The Recovery of Gallium and Germanium from Mine Tailings

By

Boingotlo Tshabang

Dissertation submitted in fulfilment of the requirements for the degree
Master of Science
(M.Sc.)

in the

DEPARTMENT of Chemistry
FACULTY OF Natural and Agricultural Sciences
UNIVERSITY OF THE FREE STATE
BLOEMFONTEIN

December 2024

Supervisor: Prof. W. Purcell

DECLARATION

I, Boingotlo Tshabang declare that the Master's research dissertation that I herewith submit at the University of the Free State, is my independent work and that I have not previously submitted it for qualification at another institution of higher education.

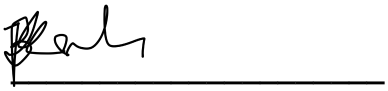

06/12/2024

Boingotlo Tshabang **Date**

DEDICATION

I dedicate this work to my mother, Tshisimogo Tshabang and my sister Keletso Tshabang.

ACKNOWLEDGEMENTS

My sincere gratitude to the following:

Prof Walter Purcell, my supervisor, thank you for accepting me as your student. Thank you for your rigorous and meticulous feedback and support while completing this study. It was an honour being your student.

Thanks to Rian Jordaan, Dr Alba Gómez-Arias, and Dr N.J Shivaramu for their assistance with sample analysis.

My colleagues from the Dept of Soil, Crop, and Climate Sciences: Thank you Dr Neo Mathinya for the encouragement, support, and assistance throughout my studies. Thank you Prof Elmarie Kotzé, my line manager, for your encouragement and for allowing me to pursue this study.

Above all, I thank God, my creator, for my life and the opportunity to pursue this study.

Table of Contents

Lists of Tables

List of Figures

List of Abbreviations

Analytical Instruments

ICP-OES	Inductively Coupled Plasma- Optical Emission Spectroscopy
XRD	X-ray Diffraction
XRF	X-ray fluorescence
SEM-EDS	Scanning Electron Microscopy and Energy Dispersive X-Ray spectroscopy
FTIR	Fourier Transform Infrared Spectroscopy

Chemical Reagents

H_3PO_4	Phosphoric Acid
H_2SO_4	Sulfuric Acid
HCl	Hydrochloric Acid
HNO_3	Nitric Acid
HF	Hydrofluoric Acid
NaOH	Sodium Hydroxide
Na_2CO_3	Sodium Carbonate
TBP	Tributyl Phosphate
N235	Tri(octyl-decyl) Amine
$H_2C_2O_4$	Oxalic acid
N_2H_4	Hydrazine

SI Units

M	Molar
g	gram
mg/kg	Milligram per Kilogram
L	Litre
°C	Degree Celcius
W	Watt

Abstract

Gallium (Ga), a posttranslational element, and germanium (Ge), a metalloid, are critical materials widely used in electronics, transport, defense, and renewable energy industries. The demand of these two elements far exceeds their supply, mainly due to these materials only being mined as by-products during the mining of other metals. This deficit will probably continue because these two materials are not found or produced in significant quantities. To address these supply challenges, attention is being given to secondary sources of Ga and Ge, such as electronic waste, coal fly ash, and mine waste.

This study aimed to recover Ga and Ge from tailings from the Tsumeb mine in Namibia. Chemical and mineralogical characterizations using various analytical techniques were performed on the sample. The total dissolution of the tailings sample revealed that the sample comprised 1.870(5) % Ga and 0.0300(2) % Ge. Other notable elements in the sample were 23(2) % Zn, 9.01(12) % Cu and 0.740(5) % Pb.

H_2SO_4 achieved the highest extraction of Ge of 40.63 % from four different mineral acids; H_2SO_4, H_3PO_4, HCl, and HNO_3 were evaluated as a suitable extraction candidate, while H_3PO_4 was the most effective for Ga (25.00 %).

The optimal dissolution conditions for Ga were determined to be 2 M H_3PO_4, solid-to-liquid ratio of 0.7 g:10 mL, at 90 °C, for one hour leaching with stirring speed of 100 rpm. For Ge, the optimal conditions were 3 M H_2SO_4, solid-to-liquid ratio of 0.1 g:10 mL, at 90 °C, for one hour leaching with 100 rpm stirring. Ge was isolated at pH 8 from the H_2SO_4 leachate, while Ga was isolated at pH 4 from the H_3PO_4 leachate. Products containing 5 % Ge and 25 % Ga were isolated.

Chapter 1 : Motivation of this study

1.1 Background

Critical Raw Materials (CRMs) are substances or materials, organic or inorganic, that are strategic and vital for a country or a region's national security, economy, energy, and medical technology development purposes (Buchert *et al*., 2009; Araya *et al*., 2020). This group of materials is considered 'critical' because they are i) usually not found or produced in sufficient quantities in these regions to meet their current and future supplies, ii) are subject to high-risk supply disruptions, and iii) are not easily substituted (Eynard *et al*., 2020). These materials are usually required in key industry sectors or future applications in the defense industry, health, consumer electronic products, super-alloy production, and aeronautics (Domaracka *et al*., 2022). Materials considered critical by the European Union include natural rubber and graphite, phosphate rock, light and heavy rare earth elements, fluorspar, lithium, cobalt, tantalum, niobium, germanium, and gallium, to name a few (European Commission, 2020). Aluminium, chrome, and manganese are included in the USA 'CRM' list (Fortier *et al*., 2022).

These CRMs are also considered critical for economic growth and sustainability for both developed and developing countries (Eynard *et al*., 2020; Guzik *et a*l., 2022). In addition to that, CRMs are crucial for modern technologies such as smartphones, computers, and LCD televisions (Buchert *et al*., 2009; Frenzel *et al*., 2017; Patel & Karamalidis, 2021). Many of these materials are also used in clean and renewable energy technologies such as electric vehicles (lithium for batteries), solar panels, and wind turbine production. Furthermore, these materials are utilized in batteries as a combination of materials that include cobalt, copper, niobium, germanium, and indium. Additionally, these materials are also extensively used in aerial imaging, defense communications, microelectronics, transportation, space exploration, aviation, and medical devices.

In 2020 the European Union (EU) listed 35 materials *as* Critical Raw Materials. This list was generated to create awareness of materials that are important to European economies and to identify their availability, supply risks, and to stimulate research in product development as well as search for alternatives. (European Commission, 2017; Eynard *et al*., 2020). **Figure 1.1** depicts the global distribution of the main suppliers of the 35 CRMs. It is evident from **Figure 1.1**, that China has global dominance in the CRM market (as identified by the EU and USA), with the country leading the production of 19 out of the 35 CRMs, which in itself is a very serious supply risk and creates the potential for geopolitical instability, tension and conflict (Gulley *et al*., 2019).

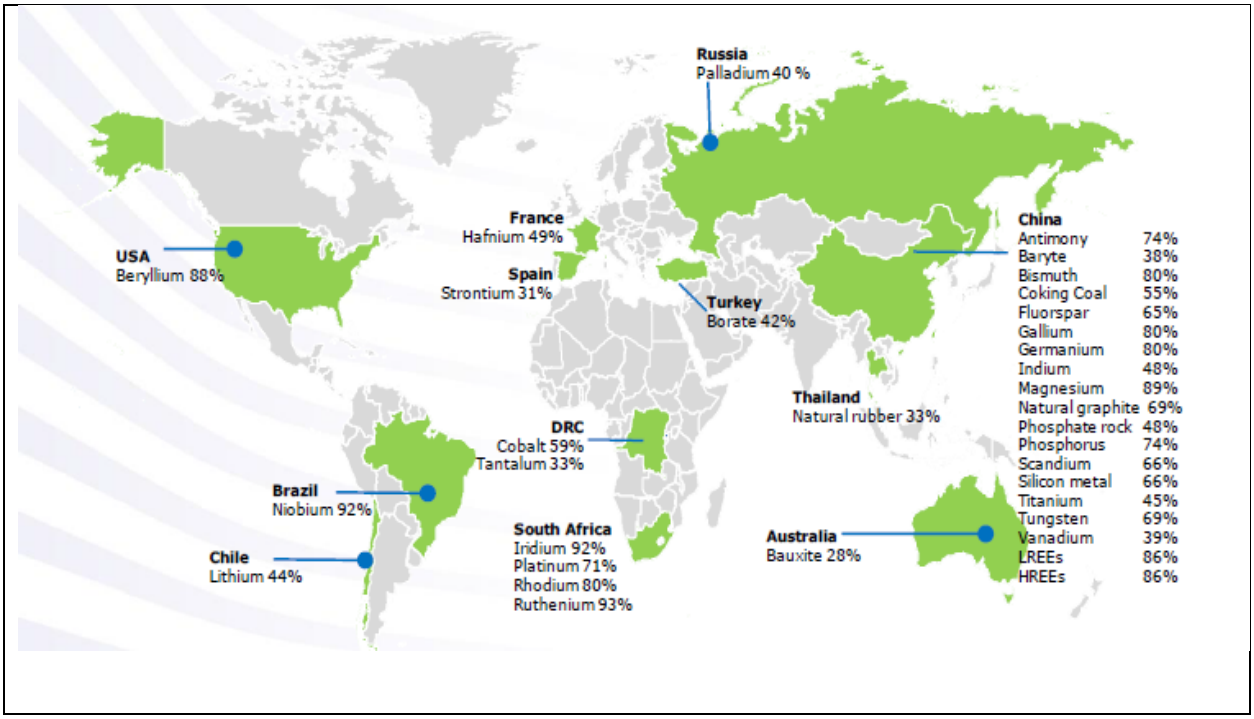

Figure 1.1: EU's Critical Raw Material List and major producers of the materials (Eynard *et al*., 2020).

These materials are of importance not only for EU member countries but for many other countries, including South Africa. Although the list indicates that South Africa is only a major producer of 4 out of 35 of the 'CRMs,' namely iridium, platinum, rhodium, and ruthenium (Eynard *et al*., 2020), the country has the largest platinum group, chrome, and manganese ore deposits worldwide, and extensive zirconium, vanadium and titanium

deposits which are included in the USA 'CRM' list. The four platinum group metals listed for SA, are used in the manufacturing of exhaust catalysts in the motor industry and as catalysts in the production of chemicals (Hughes *et al*., 2021; Ngcephe *et al*., 2020).

Of interest to this study are two CRMs, namely gallium (Ga) and germanium (Ge) (**Figure 1.2**) which are included in both the EU and USA CRM published lists. The average concentration of these two elements in the earth's crust is 16 and 6.7 ppm, respectively (Curtolo et al., 2017; Moskalyk, 2004). These two elements are critical to modern technology, green energy development, and in some instances, to the national security of countries. Germanium is extensively used in optical fibers, computer chips, infrared optical systems televisions, solar cells, computer screens, and in the electronic industry for high-speed integrated circuits. Gallium, on the other hand, is used in infrared, microwave, high-speed switching circuits, light-emitting diodes (LEDs), semiconductors, and high-temperature thermometers. It is also used in the production of mobile phones and barometers, blue and green LEDs, and pressure sensors for touch switches and in Blu-ray technology.

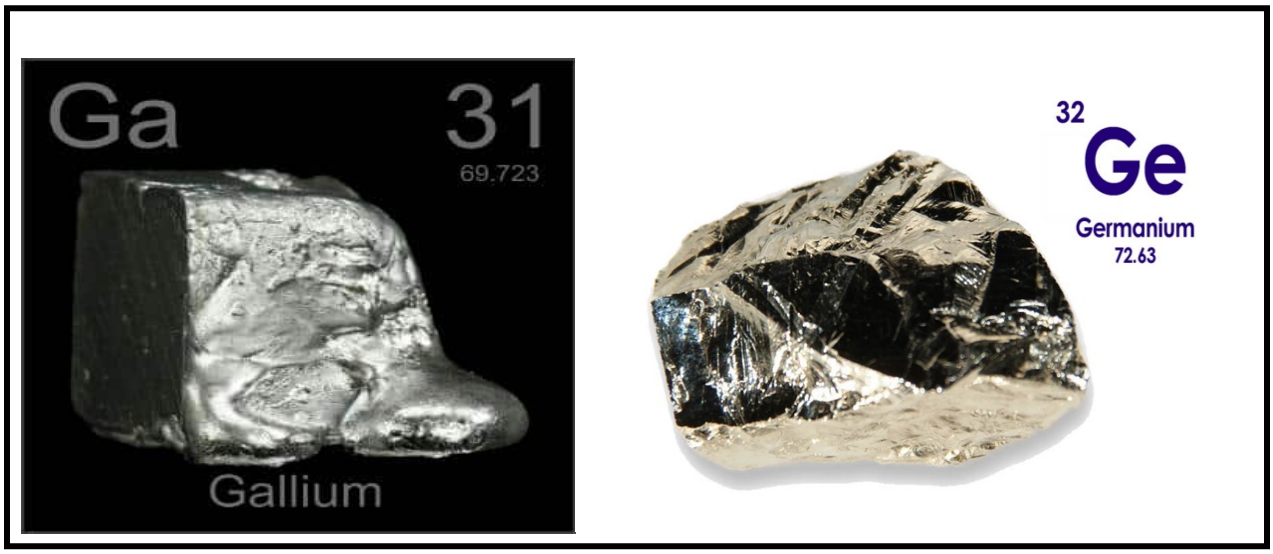

Figure 1.2: The two Critical Raw Materials of interest to this study (Gray, 2007).

Gallium and germanium are not found in nature in their elemental form and are mined mainly as by-products of aluminium and zinc ore processing (European Commission,

2023; Lu *et al*., 2017; Patel & Karamalidis, 2021; Torma & Jiang, 1991). According to the findings from a multilevel dynamic material flow analysis, the demand for Ga and Ge is is predicted to surge by 224 % and 2 130 %, respectively by 2050, in comparison to the production levels recorded in 2010 (Elshkaki & Graedel, 2013; Licht *et al*., 2015). A major supply risk of gallium can be attributed to the reported end of the aluminium production boom experienced by China (Song *et al*., 2022). China is globally the primary producer of aluminium, and gallium. Song *et al*., (2022) investigated the gallium and alumiunium supply linkages and dynamics across significant Ga-supplying regions of China, the United States of America (USA), the European Union, Japan, and the rest of the world. The result of this investigation is depicted in **Figure 1.3,** varying patterns in the gallium supply and demand across the compared regions were observed.

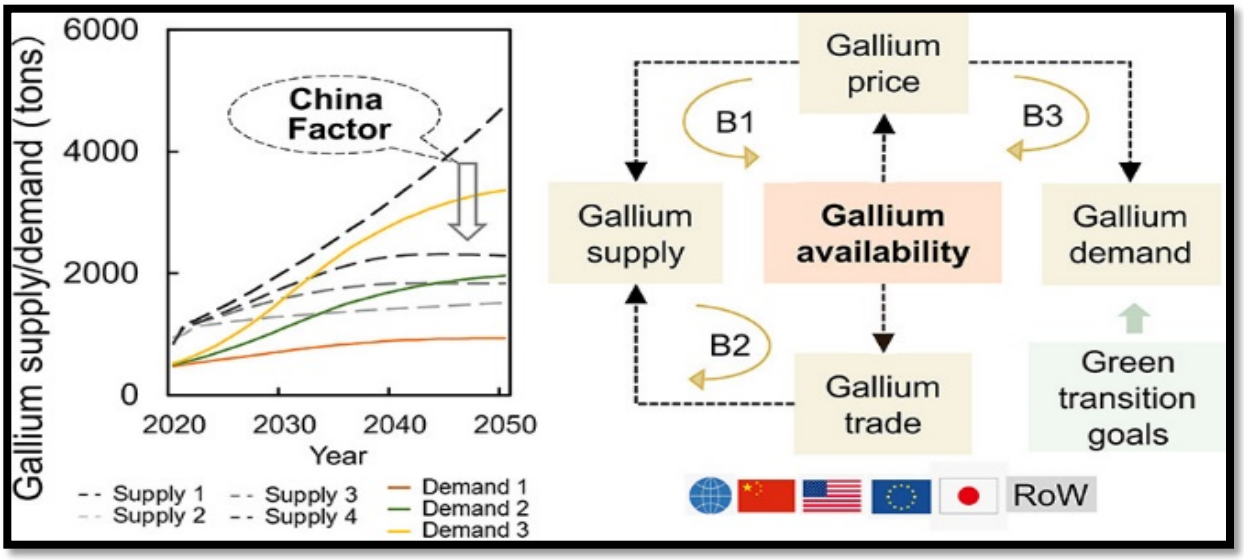

Figure 1.3: Projected gallium supply and demand (Song *et al*., 2022).

The graph of the left of **Figure 1.3** depicts the gallium supply and demand across the mentioned five regions projected from 2020 to 2050. **Supply 1-4** represents different supply potentials or scenarios. In **Supply 1**, the existing trend is assumed to continue steadily until 2050 with no major disruptions and ultimately peaking at 4800 tons/year. This supply is expected to meet the highest demand scenario (**Demand 1**). The reported reason for this is the rising gallium price that could result in a 60 % increase in the gallium recovery from bauxite by 2050. **Supply 2-4** are adjusted for any changes in the supply

capacity across the five regions. The “China Factor” is attributed to the role that China is expected to play in quenching its gallium demand and that of the other four regions. China’s gallium net exports supply 40-98 % of the gallium demand of the four other mentioned regions (Song et al., 2022). The flow diagram on the right-hand side of the same figure depicts a cycle that influences the availability of gallium. Gallium supply includes primary and secondary production. **B1** on the diagram is the linkage between the gallium supply and its market price. Limited gallium supply reduces its availability thus resulting in elevated gallium prices. **B2** illustrates the linkage between gallium supply and its trade. As previously mentioned, limited gallium supply reduces gallium availability, ultimately impacting the overall gallium trade. Regions with reduced gallium availability ultimately cut back on their Ga exports or increase their Ga imports. **B3** depicts the linkage between the gallium demand as a result of the global green transition. An increase in the gallium demand ultimately results in reduced gallium availability which leads to an increase in the gallium price.

Similar to gallium, refined germanium is largely produced in China. **Figure 1.4 a)** depicts the annual yield of Ge over a 11-year period. The dominance of China in Ge production is evident from this graph. Another significant role player in the production of germanium is Russia. As previously mentioned, geopolitical stability is at risk when political manipulation of Critical Raw Materials supply is prevalent in the global market. With the political tensions between Russia and NATO caused mainly by the war in Ukraine, and the ongoing tensions between the United States of America (USA) and China, the supply risk of Ga and Ge is at an all-time high. **Graphs b)** and **c)** in **Figure 1.4** depict the significant uses of Ge and average annual prices of refined Ge and GeO_2.

It is reported that only 30 % of the consumed Ge is recovered from secondary sources and a large portion of this is recovered from optic fibres. **Graph d)** from **Figure 1.4** shows the proportion of Ge consummation and recycling from its major uses. More details on the uses of Ga and Ge in **Chapter 2.**

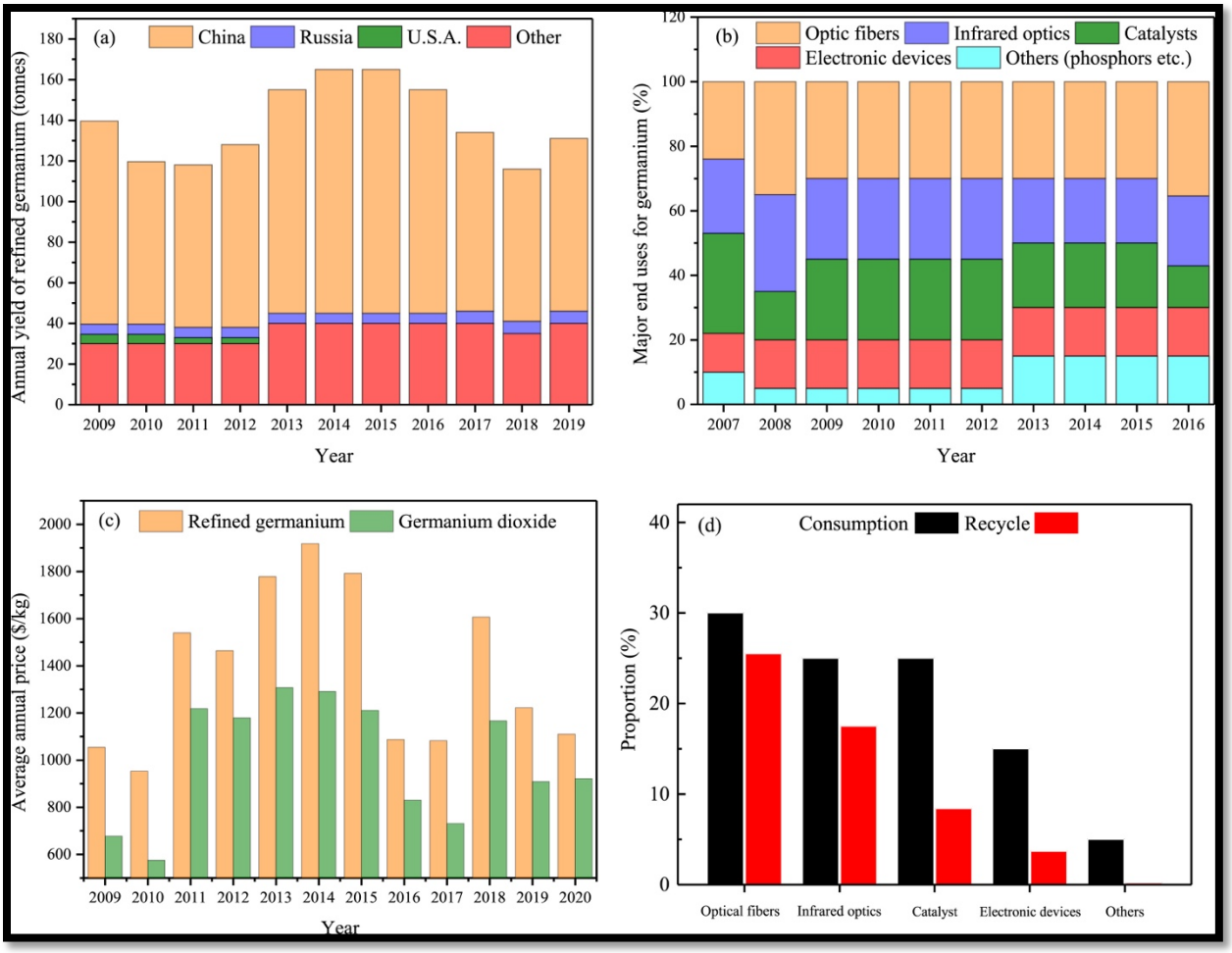

Figure 1.4: Ge annual yields, average prices, uses, consumption and recycled proportions graphs (Tao *et al*., 2021).

The mining of minerals for the sole extraction of gallium and germanium is usually uneconomical and the last recorded process was in 1985 by the Apex mine in Washington County, Utah (Bernstein, 1986). The mine was developed for the primary processing of copper, silver, trace amounts of gold, and lead and was operated between 1884 to 1962 (Bautista, 2003; Torma & Jiang, 1991; Wardell & Davidson, 1987), In 1985 the mining shifted solely to Ga and Ge processing initiated by Teck Cominco American, Inc (Bernstein & Waychunas, 1987; Dutrizac *et al*., 1986). Since the closure of the Apex mine, much attention has shifted to the recycling of the critical elements from products that have reached end-of-life stages.

Natural Ga and Ge reserves are certainly not adequate to meet the future consumption and demand for these strategic elements (Robertz *et al*., 2015). Their production is exclusively dependent on the mining of host elements such as zinc, copper, and silver from mineral deposits and ores. A disruption in the processing of minerals containing zinc and aluminium will inevitably have an adverse effect on the supply of the two by-products, Ga and Ge. This study is motivated by a need to develop a local hydrometallurgical process for the separation and isolation of the two elements from mine tailings sourced from the north of Namibia.

The mineralogy and geochemistry of different Ga and Ge bearing ores and host rocks vary significantly (Bernstein, 1985, Höll *et al*., 2007; Ettler *et al*., 2021). Different studies reported on Ge and Ga from different sources being distributed in different phases, with varying concentrations of Ga and Ge between the different phases (Cook *et al*., 2009). Added to these natural phenomena, is the fact that the original physical and chemical properties of the minerals and ores have been altered during the processing of the original target elements, such as copper and zinc. This explicitly implies that the secondary material (mine tailings) i) has new or altered properties and ii) may differ from mine to mine, depending on the processing regime that was used to extract the target elements. In essence, it means that i) an in-depth study is needed to determine both the physical and chemical properties of the secondary material, and ii) a unique chemical process may/should be developed, depending on its properties.

1.2 Problem Statement

The demand for the two critical raw materials gallium (Ga) and germanium (Ge) consistently increased due to their usage in the manufacturing of various technological components (de Oliveira *et al*., 2021; Frenzel *et al*., 2017). However, mining for the sole extraction of these materials is not economically feasible, and hence their production primarily relies on being extracted as by-products during the processing of other minerals, as well as through recycling (Charles *et al*., 2020).

Tailings from the Tsumeb Smelter in the north of Namibia has been identified as a potential secondary source of Ga and Ge (Ettler *et al*., 2021, 2022). However, a hydrometallurgical study has yet to be carried out to elucidate the best extraction process for this anthropogenic deposit, which is the main aim of the present study.

1.3 Aim and Objectives

The aim of this study is to develop a novel process to extract gallium and germanium from copper tailings samples from the Tsumeb mine in Namibia.
To achieve this aim, the main objectives of this study include:

- In-depth literature study on Ga and Ge hydrometallurgy
- Chemical, geochemical, and mineralogical characterization of Ga and Ge bearing tailings
- Selective dissolution of Ga and Ge from the tailings
- Optimization of the reaction conditions
- Isolation of Ga and Ge from the digestion solution

1.4 Justification

The production of gallium and germanium is i) mainly feasible as a by-product from processes that target other main or valuable elements present in the original ore bodies and ii) these two elements are usually found in low concentrations in the host ores and minerals (Redlinger *et al*., 2015). These two factors create insecurity in the future supply of these elements and hence create large supply risks for the industries and products that rely on their supply.

The increased demand, the scarcity, and the subsequent high prices for these two critical materials necessitate the development of new and/or alternative processes to recover the elements from secondary sources such as tailings (Robertz *et al*., 2015). Mining

companies can no longer afford for these critical materials to end up in landfill sites. Consequently, it is necessary to develop new efficient, and possibly energy-effective processes to extract Ga and Ge from mine tailings. The mineralogy and distribution of Ga and Ge between the different solid mine tailing phases is important in developing good extraction processes. This information can provide insights into the physical and chemical properties of the mineral samples, including the location, quantity, and speciation of Ga and Ge within mineral phases. By understanding the mineralogy and distribution of Ga and Ge, it is possible to identify the most efficient extraction methods and optimize the extraction conditions to achieve economically viable quantities or yields of these CRMs (Jamieson *et al*., 2015). In addition, the post-transitional element gallium and the metalloid germanium have not been extensively or sufficiently studied compared to base and precious metals. These two critical materials have been largely overlooked due to their rarity and sole production as byproducts of the processing of other minerals. This study aims to contribute to the limited body of knowledge of these two critical materials.

Chapter 2 : Introduction and natural occurrences of Gallium and Germanium

2.1 Introduction

Gallium and germanium belong to the 4th period on the periodic table with the former classified as a post-transition metal, while the latter is regarded as a metalloid. Both these elements are regarded as having critical economic importance and have been cited by both the European Commission's 2020 report and the USA's list of Critical Raw Materials (European Commission, 2020; Eynard *et al*., 2020; Fortier *et al*., 2022). This chapter aims to describe the main characteristics, occurrence and uses of both gallium and germanium.

2.1.1 Germanium

Germanium (Ge) is a greyish-white and brittle metalloid with five naturally occurring isotopes; ^{70}Ge, ^{72}Ge, ^{73}Ge, ^{74}Ge, and ^{76}Ge. The most abundant isotopes are ^{73}Ge and ^{74}Ge with later having a natural abundance of 36 %. The existence of Ge as an element was first proposed by Dmitri Mendeleyev in 1871 but was only isolated in 1886 from the mineral argyrodite (Ag_8GeS_6) by the German chemist Clemens-Alexander Winkler (Burdette & Thornton, 2018; de Laeter *et al*., 2003). Germanium has an ionization energy of 7.9 eV, a melting point of 937.4 °C, and a boiling point of 2 830 °C. The two most prevalent oxidation states of germanium are +2 and + 4.

Germanium can form complexes with halides, hydroxides, sulfides, nitrides, oxides, and alloys (Johnson, 1952). The most important Ge compounds in terms of their current uses are germanium dioxide (GeO_2) and germanium tetrachloride ($GeCl_4$). The two compounds are largely employed in electronics and as polymerization catalysts as detailed in **Section 2.2** (Shanks III *et al*., 2017).

Germanium with the [Ar]3d^{10}4s^{2}4p^2 electron configuration readily loses 2 to 4 electrons in the 4s and 4p orbitals to form the relatively stable Ge^{2+} and Ge^{+4} oxidation state. This

results in the formation of a relatively stable number of complexes with σ- and π-donating ligands such as O^{2-}, OH^- and halides (X^-) which stabilize this high oxidation state of the element. The amphoteric GeO_2 is a well-known, stable and useful germanium +4 compound, while a number of Ge-halide species with Ge present in both the +2 and +4 oxidations states, with the most important species GeX_2 (X = Cl^- and F), GeF_3^- .GeX_4^-(X = Cl^- and F) and GeF_6^{2-} have been identified. Numerous Ge-hydroxide compounds have also been identified in mild alkaline to strong alkaline solutions, with the dominant species $Ge(OH)_4$ and $GeO(OH)_3^-$ (**Figure 2.1**).

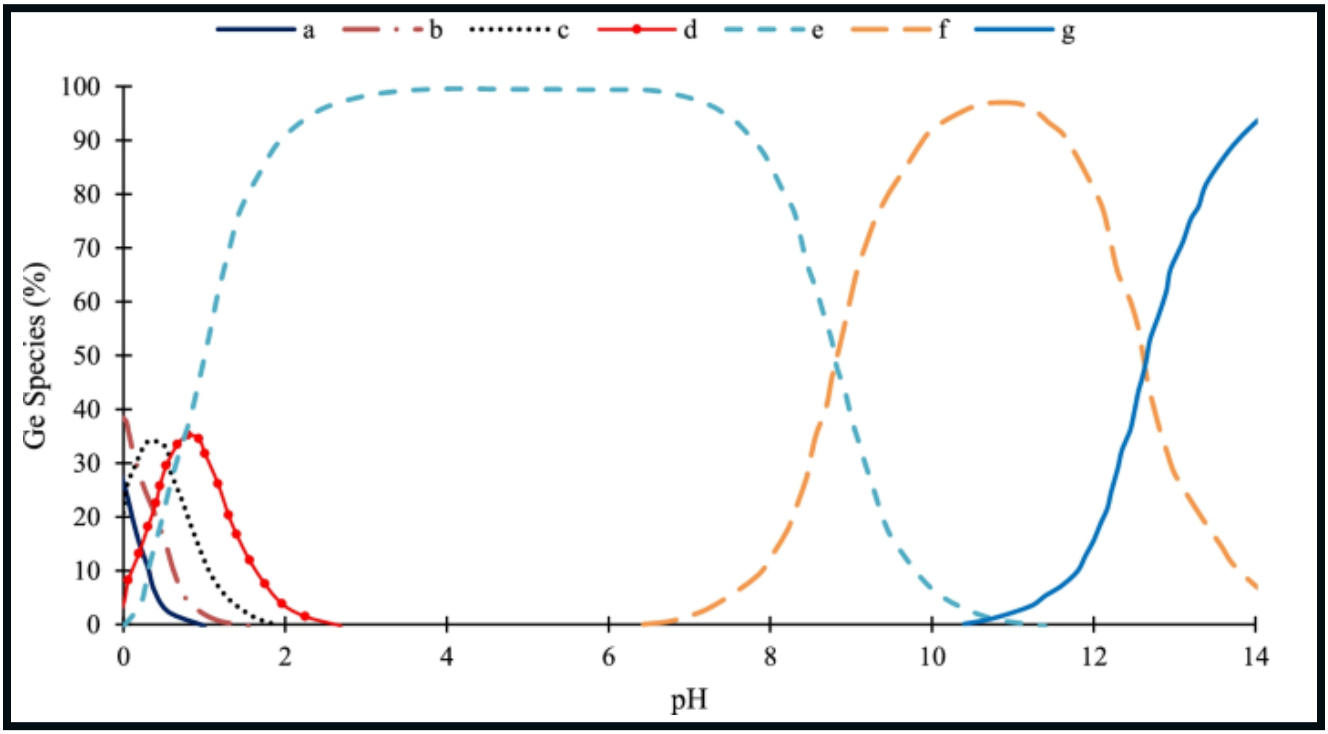

Figure 2.1: Effect of pH on germanium species: (a)Ge^{4+}; (b) $Ge(OH)_3^+$,(c) $Ge(OH)_2^{2+}$; (d) $Ge(OH)^{3+}$;(e) $Ge(OH)_4$;(f) H_3GeO^{3-},(g) H_2GeO^{4-} (Kamran Haghighi *et al.*, 2022).

Methyl and ethyl chlorides, bromides and alkyl halides reacts with heated germanium metal to form organogermanium halides and dry hydrogen reacts with Ge at high temperatures to form $GeCl_4$ and $GeHCl_3$ as indicated in **Eq (2.1)** and **Eq (2.2)** (Rochow & Abel, 1997) :

$$Ge + 4HCl \rightarrow GeCl_4 + 2H_2 \qquad \textbf{(2.1)}$$

$$Ge + 3HCl \rightarrow GeHCl_3 + H_2 \quad \textbf{(2.2)}$$

2.1.2 Gallium

Gallium (Ga) is soft and silvery in colour (Lu *et al*., 2017). It has two stable isotopes, namely ^{69}Ga and ^{71}Ga (Wei Yuan, 2021). This post-transitional element exhibits two stable oxidation states namely Ga^{+} and Ga^{3+} and it has a relatively low ionization energy of 5.99 eV. It also has a low melting point of 29.76 °C and a boiling point of 2 400 °C (Gupta & O'Sullivan, 2013). Paul-Émile Lecoq de Boisbaudran, a French chemist discovered gallium in 1875, but its existence was predicted six years prior to its discovery by Mendeleev. In his arrangement of the periodic table, Mendeleev had left placeholders for elements not yet discovered, with gallium being one of those elements (Brennan, 2014).

Gallium with the $[Ar]3d^{10}4s^{2}4^{1}$ readily loses the 4s and p electrons to form compounds in the +1 and +3 oxidation states. Gallium forms complexes of hydrides, chlorides, bromides, oxides, sulfides, and nitrides. In addition, gallium can dissolve in acids with a pH value below 2 and it also dissolves in concentrated alkali solutions due to its amphoteric nature (Lu *et al*., 2017). Gallium metal is soluble in hydroxide, resulting in the formation of a number of different hydroxide species. The element also forms different oxide systems with the formation of α- and β-Ga_2O_3.

The prevalent gallium species Ga^{3+} at different pH values is demonstrated in **Figure 2.2** The Ga^{3+} species dominates in solutions with a pH lower than 2, while $Ga(OH)^{2+,}$ $Ga(OH)^{+}_{2,}$ $Ga(OH)_3$ dominate from pH 2 -7. At higher pH values $Ga(OH)_4^{-}$ is the dominant species in solution.

In chloride and sulfate solutions gallium can form complexes with Cl^{-} and SO_4^{-} to yield $GaCl_{3,}$ $[GaCl_4]^{-}$,$[GaCl]^{2+}$,$[GaCl_2]^{+}$,$[GaCl_3]$ and $[Ga(SO_4)_2]^{-}$. Gallium has also been reported to form complexes with phosphates, although not extensively studied as other gallium complexes $[Ga(HPO_4)]^{+}$, $[Ga(HPO_4)_2]^{-}$, $[Ga(H_2PO_4)]^{2+}$ and $[Ga_2(HPO_4)^{4+}$ occur in aqueous solutions (Lu *et al*., 2017).

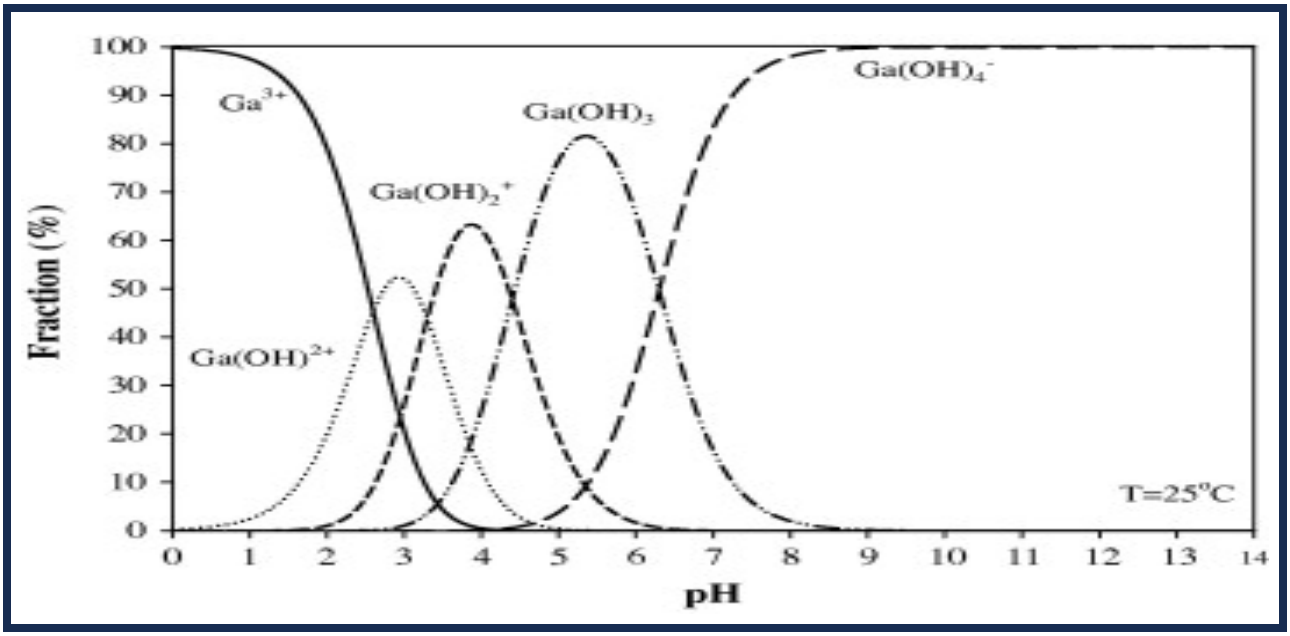

Figure 2.2: Effect of pH on Ga(III) speciation (Thanh & Liu, 2014).

The most important compounds in terms of uses are gallium nitride (GaN) and gallium arsenide (GaAs). Gallium nitride is prepared in industry by reacting Ga_2O_2 with NH_3 (as demonstrated in **Eq (2.3)** at a temperature of approximately 1000°C (Sudarsan, 2017).

$$Ga_2O_2 + 2NH_3 \rightarrow 2GaN + 3H_2O \quad \textbf{(2.3)}$$

For the preparation of gallium arsenide, elemental gallium reacts with SiO_2 to form Ga_2O_2, which is then reacted with elemental arsenide as per **Eq (2.4)** & **Eq (2. 5).** These products are mostly used in the manufacturing of optoelectronic devices (LEDs, laser diodes, and solar cells) (Foley *et al*., 2017; Vecchia *et al*., 2019; Papež *et al*., 2021).

$$2Ga + 2SiO_2 \rightarrow Ga_2O_2 + 2SiO \quad \textbf{(2.4)}$$

$$Ga_2O_2 + 2As \rightarrow 2GaAs \quad \textbf{(2.5)}$$

2.2 Natural Occurrence

2.2.1 Gallium

Gallium has a relative abundance of 17 ppm in the earth's crust (Redlinger et al., 2015). The main sources of gallium are 1) coal deposits, 2) bauxite residues, and 3) zinc-containing ores. Although coal deposits have the greatest reserves of gallium (**Table 2.1**), most of this post-transition metal is obtained from bauxite residues (Raiguel, Dehaen and Binnemans, 2020).

Table 2.1: Ga reserves reported globally (Lu *et al*., 2017).

Raw material	**Estimated reserve (10^9 tons)**	**Ga average content (ppm)**	**Ga potential resources (10^6 tons)**
Bauxite	55–75	50	> 1
Zinc ore	1.9	50	0.095
Coal	> 1000	10	10

Additionally, gallium has been determined in seawater as well as more than 80 minerals, rocks, and sediments. More than 80 percent of the thirty-three granitic type rocks examined contain Ga in concentrations ranging between 14 and 24 ppm (average 18.1 ppm) and is present in hydrolysate sediments, including clays and mudstones. The mean Ga: Al ratio for the mentioned rocks is 2.35×10^{-4} :1, while the mean gallium concentration in twenty siliceous sediments was recorded as 9.9 ppm. Residual sandstones and other sedimentary rocks rich in silica have generally low gallium content. In carbonate rocks, only minute amounts of gallium are found (mean 0.06 ppm). An average gallium concentration of 22.4 ppm with a Ga: Al ratio of 2.40×10^{-4} :1 is contained in pelagic clays from the Pacific, Atlantic, and Indian Oceans, while other pelagic sediments contain most of its gallium in the clay fraction (mean Ga: $Al = 9.7 \times 10^{-4}$)(Burton *et al*., 1959).

Examined oxide minerals with noteworthy amounts of gallium are corundum, bauxite, and magnetite. All the sulfides except blende formed at low temperatures, contain less than 3 ppm gallium. Not more than 0.15 ppm gallium was found in carbonate, sulphate, fluoride, and evaporite minerals while seawater contains 0.030 ± 0.007 *μg* of gallium/kg (0.44 ± 0.10 *μg-atom*/*ton*) and has a Ga: Al ratio of about 3.0×10^{-3}:1 (Burton *et al*., 1959).

Bauxite is a mineral ore **(Figure 2.3)** that contains mainly aluminium hydroxide and other hydroxide compounds and is also the main source of aluminium production, with gallium as an impurity. It is estimated that the Ga concentration ranges between 10 - 812 ppm, averaging at 57 ppm in global bauxite deposits (Schulte & Foley, 2014). Gallium is found in lesser amounts in sphalerite, a zinc-sulfide mineral. The sphalerite ore in which Ga is found, is processed from three different types of zinc deposits namely, Mississippi-Valley type (MVT), sediment-hosted, and volcanogenic massive sulfide (Foley *et al*., 2017) .

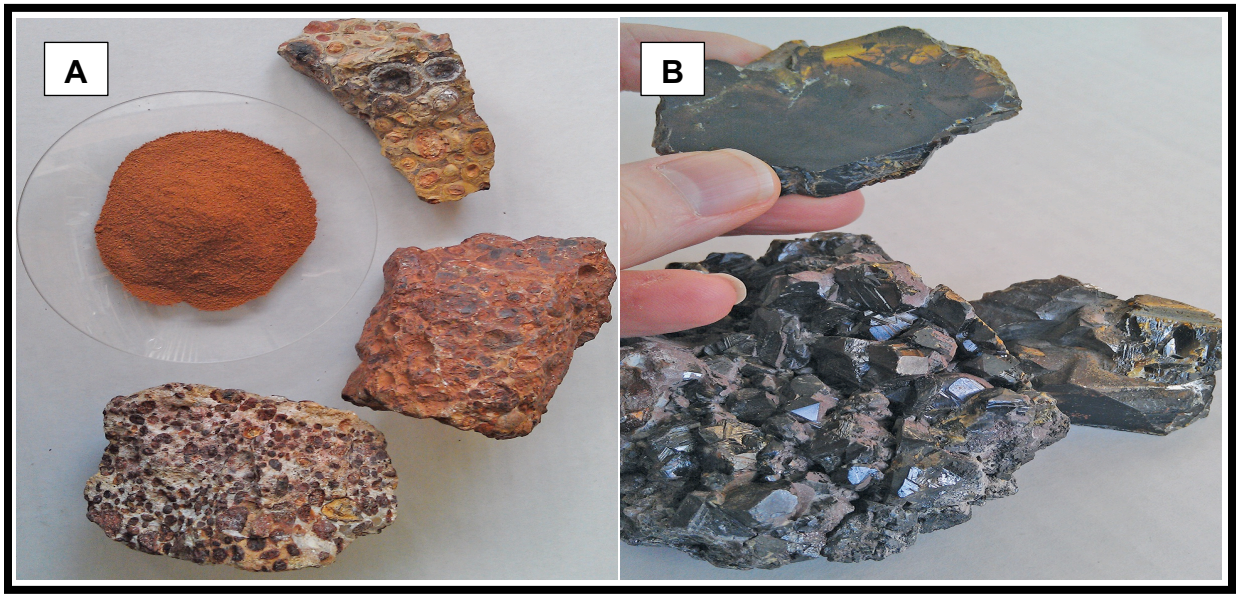

Figure 2.3: Images of the primary mineralogical sources of gallium bauxite ore sample (A) and sphalerite (B) (Foley *et al*., 2017).

Several gallium-rich minerals have been reported in Africa with the most well-known being found at the Tsumeb Mine in the Oshikoto Region of Namibia (Ettler *et al*., 2021; Hawthorne *et al*., 2012; Hearth, 2021). These minerals with their Ga content are depicted in **Table 2.2** The above-mentioned mine which mainly processes Cu, Zn, Ag, and Cd

started operations in 1907 but was subsequently closed in 1996 due to economic factors (Pitiya & Peter, 2021). The mine was re-opened in 2000 and reached production in 2001 under the stewardship of Ongopolo Mining and Processing Limited (Coakley, 2002). All mining activities have been decommissioned while only the smelter is still in operation. The Tsumeb smelter was acquired by Dundee Precious Metals in 2010 and produces blister copper (98.5 % Cu) (*Tsumeb Specialty Smelter, Namibia*, 2024) . The mineral deposits were situated on a Neoproterozoic Otavi Dolomite rock sequence (Melcher, 2003). This ore body has a pipe-like structure, and it is about 120 by 15 meters in cross-section. It is steeply dipping and extending from the surface to at least 1000 meters in depth (Hawthorne *et al*., 2012; Hearth, 2021; Melcher, 2003; Nora K. Foley *et al*., 2017).

Table 2.2: Cu-Pb-Zn deposits mined by the Tsumeb Namibia (Nora K. Foley *et al*., 2017).

Mineral	**Chemical Formula**	**Ga content (% w/w)**	**Group**
Gallite	$CuGaS_2$	35	Sulfide
Gallobeudantite	$PbGa_3[(AsO_4)_2(SO_4)]_2(OH)_6$	15	Alunite
Sohngeite	$Ga(OH)_3$	58	Hydroxide
Tsumgallite	GaO(OH)	60	Hydroxide

2.2.2 Germanium

Germanium is found in nature in Pb, Zn and Cu sulfide ores and in coal deposits with the former being the main source and it also found in phosphates, tungstates and arsenates (Etschmann *et al*., 2017). In addition, germanium was observed in over 200 minerals, rocks, and sediments, and in seawater (Burton *et al*., 1959; Sutley *et al*., 1999). Germanium has a crustal abundance of approximately 1.7 ppm, which is the average germanium content in granitic and basic igneous rocks. Similar amounts of germanium are also found in metamorphic rocks, shales and red claysand (pelagic sediments). Only minute levels of germanium were observed in the sulphates, carbonates and evaporite portions of the examined minerals. Germanium is primarily concentrated in goethite (as much as 0.5 %), hematite (maximum of 0.7 %), and limonite (as much as 0.5 %). The germanium content of most oxides and silicates is close to the mean crustal abundance, while magmatic sulphides have less than 1 ppm germanium content. In addition to this, coal reserves and zinc resources are reported to contain 100 ppm Ge, while sea water has been found to contain 0.06 ± 0.01 *μg* Ge/kg (0.82 ± 0.13 *μg-atom*/*ton*) (Nguyen & Lee, 2021). Germanium is also found in the following minerals, argyrodite (Ag_8GeS_6), germanite ($7CuS.FeS.GeS_2$) and sphalerite (Zn,Fe)S. Interestingly, germanium was first isolated in argyrodite while sphalerite is the most prevalent Pb-Zn containing ore mineral and it has been reported to contain high amounts of germanium with concentration reaching levels of up to 3000 ppm (Höll *et al*., 2007; Niu *et al*., 2023). **Figure 2.4** depicts different sphalerites (letters A-I, with C1-C5 representing different colours of sphalerite) found in the Maoping Pb-Zn deposits in the Sichuan-Yunnan-Guizhou province of China, one of the world's top germanium producers (Niu *et al*., 2023). (A) Black sphalerite (C1), (B)Symbiotic black (C1) and red-brown sphalerite (C2), (C) Dark brown sphalerite (C3) coexisting with light brown (C4), (D) Dark brown sphalerite (C3) occurring on edge of red-brown sphalerite (C2),(E) a combination of C1-C4 sphalerite, (F-G) light red sphalerite (C5) crosscutting C1 and C2, (H)light red sphalerite (C5) veining in C3 and C4, (I) Variations of C2-C4 (Niu *et al*., 2023).

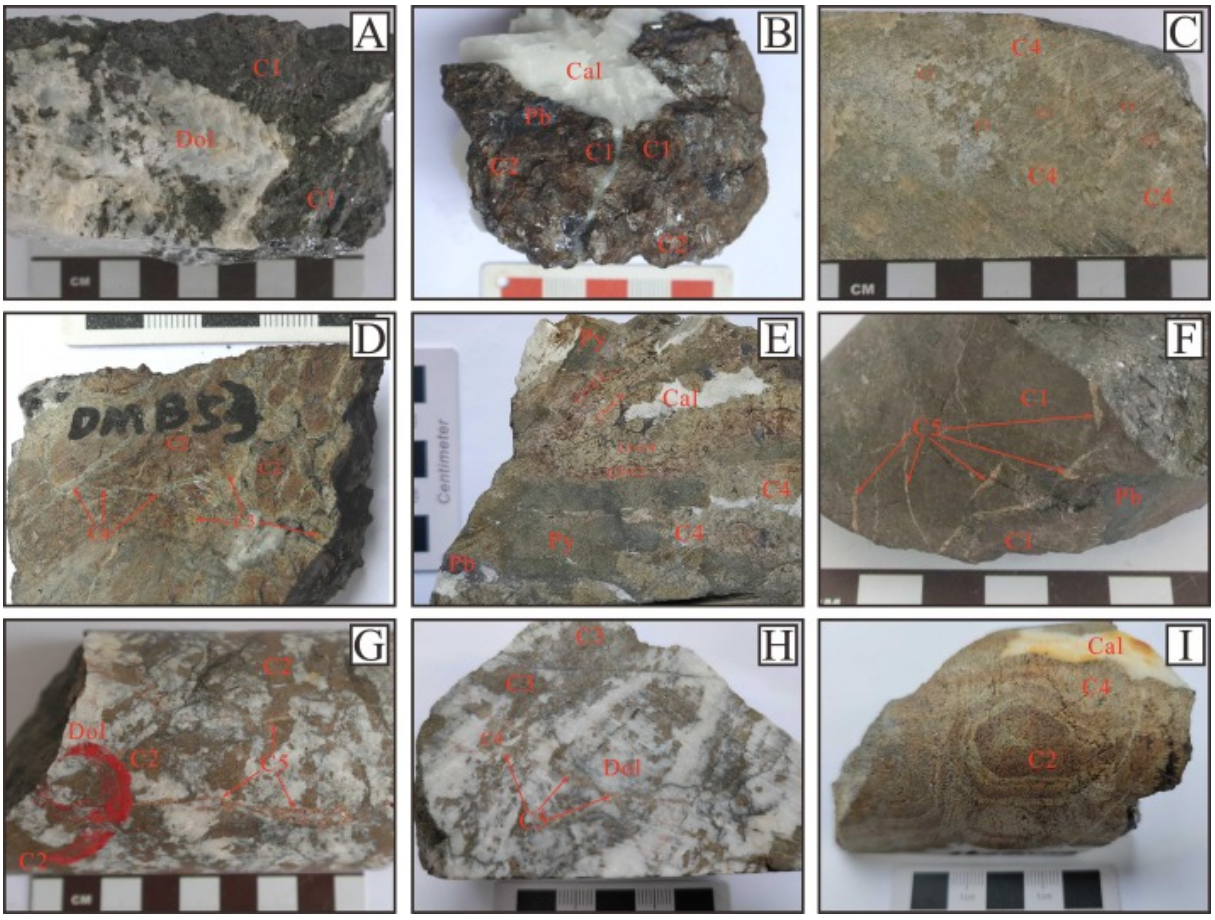

Figure 2.4: Images of different colour sphalerite from the Maoping Pb-Zn deposits of Southwest China (Niu *et al*., 2023).

Among the different Ge-bearing deposits (**Table 2.3),** the Zn-Pb deposits found in the carbonate rocks of the Irish Midlands, together with the coal deposits of Lincang, China are considered major Ge containing deposits (Nguyen & Lee, 2021). Other significant Ge-bearing deposits are the Mississippi Valley type deposits (MVT) in the United States of America (USA) and the sedimentary exhalative deposits of South China and Germany (Höll, *et al*., 2007).

It has been reported that the Kipushi Zn deposits in the Democratic Republic of Congo contain an average of 68 ppm Ge (see **Table 2.3**) (Ruiz *et al*., 2018). Other studies have reported Ge concentrations of between 100 to 250 ppm in the Cu-Co ores situated at Kupushi in the Haut-Katanga province of the DRC (Ettler *et al*., 2021). Also, in Africa, Ge-rich sulfide ores of up to 8.3 ppm Ge have been reported in Tsumeb in the northern region

of Namibia which is well known for its Cu-Pb-Zu sulfide ore deposits (Melcher, 2003; Melcher *et al*., 2006; Höll *et al*., 2007; Ettler *et al*., 2021). The geology and history of the Tsumeb is discussed in more detail in **Chapter 4**.

Table 2.3: Ge concentration in minerals deposits (Höll *et al*., 2007; Nguyen & Lee, 2021).

Deposits	Comments	Ge content, ppm
Volcanogenic massive sulfide (VHMS) Cu-Zn(-Pb)(-Ba)	Occurring in submarine volcanic rocks. Major source of the world's Zn, Cu, Pb, Ag and Au.	Average ≪ 100 ppm
Sedimentary exhalative deposits (SEDEX)	Occurring as tabular Zn-Pb-Ag deposit in carbonaceous and pyrite shales and siltstones. Major source of Zn-Pb-Ag	104 – 249 ppm
Mississippi Valley-type deposits (MVT)	Zn and Pb concentrates in carbonate sedimentary rocks that are formed in collapsed breccias. Major source of Zn-Pb with Cu, Ni and Co	The Gordonsville–Elmwood zinc-lead district in Tennessee, USA: 400 ppm MVT deposits in the United States: 50 ppm
Irish-type carbonate-hosted lead-zinc deposits	Hosted in lower carboniferous carbonate rocks of the Irish Midlands in Ireland. Major source of Zn-Pb	The southern Silvermines–Lisheen group: >100 ppm. Sphalerite: 400 – 900 ppm, galena: 200 –1300 ppm, tennantite: 200 –1000 ppm
Kipushi-type deposits	Occurring in carbonate platform rock sequences. Major source of Zn-Pb-Cu	Average 68 ppm
Coal and lignite deposits	Ge concentrated in organic matter of coal seams. Major source of Ge with As, Ba, Sb, U, and W	Lincang deposit: 850 ppm

2.3 Processing of Ga/Ge sources

From the previous discussion, it should be clear that Ge and Ga are hosted in numerous minerals at very low concentrations and only present in significant quantities in a zinc sulfide mineral such as sphalerite **(**(Zn,Fe)S) or in some deposits formulated as (Zn,Fe,Mg,Mn,Cd,In,Ga)S, which are relatively high in Cd, In, and Ga content. Another mineral called gallite with the general formula $CuGaS_2$, is relatively high in Ga content, but it is very rare and interestingly, this mineral is strongly associated with Tsumeb in Namibia. The closure of the Apex mine in Washington County, Utah, the only mine that exclusively processed Ga and Ge during its later life, happened in 2002 due to economic considerations.

The recent rapid growth in Ga and Ge demand worldwide due to the development and production of innovative products, was accompanied by a rapid growth in the spot price of these elements, which prompted businesses and governments to find new or alternative sources of Ga and Ge. One of the more recent strategies is called “industrial symbiosis,” which embraces the concept that the waste produced by one industrial process becomes the valuable input of another. The methodology is also very useful in the reduction of production costs and inputs. This strategy is especially useful in the metallurgical industry, which also reduces waste and therefore reduces the impact of mining on the environment, health, and other social aspects (Yuan and Shi, 2009). In this context, it implies that waste produced by Zn and Al production does not end up in mine tailing or waste sites but is sent to another business that extracts the two elements in question from these sources.

However, before the rapid increase in demand for Ga and Ge, and hence its economic benefits, these two elements which are present in relatively low concentrations in minerals and hence the tailings, were regarded as waste or impurities which ended up in mine tailings near mining or processing sites. In reality, it means that large quantities of valuable elements, like Ga and Ge, are present in mine waste or tailings and lying unprocessed on the earth’s surface.

These mine tailings are waste consisting of crushed rocks or solid material, chemicals, and effluents from the processing plants and are often a reserve of valuable metals that have a) not been entirely exploited because the technology at that time was not efficient, b) financial considerations or c) contained elements that were not of economic interest at the time of production (Xiaolong *et al*., 2021). Thus, more research is needed to efficiently recover any critical or economically valuable elements from these waste materials to meet current and future demand (Bodénan *et al*., 2015; Lu *et al*., 2017).

Recovery of these critical elements from mine tailings poses considerable challenges due to a number of factors. Firstly, these elements are present in the tailings in low quantities, which makes their recovery a very delicate process. Secondly, the inherent physical and chemical properties of the ore minerals, and the type of mining or the processing methodology of the minerals, produce tailings with different, or new characteristics compared to the starting mineral ores. Therefore, a process used for extraction and recovery of the same elements in one tailing may not be applicable to different tailing deposits. Finally, it is important to consider the possibility of the tailings containing toxic elements at considerably high concentrations (Falagán *et al*., 2017).

Ga (III) and Ge (IV) are commonly recovered from zinc ores by sulphuric acid leaching followed by solvent extraction (Harbuck *et al*., 1991; Liu *et al*., 2017). Less than 3% of the Ge embedded in zinc ores and coal fly ash is recovered globally. Less efficient and uneconomical extraction processes contribute to new waste containing scarce resources of gallium and germanium, which worsen their scarcity (Patel & Karamalidis, 2021) and increase their abundance in mine tailings.

Several recent examples are known where Ga and Ge were successfully extracted from secondary material. A recent study on the extraction of Ga and Ge from secondary sources (Macías-Macías *et al*., 2019) shows that total dissolution of gallium from iron mine tailing was reached by leaching with 8 M HCl for 48h. Solvent extraction using tributyl phosphate and trioctylphosphine was used to recover Ga. The tailings were reported to have approximately 13 mg/kg of Ga and 100 % of the Ga in the tailings was

extracted. In another study, 70 % of the gallium present in bauxite obtained from aluminium processing was recovered by its leaching with sodium hydroxide. The aluminium crystallized as alumina trihydrate (Al $(OH)_3$) at a pH of 10, while $Ga(OH)_3$ initially remained in the liquid phase and precipitated at a pH between 9.4 and 9.7 (Lu *et al*., 2017),

Gallium was also extracted by a roast-leach electro-winning from zinc residues obtained from a zinc smelting plant at a recovery rate, ranging between 70 % to 99 % (Fugleberg, 1999; Phatak *et al*., 1988). In one notable study, Ga was recycled from gallium arsenide scrap. In this study, 99 % of Ga was extracted using 2N HNO_3 as a leaching reagent. The study also reported that more than 80 % of the GaAs scrap was wasted and not reclaimed, hence the need to develop a process to recover Ga from that scrap (Sook Lee & Woo Nam, 1998).

Generally, germanium is recovered from zinc residues by acid or alkali leaching followed by precipitation of the germanium concentrate (Shanks III *et al*., 2017). An earlier study by Johnson, (1952) reported on extraction processes of germanium from secondary sources such as coal fly ash, from gasification fly ash, as well as Cu smelting flue dust and waste optical fibers These processes generally involve the physical separation of the waste material and subsequently its mineral or organic acid leaching. Finally, the Ge concentrate is chlorinated and purified to produce $GeCl_4$ which is extensively employed in fiber optics (Johnson, 1952; Ruiz *et al*., 2018).

Various studies have reported on the recovery of germanium from gasification fly ash. In many of the reports, the fly ash was leached/washed with water, followed by solvent extraction with catechol which resulted in a recovery of 85 % Ge in the fly ash sample (Arroyo Torralvo *et al*., 2010). Another study performed on gasification fly ash, extracted 84 % Ge by the initial washing of the ash with water (Font *et al*., 2005). Exceptional Ge recoveries of up to 98.3 % was obtained from coal fly ash water leachates and its subsequent separation and isolation using anion resin ion-exchange (Torralvo & Fernández-Pereira, 2011). González also reported the extraction of Ge from copper

smelting flue dust. The ash was leached with various chemical reagents such as sodium acetate, hydroxylamine hydrochloride, nitric acid/hydrogen peroxide, and the Ge was extracted with water and finally yielded between 97 % and 100 % Ge (González et al., 2017). In addition, the leaching of Ge from optical fibres reported that up to 99 % Ge was extracted by its leaching with H_2SO_4 followed by HF addition (Chen *et al.*, 2017). The recovery and reagents from these secondary sources are reviewed more in detail in **Chapter 3**.

2.4 Uses of Gallium and Germanium

2.4.1 Uses of Germanium

One of the main uses of germanium is in fibre optics (25 %), largely due to its ability to increase the refractive index of the optical fibre (see **Figure 2.5**) (Ruiz *et al*., 2018). Germanium is transparent to infrared light; hence it is also extensively used in infrared sensors used by aircrafts, ships, and military equipment and vehicles (Fink and Culver-Hopper, 1991; Nguyen and Lee, 2021). Once decommissioned, these objects become a great source of Ge bearing scrap that can or should be recycled and added to the value chain. The biggest producers of Ge are China (80 %) and Russia (5 %), as demonstrated in **Chapter 1**, **Figure 1.6** (European Commission, 2020) which is extensively used in their high-tech industries and sophisticated military machinery.

Germanium oxides are employed as catalysts in the manufacturing of PET plastic (Robertz *et al*., 2015),while about fifteen percent of the worldwide germanium are used in the manufacturing of solar panels. The metalloid is also resistant to deteriorating or corrosive environment conditions, including chemicals, moisture, and atmospheric oxidation (Patel & Karamalidis, 2021). In addition, germanium also serves as semiconductor in LED devices such as cameras, TV and smartphone screens (Patel & Karamalidis, 2021).

2.4.2 Uses of Gallium

Ga is extensively used in the defense, electronics, and renewable energy industries. Gallium based chips are utilized in military technology. GaAs is used in precision-guided weapons and radars (Funaiole *et al*., 2023). GaAs is also used as semiconductors and GaP is used in light-emitting and laser diodes (Maarefvand *et al*., 2020). In addition, gallium oxide (Ga_2O_3) has a large band gap of 4.7-4.9 eV and thus it is employed in electronic devices (Masataka Higashiwaki, 2014), as well as in electro-luminescence applications (Shi & Qiao, 2022).

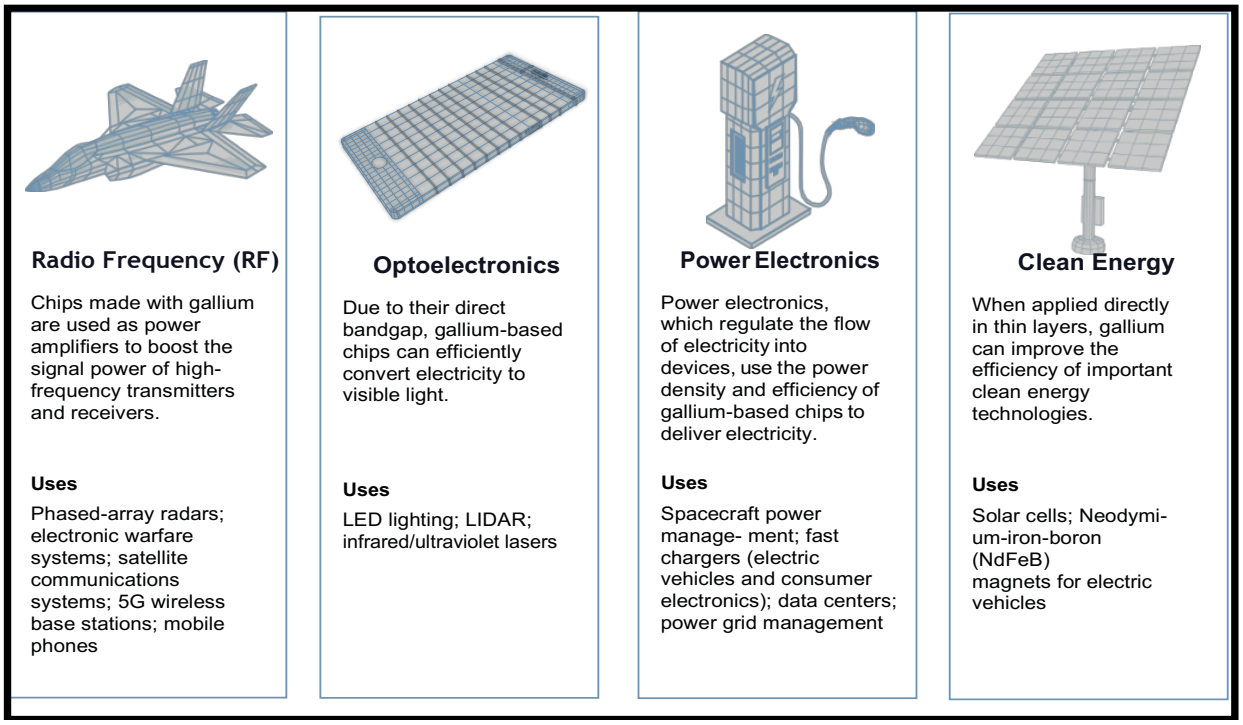

Figure 2.5: Main uses of gallium in industry (Funaiole *et al*., 2023).

Gallium semiconductors are used in the manufacturing of the products (**Figure 2.7**) such as photo detectors, computer memory devices, power electronics, and optoelectronics (Patel, 2021). Additionally, gallium halides are also used as Lewis's acid catalysts in organic synthesis to afford allylation, alkylation, radical reactions, and several coupling reactions due to its low ionization energy and their non-reactivity with acid-sensitive

groups during synthesis, as highlighted by Gupta and O'Sullivan (2013) (Hirashita *et al*., 2007).

Chapter 3 : Literature Review

3.1. Introduction

An evaluation of the hydrometallurgical extraction of gallium (Ga) and germanium (Ge) from primary and secondary sources will be given in this chapter. Some of the processes reviewed in this chapter are only applicable to the extraction of gallium or germanium individually, while others applied to both elements. Numerous review articles on the beneficiation of Ga and Ge resources as well as their extraction methods have been published (Torma and Jiang, 1991; Zhao *et al.*, 2012; Qin *et al.*, 2015; Lu *et al.*, 2017). However, these published articles predominantly focus on gallium and germanium recovery methods from natural resources. Bayer liquor and zinc residue were the main exploitable sources of gallium hence the sharp focus on developing and improving methods to recover gallium from those sources (Lu *et al*., 2017). In contrast, much fewer review articles were published on the recovery of gallium mine tailings (de Oliveira *et al*., 2021; Z. Liu & Li, 2015; Swami & Patel, 2021). Similarly, a high number of review papers have been published on recovery methods of germanium from its natural resources. Only recently research on recovery methods of Ge from waste material has gained momentum (Geng *et al*., 2022a, 2022b; Hoffmann, 1987; Höll *et al*., 2007; Meshram & Abhilash, 2022; Nguyen & Lee, 2021; Patel & Karamalidis, 2021; Robertz *et al*., 2015; Ruiz *et al*., 2018).

The natural sources of germanium and gallium are varied and diverse as discussed in **Chapter 2**. As a result, different processes were developed to concentrate and isolate these minerals (Dumortier *et al*., 2005). To date, the beneficiation of gallium and germanium from ores and scrap materials have yet to be sufficiently or extensively studied, despite the two metals demand and importance. As stated previously, Ga and Ge are included in the 2020 European Union (EU) Critical Raw Materials (CRM) list. This list (**Figure 1.1**) identified and prioritized raw materials that are of crucial importance to the EU and are at risk of supply disruptions (European Commission, 2020). Another aim of the CRM list is to stimulate research and innovation into recycling, as well as to find

alternatives or substitutes of these CRMs. Limited research has been conducted on the beneficiation of these critical elements from mine tailings, although the global volume of tailings is reported as significant, compared to that present in natural deposits (Ceniceros-Gómez *et al*., 2018; Jamieson *et al*., 2015). Edraki *et al*. (2014) estimates that about 1150 million tons of heavy metals have been mined since the inception of mining, and between 5 and 7 billion tons of mine tailings are annually produced globally. Mine tailings are composed of residual crushed rock (ranging from 1 to 600 micrometers in size) that remains after valuable the target elements at that stage, have been extracted from the ores (Ceniceros-Gómez *et al*., 2018).

Mine tailings have different characteristics to that of the virgin ores that were mined and processed, and in turn, require different extraction and separation techniques or processes to isolate the newly identified valuable materials. A well-known technique to access Ga and Ge from the ores is to use inorganic or mineral acids as leachant, but recent literature indicates that organic acids are becoming more popular than before as leachant. The solutions containing Ga and Ge can be complex and diverse due to the dissolution of other elements under the selected experimental conditions, which poses complex challenges to the isolation of these elements from the leachate. Special attention needs to be paid to the following factors, i) the composition of the mine tailings, ii) possible extraction methods and iii) reagents and chemicals needed for the beneficiation. Co-extraction of the non-target elements is one of the challenges faced in the recovery of these strategic elements, hence the need to not only know the composition of the tailings sample, but also the general inorganic chemistry of the target, as well as the non-target elements to successfully plan and execute a dissolution and separation process (Tao *et al*., 2021).

3.2. Beneficiation of gallium and germanium

3.2.1 Beneficiation of Germanium

The recovery of Ge from coal deposits and sulfide ores of Zn, Cu, and Pb is mainly through pyro– and hydrometallurgical processes (Ruiz et al., 2018). Numerous studies, although somewhat limited in scope, have been published on the recovery of Ge since its first isolation as germanium chloroform ($GeHCl_3$) and germanium tetrachloride ($GeCl_4$) with excess hydrochloric acid by Winkler in 1886 (Burdette & Thornton, 2018; Dennis & Hunter, 1929). The focus of Ge beneficiation has since moved to the extraction of the metalloid from secondary resources such as scrap material, which includes electronic waste, red mud, and mine tailings.

Melcher & Buchhilz, (2012) developed a germanium extraction method/process that can be applied to both Ge-containing ores and scrap material as depicted in **Figure 3.1** (Gunn, 2013). The only difference is that the Ge-containing ores undergo physical separation processes prior to the application of a common hydrometallurgical process. This process entails the chlorination of Ge in the samples to form $GeCl_4$, a compound extensively used in fiber optics. Subsequently, the $GeCl_4$ undergoes hydrolysis by the introduction of water to form GeO_2, a compound that is used as a PET catalyst. The GeO_2 can subsequently be reduced with hydrogen to form metallic Ge that is used in the production of different metal alloys such as Ge-Al, Ge-Si, Ge-Ga, etc., which are used as infrared lenses and solar cells. This is an elaborate process with different pathways to produce the three products that have important industrial applications (Ruiz *et al*., 2018).

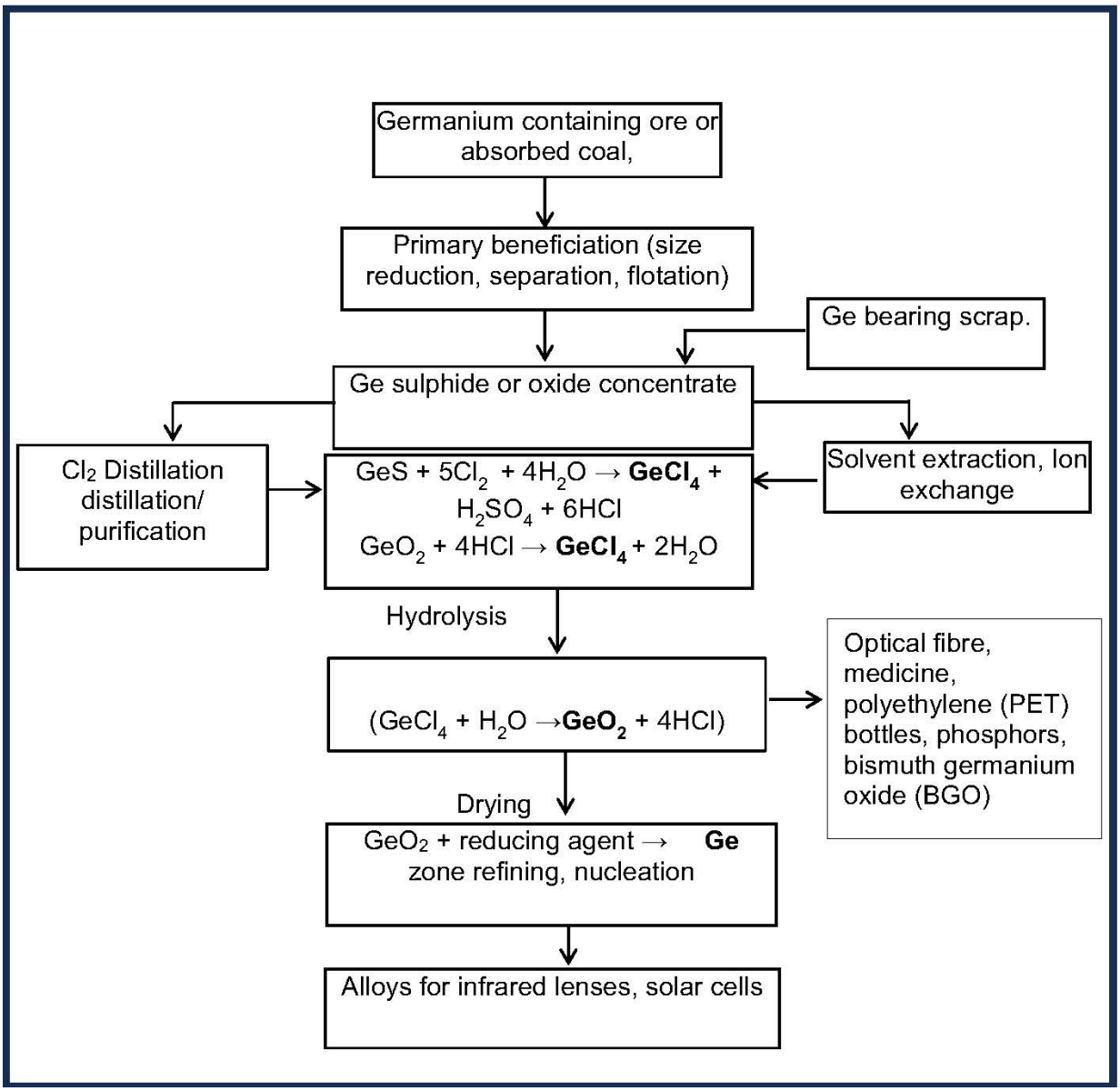

Figure 3.1: Processing of germanium resources to $GeCl_4$, GeO_2 and Ge metal adapted from Gunn (2013).

3.2.2 Beneficiation of Gallium

Gallium is usually produced as a by-product of aluminium processing from bauxite, processing of zinc ores, and coal fly ash. Bayer liquor is the largest natural resource for the production of gallium and four different methods have been employed in the separation of gallium from this source. These methods are solvent extraction, fractional

precipitation, electrochemical deposition, and ion-exchange (Zhuo Zhao, 2012). These methods are explained in detail in **Section 3.4**.

Approximately 70 % of gallium is usually recovered from the Bayer liquor while the remaining 30 % is lost as red mud (Bayer liquor waste), which is enriched in alumina, soda, and other rare metals (Zhuo Zhao, 2012). Several researchers have conducted research on the recovery of gallium from Bayer red mud. One such process is based on acidic leaching, followed by ion-exchange, and up to 97 % of the Ga present in the Bayer red mud was recovered (Lu *et al*., 2017). The researchers that developed this process investigated the following mineral acids for suitability as extracting reagents; HCl, H_2SO_4, and HNO_3. The Bayer red mud sample was leached with 4 M acid for 4 hours at 100 °C with a liquid-to-solid ratio of 8 mL/g. The extraction rate for HCl, H_2SO_4 and HNO_3 was 97 %, 90 %, and 78 % respectively. According to the authors, the observed low leaching efficiencies for sulfuric and nitric acids could be attributed to the large number of other sulfate and nitrate species present in the solutions that could potentially reduce the amount of gallium in H_2SO_4 and HNO_3 solution by precipitation or adsorption.

The isolation of gallium from an alternative source such as coal fly ash, will differ based on the type and origin of the coal of the fly ash. Coals of different origins differ in chemical composition, particle size, and major and trace elements. Hence the gallium content varies in coals from different locations. A study published by Fang and Gesser (1996) found that the gallium content of 13 different ashes sampled from various parts of the world ranged between 30 mg/g and 100 mg/g (**Table 3.1**).

Table 3.1: Ga content of fly ash from 13 different sources (Fang & Gesser, 1996).

Location	Ga content (ppm)
Ontario Hydro, Lakeview	64.3 ± 2.7
N.B Power, Dalhousie Generating Station	55.0 ± 4.2
N.B Power, Grand Lake Generating Station	86.8 ± 4.8
Saskatchewan Power, Popular River	112.0 ± 2.6
Saskatchewan Power, Shand	120.0 ± 0.6
Trasaita Utilities, Sundance, Alberta	104.0 ± 1.0
Trasaita Utilities Keephills Plant, Alberta	80.0 ± 4.7
Alberta Power Limited, Sheerness Generating Station	62.1 ± 3.5
Wabamun Generating Plant, Alberta	66.6 ± 3.7
Ontario Hydro, Nanticoke	56.5 ± 5.3
Manitoba Hydro, Brandon	64.6 ± 4.1
City Power, Changsha, P.R. China	37.5 ± 5.4
Hadera Power Plant Israel	60.0 ± 3.3

3.3 Leaching processes

3.3.2 Mineral acids

Germanium and gallium are recovered from different sources by leaching with acidic or alkaline solutions and a few reported cases where water was used as leachant. Acid and alkaline leaching of both germanium and gallium have been widely investigated and the type of leaching usually depends on the nature of the sample. Most of the published studies are skewed towards acid leaching with only a few on alkaline leaching.

Leaching with sulfuric acid, followed by solvent extraction was successfully applied to the recovery of germanium from processing residues. Wardell and Davidson (1987) studied the sulfuric acid extraction of gallium and germanium from zinc refinery residues. In this

study, 88.2 % of gallium and 57.3 % of germanium were extracted using 4 M H_2SO_4, at a temperature of 80 °C (Wardell & Davidson, 1987). In another study Harbuck *et al*., (1991) extracted and separated 95 % gallium and 73 % germanium from zinc tailings by using 2.9 M H_2SO_4 and 0.6 M H_2SO_4 respectively. The zinc residue sample was leached for 6 hours at 80 °C. Major drawbacks of sulfuric acid leaching are i) the co-extraction or dissolution of non-target elements and ii) the formation of silica gel which in turn results in a loss of Ga and Ge. To circumvent this silica gel formation problem, several researchers proposed various methods. Rao *et al*. (2019) proposed an alkaline leaching process for zinc tailings. The authors reported that Si and Ge exist in stable forms of $SiO_3(OH)^{3-}$ and $HGeO_3^-$ in solutions of pH higher than 12. Furthermore, it was reported that the two complexes can be separated by adjusting the pH of the solution. Harbuck (1993) on the other hand recommended the use of hydrofluoric acid (HF) as a supplementing agent to dissolve SiO_2 and subsequently release Ge from the SiO_2-GeO_2 complex (Rao *et al*., 2019). In this study, a zinc residue sample that remained from prior H_2SO_4 leaching was treated with 11 M HF for 2 hours at 80 °C. Germanium extraction in this process increased from 70 % to above 90 %. In another study conducted by Wen *et al*. (2018), a mixture of H_2SO_4 and HF was employed to extract Ga from a silica-rich copper flue dust sample. In this study 91 % Ga was leached using a mixture of H_2SO_4 and HF as compared with only 38 % Ga leached when only H_2SO_4 was used. Similarly, as with released Ge from the SiO_2-GeO_2, HF dissolves SiO_2 resulting in the liberation of Ga from the SiO_2-Ga complex. The optimal experimental conditions were 1.5 M H_2SO_4 and 6.4 M HF, a leaching time of 4 hours, a temperature of 80 °C and with a liquid-to-solid ratio of 5:1 mL/g.

Another alternative suggested by Liu *et al*. (2016) involves the pressure acid leaching of a zinc refinery residue and found a significant decrease in Ge recovery losses (as a result of SiO_2-GeO_2 complex formation) which they attributed to SiO_2 aggregation. The zinc residue was leached with 1.5 M H_2SO_4 for 3 hours at 150 °C and a total pressure of 0.40 MPa. Under these conditions, 98 % of Ge was successfully leached.

Hydrochloric acid has also been investigated as leachant for the extraction of gallium and germanium. A process was developed by Fang & Gesser (1996) to extract Ga from coal fly ash. The sample was initially roasted at 500 °C for 10 hours, followed by its leaching with 2 M HCl at room temperature. The liquid-to-solid ratio was 6:1 and 95 % gallium was recovered. In a study by Gutiérrez et al (1997), HCl was also used to extract gallium from fly ash. The sample was leached with 6 M HCl, and 83 % Ga was extracted.

Other studies revealed that nitric and hydrochloric acids were more efficient than sulfuric acid in the leaching of gallium from gallium arsenide (GaAs) scrap. A study by Chen *et al*. (2011) indicated the complete leaching of gallium is possible from GaAs scrap with 4 N HNO_3 at room temperature, stirred for 1 hour with a liquid-to-solid ratio of 100 mL: 3 g. In a study with different Ga-bearing material to that used in the study published by Chen *et al*. (2011), Pourrahim *et al.* (2017) obtained results that indicated that the dissolution of gallium from zinc oxide was superior in hydrochloric acid compared to that obtained using sulfuric or nitric acid. A leaching percentage of 91.3 % in hydrochloric acid was obtained compared to 86.7 % with sulfuric acid and 83.4 % with nitric acid. The reactions were carried out at 90 °C and leached for four hours at 600 rpm at a leachate concentration of 6 M (Pourrahim *et al*., 2017). Another study that also demonstrated the superiority of HCl in the leaching of Ga, 100 % Ga was extracted from a mine tailings sample (Macías-Macías *et al*., 2019). The iron tailings sample was leached with 8 M HCl for 48 hours. This study is one of a few studies in which gallium is extracted and recovered from mine tailings. Further details and a schematic diagram of the proposed process are provided in **Section 3.4.1**

The challenge of non-target elements co-extraction mentioned in **Section 3.1,** was investigated by several researchers using selective extraction of the two elements from leach liquors (Arrambide Cruz *et al*., 2018; Rao *et al*., 2019). An elaborate stepwise leaching process of Ga, Ge, Zn, and Pb from a zinc refinery residue is illustrated in **Figure 3.2**. In this process, leaching with 2 M sulfuric acid, at 80 °C for 2 hours, with a liquid-to-solid ratio of 10 mL:g dissolved 99 % of Ga and 90 % of Zn while 92 % of Ge remained in the residue (Rao *et al*., 2019). The Ge that remained in the residue was subsequently

leached with 1 M NaOH for 2 hours at 80 °C, with a liquid-to-solid ratio of 20 mL:g. During this step, 90 % of Ge was successfully extracted

.

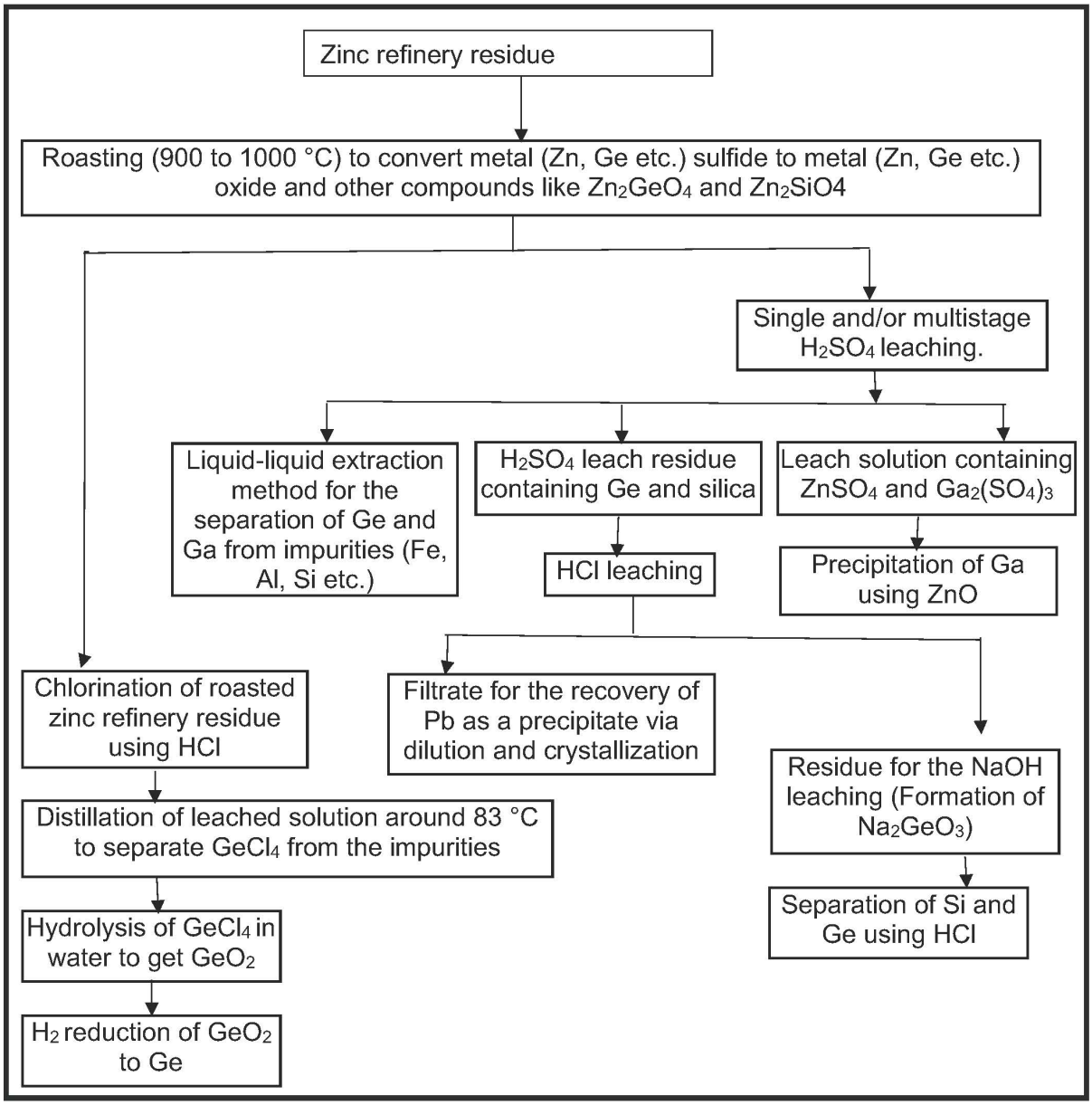

Figure 3.2: Production of germanium and gallium metals from zinc refinery waste (RAO *et al*., 2021).

3.3.2 Organic acids

A number of studies reported the use of organic acids for the leaching of germanium. Liu *et al*. (2017) used a two-step leaching process that extracted 96 % Ga and 99 % Ge. In

the initial step of this process, 0.6 M H_2SO_4, leached 92 % of Zn and 94 % of Cu at 60 °C, with a liquid-to-solid ratio of 10:1 and a leaching time of 2 hours. Finally, 0.8 M $H_2C_2O_4$ was used to extract Ga and Ge. The optimal second step leaching experimental conditions were the leaching at 90 °C for 2 hours with a liquid-to-solid ratio of 10 mL:g. Tannic acid (0.001) M was then added, and an insoluble Ge precipitate was isolated. This study was published in two parts; part 1 (described above) only dealt with the leaching of the elements while part two dealt with the subsequent isolation thereof which is discussed in **Section 3.4.1**

Oxidative leaching, using a combination of an oxidizing agent in conjunction with an acid, has also been reported. An oxalic acid and hydrogen peroxide extraction process to recover gallium and germanium from zinc residues was developed by Liu *et al*., (2017c). This process selectively extracted gallium and germanium at 99.3 % and 98.9 % respectively from the zinc processing residue which contained Zn, Fe, Cu, Ga, and Ge. The recovery of the non-target elements was much less, with 30.3 % of Fe, 0.3 % of Zn, 0.8 % of Cu, and 0.4 % of Si recovered with the same process. The optimal experimental conditions for this process were as follows: 1 M $H_2C_2O_4$ with a liquid-to-solid ratio of 8 mL: g leached at 40 °C for 30 minutes. The Fe in this residue was removed as $FeC_2O_4.2H_2O$ during a subsequent purification step using an ultrasound-aided Fe powder precipitation method, which resulted in the loss of only 1 % of gallium and germanium. The experimental parameters for the iron removal process were as follows: ultrasound (200 W) for 15 minutes, Fe/Fe^{3+} mole ratio 1:7, and temperature of 30 - 70 °C (Liu *et a*l., 2017c). **Figure 3.3** outlines the process described above.

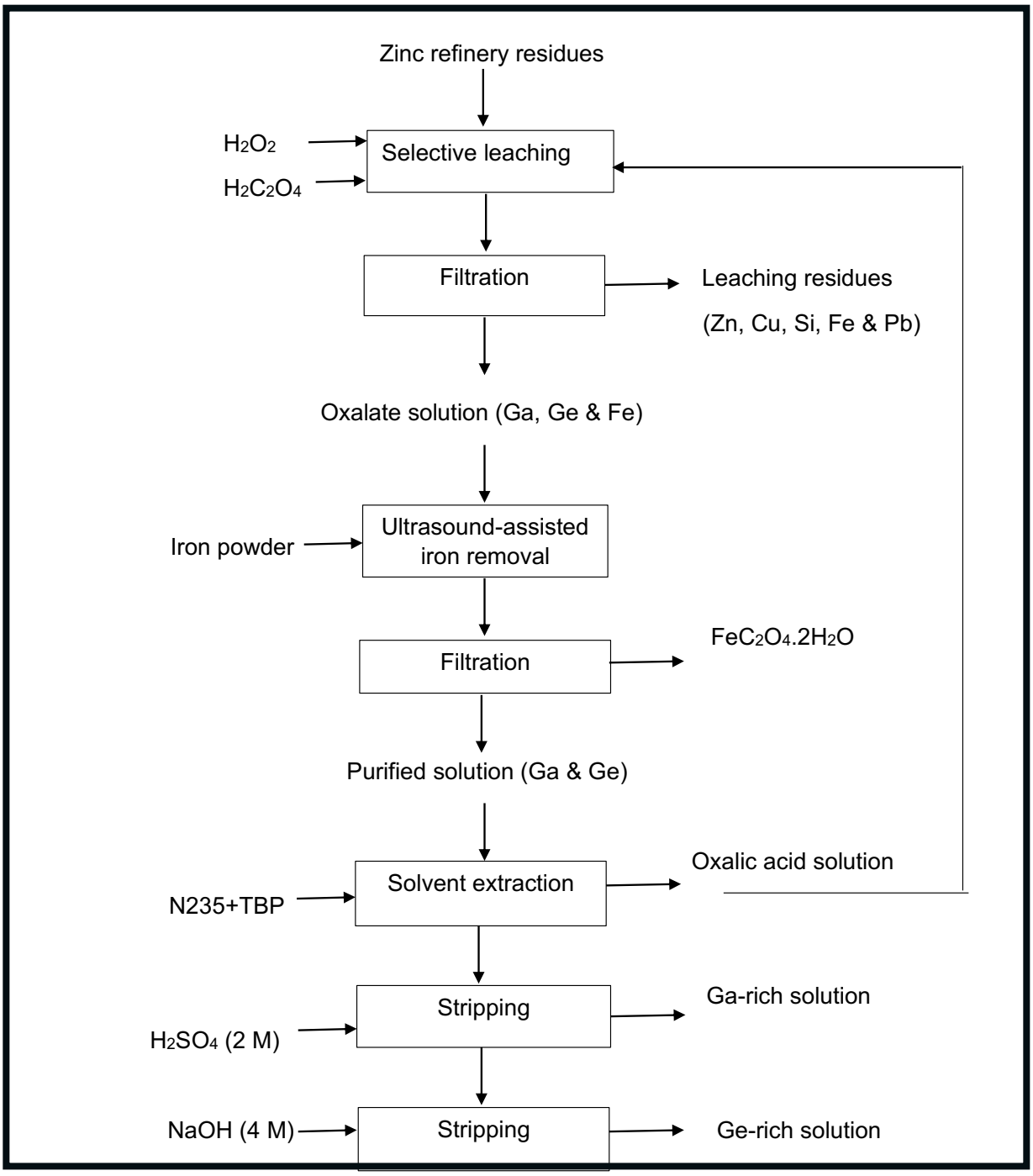

Figure 3.3: Flow diagram for the oxalic acid and hydrogen peroxide extraction of Ga and Ge from zinc refinery residues (Liu *et al*., 2017c).

In a comparative study by Drzazga *et al*. (2018), the leaching efficiencies of Ge using H_2SO_4 and $H_2C_2O_4$ were investigated. In this study, 85 % of Ge was leached from 'Dros' (a zinc metallurgy by-product) using 3 M H_2SO_4 while only 80 % of Ge was leached using 3 M $H_2C_2O_4$. These results indicate that leaching with sulfuric acid is more effective than

leaching with oxalic acid under the following optimal experimental conditions: a leaching time of 3 hours at 80 °C with a liquid-to-solid ratio of 10 mL:g.

Furthermore, oxalic acid has also been investigated for the leaching of Ga and Ge from coal sources as well as from zinc processing residues (Arroyo *et al*., 2014). Besides oxalic acid leaching of Ge, leaching of Ge with citric acid and acetic acid has also been reported. Rezaei *et al*. (2022) investigated the use of citric acid as a sustainable process to extract Ge, V, and Li from coal fly ash. In this process (depicted in **Figure 3.4**) 0.5 M citric acid was used and 98 % of Ge, 75 % of V, and 97 % of Li was leached from coal fly ash after roasting with Na_2CO_3.The optimal experimental conditions were as follows: a leaching temperature of 30 °C, a leaching time of 1 hour, and a sample-to-Na_2CO_3 ratio of 1:0.5.

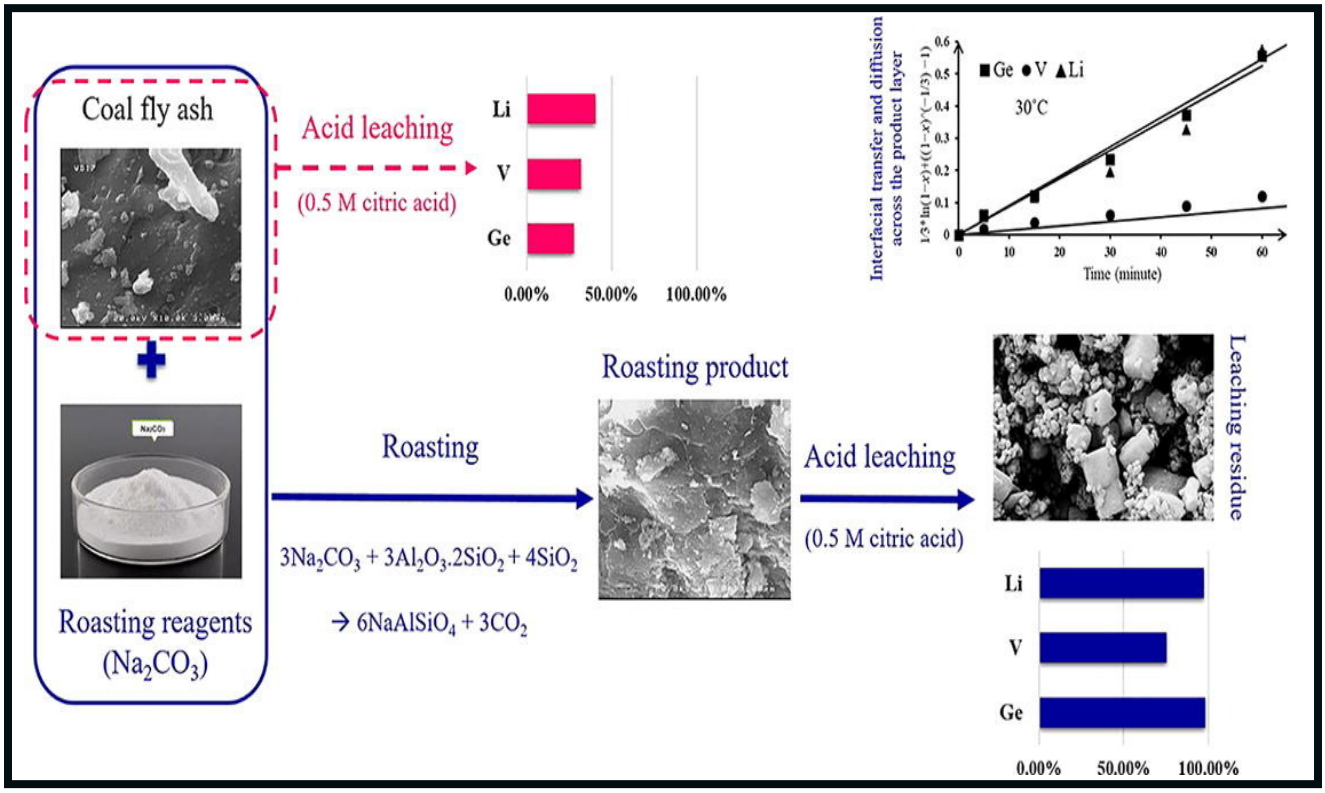

Figure 3.4: Graphical abstract of the proposed citric acid leaching process (Rezaei *et al*., 2022).

Zhou *et al*. (2019) reported an exceptional leaching efficiency from E-waste, using oxalic compared to hydrochloric acid and citric acid. With the aid of oxalic acid, 90 % Ga was leached compared to 80 % in hydrochloric acid and 71 % in citric acid. The optimal

experimental conditions were as follows: 0.7 M acid, with a pulp density of 10 g: L, leaching at 90 °C for 1 hour.

Rafiee *et al*. (2021) investigated the use of acetic acid to recover Ge from E-waste. In this study, 70 % of Ge was leached from diode waste samples using 2.5 M acetic acid at 90 °C after a leaching time of 4 hours. A graphical abstract of this process is provided in **Figure 3.5.**

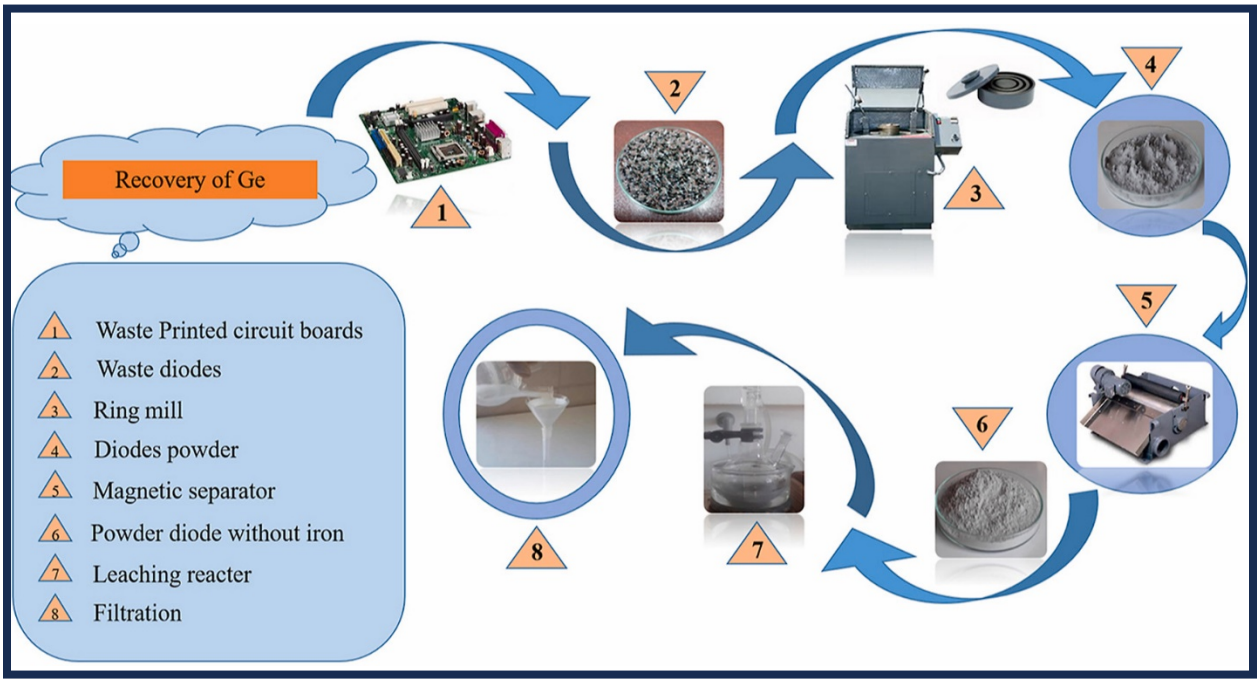

Figure 3.5: Graphical abstract of the proposed acetic acid leaching of E-Waste process (Rafiee *et al*., 2021).

Novel leaching methods

In addition to mineral acids, organic acids, and alkaline leaching, unconventional or novel leaching processes have also been reported. In one study, a regular HCl-$CaCl_2$ leaching of germanium assisted with $Ca(ClO)_2$ as oxidant, was compared with an ultrasonic-assisted HCl-$CaCl_2$ leaching process. The ultrasonic-assisted leaching recovered 92.7 % of germanium, while the regular leaching yielded 88.4% of germanium. The leaching efficiency of ultrasonic assisted resulted in a 4 % increase in Ge recovery compared to the non-ultrasonic aided leaching. In addition to that, the leaching time of the ultrasonic-assisted leaching was 40 minutes while regular or non-ultrasonic leaching was 100

minutes. The rest of the optimal experimental conditions were the same: 3.5 M HCl, 1.4 M $CaCl_2$, 58.33 g/L $Ca(ClO)_2$, and a reaction temperature of 80 °C. Zhang *et al.*(2016) question whether the additional energy input costs (700 watts of power employed in the ultrasonic-assisted leaching) were worth the additional 4% recovery improvement increment.

Xu *et al*. (2023) proposed an ultrasonic-enhanced hydrazine sulfate reduction process for the leaching of germanium from Ge bearing zinc oxide dust. In this novel process, Ge was extracted with H_2SO_4 and $N_2H_4.H_2SO_4$ (hydrazine) as reductant, from the zinc oxide dust sample as Ge^{2+} and 97 % Ge was leached. The hydrazine was used to reduce Ge^{4+} to Ge^{2+} to avoid the precipitation of Ge during the leaching process. The optimal experimental conditions of this process were as follows: 1 M H_2SO_4, with a liquid-to-solid ratio of 7 mL: g, leached at 60 °C for 1 hour aided with an ultrasonic power of 300 W. The novel process is illustrated in **Figure 3.6**.

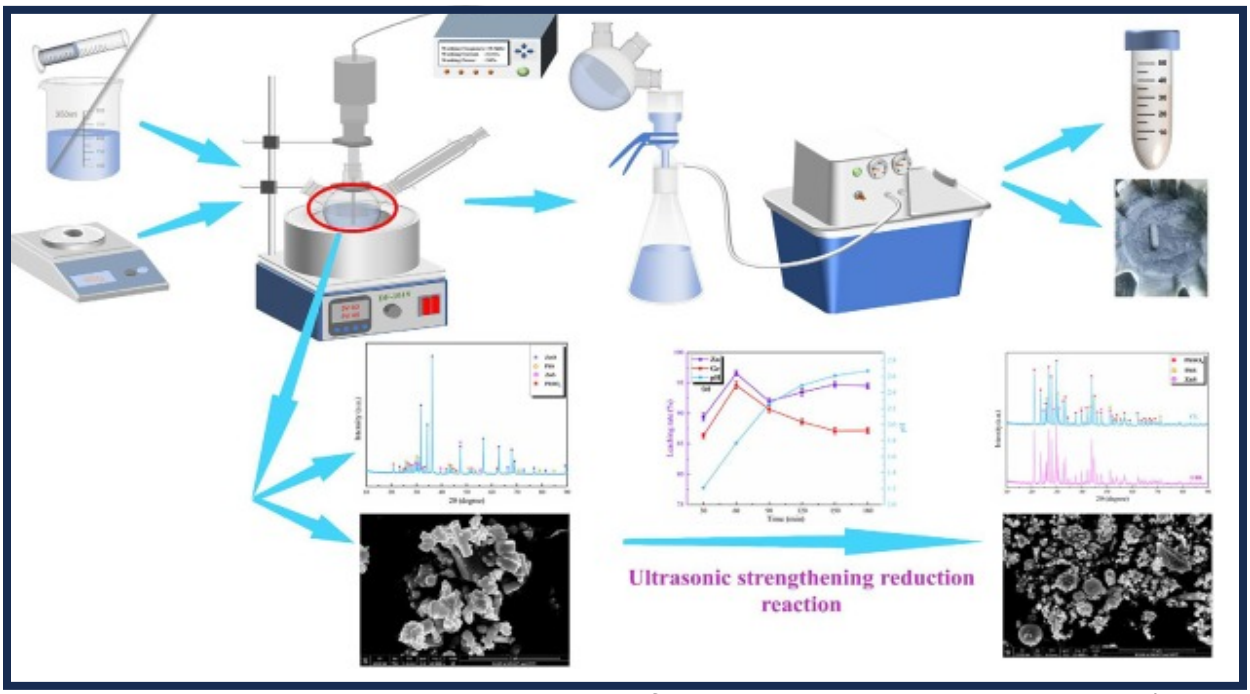

Figure 3.6: Ultrasonic enhanced hydrazine sulfate leaching process proposed by (Xu *et al*., 2023).

In another study published by Li *et al*., (2022) , gallium and indium were selectively leached from a secondary waste source which originated from a copper/indium/gallium/diselenide (CIGS) product, which is used as a thin film solar cell in industry. This study was a follow-up to a previous study in which copper and selenium were successfully separated from CIGS leaving behind a residue containing indium gallium oxide (IGO) (Lv *et al*., 2019; Ma *et al*., 2020). The selective leaching in an alkali medium obtained 97.3 % of gallium under the following optimal conditions: 7 M NaOH, solution for period of 3 hours at 60 °C (X. Li *et al*., 2022). A graphical abstract of the process is shown in **Figure 3.7**, in which Ga_2O_3 and In_2O_3 are leached from $InGaO_3$.

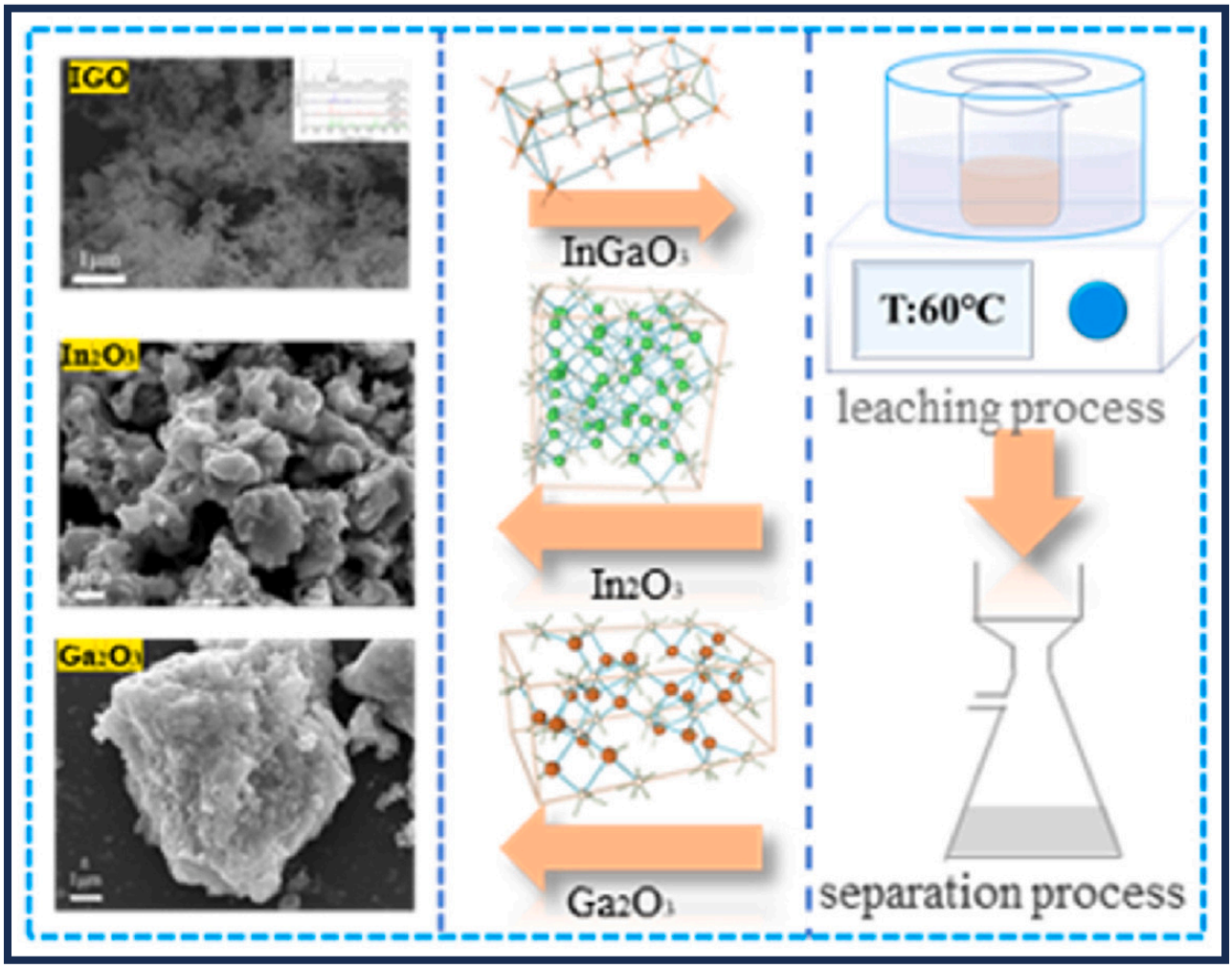

Figure 3.7: Graphical presentation of the Ga alkaline leaching process from CIGS (Li *et al.*, 2022).

Water as leaching agent

Although leaching of Ga and Ge with water has been reported, low leaching yields were observed. Arroyo *et al*. (2014) reported 22 % Ge leaching from coal fly ash, the same sample was leached with oxalic acid and the leaching rate increased up to 65 %. For these yields, the leaching time using water was 24 hours, compared to the leaching time of 2 hours using oxalic acid. Optimal experimental conditions were as follows: water and 0.16 M $H_2C_2O_4$ leached at 50 °C with a liquid-to-solid ratio of 5: 1 (mL/g).

3.4 Separation Techniques

After solubilizing germanium and /or gallium in an aqueous medium, solvent extraction, precipitation, and ion-exchange is used to either separate or isolate the elements in question. From the above-mentioned separation processes, solvent extraction is the method that has been most extensively used in the recovery of germanium while ion-exchange has widely found its application in the recovery of gallium.

3.4.1 Separation /isolation of Ga and Ge using solvent extraction

In a review paper published by Tao *et al*. (2021) they reported that solvent extraction is highly selective and efficient in the extraction of germanium. Using different extractants, such as 1) chelating extractants, 2) basic extractants, 3) acidic extractants, and 4) neutral extractants, the researchers were able to extract more than 90 % of gallium from the samples that they investigated. Chelating extractants include oximes, extractants that have ═N–OH and O═C(R)–NH-OH as active groups, hydroxamic acid and quinolines. Examples of chelating extractants include Lix 63, 7815, G315, Kelex 100, N601 and N604. Basic extractants include Alamine 336, Adogen 364, HOSTAREXA–327 and N235, while acidic extractants include D2EHPA, P204, Ionquest and Cyanex 301. Lastly, neutral extracts include the Cyanex 923 and MIBK. It is reported that the characteristics (physical and chemical) and the price of an extractant seriously influence the selection of that extractant (Tao *et al*., 2021).

One notable industrial available chelating agent 7-(4-ethyl-1-methyloctyl)-8-hydroxyquinoline (Kelex 100), was used in the selective extraction of gallium from alumina solutions (Pesic & Zhou, 1988). The optimal experimental conditions were as follows: 8 % (v/v) Kelex 100, 10 % (v/v) decanol, 82 % (v/v) Kermac 470B, 5.6 M NaOH, and at a temperature of 40 °C. This method recovered 80 % gallium.

In the second part 2 of the study mentioned in **Section 3.3,** Liu *et al*. (2017a) reported a two-step H_2SO_4 and $H_2C_2O_4$ leaching process that was used to separately leach Zn, Cu and Ga, Ge. The researchers (Liu *et al*., 2017b) used solvent extraction to recover 99 % Ga and 100 % Ge from the oxalic acid leach solution. They used a 20 % (v/v) tri(octyl-decyl) amine (N235), 10 % (v/v) tributyl phosphate (TBP) in 70 % (v/v) sulfonated kerosene to extract Ga and Ge from the leach solution. The optimal conditions for the selective stripping of Ga from the organic phase were 2 M H_2SO_4 at 30 °C for 15 minutes with A/O ratio of 1:2. The optimal conditions for the Ge stripping were 4 M NaOH at 40 °C for 15 minutes with an A/O ratio of 1:3. A flow diagram of the above process is displayed in **Figure 3.8.**

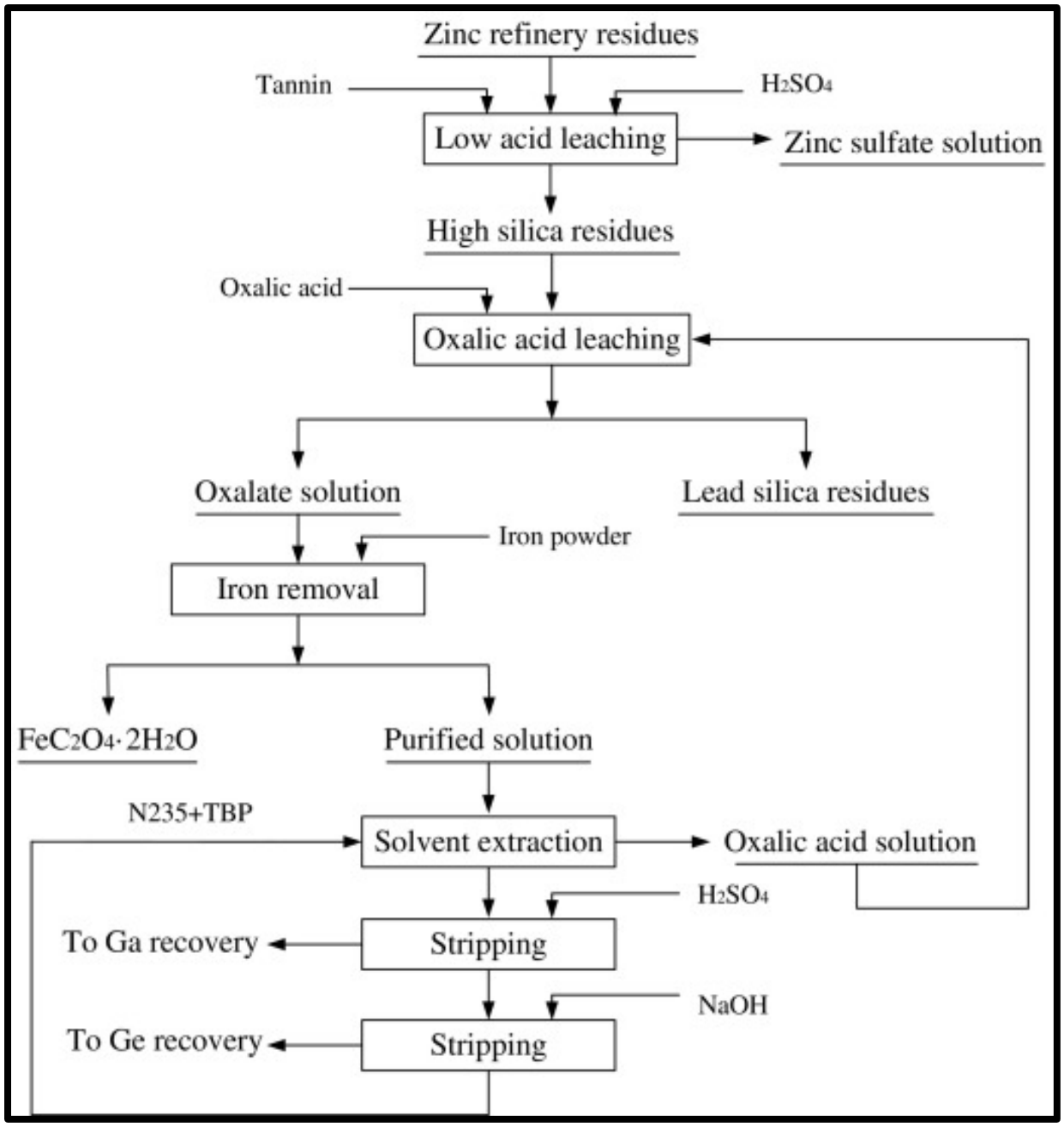

Figure 3.8: Solvent extraction of Ga & Ge from oxalic acid leach solution (Liu *et al*., 2017b).

Nayak and Devi (2017) developed an extraction process that recovered 99.8 % gallium from E-Waste (photodiodes). The researchers used 0.005 M cyphos IL 101 (trihexyl(tetradecyl) phosphonium chloride) in kerosene as an extractant in the presence

of 2 M HCl solutions. This extractant combination of cyphos IL 104 and HCl was also employed by Cieszynska and Wiśniewski (2012) for the extraction of Pd(II) and Cd(II) in hydrochloric acid solutions.

In another study 100 % Ga was extracted from hydrochloric acid solutions, using tributylphosphate (TBP) in benzene (Macías-Macías *et al*., 2019). As mentioned in the **Section 3.3**, 8 M HCl was used to leach 100 % Ga from an iron tailings sample. The optimal experimental conditions for this process included 10 % (v/v) TBP in benzene, an aqueous-organic phase ratio of 1:1, and a 0.1 M H_2SO_4 stripping agent. This process is illustrated in a flow diagram in **Figure 3.9**

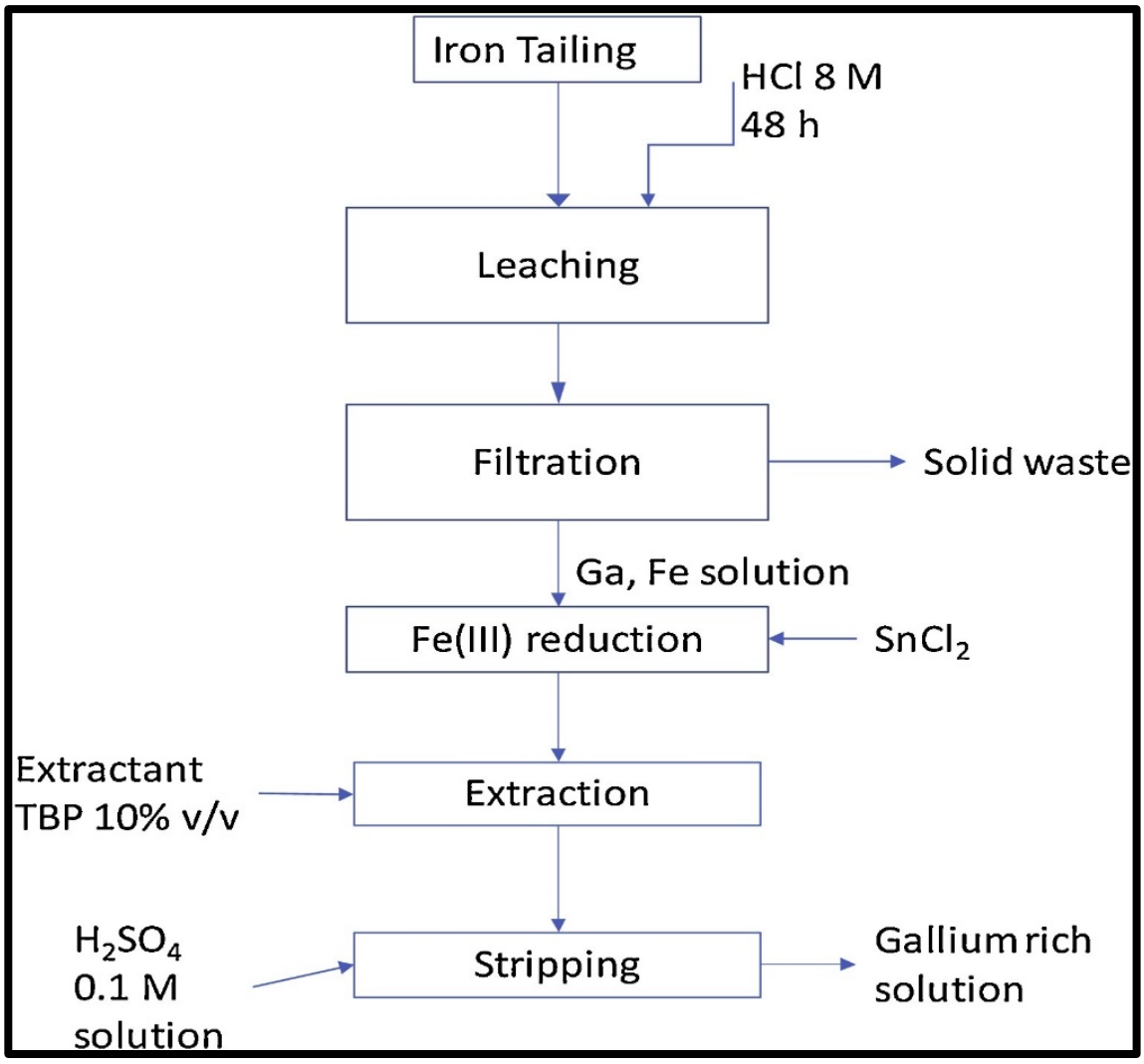

Figure 3.9: Extraction of gallium from iron tailings process (Macías-Macías *et al*., 2019).

Ma *et al*. (2013) also investigated the extraction of germanium from sulfuric acid solutions using solvent extraction. In this study, di-(2-ethylhexyl) phosphoric acid (P204) was utilized as an extractant and tributyl phosphate (TBP) as a modifier and obtained a recovery of 94.3 % germanium. The optimum extractant concentration was 30 % (v/v) D2EHPA with 15 % v/v) TBP. Stripping was carried out with 6.25 M NaOH, and the A/O phase ratio was 2:1.

A novel extraction process that used a phosphate ester (H_2R) as an extractant, was developed by Zhang *et al*. (2019) to extract Ga from zinc refinery residues. This method selectively extractant extracted 98.5 % Ga in a strong sulfate solution which also contained Ge, Zn, and Cu. The authors then also compared the extraction efficiency of this H_2R ester with that of two others widely used phosphate ester extractants, namely P507 (2-ethylhexylhydro-2-ethylhexylphosphonate) and P204 (di-2-ethylhexylphosphoric acid). The Ga extraction efficiency with the H_2R ester proved to be superior to that of P507 and P204 in strongly sulfuric and hydrochloric solutions (Zhang *et al*., 2019). The gallium extraction using P507, P204, and H_2R was 100 % from low-concentration sulfuric acid solutions. However increased H_2SO_4 concentrations (20 g/L) caused the percentage Ga extractions to decrease sharply below 50 % using P507 and P204, while the percentage Ga extracted using H_2R remained above 90 %. The optimal experimental conditions for this process were: 2 M H_2SO_4 that was used for stripping Ga from the organic phase, 40 % (v/v) H_2R in sulfonated kerosene with an A/O phase ratio of 1:1. The molecular structure of the phosphate ester is presented in **Figure 3.10**.

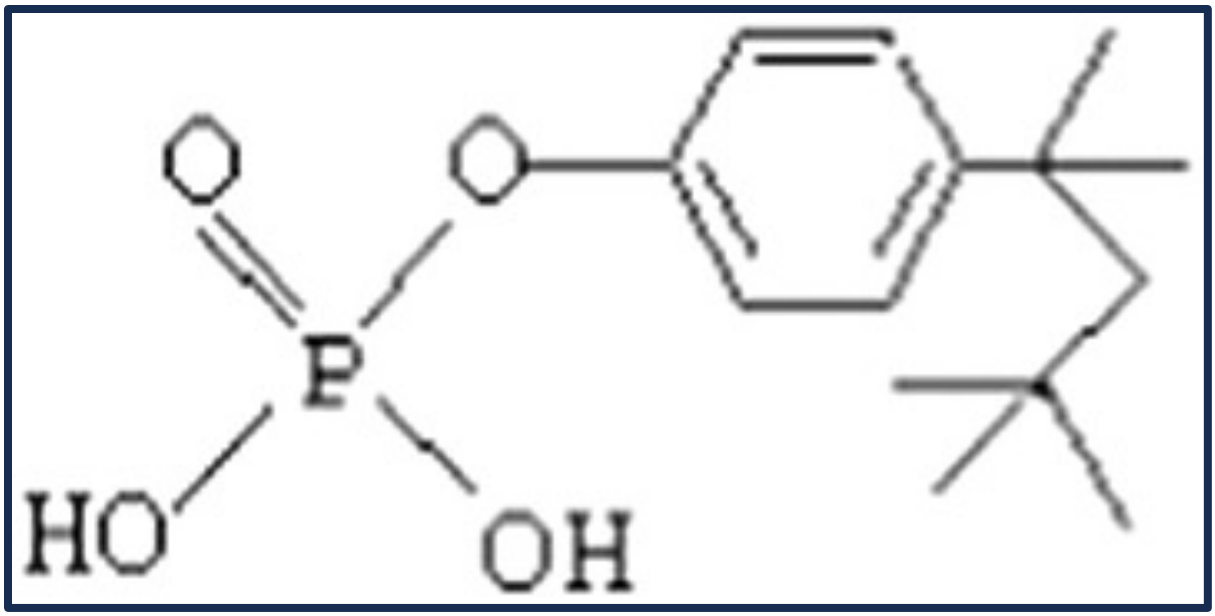

Figure 3.10: Molecular Structure of novel H_2R phosphate ester employed by Zhang *et al.*, (2019).

The comparative results of H_2R, P204 and P507 are illustrated in **Figure 3.11**. The increase in H_2SO_4 concentration resulted in a sharp decrease in the extracted Ga in P507 and P204 extracting systems. On the other hand, a slow and steady decrease in gallium extraction is observed for H_2R as the H_2SO_4 concentration is increased. Both P507 and P204 are alkyl phosphate esters and esterification will result in product formation containing alkyl groups which are now weakly electrophilic and cannot yield enough protons to exchange with the gallium ions. On the contrary, the phenyl group in H_2R triggers stronger electrophilicity in the extractant. Unlike P507 and P204, H_2R is synthesized by the esterification of phosphorus pentoxide and phenol (rather than alcohol) producing an organic solvent less prone to esterification (Zhang *et al*., 2019).

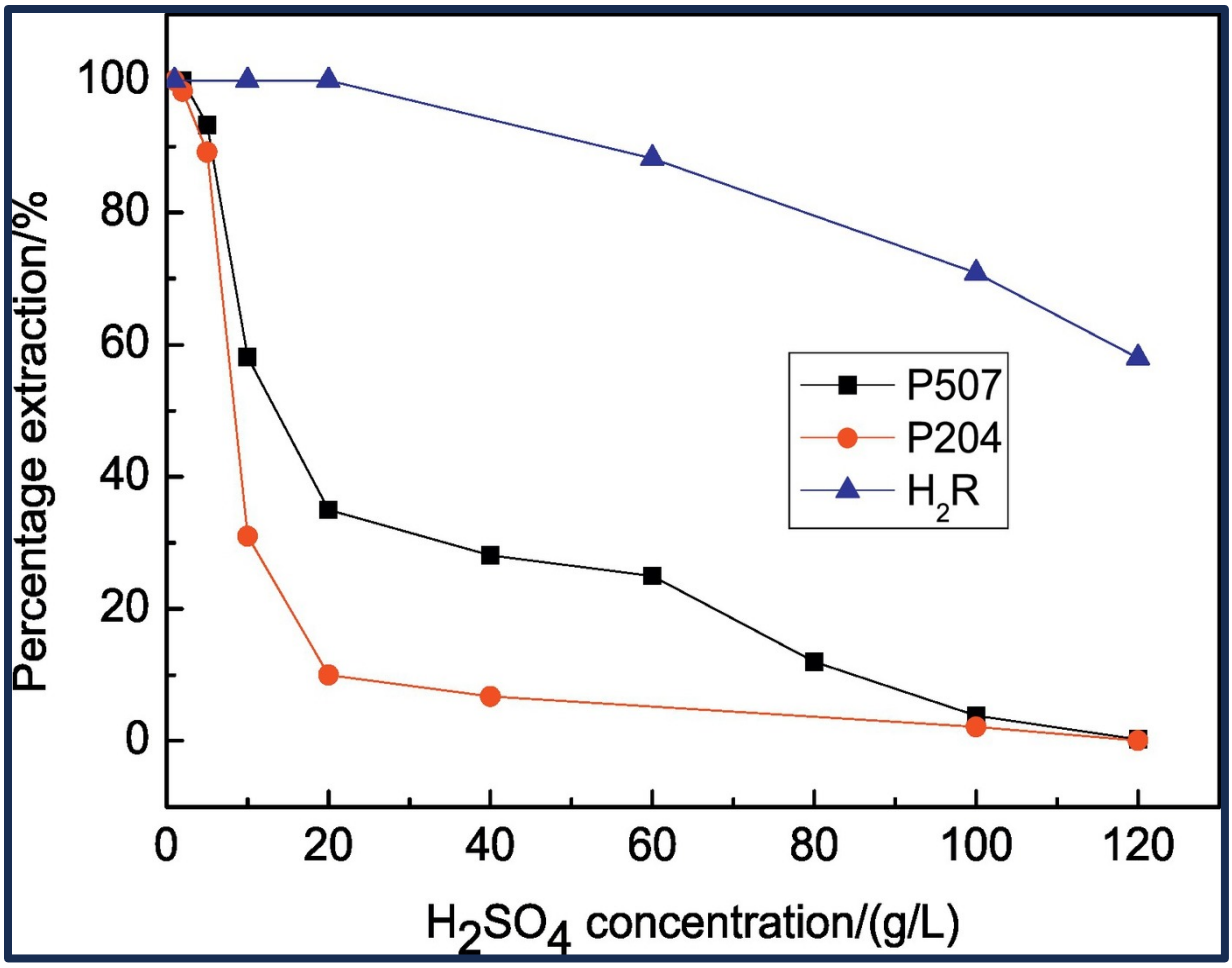

Figure 3.11: Comparison of Ga extraction efficiency of H_2R, P507, and P204 at increasing leaching acid concentration (Zhang *et al*., 2019).

Another study reported a 92 % extraction of gallium in the presence of Zn and Cu, using Cyanex 923 (a mixture of four trialkyl phosphine oxides) and Cyanex 925 (bis(2,4,4-trimethylpentyl) octyl phosphine oxide) as extractants (Ahmed *et al*., 2013). The optimal experimental conditions and the proposed flow chart illustrating the sequential extraction of Ga, Zn and Cu is depicted in **Figure 3.12.**

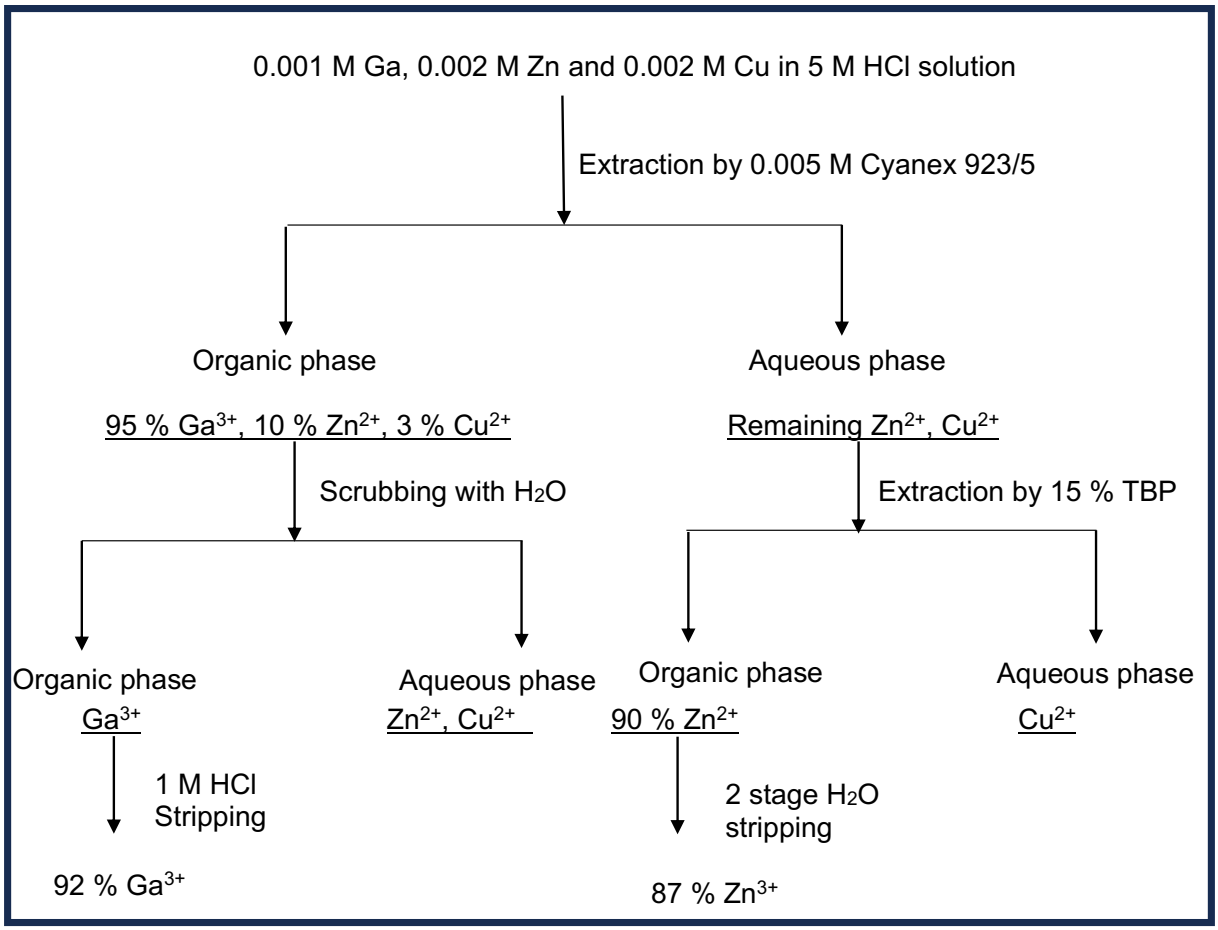

Figure 3.12: Sequential extraction of Ga, Zn and Cu using Cyanex 923/5 (Ahmed *et al*., 2013).

3.4.2 Separation of Ga and Ge using ion exchange

Gallium

Several processes have been developed for the separation and isolation of gallium with ion exchange from gallium scrap and Bayer process waste. In the published studies, gallium and germanium are either complexed with anionic ligands or chelating agents resulting in an anionic complex that binds with resins through ionic interactions, or alternatively, the complexing agent is chelated onto the resin, and the Ga and Ge ions interact with anionic groups on the resin.

A hydroxamic acid-containing resin was utilized by Rao *et al*. (2003) to selectively separate gallium from aluminium, while also minimizing the co-extraction of vanadium in

a Bayer liquor. The researchers synthesized the resin by chelating a hydrolyzed polymer with a mixture of sodium acetate, sodium hydroxide and hydroxylammonium chloride. The optimal experimental conditions for this process were: 6.25 M NaOH leachant, 1.5 M HCl (eluent), 20 mL resin with a solution-to-resin ratio of 50:1. At 1.5 M HCl, 100 % of Ga and 0 % of V was eluted only at 20 M NaOH. The recovery of V was 24 % V and 0 % Ga eluted under these extreme conditions.

Cheng *et al*. (2019) proposed a leaching process, combined with an ion-exchange separation step to recover Ga from gallium arsenide scrap. In this process, the GaAs scrap was leached with 2 N nitric acid at 30 °C for 1 hour. The leaching was followed by separation with a Diaion CR-11 resin. The Ga was eluded with 0.1 M sulfuric acid and the process recovered 99.3 % of Ga in the sample (Cheng *et al*., 2019).

Gallium was also recovered from Bayer red mud using a so-called 'acidic-leaching ion exchange" process from (Lu *et al*., 2018). The described process involved three steps and just like its name indicates, the sample was initially leached with mineral acid, followed by the removal of impurities, and then finally its separation using the ion exchange. The leaching of the Bayer red mud was carried out with 4 M HCl, with a liquid-to-solid ratio of 8 mL:g, leached at 55 °C for 5 hours. Gallium was successfully recovered with an efficiency of 95 % from this Bayer red mud. Fe^{3+} as an impurity was removed with a 0.6 g/mL LSD-396 resin. Finally, the gallium was recovered utilizing LSC-500S resin. The resulting Ga adsorption and desorption rates were 60 % and 95 % respectively. The proposed mechanism of the adsorption of Ga^{3+} is indicated in **Figure 3.13.**

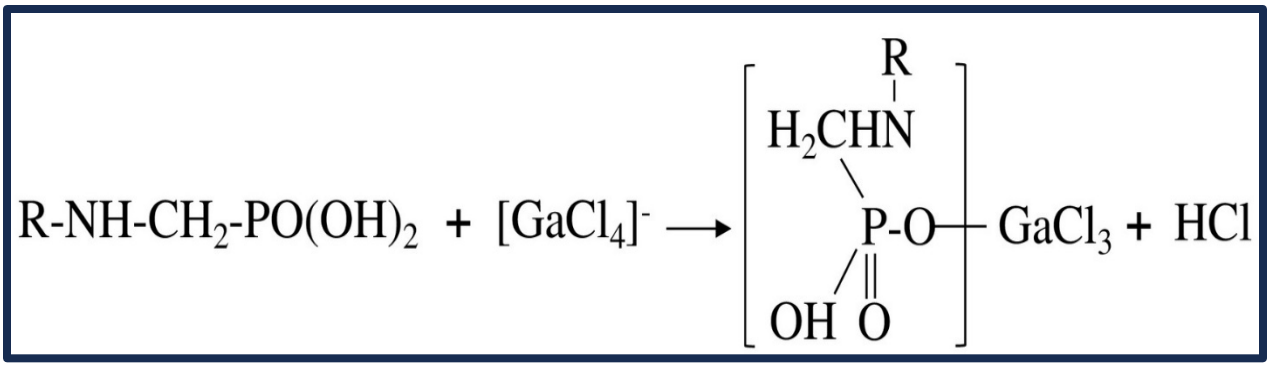

Figure 3.13: Proposed mechanism of Ga adsorption onto LSC-500S resin (Lu *et al*., 2018).

The Guizhou branch of the Aluminium Corp of China (Chalco) also employs ion-exchange to recover Ga from Bayer liquor (Lu *et al*., 2017). The mechanism for the adsorption of Ga is depicted in **Figure 3.14** while **Figure 3.15** indicates the process the company developed. The optimal experimental conditions for the process were 16 h for elution, at 45 - 50 °C, 6 M H_2SO_4 for desorption or elution. A Ga product was precipitated with 10 M NaOH, and a resin dosage 8 g/L was maintained during the separation process.

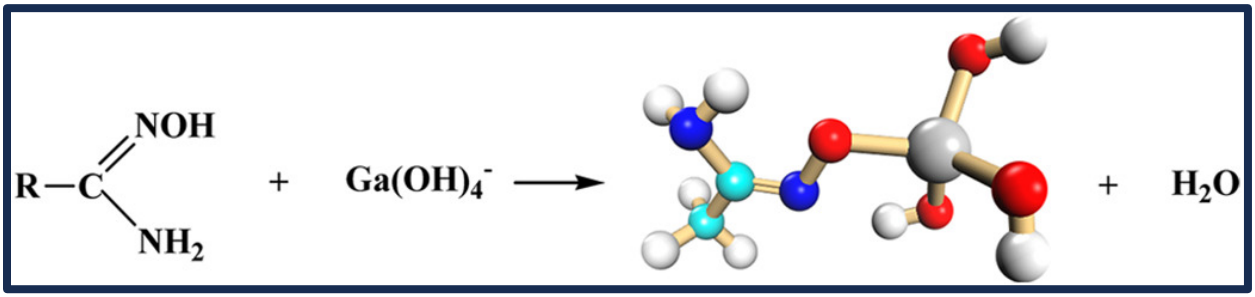

Figure 3.14: Adsorption mechanism schematic diagram of Ga onto LSC-600 (Lu *et al*., 2017).

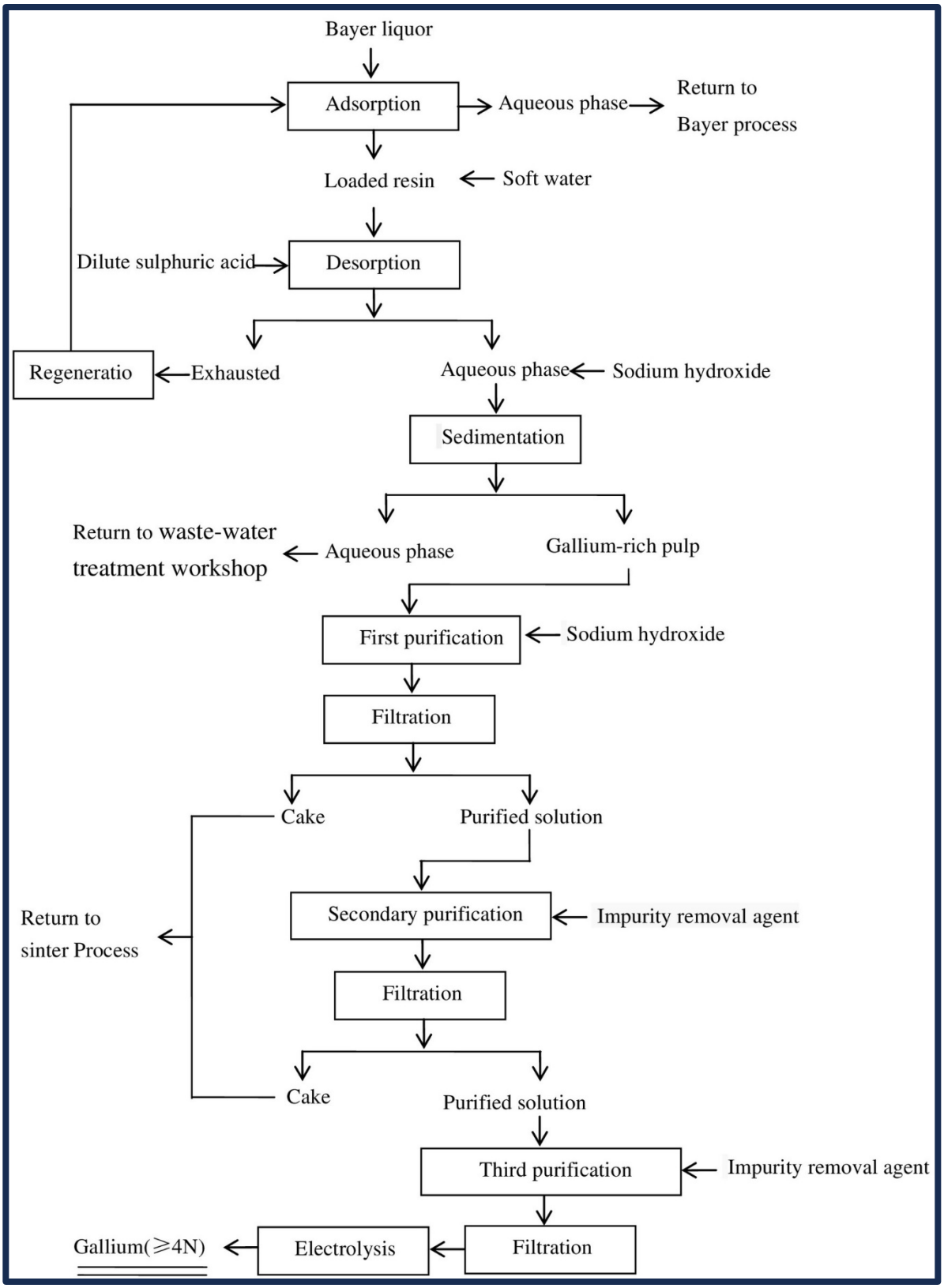

Figure 3.15: Flow diagram of Ga ion-exchange recovery process employed at Chalco Guizhou branch (Lu *et al*., 2017).

Germanium

The coordination chemistry of germanium can be used to change its chemical character to afford the use of anionic resins to separate it from the other elements in solution. Research indicated that Ge forms stable, water-soluble complexes with different catechol ligands (Takemura *et al*., 2013; Arroyo Torralvo *et al*., 2010; Kuroiwa *et al*., 2014).

In a study by Nozoe *et al*. (2012), an anion exchange membrane was utilized to isolate germanium after it was complexed with 3-methylcatechol. Germanium was selectively recovered over silicate at a pH of 8. At this pH, complexation is selective towards Ge compared to Si. In the recovery step, ionic interactions captured Ge as it passed through the membrane as an anionic methyl catechol complex. A flow diagram of the above-described study is presented in **Figure 3.16**.

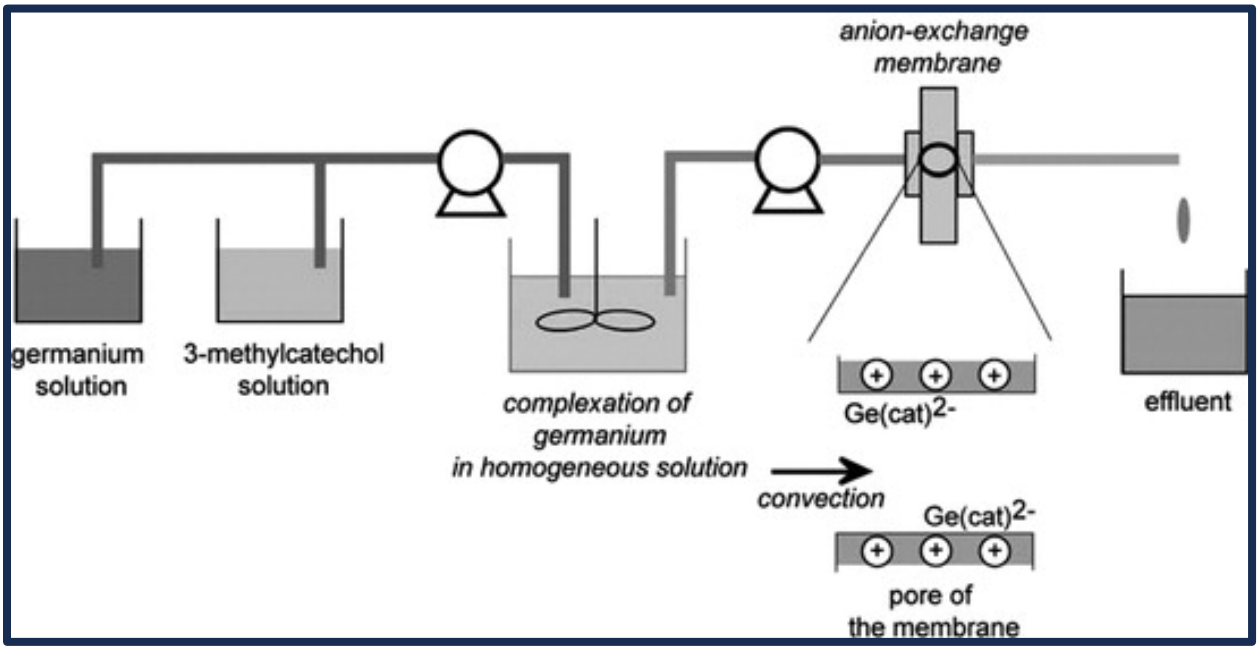

Figure 3.16: Flow diagram of the catechol complexation/anion-membrane isolation of Ge (Nozoe *et al*., 2012).

A similar study was reported by Kawakita *et al*. (2014) . Their “novel” extraction process recovered germanium using catechol to complex germanium which was then transported through a quaternary-ammonium-group-containing-membrane. The results suggested that strong anionic interactions resulted in the adsorption of germanium catechol complex

to a membrane resin. They employed the following experimental conditions: 15 mM catechol, a reaction time of 6 hours at 30 °C, pH 3 and 0.1 M HCl as eluent. The catechol was stripped from the Ge-complex with a mixture of 10 ml of 0.1 M trioctylphosphine oxide (TOPO) and 10 mL hexane. This solution was stirred at 300 rpm for 3 hours at 30 °C.

Chen et al (2018) also employed ion-exchange to recover germanium from optical fibre waste by adding citric acid as a complexing agent. In the proposed process, the first part of the process involved the pretreatment and leaching of the fibre waste, followed by the separation and recovery of germanium. The resin of choice for this process was IRA-900 with the addition of citric acid. Germanium was recovered with a 99 % efficiency under the following optimal experimental conditions: roasting at 500 °C, leaching with 0.4 H_2SO_4 at pH 6 for 1 hour, a temperature of 25 °C, pH of 3,1 M HCl eluent, citric acid/Ge ratio of 4:1.

The ion exchange resin IRA900 was also used by Arroyo Torralvo *et al*. (2018) to recover germanium from 'Integrated Gasification Combined Cycle' fly ash. They used tartaric acid to complex with germanium ion. The resulting germanium tartrate complex was retained on the IRA-900 resin. Subsequently, germanium was eluded and precipitated with tannic acid. The precipitation of germanium using tannic acid is dealt with more in-depth in **Section 3.4.3.** A graphical abstract outlining the above-mentioned process with optimal experimental conditions is provided in **Figure 3.17.**

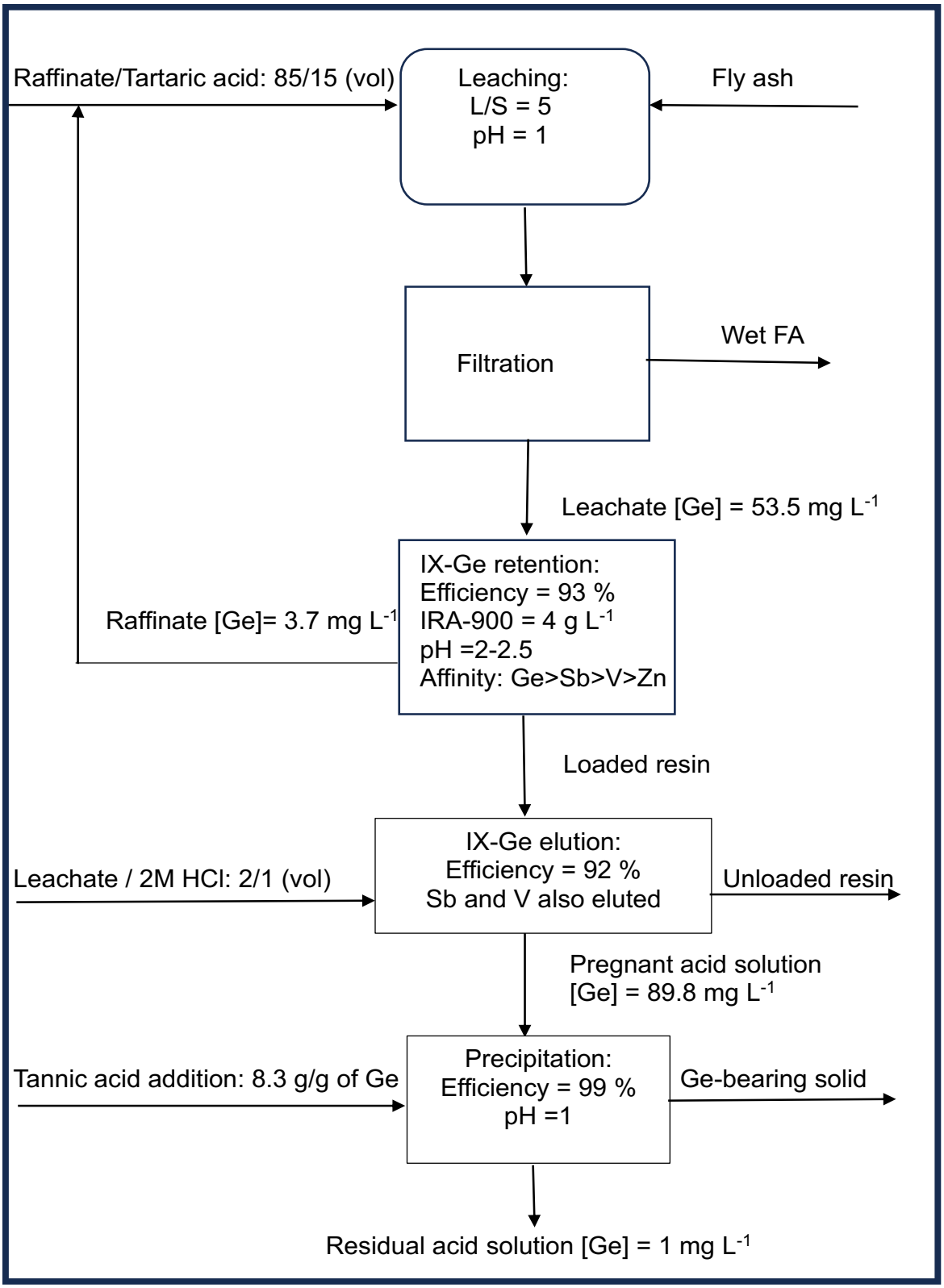

Figure 3.17: Graphical abstract of IRA-900 ion exchange and tannic acid Ge recovery (Arroyo Torralvo *et al*., 2018).

In another study, it was reported that catechol phenolic polymers are selective towards germanium in solutions that also contain zinc, copper, or silicon (Arrambide Cruz *et al*., 2018). In this study, polymeric resins in the form of a catechol-based resin were used to extract germanium from coal fly ash and recoveries of 80 % germanium were reported. The resin was synthesized by the alkaline poly-condensation of 8-hydroxyquinoline and catechol with the aid of formaldehyde. The optimal experimental conditions for this study were: 2.5 g/l resin, pH 6, 1 M HCl for stripping.

3.4.3 Isolation of Ga and Ge using precipitation

Gallium

Tannins that are used for elemental recovery, are biodegradable polyphenolic compounds that readily dissolve in acid solutions (Geng *et al*., 2022a). These tannins contain ortho-dihydroxyls groups and these hydrolyzable tannins readily chelate with metal ions to form metal complexes (Geng *et al*., 2022a; Tan *et al*., 2023).

Research has been done on the isolation/precipitation of heavy metals by using sodium derivatives of di-n-alkyl phosphinic acid (Dumortier *et al*., 2004; Esalah *et al*., 1999, 2000; Rodil *et al*., 2004). Dumortier *et al*. (2005) reported a new method for the precipitation of gallium from an alkaline medium, using sodium di-(n-octyl) phosphinate, resulting in the formation of a water-insoluble complex. This precipitation method is ideally suited for alkaline media since the presence of sulfate and chloride ions may inhibit ligand selectivity towards gallium Dumortier et al., (2005). The reactions were performed at 22 °C, ligand-to-gallium ratio of 3:1, pH adjustment of between 2 and 7.5. More than 98 % of gallium was recovered by this process.

In the ‘Bayer Process’, the Al is isolated as $Al(OH)_3$ at pH < 10.6, while the gallium precipitates as $Ga(OH)_3$ at pH ranging between 9.4 and 9.7 (Lu *et al*., 2017). In a process called fractional precipitation, Al and Ga were both precipitated utilizing lime or carbon dioxide (Zhao *et al*., 2012). Gallium and aluminium are separated by dissolving the subsequent precipitate in lime. Gallium is recovered from the solution by a second

carbonation precipitation process, re-dissolved and purified. This process is illustrated in **Figure 3.18.**

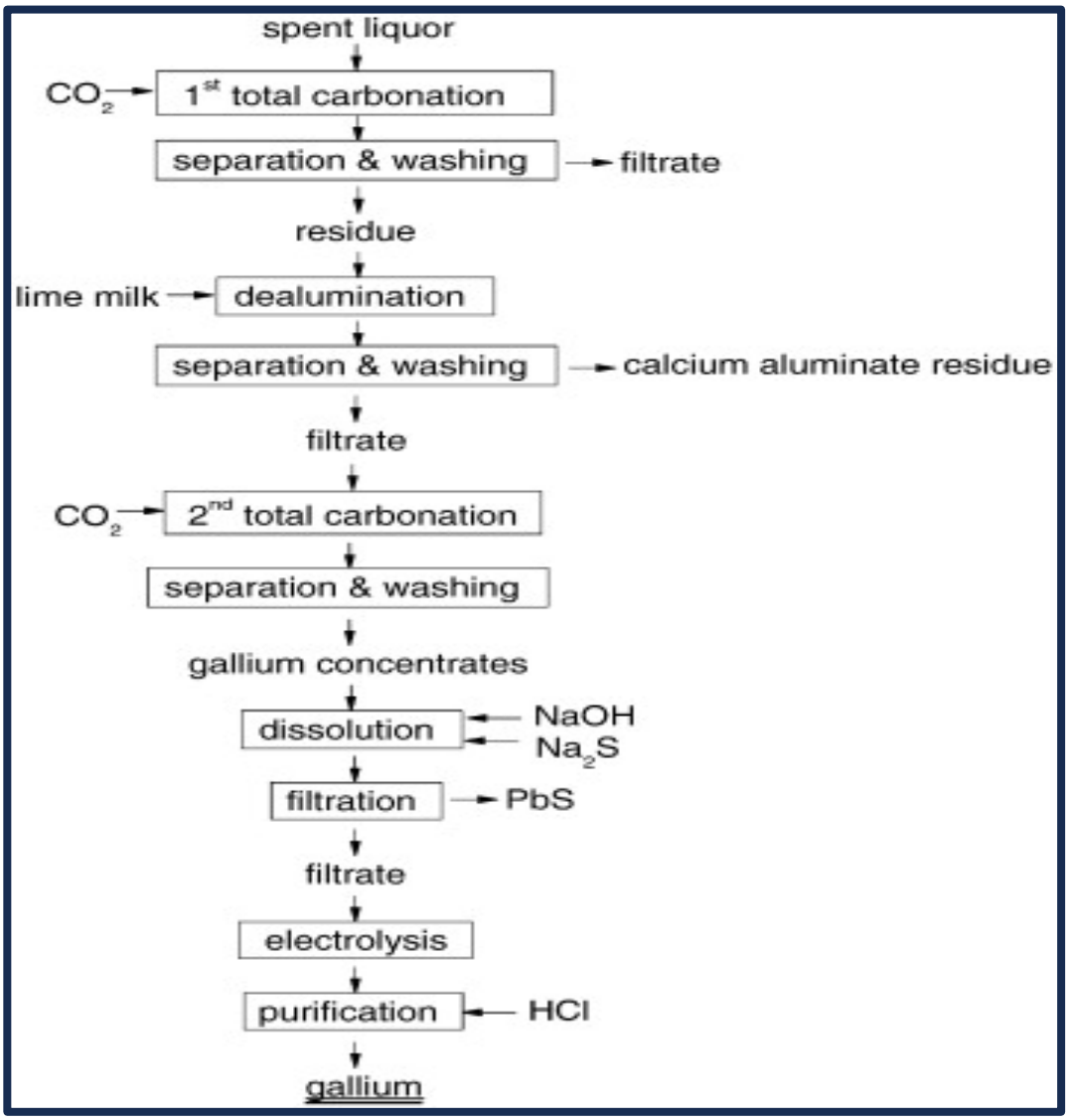

Figure 3.18: Flowsheet of the Ga fractional precipitation method (Zhao *et al*., 2012).

Several researchers reported the use of precipitating agents to recover Ga from aqueous solutions. Hu *et al*. (2015) reported the selective isolation of As from a GaAs scrap leachate, leaving Ga remaining in solution. The finely ground sample was leached using 1.5 M HNO_3 at 40 °C, and a leaching duration of 1.5 hours. The precipitation was afforded using 0.1 M sodium sulfide. The process precipitated 98.5 % As and 1.5 % Ga.

Germanium

Research indicates that germanium can be precipitated from hydrochloric and sulphate solutions by using H_2S or tannic acid (Liang *et al*., 2008; Tan *et al*., 2023). Tannic acid precipitation is preferred with low Ge solutions, while H_2S is employed in solutions with higher Ge content (Kul & Topkaya, 2008). As already mentioned tannins represent a category of biodegradable polyphenolic compounds and contain a number of ortho-dihydroxyl groups as depicted by **Figure 3.19(a)** tannic acid and in **(b)**1,2,3,4,6-penta-O-galloyl-ß-D-glucose (PGG).The coordination between germanium and the tannin molecule is illustrated in **Figure 3.19 (c)** while the Ge -tannin reaction is given in **Eq (3.1)** Geng *et al*., (2022a).

$$Ge^{4+} + O_2 + H_6T \rightarrow GeO_2H_6T \qquad \textbf{(3.1)}$$

T = Tannic acid = $(C_{14}H_{10}O_9)$

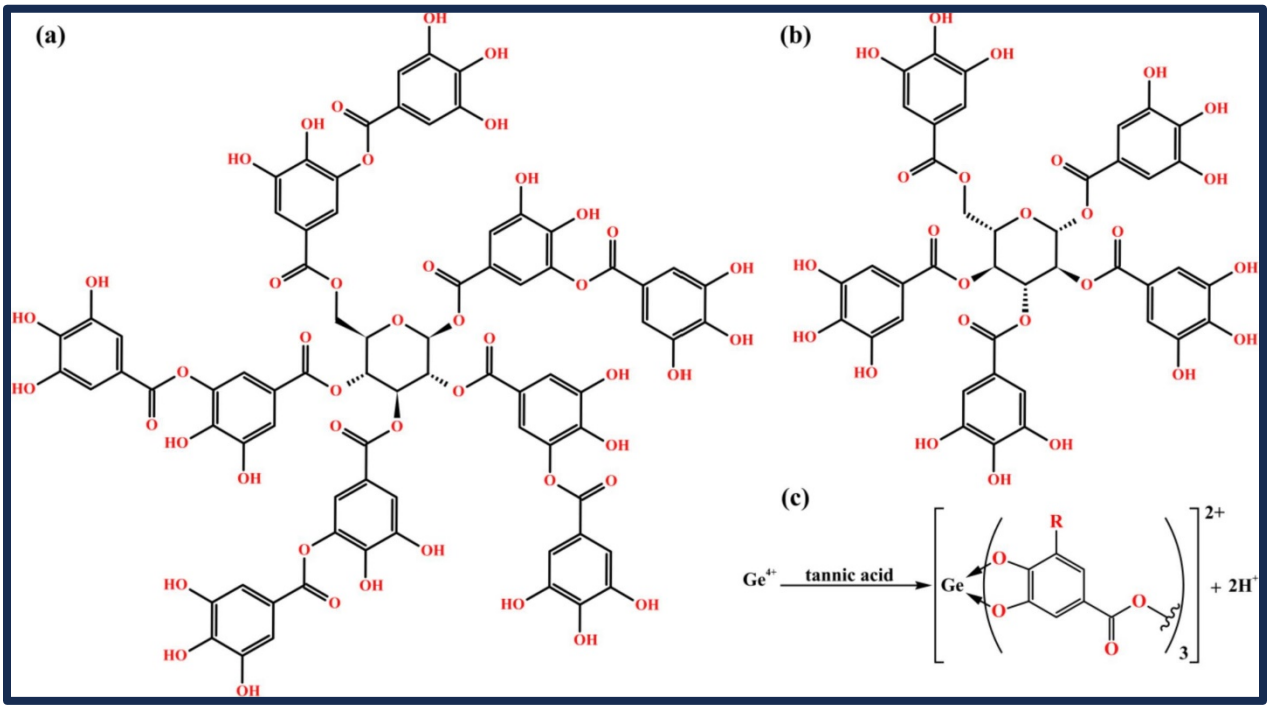

Figure 3.19: Hydrolyzable tannins (a & b) and chelating mechanism (c) to Ge (Geng *et al.*, 2022a).

Drzazga *et al*. (2019) successfully precipitated germanium from sulphate solutions using tannic acid and reported tannic precipitation is highly pH dependent. In this process, more

than 99 % of the dissolved Ge was precipitated. The optimal experimental conditions include 12 g tannic acid/1 g dissolved Ge at 90 °C, 90 minutes reaction time. Another study confirmed these results, which indicate that tannic precipitation of germanium is better compared to sodium hydroxide and ammonia precipitation or isolation (Bayat et al., 2016). Disadvantages of using tannic acid to precipitate Ge include i) it's a relatively high-cost and ii) the large excess of tannic acid that is needed for Ge precipitation, making it an expensive process (Patel & Karamalidis, 2021).

Comparative studies of different agents that can be used for Ge precipitation have also been reported (Arroyo *et al*., 2009). In one comparative study, the precipitation of germanium using 1,2-dihydroxyl benzene pyrocatechol (CAT) and cetyltrimethylammonium bromide (CTAB) was compared to germanium precipitation using H_2S. The comparison was performed on coal fly ash from the 'Puertollano Integrated Gasification Combined Cycle' (IGCC) power station. In addition to this comparison of precipitation efficiencies, the purity of Ge end-products was also compared. The results indicated the germanium precipitation efficiency of CAT and CTAB and H_2S to be 99 %. However, the purity of the Ge end-products was 90 % using CAT and CTAB, and 93 % from H_2S precipitation. The advantages of employing the H_2S precipitation besides the higher purity end-products include the low solubility of GeS_2 in acidic media as well as the fact that H_2S is produced as a by-product in IGCC plants which can conveniently be used for precipitation. However, the environmental impact and handling of H_2S pose a disadvantage. The precipitation of Ge by H_2S occurs according to **Eq (3.2)**.

$$(GeCl_6)^{2-} + 2H_3O^+ + 2H_2S + 4H_2O \leftrightarrow \downarrow GeS_2 + 6\ H_3O^+ + 6Cl^- \qquad \textbf{(3.2)}$$

The germanium catechol complex is highly soluble in water, hence the addition of CTAB to stabilize the Ge-CAT complex as per **Eq (3.3)** (Arroyo *et al*., 2009). The optimal experimental conditions for the comparison were as follows: leaching with water at 90 °C with a liquid-to-solid ratio of 5 L:kg, leaching time of 6 hours, 1) precipitation with 100 %

H_2S, roasting at 700 °C for 4 hours, 2) CAT:Ge ratio of 5 and CTAB/Ge ratio of 3, pH (9-11), roasting at 750 °C for 7 hours.

$$2CTA^{+} + GeCAT_3^{2-} \leftrightarrow CTA_2GeCAT_3 \quad \textbf{(3.3)}$$

In another study, the selective Ge precipitation using tannins was investigated (Kul & Topkaya, 2008). Prior to the precipitation reactions, a leaching comparison study was undertaken. The selective Ge leaching and collective leaching of non-target elements were compared. The comparison was performed on a copper cake sample obtained from the Çinkur Zinc Plant in Turkye. Under selective leaching conditions, the copper cake sample was leached with 1 M H_2SO_4, with a liquid-to-solid ratio of 4:1 (mL: g) at 60 °C for 30 minutes. Germanium was leached with 78 % efficiency and 94 % was successfully precipitated using the tannin. The extraction was regarded as low and unsatisfactory. Finally, GeO_2 was produced by atmospheric roasting. For the collective leaching, 93 % of Ge was successfully extracted, while the same experimental conditions extracted more than 95 % of the Cu, Zn, Cd, Ni, Fe, and Co present in the sample. The leaching experiment was performed using 1.5 M H_2SO_4, with a liquid-to-solid ratio of 8 :1 (L:g), leaching temperature of 85 °C and a leaching time of 1 hour (Kul & Topkaya, 2008) . In summary, the study found that while it is possible to extract more than 90 % of Ge and non-target elements from copper cake, selective extraction is possible although it reduces the overall extraction efficiency to below 80 %. The process is illustrated in **Figure 3.19**.

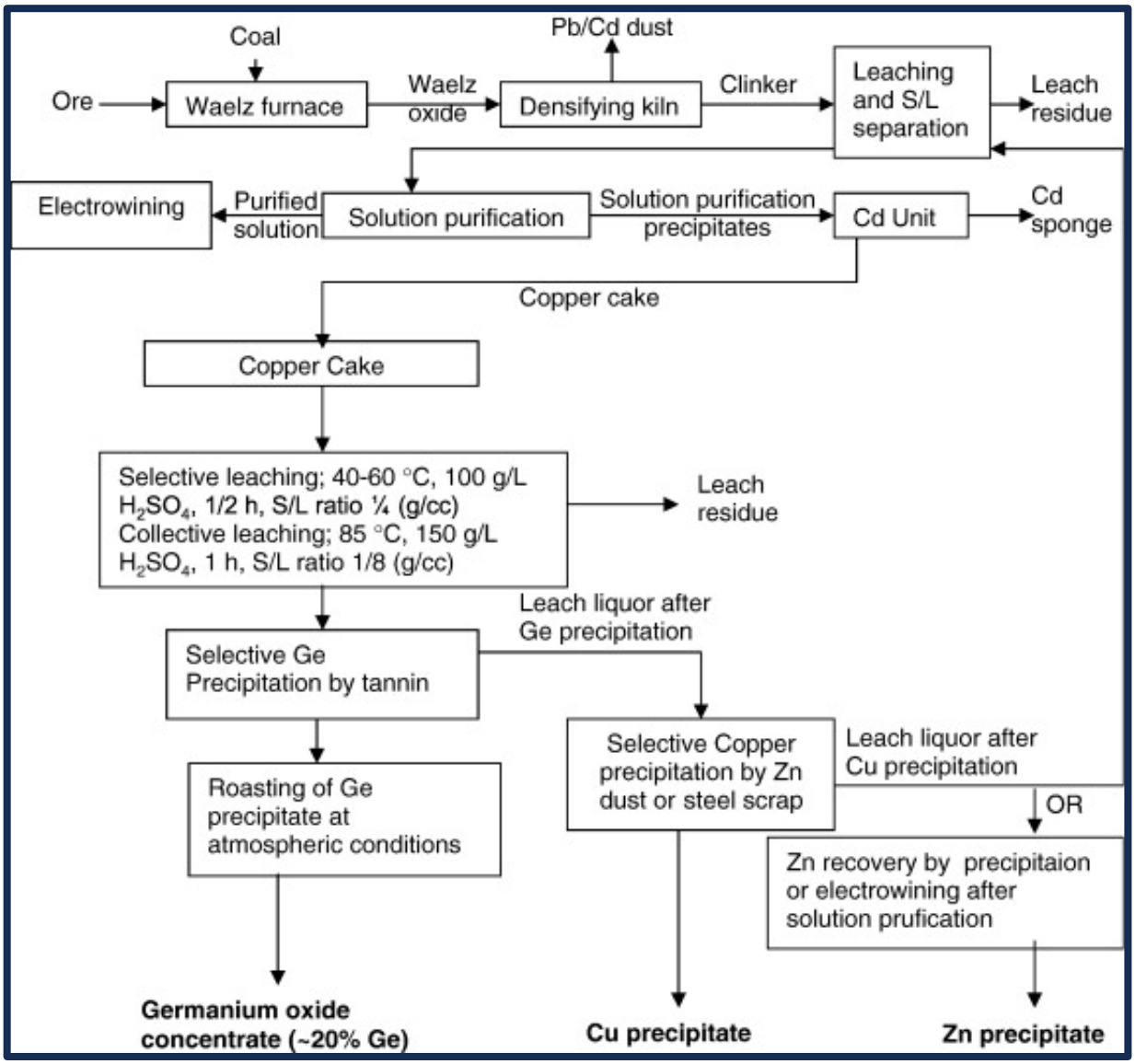

Figure 3.20: Selective Ge tannin precipitation from copper cake flow diagram (Kul & Topkaya, 2008).

3.5 Conclusion

Gallium and germanium have been described as critical and included in the critical material lists of both the USA and EU, but a well-known fact is relatively little is known about their chemistry, compared to other elements on the periodic table. There are only a limited number of well-known and isolated products recorded in literature, and the availability of articles on their processing, leaching solution and purification is limited. (Frenzel *et al*., 2016; Höll *et al*., 2007; Kamran Haghighi & Irannajad, 2022; Liao *et al*., 2017; Lu *et al*., 2017; Moskalyk, 2004; Swami & Patel, 2021; Zhao *et al*., 2012)

The reviewed literature indicate that Ga and Ge is present in a large number of minerals, but in all cases at very low concentrations. Mineral and organic acids have successfully been employed to extract/leach the two elements from secondary sources. Solvent extraction, ion exchange as well selective precipitation have all been successful in the separation of the two elements while selective precipitation proved to be a viable method for the isolation of the two scarce elements form solution.

Although Ga and Ge have been recovered successfully from various secondary sources (primarily electronic waste), these elements have not been recovered from the Tsumeb Mine tailings. This study aims to recover these two critical materials from Tsumeb Mine tailings.

Chapter 4 : Characterization Techniques

4.1: Introduction

The selection of analytical techniques used for this study was dictated by the different insights that each technique brings. Information such as the mineralogical composition, the elemental (major and trace) composition, and metal speciation are crucial in developing the Ga and Ge recovery process aimed for by this study. Mineralogical characterization aids in the identification of the specific minerals present in the sample. Understanding which minerals host the target elements is crucial for selecting the appropriate extraction techniques or reagents. Sample characterization also helps in understanding the associations of minerals; for example, the presence of minerals such as quartz has been reported to have a negative impact on the leaching efficiencies of Ga and Ge. The characterization of the chemical composition and metal distribution also helps to guide the selection of the most suitable extraction reagents.

This chapter discusses the different destructive and non-destructive techniques applied in the characterization of the Tsumeb mine tailings that are important in formulating Ga and Ge recovery from the tailings sample. The non-destructive analytical techniques used for mineralogical characterization were X-ray fluorescence, SEM-EDS, and XRD while ICP-OES, total dissolution, and sequential extraction were the destructive techniques used for the chemical composition characterization.

4.2 X-ray Fluorescence (XRF)

X-ray Fluorescence (XRF) is a non-destructive analytical technique used to determine the elemental composition of materials (Brouwer, 2003; Feng *et al*., 2021; Oyedotun, 2018). XRF can be used to analyze different materials, such as solids, liquids, and powders. This technique is based on the interaction of X-rays and atoms. XRF spectroscopy is employed for both qualitative and quantitative analysis and has been applied in fields such as ecology, environmental analysis, metallurgy, geology, mining, forensics, polymers, archaeology, and soils (Oyedotun, 2018).

A sample's elemental composition is determined by measuring the secondary X-ray's emitted from the sample when irradiated by a primary X-ray source. **Figure 4.1** illustrates this basic principle of XRF, which demonstrates the interaction of an atom with an incident X-ray beam. Depicted in **Figure 4.1** is an elemental nucleus surrounded by electrons housed in different shells or orbitals. The K-shell is the innermost, followed by the L-shell and M-shells, and the outermost N-shell (Ermrich & Opper, 2013; The Editors of Encyclopaedia, 2024). When a sample is radiated with an incident beam, some of the radiation is absorbed by the electrons while the rest is scattered. The energy absorbed from the incident beam expels an electron from the K-shell, thus creating a vacancy (core-hole) in the atom. The atom is now in an unstable higher energy state and will revert to its original configuration by transferring an electron from the outer L-shell. As an electron from a higher energy level moves to a lower energy level, surplus energy in the form of a fluorescent X-ray photon is emitted. Each element produces characteristic fluorescent X-rays that are unique to that element. These photons are seen as lines in a spectrum. XRF spectroscopy is employed for both qualitative and quantitative analysis of solid material.

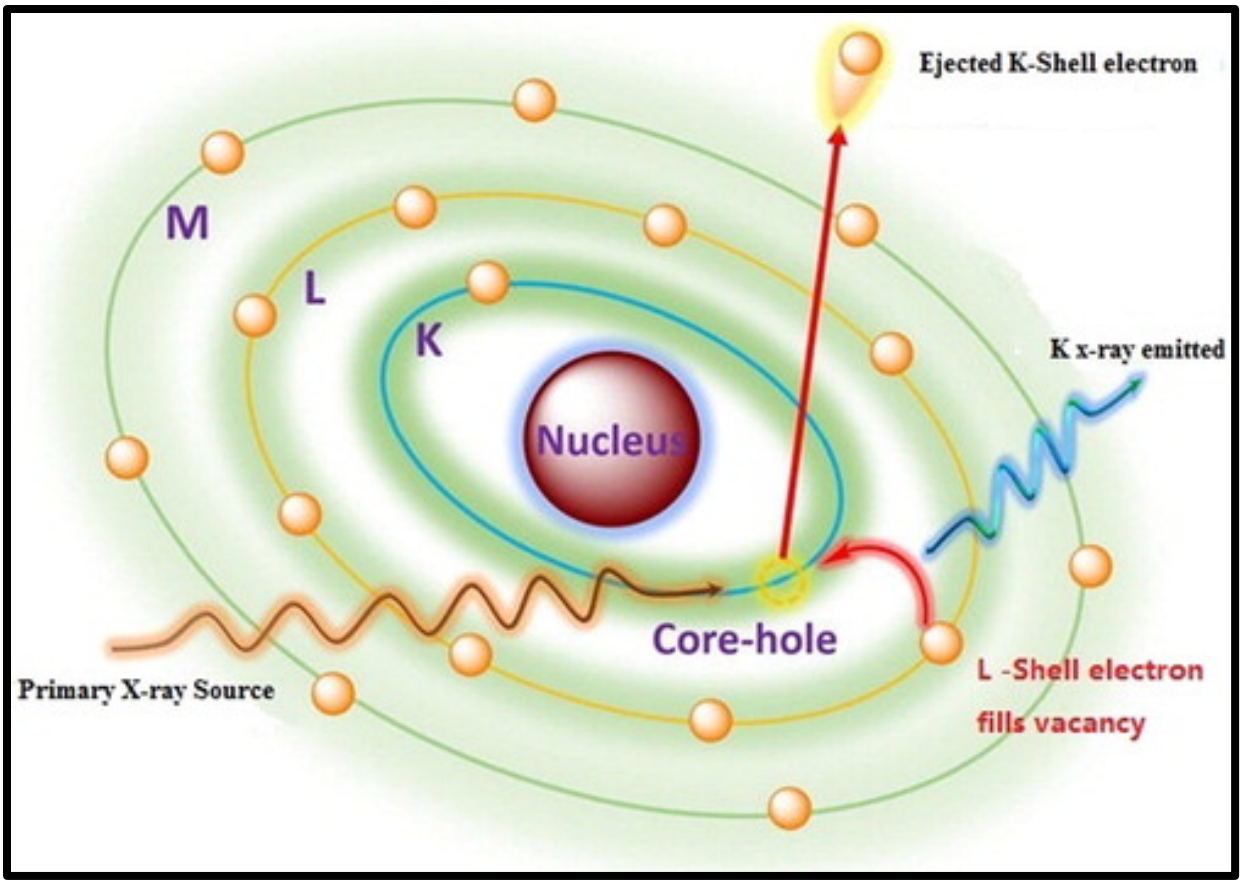

Figure 4.1: Graphical illustration of the interaction of an atom with an incident ray (Feng *et al*., 2021).

XRF spectrometers can be divided into two main categories: energy dispersive systems (EDXRF) and wavelength dispersive systems (WDXRF). These two XRF systems have different dispersion methods (F. Li *et al*., 2020; Wegrzynek, 2004).

WDXRF spectrometers

WDXRF devices use Bragg's law and X-ray reflection from crystal lattices for sequential elemental composition determination of a sample (Wegrzynek, 2004). In this type of spectrometer, the characteristic X-rays of elements are directed toward the detector, where the optical signal is converted to electrical energy (Li *et al*., 2020). Furthermore, the WDXRF spectrometer has a more comprehensive elemental range of beryllium to uranium, whereas the EDXRF elemental range starts from sodium and ends with uranium (Brouwer, 2003; Oyedotun, 2018).

EDXRF spectrometers

For EDXRF spectrometers, characteristic X-rays and scattering rays are emitted when a sample is excited by a source. The characteristic X-rays and the scattered rays are directed towards the detector, where the intensity is measured, and nuclide concentration is calculated (Li *et al*., 2020). In comparison, EDXRF has a better spectral resolution than WXRF; however, it is slower and less convenient to use (Wegrzynek, 2004).

A) Sample preparation: Sample preparation is variable and largely depends on the nature of the samples being analyzed. Geological samples must be larger than the largest sample particle size.
B) Analysis: XRF is used for both qualitative and quantitative analysis. It can be used for quantitative elemental composition determination because the X-ray fluorescence intensity (peak height) of an element depends on the concentration of the sample. Two techniques are used in XRF quantitative analysis: the Fundamental Parameters Method (FPM) and the standards calibration method. FPM calculates element concentration based on peak intensity, while the standards calibration method relates the intensity of the elements to the calibration curve derived from certified reference materials.

4.3 X-Ray Diffraction

X-ray diffraction (XRD) is a non-destructive analytical technique used to characterize a sample's phase composition and crystal properties (structure, size, shape, and orientation). XRD is used to analyze various sample types, such as powder, solid, or liquid (Ermrich & Opper, 2013). XRD analysis is applied in industries such as pharmaceuticals, automotive, material science, geology, forensic science, electronics, and the environment. The specific applications of XRD in these industries and others are listed in **Figure 4.2**.

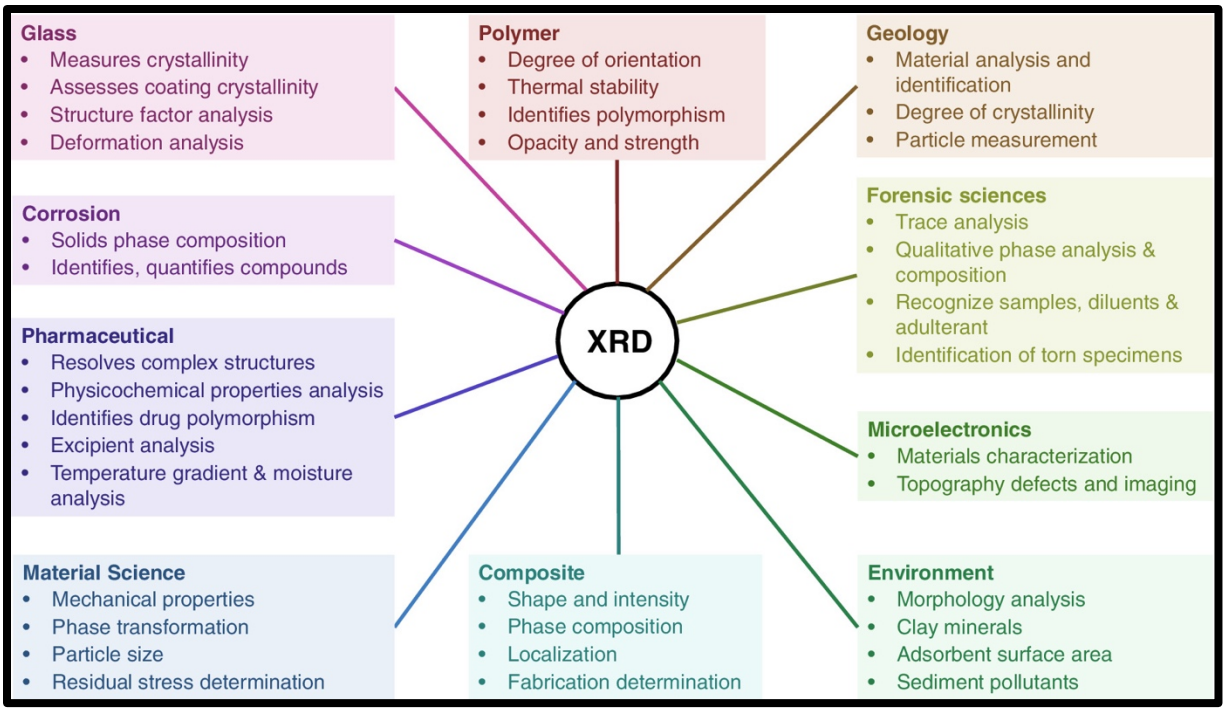

Figure 4.2: Different applications of XRD (Khan *et al*., 2020).

Materials consist of crystal microstructures; these materials' chemical composition and structural type are referred to as their phase. Based on the internal arrangement of atoms, solid-state compounds are classified as amorphous, single-crystalline, or polycrystalline materials. The arrangement of atoms in amphormous materials is irregular, making the materials isotropic. In contrast, the arrangement of atoms in crystalline materials is repetitive and regular, making it anisotropic. Polycrystalline materials are a combination of different crystals of varying sizes and shapes; these crystals' arrangement, orientations, and sizes strongly influence these materials. In summary, amorphous materials have similar properties in all directions, while crystalline materials display changes in properties with direction (Ali *et al*., 2022).

In XRD analysis, different crystalline phases have different diffraction patterns. The arrangement of atoms within a crystal lattice dictates the peak intensities. As a result, atom distribution in a lattice is regarded as the fingerprint of a specific material (Bunaciu *et al*., 2015). Phase identifications are performed by comparing X-ray diffraction patterns of unknown samples to patterns of those in a reference library, The International Center

of Diffraction Data (ICDD) being the most comprehensive. Alternatively, laboratories can also create reference libraries from measured pure-phase diffraction patterns either from their own measurements or literature (Ali *et al*., 2022; Ermrich & Opper, 2013).

Components and working of XRD diffractometer

An XRD diffractometer is made up of three main components: an X-ray source (cathode ray tube), a sample holder, and a detector (scintillation counter or semiconductor). The interaction of the incident X-rays with a sample either generates constructive or destructive interference based on the direction of the rays. When an incident X-ray beam strikes a crystalline sample, it is diffracted by the atomic planes within the crystal, producing a pattern that reveals the structural information of the sample. Diffraction occurs due to constructive interference between scattered X-rays (Ali *et al*., 2022). Bragg's Law (**Eq 4.1**) must be satisfied for diffraction to occur. Bragg's diffraction condition is satisfied when the path difference *d* equals $n\lambda$ (Ali *et al*., 2022; Bunaciu *et al*., 2015).

$$n\lambda = 2d sin\,\theta \qquad \textbf{Eq 4.1}$$

where:

- n is the diffraction peak order
- λ is the wavelength of the incident X-ray
- d is the spacing of the crystal lattice
- θ is the angle between the incident X-ray and the crystal plane

A schematic representation of the XRD operation is depicted in **Figure 4.3**, where a sample to be analyzed by this technique is radiated by X-rays generated by the source. The diffracted X-rays are measured by a detector, which determines the intensity of the diffracted X-rays as a function of the diffraction angle (2θ) (Surdu & Győrgy, 2023).

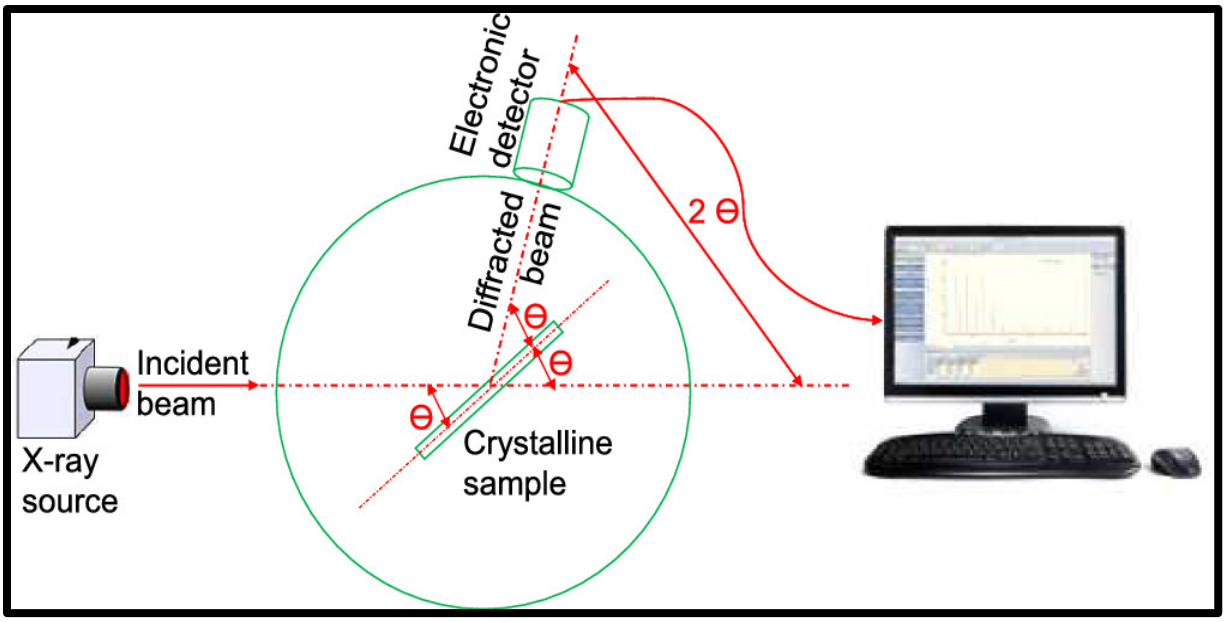

Figure 4.3: Diagram of XRD components and operation (Khan *et al*., 2020).

XRD graphs of crystalline substances are easier to interpret than those of amorphous materials. As previously mentioned, the arrangement of atoms in amphormous materials is irregular, while the arrangement of atoms in crystalline materials is regular and periodic. The lack of periodic arrangement of atoms in amorphous materials leads to average peaks (**Figure 4.4 a**), while the periodic arrangement in crystalline materials results in distinct peaks (**Figure 4.4 b**) (Ali *et al*., 2022).

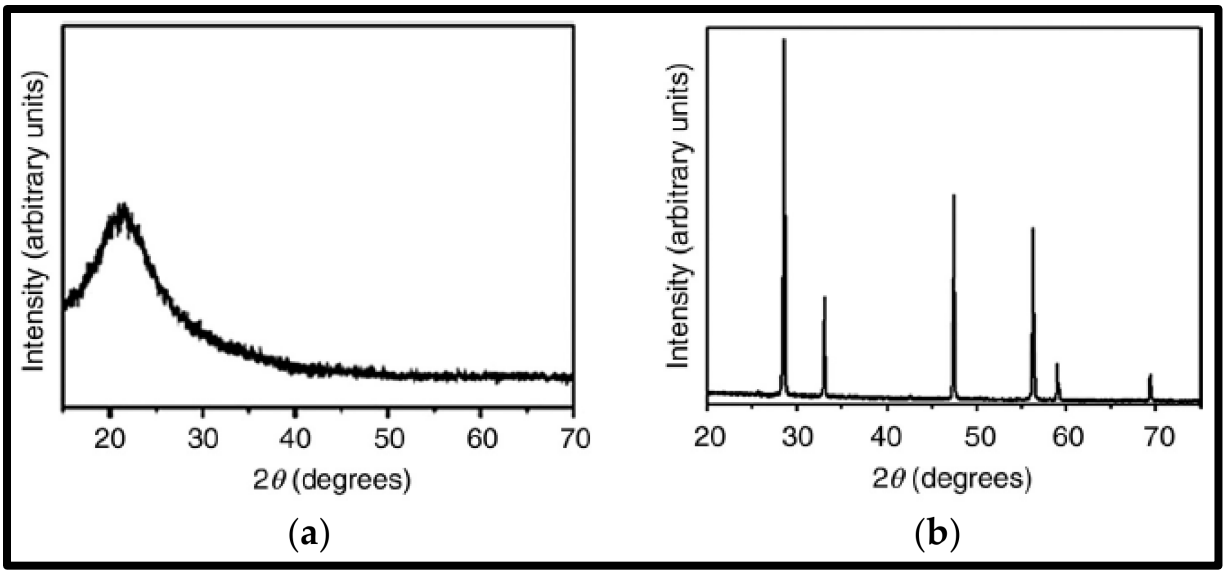

Figure 4.4: XRD graphs of (a) amophous material and (b) crystalline material (Ali *et al*., 2022).

X-ray diffractometers are categorized into two groups, namely powder XRD (PXRD) and single crystal XRD (SCXRD). PXRD's advantage over SCXRD is that it does not require individual crystals, and the diffraction pattern can be obtained from powdered substances, thus making it easier and more convenient, especially for mineral or naturally occurring samples.

Differences in Data Collection

In PXRD, a sample is irradiated with a beam of X-rays, and the diffracted X-rays' intensity is measured as a function of the diffraction angle. This results in a diffraction pattern of a series of peaks corresponding to different sets of crystal planes (Drawell Analytical, 2023).

In SCXRD, the sample is rotated in an X-ray beam while measuring the intensity of the diffracted X-rays as a function of the diffraction angle. The diffraction results in a three-dimensional map of the crystal structure (Drawell Analytical, 2023).

Differences in Data Analysis

PXRD is utilized to elucidate the crystal structure and phase composition of the sample, while SCXRD is used to elucidate both the crystal structure and phase composition and,

in addition, atomic positions and angles within the sample. In PXRD, the crystal structure is determined by comparing the diffraction pattern of the sample with that cited by a reference database. In contrast, SCXRD determines the crystal structure by applying mathematical methods to the diffraction pattern. The phase composition of both diffractometers is determined by the relative intensities of the diffraction peaks. Lastly, the atomic positions in SCXRD are determined by the intensity of the diffracted X-rays as a function of the diffraction angle (Drawell Analytical, 2023).

4.4 Scanning Electron Microscopy (SEM)

Scanning electron microscopy (SEM) is an analytical technique that uses a focused beam of electrons to capture magnified or high-resolution images of a sample (Joy, 2019; Zhou *et al*., 2007). This technique has been widely applied in material science, geology, and mining (Ali *et al*., 2023). When a high energy (up to 50 keV) electron beam strikes a sample, the results are multiple interactions between the electron beam and the atoms on the sample's surface. These interactions relay information regarding the surface topography, crystalline structure, electrical properties, and chemical composition of the surface of a sample (Vernon-Parry, 2000). Furthermore, these interactions are categorized as elastic and inelastic interactions (Zhou *et al*., 2007).

Elastic interactions emanate from the deflection of the incident electron beam by the sample's atomic nucleus. Elastic interactions experience negligible energy loss during collision and directional change. Backscattered electrons are elastically scattered through an angle greater than 90 ° C. These electrons are used to image the sample under investigation (Zhou *et al*., 2007).

Inelastic scattering leads to a transferal of substantial energy from the primary beam electron to the atom of the sample. The excitation of the sample's electrons leads to the generation of secondary electrons that contain less than 50 eV and are also used to image the sample (Vernon-Parry, 2000; Zhou *et al*., 2007). Furthermore, there are other electron signals, such as Auger electrons and X-rays, that are not used to image samples.

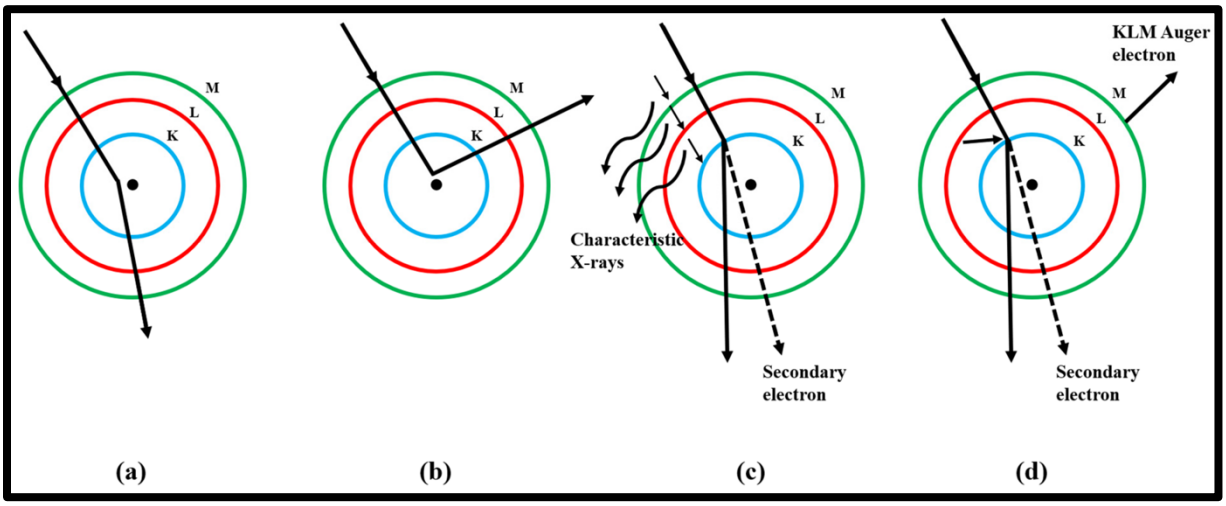

Figure 4.5: Schematic depiction of high energy electrons with atoms a) Low angle scattering, b) high angle/backscattering, c) characteristic X-rays & secondary electron emission, d) secondary electron & Auger-electron emission (Ali *et al*., 2023)

Secondary electrons

Secondary electrons (SEs) are those released when a primary electron beam strikes the sample surface, resulting in the ionization of the sample's atoms (Haque *et al*., 2017). These SEs have low energy with an average of 3-5 eV and can only be released for a few nanometers of the sample's surface. The SE emission signal is the most extensively used signal that results from the interaction of the primary electron beam with a sample (Cazaux, 2012; Scholtz *et al*., 1996). Thus, SEs indicate the beam's position and capture the topography of the sample surface with good resolution. In summary, secondary electrons are used for topographic (surface texture and roughness) imagery (Zhou *et al*., 2007).

Backscattered electrons

A backscattered electron is an electron that has been scattered once or multiple times and is emitted from the sample surface with energy greater than 50 eV (Cazaux, 2012; Vernon-Parry, 2000). Backscattered electrons (BSE) provide compositional and topographic information. The lateral resolution of BSE (1μm) is larger than that of SE (10 nm) due to BSE having larger energy, which prevents it from being absorbed by the sample (Zhou *et al*., 2007).

Characteristic X-rays

Characteristic X-rays are another group of signals generated by the interaction of the primary electron beam and the sample (Vernon-Parry, 2000). The detection of characteristic X-rays is a microanalytical technique in SEM, employed to provide the chemical composition of a sample. When an incident beam strikes a sample, an electron in the inner shell is displaced, thus creating a vacancy in the shell. An electron from the outer shell will fall into the vacant shell to reestablish the original configuration. As the electron from a higher energy level is transferred to a lower energy level, X-rays characteristic of the sample element are emitted. Microanalysis of the sample's surface is achieved using energy-dispersive X-ray spectroscopy (EDS) detectors to read the characteristic X-ray signals (Zhou *et al*., 2007).

Basic SEM operation

Incident electrons with energies ranging from 2 – 40 keV are produced by an electron source (Chen *et al*., 2015; Vernon-Parry, 2000). The three types of electron sources employed are i) a tungsten hairpin filament, ii) a lanthanum hexaboride source, and iii) a field emission gun (Ali *et al*., 2023). The tungsten filament gun operates by thermal emission and is heated to over 2500 ° C (Vernon-Parry, 2000). Lanthanum hexaboride also operates by thermal emission but has a brighter beam and a prolonged lifespan. Field emission guns are not heated and are called cold cathode emitters (Ali *et al*., 2023).

An image of all these different interactions can be produced with a suitable detector. The two most common detectors utilized by SEM instruments for high-resolution imaging of a sample's surface are the secondary electron detector (SED) and backscattered detector (BSD).

4.5 Total Sample Dissolution

Complete and reliable sample dissolution is one of the most crucial steps for any analytical procedure (Sill & Sill, 1995). This requirement must be satisfied for the sample matrix's accurate and complete/total elemental quantification (Harms, 2007; Sill & Sill, 1995). Each insoluble component must be converted into a soluble form for a sample to be dissolved entirely. The three major categories of sample decomposition are wet ashing or acid dissolution, flux fusion, and microwave digestion (Bock, 1979; Epa & Protection Division, 2004).

Flux Fusion

In this study, flux fusion was employed to achieve total sample dissolution. This technique is used on samples that are difficult to dissolve in acids (Harms, 2007). The requirement for a fusion to succeed is that the sample must contain chemically bound oxygen in oxides, carbonates, or silicates. Samples that do not meet this requirement must first be oxidized prior to the fusion process.

Flux fusion involves heating a salt (called the flux) and mixing it with a specified amount of the investigated sample. The resulting mixture is heated at an elevated temperature above the melting point of the salt, usually 1000 ° C. Upon completion of the reaction, the mixture is cooled to room temperature. The fused sample is dissolved and analyzed with ICP-OES. The complete dissolution of a sample matrix depends on the temperature required to melt a flux salt, the ratio of the flux salt to the sample matrix, and the nature of the sample (basic, acidic, or oxidation/reduction requirements).

Flux Fusion preparation

Solid samples to be fused must be finely ground to increase the surface area, which readily allows for the dissolution process. The sample is thoroughly mixed with salt in an appropriate ratio, normally in a 1:10 ratio. Fusions are usually performed using sand or oil baths or in a muffle furnace and platinum, zirconium, nickel, or porcelain crucibles. The selection of the type of crucible depends on the salt used for the fusion. The platinum

crucible is the most extensively used in flux fusion due to its inert nature to many of the fluxes that can be used. Platinum crucibles are resistant to molten alkali metals, borates, fluorides, nitrates, and bisulfates. A wide variety of salts are used in flux fusion; **Figure 4.1** lists the salts, their melting points, fusion temperatures, types of crucibles used, and the nature of samples which they dissolve.

Table 4.1: Types of fusion fluxes (Bock, 1979; Epa & Protection Division, 2004).

Flux (MP, ° C)	**Fusion Temp, ° C**	**Type of Crucible**	**Types of samples Decomposed**
$Na_2S_2O_7$ (403) or $K_2S_2O_7$ (419)	Up to red heat	Pt, quartz, porcelain	Insoluble oxides and oxide-containing samples, particularly those of Al, Be, Ta, Ti, Zr, Pu, and the rare earths
NaOH (321) or KOH (404)	450-600	Pt, quartz, porcelain	Silicates, oxides, phosphates, and fluorides
Na_2CO_3 (853) or K_2CO_3 (903)	900-1,000	Ni Pt for short periods (use the lid)	Silicates and silica-containing samples (clays, minerals, rocks, glasses), refractory oxides, quartz, and insoluble phosphates and sulfates
Na_2O_2	600	Ni, Ag, Au, Zr, Pt	Sulfides; acid-insoluble alloys of Fe, Ni, Cr, Mo, W, and Li; Pt alloys; Cr, Sn, and Zn minerals
H_3BO_3	250	Pt	For analysis of sand, aluminum silicates, titanite, natural aluminum oxide (corundum), and enamels
$Na_2B_4O_7$ (878)	1000 - 1200	Pt	Al_2O_3; ZrO_2 and zirconium ores, minerals of the rare earths, Ti, Nb, and Ta, aluminum-containing materials; iron ores and slags
$Li_2B_4O_7$ (920) or $LiBO_2$ (845)	1000 - 1100	Pt, graphite	Almost anything except metals and sulfides. The tetraborate salt is especially good for basic oxides and some resistant silicates.

4.6 Acid/Wet Ashing Dissolution

Acid dissolution or wet ashing is used to decompose a sample matrix using hot concentrated acid solutions. Several inorganic matrices, such as oxides, silicates, nitrides, carbides, and borides, are challenging to dissolve completely. Single or combined mineral acids are employed to decompose specific materials present in the sample. The most common wet ashing procedures use acids such as HCl, HNO_3, H_2SO_4, $HClO_4$, and HF, or a combination of these acids (Balaram & Subramanyam, 2022; Epa Protection Division, 2004). **Table 4.2** lists various acids and the compounds that these acids generally decompose during wet ashing.

At times, acid dissolution is used to dissolve a major fraction of the sample, leaving a small portion as residue. Further, wet ashing or flux fusion treatment may be applied to dissolve the remaining residue (Epa Protection Division, 2004). The use of HF is the last resort due to its highly corrosive nature, but, in some instances, it becomes inevitable for some sample decompositions because of its ability to dissolve silica and other silicates (Balaram & Subramanyam, 2022; Kline & Fogler, 1981; Muratli *et al*., 2012).

Table 4.2: Mineral acids used in wet ashing and its usual applications (Epa & Protection Division, 2004).

Acid	Common uses
HF	The removal of silicon and the destruction of silicates, dissolves oxides of Nb, Ta, Ti, and Zr, and Ta ores.
HCl	Dissolves many carbonates, oxides, hydroxides, phosphates, borates, and sulfides; dissolves cement.
HBr	Distillation of bromides (e.g., As, Sb, Sn, Se).
HI	Effective reducing agent; dissolves Sn^{+4} oxide and Hg^{+2} sulfide.
H_2SO_4	Dissolves oxides, hydroxides, carbonates, and various sulfide ores; hot concentrated acid will oxidize most organic compounds.
H_3PO_4	Dissolves Al_2O_3, chrome ores, iron oxide ores, and slag.
HNO_3	Oxidizes many metals and alloys to soluble nitrates; organic material oxidizes slowly.
$HClO_4$	Powerful oxidizer; reacts violently or explosively to oxidize organic compounds; attacks nearly all metals.

4.7 Sequential Extraction

Many metals are partitioned across different physiochemical phases in soils and sediments (Li *et al*., 1995; X. Li & Thornton, 2001; Pickering, 1986). These phases **(Figure 4.6)** act as reservoirs for these metals and are classified broadly as exchangeable, carbonates, Fe and Mn oxides, organic matter, sulphides, and silicates or residual (X. Li & Thornton, 2001; Tessier *et al*., 1979). A fractionation or partitioning

method called sequential extraction was developed to determine the different elements' distribution across the different phases (Tessier *et al*., 1979).

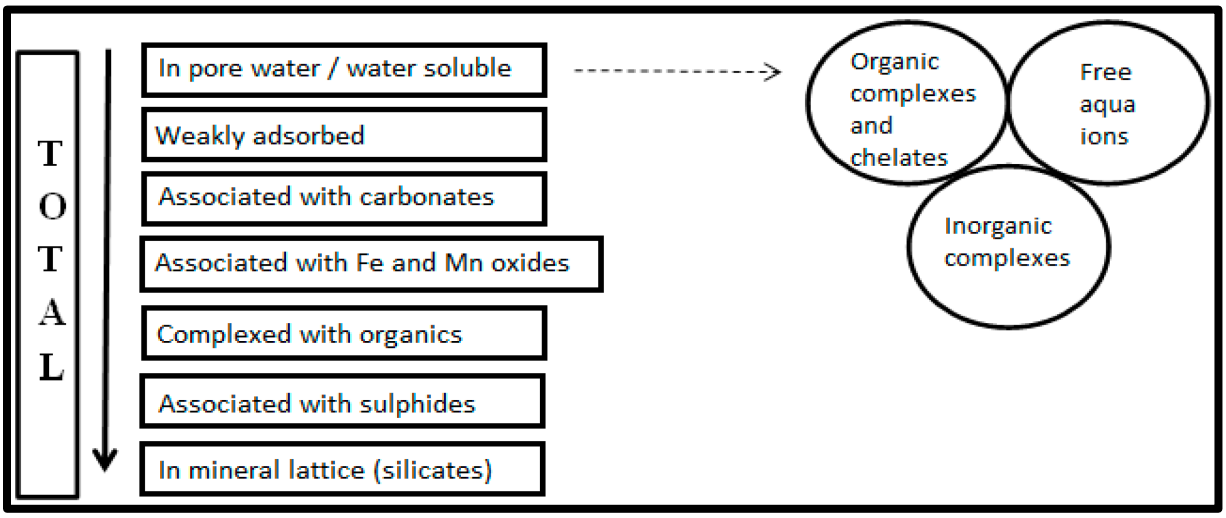

Figure 4.6: Different forms of metals in soils and sediments (Rodgers *et al*., 2015).

Sequential extraction extracts the different fractions of a material using various reagents in a stepwise process. This method is employed to determine the different reactivities and mobilities of elements in the sample. In this method, the extractants are used in order of increasing reactivity or dissolution strength (Du Laing, 2011; Wenzel *et al*., 2001). The increasing order of extractants' reactivity corresponds to successive fractions with less reactive trace elements. Extractants extensively used in sequential extractions are part of the following groups: salts, weak acids, reducing agents, and strong acids (Du Laing, 2011). Various sequential extractions have been developed and can differentiate between reducible or oxidizable metal species. In 1992, the European Community Bureau of Reference (BCR) proposed a three-step sequential extraction method called the BCR sequential extraction method to standardize the many sequential extraction methods used during elemental analysis. This method was subsequently revised and improved following further collaborations and is now called the modified BCR sequential extraction method. **Figure 4.7** graphically depicts an example of a modified BCR extraction method used by Šebesta *et al*. (2020) to determine the mobility of three different Zn forms ($ZnSO_4$, ZnO nanoparticles, and larger ZnO particles) in acidic and alkaline soils. The Zn in the

soil samples was extracted into three fractions: ion exchange, reducible, and oxidizable fractions.

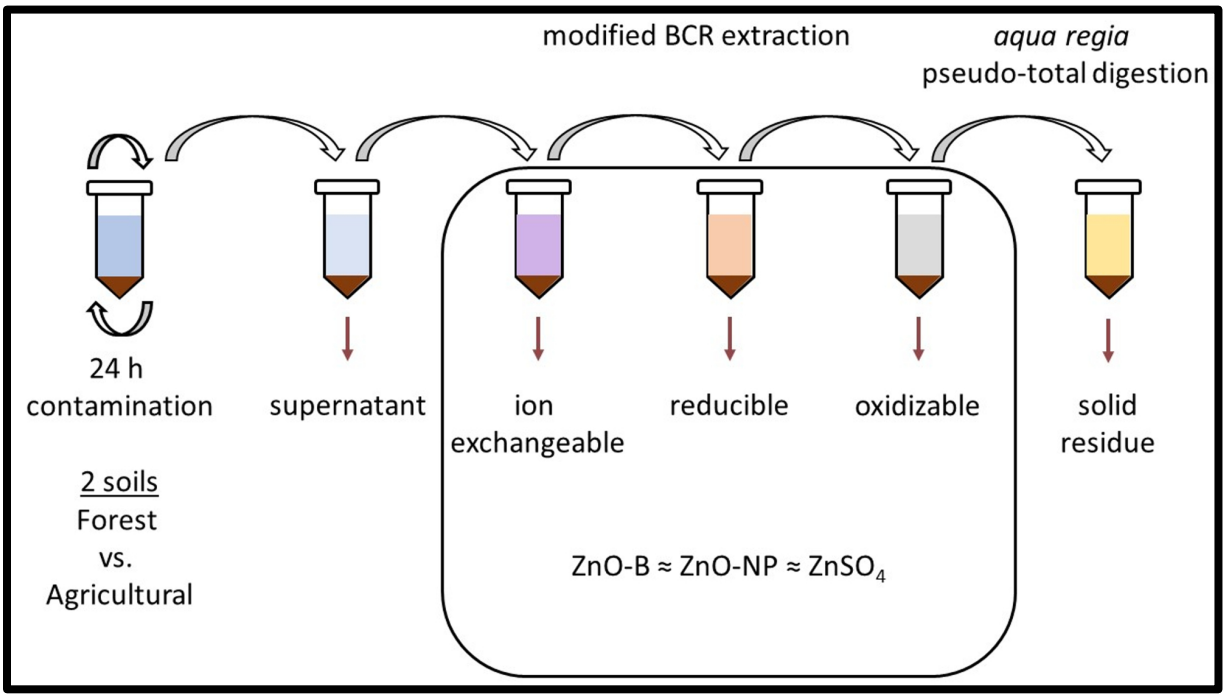

Figure 4.7: Graphical abstract of modified BCR sequential extraction method (Šebesta *et al.*, 2020).

Sequential extraction chemically separates into the following fractions: a) exchangeable, water and acid-soluble, b) reducible, c) oxidizable, and d) residual/silicate bound (Frentiu *et al*., 2009; Žemberyová *et al*., 2006; Zimmerman & Weindorf, 2010). Elements that are weakly absorbed on the solid sample's surface by weak electrostatic forces are readily released by ion-exchange processes and can be co-precipitated with carbonates. Fraction 1 comprises exchangeable, water, and acid-soluble trace elements originating from carbonates. The reagents often used to extract metals in this fraction are acetic acid (buffered to pH 3-5) and ethylenediaminetetraacetic acid (Na_2EDTA) (pH 4.6). Fraction 2 is the reducible portion and elements found in this fraction are bound to iron and manganese oxides and hydroxides. Elements found in the reducible fraction are released in the presence of a suitable reducing agent, the common being hydroxyl-ammonium chloride. Fraction 3 is the oxidizable portion, and it contains elements that are bound to organic matter and sulfides; hydrogen peroxide, followed by acetic acid, is employed to liberate elements in this fraction. Lastly, fraction 4 contains elements tightly bound and incorporated into the crystal lattice of primary and secondary minerals with the sample. A strong acid digestion, one or a combination of two acids, is required to release elements in this fraction. Hydrofluoric acid and aqua regia are the most used reagents for extracting elements in this fraction (Bacon & Davidson, 2008; Tessier *et al*., 1979; Zimmerman & Weindorf, 2010). **Table 4.3** lists several modifications to the BCR sequential extraction between 1993 and 2008.

Table 4.3: Modifications of BCR sequential extraction procedure (1993–2008) (Rodgers *et al.,* 2015).

Sample Type	Fraction 1 (Exchangeable, Water and Acid Soluble)	Fraction 2 (Reducible (Fe and Mn Oxyhydroxides)	Fraction 3 (Oxidisable-Organic Matter and Sulphides)	Fraction 4 (Residual-Silicate Bound)
Soils and sediments (Muratli *et al*., 2012)	0.11 M acetic acid	0.1 M hydroxyl ammonium chloride pH 2, 4h	hydrogen peroxide followed by 1.0 M ammonium acetate at pH 2	aqua regia
Sewage sludge (Muntau *et al*., 1993) and sediment (Guevara-Riba *et al*., 2004)	0.11 M acetic acid	0.5 M hydroxyl-ammonium chloride pH 1.5	Hydrogen peroxide followed by 1.0 mol/L ammonium acetate at pH 2	aqua regia
Sediments (Bacon & Davidson, 2008)	0.11 M acetic acid	0.5 M hydroxyl-ammonium chloride	H_2O_2, 1.0 mol/L CH_3COONH_4	aqua regia
Sewage sludge (Nyamangara, 1998)	40 mL 0.11 M acetic acid	40 mL 0.10 M hydrochloride (pH 2 $HNO_{3)}$	10 mL 8.8 M H_2O_2	HF
Solid waste (Bruder-Hubscher *et al*., 2002)	0.11 mol/L acetic acid	0.1 M hydroxylamine hydrochloride (pH 2 HNO_3)	8.8 M H_2O_2 followed by 1 M ammonium acetate	Perchloric acid-hydrofluoric acid, hydrochloric acid

Total dissolution and strong acid leaching techniques can determine the total elemental concentrations in sediments but are limited when it comes to the distribution or speciation of these different metals. The results obtained from sequential extraction aid in understanding the speciation of the elements under investigation. Based on the distribution of the target elements, appropriate reagents can used to selectively target the phase in which the target elements are mainly located. Sequential extraction has its own limitations with it being regarded as semi-quantitative rather than fully quantitative due to the possibility of the analyte being redistributed in successive steps due reagents not being fully selective to the phase or due to incomplete extraction (Rodgers *et al*., 2015).

4.8 Inductively Coupled Plasma – Optical Emission Spectroscopy (ICP-OES)

Inductively Coupled Plasma-Optical Emission Spectroscopy is an analytical technique that was developed in 1974 (Douvris *et al*., 2023). ICP-OES analysis technique is well established in trace and ultra-trace elemental composition determination and has subsequently been employed in industries (**Figure 4.8**) of water quality monitoring, environmental protection, agricultural analysis, pharmaceutical, mining and petrochemical analysis (Douvris *et al*., 2023; Khan *et al*., 2022; Levine, 2021).

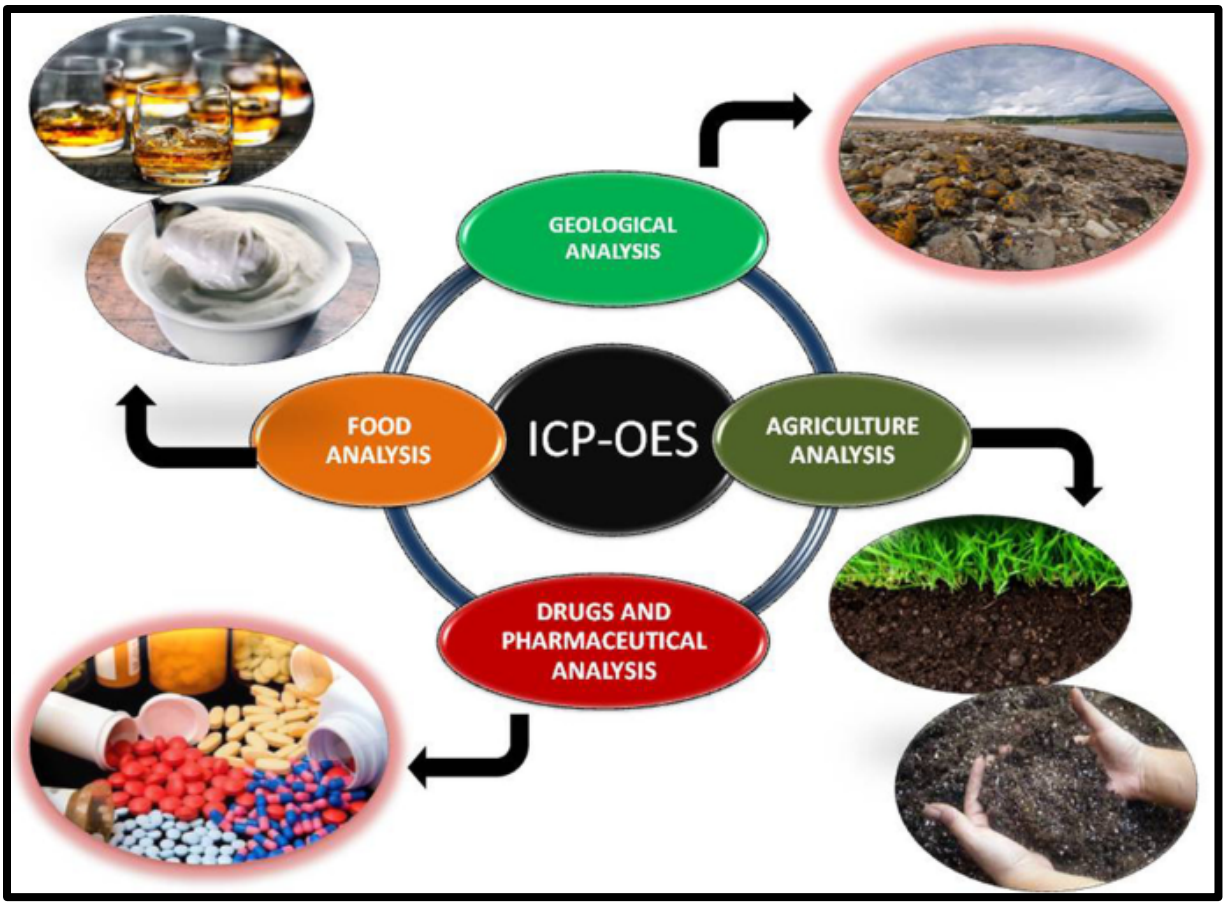

Figure 4.8: Depiction of industries that uses ICP-OES analysis (Khan *et al*., 2022).

The advantages that ICP-OES analysis has over other elemental analysis techniques such as ICP-MS or AAS are its extensive linear dynamic range, strong matrix tolerance, faster analysis speed and its ability to analyze numerous elements simultaneously. ICP-OES works on the principle that atoms and ions can absorb energy to elevate its valence electrons from the ground state to a higher, excited state. The absorbed energy, normally comes from the heat of an argon plasma that operates at approximately 10 000 K. The excited atoms emit light at a specific wavelength (unique for every element- finger print) as they transition from the excited state to a lower energy level. The concentration of an element is calculated by measuring the amount or intensity of emitted light at a selected wavelength or wavelengths. The amount of light emitted at each wavelength is directly proportional to the number of atoms or molecules releasing their energy and the concentration is calculated according to the Beer Lambert's law.

An ICP-OES instrument is calibrated, using stock solutions containing known amounts of each element being measured and calibrations curves are constructed for quantification. The concentration of an unknown is determined by comparing (plot on calibration curve) the intensity of light emitted at the unique selected wavelengths to that of the calibration data (intensity of the standard solutions of known concentrations).

Components of an ICP-OES

An ICP-OES consists of several key components which include a) a high energy plasma, b) sample aerosolizer or introduction system, c) wavelength separation mechanism, d) detector, and signal processor. These key components required to perform an ICP-OES analysis are illustrated in **Figure 4.9**.

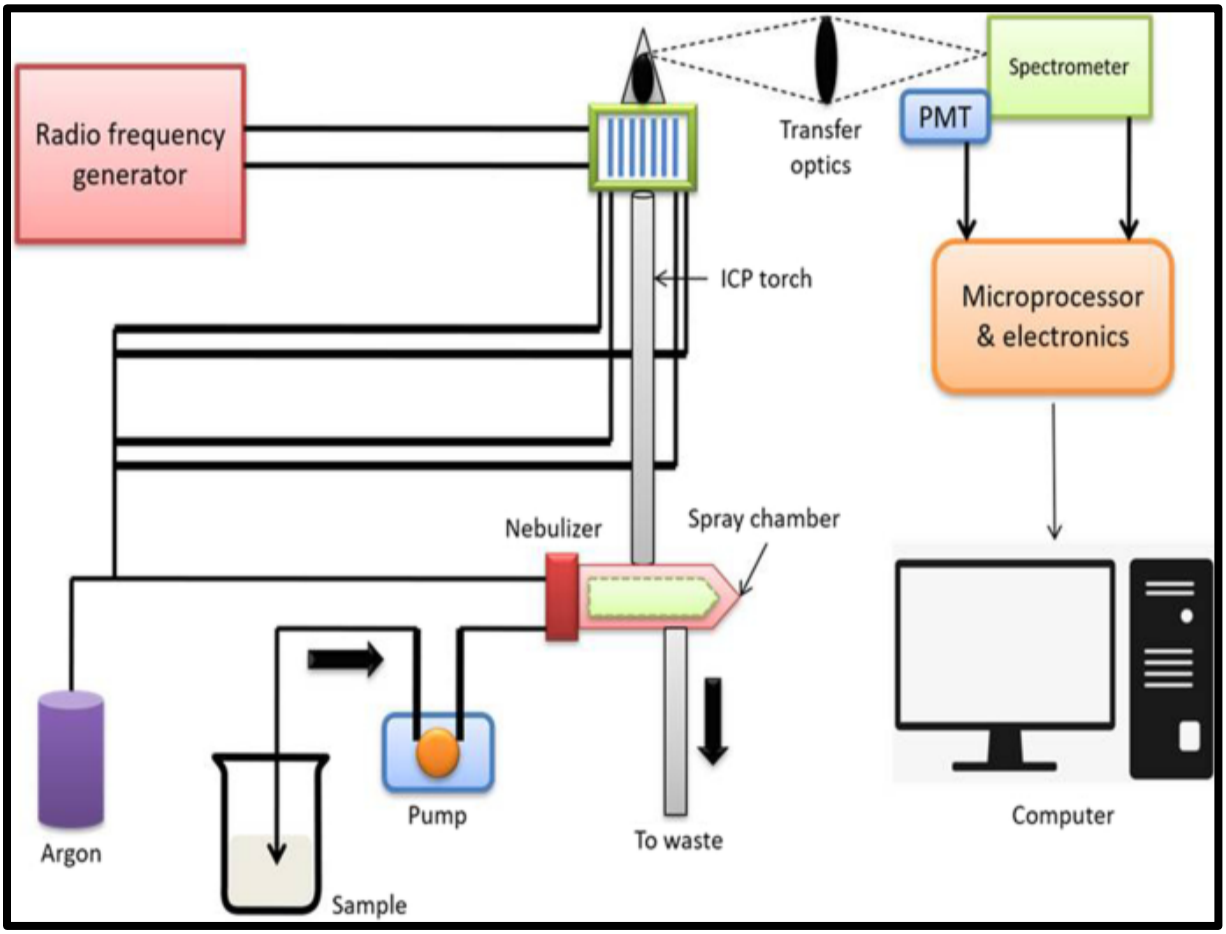

Figure 4.9: ICP-OES set-up diagram (Khan *et al*., 2022).

a) High energy plasma: The high energy plasma is formed when argon gas is ionized in a radio frequency field. The high energy is generated when the gaseous ions and electrons oscillate in opposite directions in the radio frequency field. The friction caused by the movement of ions and electrons in opposite directions within the high-frequency generator is responsible for providing the energy to the plasma flame.

b) Sample introduction system: The sample introduction system consists of a peristaltic pump, nebulizer and a spray chamber. The peristaltic pump transports the sample to the nebulizer and the amount of sample being transported to the nebuliser can be varied by changing the speed of the peristaltic pump or the diameter of the pump tubing. Injection of the sample into the plasma requires the nebulizer to convert the samples into an aerosol. The spray chamber transports the aerosol from the nebuliser to the ICP torch, where the aerosol is desolvated, vapourised and atomized into the plasma flame.

c) Wavelength separation mechanism: Each element absorbs and emits light at a specific wavelength, however, emission lines for multiple elements can overlap or be very close to one another, causing challenges in interpreting the obtained results. This challenge is usually addressed by employing wavelength separation mechanism in the form of an optical grating device (spectrometer) (Levine, 2021). The spectrometer analyses the photons of light emitted by excited electrons as they transition to a lower energy level, subsequently the different wavelengths are either separated sequentially (monochromator) or simultaneously (polychromator) (Khan *et al*., 2022).

d) Detector and signal processor: A detector converts the light energy into an electrical energy/signal. In ICP-OES, signal detection is performed by a so-called 'Charge Injection Device' (CID) or 'Charge Coupled Device' (CCD) (Khan *et al*., 2022; Levine, 2021).

4.9 Conclusion

The successful chemical analyses of complex natural samples and their beneficiation requires a variety of techniques and several different pieces of equipment. Each of the different techniques discussed in this chapter offers unique and complementary insights into the tailings sample that was analyzed. XRD provides structural information, XRF gives a brad elemental overview, SEM, offers detailed morphological and microstructural analysis, while ICO-OES delivers highly sensitive (ultra-trace) elemental data. Sequential extraction aids in the determination of the specific chemical forms in which metals exist within the sample, metals bound to carbonates, Fe or Mn oxides, organic matter or silicates. Together, these techniques provided a comprehensive toolkit for characterization of the Tsumeb tailings sample.

Chapter 5 : Sample Characterization

5.1 Introduction

The mine tailings investigated in this study were obtained from the Tsumeb mine, located in the Northern Oshikoto region of Namibia (**Figure 5.1**) (Cairncross, 2017). The mine's location is regarded as one of the most abundant mineral localities in the world, boasting more than 350 different minerals. It is also renowned for the high quality of the minerals excavated at the site. Perhaps most famous are the excellent examples of azurite (deep-blue copper mineral), cerussite (colourless, white, gray, blue, or green $PbCO_3$ compound), and dioptase (intense emerald-green to bluish-green copper cyclosilicate mineral) that was excavated at this location. The Tsumeb mineral deposits are present in Precambrian carbonates that consist mainly of dolomite and limestone (Cairncross, 2017). These mineral deposits are renowned for their Cu-Pb-Zn-Ag-Ge-Cd deposits.

Figure 5.1: Location of the Tsumeb mine in Northern Namibia (Cairncross, 2017).

Natives from this area knew about the Tsumeb copper-lead deposit long before Europeans explored Africa. The local tribes who knew about the "green stained low hill of

rocks', collected the surface specimens, which they traded with other tribes like the Ovambo tribe, who successfully mastered crude smelting methods to recover the copper from these minerals. Formal mining operations at Tsumeb started in 1906 and continued until 1996, when, at a depth of 1.2 km, mining activities became too expensive to continue, and the mine was subsequently closed. In 2000, under the stewardship of Ongopolo Mining and Processing Limited, the mine re-opened.

The mineral deposits at Tsumeb are present in a nearly vertical pipe that surfaced at the "green-stained low hill." Unique to this deposit is that the elements in these deposits are heavily oxidized to extensive depths, which is attributed to the "Great Fault," which developed some distance away. This major fault lengthened diagonally and systematically deeper from a distance and eventually cut through the Tsumeb ore body at an abnormal depth, causing the oxidation of minerals. Contrary to "normal" upper oxide zone deposits, the Tsumeb mineral deposit has three oxidation zones separated by primary sulfide ore deposits. In addition, these different oxide zones contain various combinations of minerals with their own diversity and dominant species present.

The explanation is that normal ore bodies exposed to the atmosphere contain an upper oxide zone where the primary sulfide ores have decomposed and converted to atmospheric or oxide components. Below this oxide zone, the primary ores remain untouched. Still, at Tsumeb, both primary and secondary minerals occur together in some areas due to the exposure to atmospheric conditions due to the "Great Fault." This unique situation at Tsumeb meant that the upper oxide zone stretches much deeper into the earth than usual. After the initial oxide zone was removed, the miners encountered the expected sulfide ores, but deeper, they encountered a second oxide zone containing another treasure trove of specimens like scorodite and wulfenite.

Figure 5.2: Scorodite ($Fe^{3+}AsO_4.2H_2O$) from Tsumeb mine (Origlieri, 2005).

Figure 5.3: Wulfenite (PbMoO4) from Tsumeb mine (Watzl, 2013).

In the upper oxide zone at Tsumeb, exceptional quality azurite and malachite (**Figure 5.4**) were unearthed, the middle zone was well known for cerussite and dioptase discoveries, while the lowest oxide zone for high-quality smithsonite deposits as well as rare scorodite crystal deposits. The lower oxide zones also contain the primary metals and rare elements such as germanium, gallium, and rare earths.

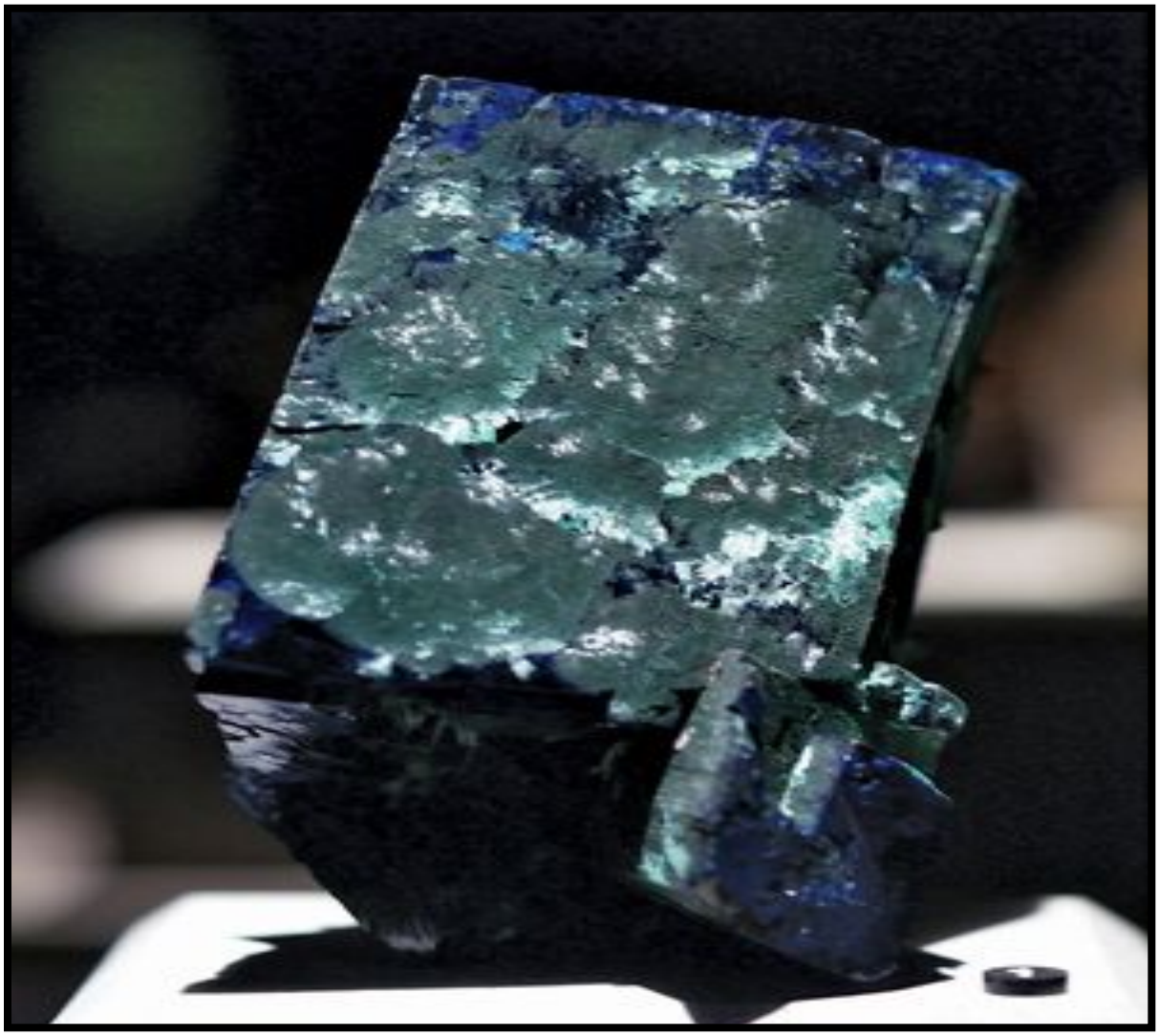

Figure 5.4: Azurite with malachite crystals from the Tsumeb Mine in Namibia (Grimm, 2018).

This mine was home to the largest single sulfidic accumulation of Ge (Melcher, 2003). The mine was decommissioned, but the smelter is in operation after being acquired by Dundee Precious Metals (DPM) in 2010 (*Tsumeb Specialty Smelter, Namibia*, 2024). The smelter is primarily used to process complex Cu concentrates from DPM's Chelopech mine in Bulgaria and other third-party mines. On 7 March 2024, Dundee Precious Metals announced the sale of the Tsumeb smelter for US$ 49 million to Sinomine Resource Group Co. Ltd (Webb, 2024).

Tailings/sample characterization

5.2 Introduction

The initial step in developing a hydrometallurgical process to recover valuable materials from the mine tailings involves a comprehensive physical and chemical characterization of the collected samples. Results obtained from this mineralogical and elemental characterization of the tailings sample will be used to select and guide the chemical processes to recover the two target elements, Ga and Ge, from the tailings.The mineralogical characterization entails solid phase or non-destructive analysis, which includes X-ray diffraction (XRD) and scanning electron microscopy (SEM) with Energy Dispersive X-ray (EDX) analysis that determines the solid phases and characteristics of the tailings (Jamieson *et al*., 2015). A common problem encountered in the characterization of Ga and Ge-bearing samples is their sparse distribution attributed to their low concentration; hence, there are instances where SEM-EDX could not quantify or detect Ga or Ge from Ga and Ge-bearing samples (Rao *et al*., 2019).

The chemical characterization, however, is destructive and determines and quantifies the elemental composition of the tailings. The elemental characterization in this study in this study was carried out with analytical instruments, which included Inductively Coupled Plasma Optical Emission Spectroscopy (ICP-OES), Atomic Absorption Spectroscopy (AAS), and X-ray Fluorescence Spectroscopy (XRF) (Ceniceros-Gómez *et al*., 2018). The low sensitivity of XRF to trace elements limits its application in trace and micro-analysis of elements present in samples. The same can be said about AAS; these two analytical

techniques are more suited for major elements in Ga and Ge resources (Qin *et al*., 2015). The chemical characterization also included a sequential extraction process to try and identify the type of components in the sample (possible cation and anion association) to explain sample solubility and characterization, as well as a total dissolution step to identify and quantify all the elements in the sample.

5.2.1 General experimental procedure, equipment, and chemicals

5.2.1.1 General Experimental Procedure

The tailings sample was homogenized and finely milled (10 minutes at 30 Hertz) using an Anton Paar Ball Mill BM500 and passed through a sample splitter. All reactions were performed in triplicate. All chemicals and reagents used were of analytical grade (AR); the suppliers and purity of the reagents are provided in **Table 5.1.** Analytical standards were supplied by Sigma-Aldrich, South Africa. Ultra-pure water produced from a Hydro Health Reverse Osmosis Unit was used.

Table 5.1: Chemical Reagents and respective suppliers.

Reagent	Formula	Purity	Supplier
Acetic acid	CH_3CO_2H	99.7 %	Sigma-Aldrich
Nitric acid	HNO_3	65 %	Sigma-Aldrich
Sulfuric acid	H_2SO_4	98 %	Sigma-Aldrich
Phosphoric acid	H_3PO_4	85 %	Merck
Hydrochloric acid	HCl	32 %	Minema Chemicals
Sodium hydroxide	NaOH	AR	Sigma- Aldrich
Lithium metaborate	$LiBO_2$	AR	Sigma-Aldrich
Hydrogen peroxide	H_2O_2	30 %	Sigma-Aldrich
Hydroxylamine	NH_2OH	50 %	Sigma-Aldrich
Ga Standard for ICP	Ga	-	Sigma-Aldrich
Ge Standard for ICP	Ge	-	Sigma-Aldrich
ICP multi-element standard	-	-	Supelco

Calibration standards for ICP analysis were prepared using 1005 mg/l ± 2mg/l Ge, 1000 mg/l ± 2 mg/l Ga and 100 mg/l multi-element standard (Sb, Al, As, Be, Cd, Ca, Cr, Co, Cu, Fe, Pb, Li, Mg, Mn, Mo, Ni, Se, Si, Sr, Tl, Ti, V, Zn). The calibration standards for Ga and Ge were prepared by quantitatively transferring 0.025, 0.05, 0.1, 0.15, 0.2, and 0.3 ml into 100 ml volumetric flasks and filled to the mark with 0.1 M HNO_3 solution. Similarly, the calibration curves were prepared for the multi-element standard by quantitatively transferring 0.05, 0.1, 0.3, 0.5, 0.7, and 1 ml of the standard into 100 ml volumetric flasks and filling to the mark with 0.1 M HNO_3 solution. The selected wavelengths for ICP analysis are provided in **Table 5.2.**

Table 5.2: Selected wavelengths for Tsumeb tailings ICP-OES analysis.

Element	Wavelength
Ga	287.424
Ge	219.871
Cu	327.396
Pb	280.200
Zn	202.548
Al	396.152
Fe	259.940
Mn	259.372
Si	288.158

Total dissolution

0.1 g (accurately weighed to 0.1 mg) of the finely milled tailings sample was digested with 1 g lithium metaborate in a muffle furnace for 3 hours. The resulting molten solution was cooled, and 4 ml of 65% HNO_3 was added. The solution was transferred into a 100.0 mL volumetric flask and filled to the mark with deionized water.

5.2.1.2 Equipment

- XRD analysis was conducted using a PANalytical Empyrical with a Cu-anode X-ray tube.
- Teledyne Leeman Prodigy 7 ICP-OES
- Rigaku Primus IV WD XRF spectrometer
- JSM-7800F Extreme-resolution Analytical Field Emission SEM-EDX
- Disk rotator
- Eppendorf 5800R Centrifuge
- Muffle furnace
- Water Bath
- Analis Namur horizontal Sieve Shaker
- Sartorius CP64 analytical Balance

5.2.2 Mineralogical Characterization and Discussion

Mineralogical characterization refers to the comprehensive analysis and identification of minerals contained in a rock, ore, soil, or sediment sample. This process is crucial for understanding the minerals' composition, structure, and properties, essential in fields such as mining, metallurgy, material, and environmental sciences. Mineralogical characterization aims to identify the types of minerals, their abundance, distribution, mineral associations, and their physical and chemical properties.

Mineralogical characterization is widely performed with the aid of non-destructive analysis techniques. Non-destructive analysis techniques are diverse and powerful tools that enable molecular and elemental analysis to be carried out without sample pre-treatment (Gredilla *et al*., 2016; Olivares *et al*., 2009). Solid samples' pre-treatment (extraction or digestion) is generally long and expensive and usually generates hazardous waste (Gredilla *et al*., 2016). Non-destructive techniques allow for sample analysis without alteration or damage to the sample.

This study used the following non-destructive techniques: XRD, XRF, SEM-EDS, magnetic separation, and particle size characterization. XRD was used to determine the different mineralogical phases, while XRF and SEM-EDS were employed to characterize the elemental composition of the Tsumeb tailings sample. Magnetic separation was used to separate the tailings sample into magnetic and non-magnetic fractions to determine further the possible distribution of the target elements between the two fractions. Finally, particle size characterization was performed to determine fraction sizes and the concentration of Ga and Ge between those fractions.

5.2.2.1 XRD characterization

The mineralogical composition of the Tsumeb tailings was performed using a Panalytical Empyrean X-Ray Diffractometer (XRD) equipped with a side-window tube (anode consisting of copper and tungsten cathode) with an X-Celerator detector. Samples were scanned between 3.5° and 70° 2θ at tube settings of 45 kV and 40 mA. Data Collector v3.0c was used for data collection, and phase identification was performed using the

X'Pert Highscore Plus software. Rietveld method was used to estimate the relative phase amounts.

The Tsumeb mine is known for its diverse mineralization. Several geological studies, research papers, and reports have been published on the mineralogy of the Tsumeb mine and its host region (Ettler *et al*., 2009, 2021; Lohmeier *et al*., 2021). The results obtained from the XRD analysis are reported in **Table 5.3**. The XRD analysis results depict an even distribution of quartz (silicon element (SiO_4)) and orthopyroxene at 24 %, the least fraction is olivine at 19 %, while magnetite (iron ores (Fe_3O_4) is the dominating fraction with 37 %.

Table 5.3: Mineralogical determination by X-ray diffraction Analysis (XRD).

	Quartz	Orthopyroxene	Olivine	Magnetite
Tailings sample	24 %	24 %	19 %	33 %

The occurrences of quartz in the Tsumeb mine have been reported (Foord & Conklin, 1982; Schlüter *et al*., 2013). Furthermore, quartz is known not to react with most acids except HF and concentrated phosphoric acid (Pan et al., 2022). Magnetite is an iron oxide mineral not commonly reported in the Tsumeb mine (Nadoll *et al*., 2014; Pitiya & Peter, 2021). Its appearance in the tailings sample can be attributed to its being localized to specific zones or because of mineralization events at the mine. Olivine, a magnesium iron silicate $(Mg,Fe)_2SiO_4$, has been reported in Tsumeb tailings and slag. These Olivines were reported to be Zn-bearing (8.74 wt.%) (Ettler *et al*., 2009). The XRD spectrum of the tailing showing the mineral peaks is provided in **Figures 5.5 and 5.6.**

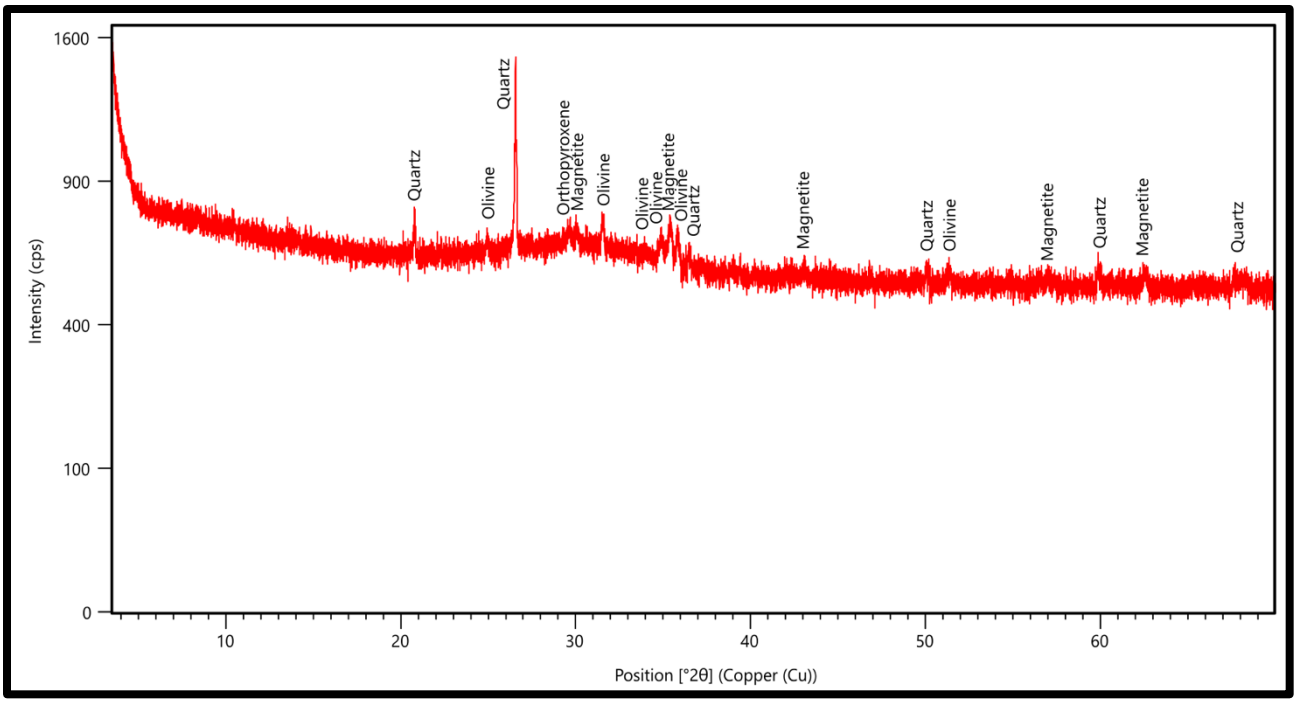

Figure 5.5: XRD spectrum of the Tsumeb tailings.

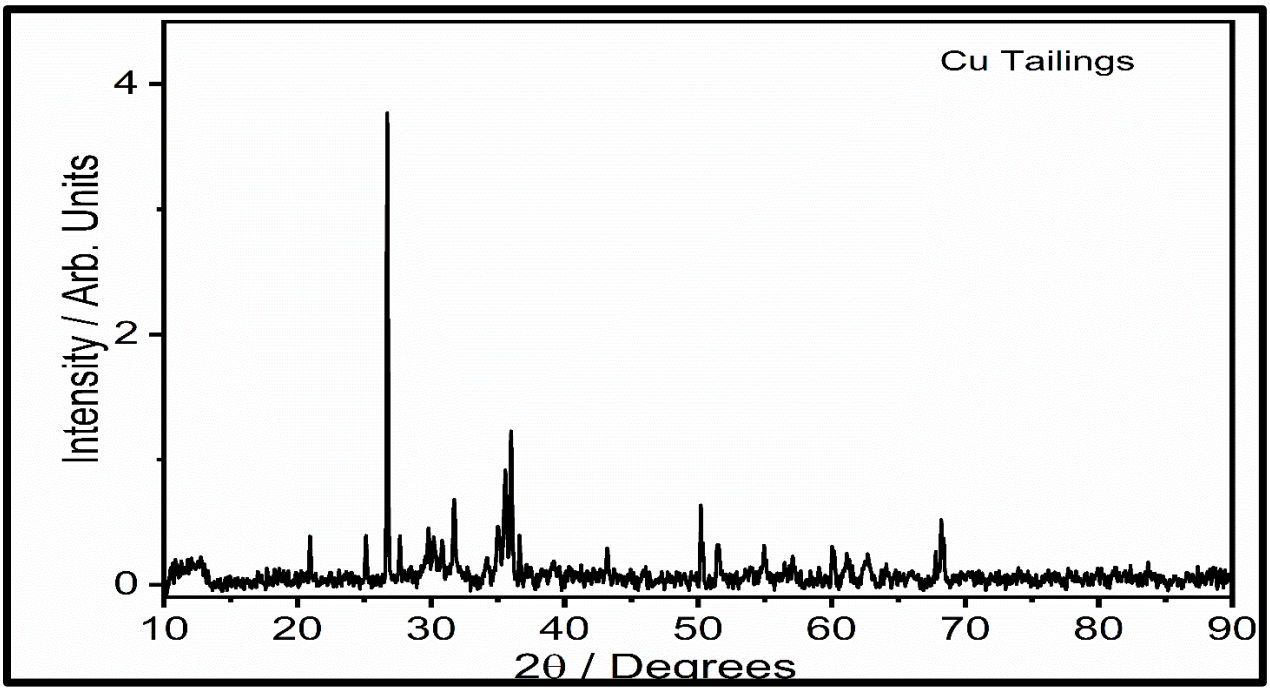

Figure 5.6: Refined XRD spectrum of Tsumeb tailings.

5.2.2.2 XRF characterization

The concentration of the major and minor elements was determined using a Rigaku Primus IV WDXRF spectrometer equipped with a 4 – kW Rh-anode, X-ray tube, four filters, five crystals, a scintillator detector, and a P10 flow detector. The pellets were prepared by mixing an 8 g sample of the Tsumeb tailings with 3 g Hoechst wax (binder material). Subsequently, the mixture was compressed to 30 tons of pressure, forming flat-like discs measuring 27 mm in diameter and 9 mm thick. The results of the major and minor elements are reported in **Table 5.4** and **Table 5.5,** respectively. Silicon dioxide (SiO_2) was found to be one of the major constituents, with a content of 38.34 wt.%. Other major elements present in the tailings were Fe_2O_3 at 31.40 wt.%, CaO at 11.66 wt.%, Al_2O_3 at 4.18 wt.% and finally MgO at 3.40 wt.%. Previous reports on the mineralogical characterization of slags from the Tsumeb mine indicated the presence of 9.82 -35.50 wt.% SiO_2, 8.42-64.22 wt.% Fe_2O_3, 3.85 -17.44 wt.%, CaO, and 2.82-18.50 wt.% Al_2O_3 and the results obtained from the current study fall within the ranges previously reported (Ettler *et al*., 2009; Lohmeier *et al*., 2021).

Table 5.4: XRF major element analysis of Tsumeb tailings.

Major elements	**Wt.%**		
	This study	Ettler *et al*., (2009)	Lohmeier *et al*., (2021)
SiO_2	38.34	9.82-35.50	34.34
Al_2O_3	4.18	2.82-18.50	3.91
Fe_2O_3	31.40	8.42-64.22	33.86
CaO	11.66	3.85-17.44	12.60
MgO	3.40	0.69-5.01	4.22
TiO_2	0.33	0.15-0.70	0.22
MnO	0.26	0.08-0.26	0.28
Na_2O	0.37	0.80-4.31	1.20
K_2O	0.48	0.10-0.61	0.34
P_2O_5	0.28	0.22-0.59	0.30

In addition, the previously reported data also reported the presence of metal and metalloid elements such as Pb (0.97-18.38 wt.%), Cu (0.49-12.18 wt.%), Zn (2.8-12.09 wt.%), As (0.09-7.59 wt.%), Ga (0.97-48 mg/kg), Ge (2.4-123 mg/kg). Similarly, the trace elements in the Tsumeb tailings in this study correlate well with those reported in previously studied Tsumeb slags (Ettler *et al*., 2009; Lohmeier *et al*., 2021).

Table 5.5: XRF trace element analysis of Tsumeb tailings.

Trace elements	**mg/kg**		
	This study	Ettler *et al*., (2009)	Lohmeier *et al*., (2021)
Ga	-	0.97-48	101
Ge	-	2.4-123	-
Cr	1002	201-1576	331
Co	6972	27-4244	203
Ni	137	8-252	-
Cu	8482	4963-121850	7290
Zn	32277	28188-120850	47000
As	10145	930-75865	5607
Sr	178	-	331
Zr	202	-	-
Mo	1776	-	910
Ba	2327	240-3150	3692
Pb	30970	9763-183800	26800
V	85	-	128

5.2.2.3 SEM/EDX Characterization

The Free State's Centre for Microscopy analyzed a sample of the Tsumeb tailings for semi-quantification using scanning electron microscope-energy dispersive spectroscopy (SEM-EDX). The sample was mounted on aluminum pin stubs using double-sided carbon tape and coated with approximately 10 nm of iridium using a Leica EM ACE600 sputter coater. The sample was imaged and analyzed using Aztec software with a JSM-7800F Extreme-resolution Analytical Field Emission SEM equipped with an Oxford instrument X-Max 80 mm EDX detector. Samples were imaged at 5 kV at a WD of 10 m.m. EDX analysis was performed at 20kV. The composition analysis of the tailings revealed high levels of Fe (24.9 %) and Si (16.2 %). These high levels of Fe and Si agree with the XRF and XRD results that revealed the major elements and phases to be SiO_2 and Fe_2O_3. **Figure 5.7** depicts the EDS spectrum percentage of the elements detected in the sample.

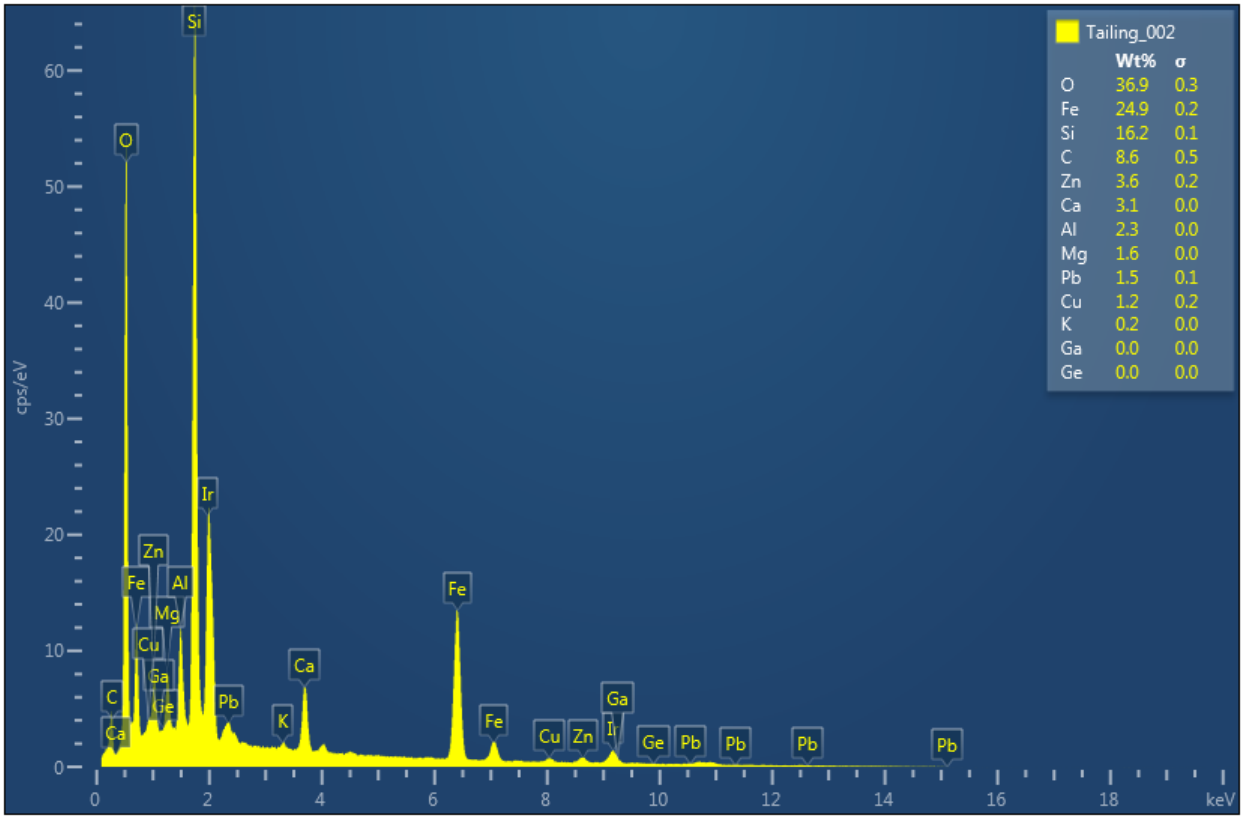

Figure 5.7: EDS results obtained for the Tsumeb tailings.

Figures 5.8 and **5.9** depict images of the microstructures of the Tsumeb tailings sample. These images display glassy fragments indicative of quartz/amorphous materials.

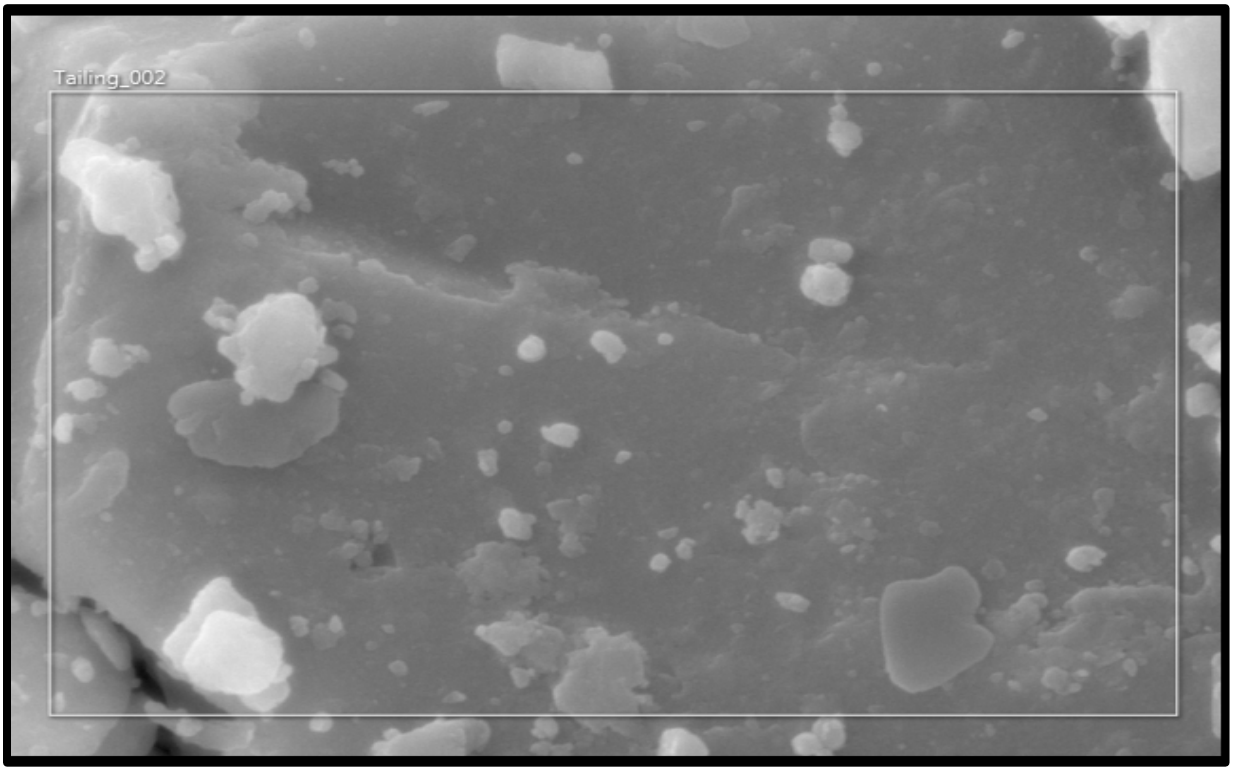

Figure 5.8: Microstructure of the Tsumeb tailings.

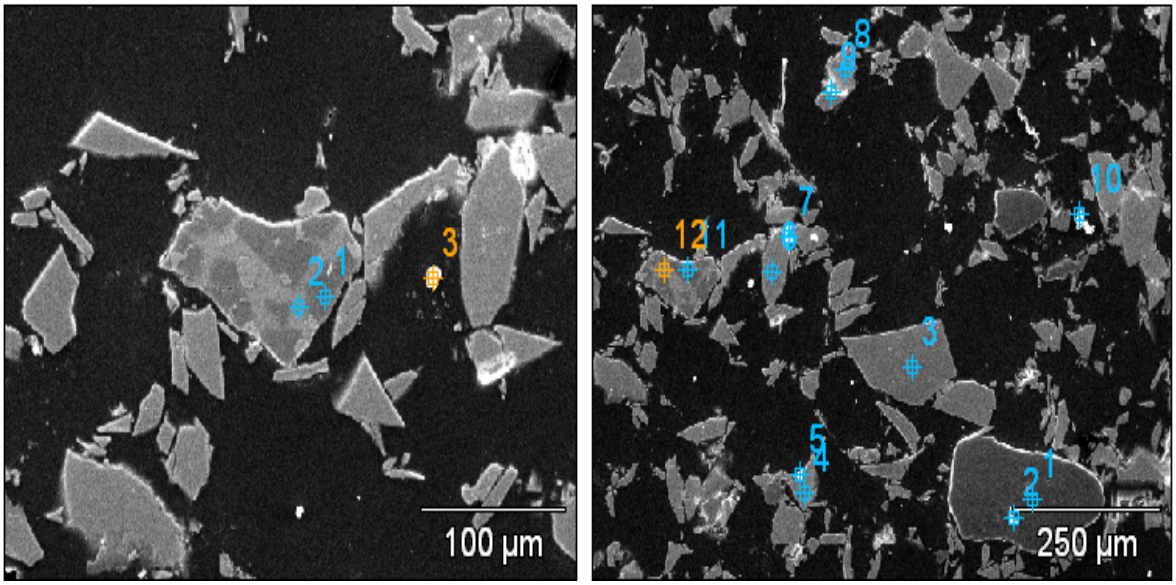

Figure 5.9: Microstructure of the Tsumeb tailings.

5.2.2.4 Magnetic separation

Magnetic separation is a valuable tool for pre-concentrating ore or tailings samples and removing magnetic impurities in the initial stages of a beneficiation process. In this study, magnetic separation was applied to try and concentrate Ga and Ge in one of the portions and to try and separate them from Cu, Pb, and Zn. As the XRD and XRF analysis already established, the major phases of Tsumeb tailings are quartz, magnetite, orthopyroxene, and olivine. Magnetite is ferrimagnetic and is known for its high magnetic susceptibility. In contrast, the other three mineralogical phases are characterized by low magnetic susceptibility; quartz is diamagnetic, and orthopyroxene and olivine are both paramagnetic. The reasons mentioned above informed the decision to separate a sample of the Tsumeb tailings into magnetic and non-magnetic portions.

Triplicate portions of a 1 g (accurately weighed to 0.1 mg) samples of the Tsumeb tailings were evenly spread over a glass surface. The magnetic fraction was separated from the non-magnetic fraction using a handheld magnet. The two portions were digested with 1 M H_3PO_4 and analyzed using ICP-OES. The leaching results from the magnetically separated portions showed that Ga and Ge were present in both portions. The magnetic portion was weighed and determined to constitute 43 % of the tailings sample, while 57 % comprised the non-magnetic portion. The percentages for Ga and Ge differed by only 10 % and 17 %, respectively. Furthermore, Cu, Pb, and Zn were also similarly present in the magnetic and non-magnetic fractions with differences of 10% or less **(Table 5.6).** Thus, it is concluded that magnetic separation does not aid the separation recovery of Ga or Ge.

Table 5.6: Leaching results of the magnetic and non-magnetic portions.

Element	Magnetic (%)	Non-magnetic %
Cu	76.19	68.07
Ga	63.34	53.08
Ge	74.17	91.39
Pb	71.65	62.10
Zn	78.23	72.12

5.2.2.5 Particle Size Characterization

The particle size distribution of the Tsumeb tailings was mechanically determined as follows: three sets of four different sieves sizes of 53μm, 106μm, 250μm, and 500μm were stacked on a horizontal vibrating sieve shaker as displayed in **Figure 5.10.** A 10 g sample of the Tsumeb tailings was transferred to the top of the biggest top sieve, and the mixture was allowed to shake for 5 minutes. Fractions with different sizes were transferred from the largest sieve to the smallest that passed through, and the ones that remained on the different sieves were collected and weighed.

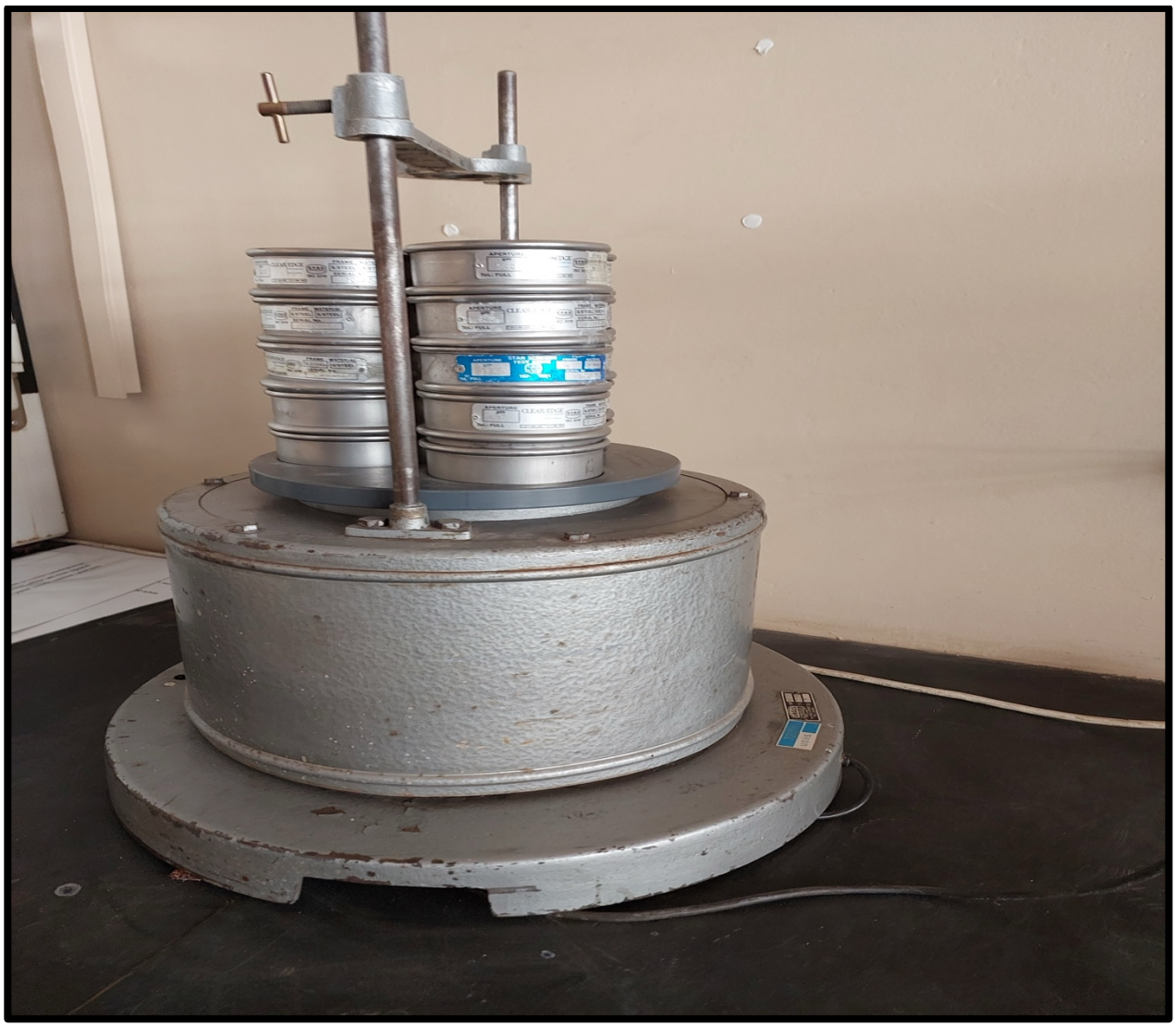

Figure 5.10: Image of horizontal vibrating sieve shaker and sieves used.

Results of the different size fractions were 50.75(4) % for the portion with particle size smaller than 53 μm and 49.43(3) % for the portion with particle size between 53 μm and 106 μm, with a sample loss of 2.6 %**.** The tailings distribution was nearly uniform between the fractions smaller than 53 μm and between 53 μm and 106 μm fractions. No particles were collected for sizes larger than 106 μm. In the next step, Ga and Ge were extracted from 1 g (accurately weighed) of both fractions and digested with 10 mL of 1 M H_3PO_4 for one hour at 300 rpm. The results of the leaching procedure indicated a greater extraction of both Ga and Ge for the fraction smaller than 53μm as compared to the portion size between 53 μm and 106 μm (**Figures 5.11** and **5.12)**. Additionally, Zn was more prevalent in the fraction smaller than 53 μm than in the fraction between 53 μm and 106 μm. The extraction of Cu was extremely low and negligible in both fractions. This observation guided the decision to finely mill all the Tsumeb tailings for subsequent investigations to a size smaller than 53 μm to improve the separation and possible isolation of the two target elements.

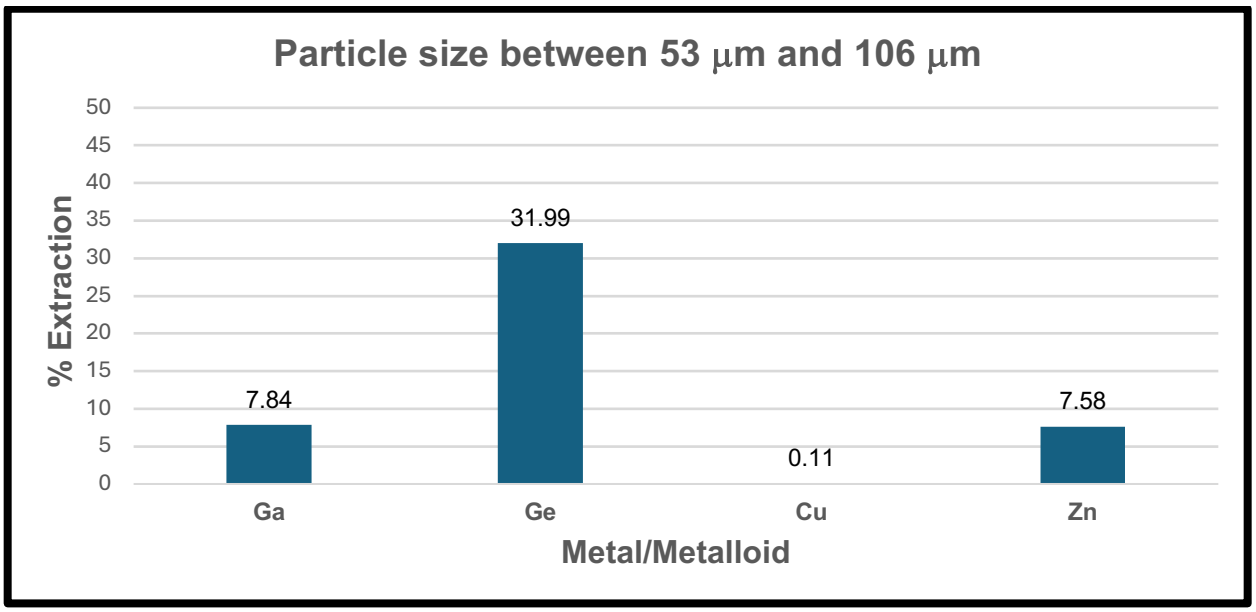

Figure 5.11: Graph of elements present in the portion collected between 53 μm and 106 μm.

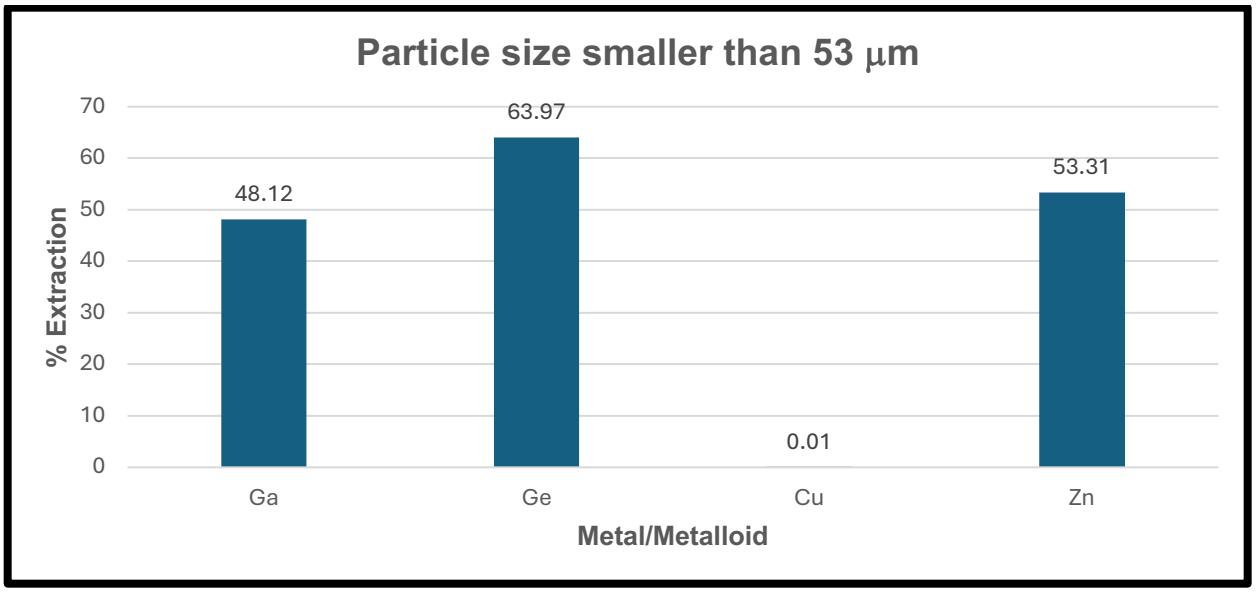

Figure 5.12: Graph of elements in the sample fraction smaller than 53 μm.

5.2.2.6 Comparison of XRD, XRF, and SEM/EDS Results

XRF and SEM-EDS analysis are well-established methods for determining the composition of geological samples, mineral ores, mine and industrial was*te (*Lohmeier *et al.,* 2021*)*. However, the two techniques have limitations in determining Ga and Ge from low-concentration and sparsely distributed Ga and Ge-bearing samples such as mine tailings (Rao *et al*., 2019*)*. This may also be the reason why the XRF or SEM-EDS analysis were unable to detect any Ga and Ge in the Tsumeb tailings.

These two techniques however successfully determined the presence and concentration of other elements such as Cu, Pb, and Zn, which are also of interest to this study. The results are displayed in **Table 5.7.** Pb and Zn results obtained using XRF and SEM/EDS reveal a factor 2 difference for the Pb content. A possible reason for the 2-factor difference in the Pb content result is distribution of Pb in the tailings sample. SEM-EDS analyzes smaller, localized areas, whereas XRF determines an average composition over a larger area. Only minor differences in the Cu and Zn results were obtained. Furthermore, the Cu, Pb and Zn results from both techniques are within range of those previously reported from Tsumeb mine slags (Ettler *et al*., 2009; Lohmeier *et al*., 2021).

Also compared in **Table 5.8** are the mineralogical phases/major elements obtained using XRD and XRF techniques. Two of the phases, quartz, and magnetite, that were determined by XRD were also confirmed by XRF. In addition, these results obtained using the non-destructive techniques as listed in **Table 5.7** have compared with previously conducted studies and are in agreement with those reported studies as depicted in **Tables 5.4** and **5.5.**

Table 5.7: Comparison of XRF, SEM-EDS and XRD analysis results.

XRF analysis		**SEM-EDS analysis**	
Trace elements	**Wt.%**	**Elements**	**Wt.%**
Ga	Not detected	Ga	Not detected
Ge	Not detected	Ge	Not detected
Cu	0.85	Cu	1.2
Pb	3.10	Pb	1.5
Zn	3.23	Zn	3.6
Ni	0.70	Ca	3.1
Cr	0.10	Al	2.3
As	1.01	Mg	1.6
Ba	0.23	K	0.2
Mo	0.20		
XRF analysis		**XRD analysis**	
Major elements	**Wt.%**	**Phases**	**Wt.%**
SiO_2	38.3	SiO_2	24
Fe_2O_3	31.4	Fe_2O_3	33

5.2.3 Chemical Characterization and Discussion

5..2.3.1 Sequential Extraction Procedure

Sequential extraction was performed to partition or fractionate the target elements into their various chemical forms by using a series of chemical reagents with increasing reactivity.

Step1: Extraction of exchangeable, water, and acid-soluble elements

1. A 1g (accurately weighed to 0.1 mg) dry sample was weighed and placed in a 50 ml polypropylene centrifuge tube.
2. 40 ml of 0.11 mol/L acetic acid was added to the tube.
3. The tubes were shaken in a disk rotator at 40 rpm for 16 hours at room temperature.
4. The tubes were centrifuged at 5000 rpm for 20 minutes to separate the solid residue.
5. The supernatant was extracted and stored in polyethylene tubes after acidification with $HNO_{3.}$
6. The solid residue was washed with 20 mL of distilled water at 40 rpm for 15 minutes in a rotator.
7. The washings were decanted into polyethylene tubes and acidified with HNO_3.
8. The supernatant and washings were stored at 4 °C for further analysis, referred to as **Fraction 1 (F1)**.

Step2: Extraction of reducible elements

1. The residues from Step 1 were used for chemical digestion.
2. 40 ml of 0.1 mol/L hydroxylamine hydrochloride (adjusted to pH 2 using HNO_3) was added for digestion.
3. The extraction procedure described in Step 1 was followed.
4. The extracted supernatant was stored as **Fraction 2 (F2)**.

Step 3: Extraction of oxidizable elements

1. The residue from Step 2 was further digested.
2. 10 ml of 8.8 mol/L H_2O_2 (pH 2-3) was carefully added into the tubes.

3. The tubes were covered, and the contents were allowed to react for 1 hour at room temperature.
4. The contents were digested at 85 % in a water bath until the volume was reduced to around 2-3 mL.
5. This step was repeated twice.
6. After cooling, 50 mL of 1 mol/L ammonium acetate (adjusted to pH 2 with HNO_3) was added to the residue.
7. The tubes were shaken in a disk rotator at 40 rpm for 16 hours.
8. The extraction procedure described in Step 1 was followed.
9. The extracted supernatant was stored as **Fraction 3 (F3).**

Step 4. Residual/Silicate bound

1. 10 ml of aqua regia (a mixture of 12 mol/l HCl and 15.8 mol/l HNO_3 in the ratio 3:1) was added to the residue from step 3
2. The mixture was digested for 24 h inside fume hood.
3. It was then boiled on a hot plate for 1 h at 100°C.

5.2.3.2 Results

The first step in the chemical or stepwise destructive characterization of the Tsumeb mine copper tailings was performed with a sequential extraction evaluation process. High levels of Fe, Zn, and Pb were obtained from this sample. The sequential extraction results **(Table 5.8 and Figure 5.12)** revealed that Fe was primarily contained in **F3** in the oxidizable portion in the form of sulfides. A lesser, but still considerate amount of Fe (> 20 000 ppm) was found in the exchangeable, water and acid-soluble portion **(F1)**, while a small fraction of this element was found in the reducible portion of **F2**. Other metals that were also primarily found in the oxidizable fraction **(F3)** included Zn (10 000 ppm), Si (5 600 ppm), and Al (5 600 ppm). Pb, however, was primarily found in the reducible fraction **(F2)**; at concentration levels of 16 900 ppm.

The total quantity of the extracted elements of interest across the different fractions to the total dissolution results performed using flux fusion are reported in **Table 5.8**. Sequential

extraction analysis was unable detect Ga and Ge whereas flux fusion was able to quantify both elements. The total Cu and Zn extracted using sequential extraction is significantly lower than that of flux fusion. A possible reason for the lower quantities is the inability of milder stepwise conditions applied during sequential extraction to not completely extract all the elemental forms, especially those tightly bound. In contrast the amount of Pb extracted from sequential extraction is higher than that of flux fusion.

Other elements found in trace amounts are reported in **Figure 5.12.** As previously mentioned, this sequential extraction procedure did not successfully elucidate the fractionation of Ga and Ge in the mine tailings. Possible reasons for this could be that the Ga and Ge are present in forms resistant to the extraction reagents used or that Ga and Ge are bound with mineral structures that require more aggressive extraction conditions to release them, or their concentration levels were so diluted that they were below the detection levels for the ICP. For **Fraction 4** extraction, little to no residue was left to analyze after the initial three fractional dissolutions. Excessive washing, centrifugation, or decanting may be the cause for inadvertently not having enough residue for the residual portion extraction. Limitations of sequential extraction methods have been well documented; errors between steps can lead to irreproducibility and residue losses during the inter-step washing process.

Table 5.8: Sequential extraction results.

Element	Fraction 1	Fraction 2	Fraction 2	Total	Total dissolution
	mg/kg	mg/kg	mg/kg		
Mn	476	140	777	1393	-
Fe	23366	12727	48795	84888	-
Al	2162	708	5698	8568	-
Si	3097	784	5630	9511	-
Sn	-	-	-	-	-
Ni	-	-	-	-	-
Co	-	-	35	35	-
Cu	1077	116	1994	3187	90100
K	9	-	390	399	-
Zn	6390	2824	10708	19922	234000
Ti	73	-	310	383	-
In	-	-	-	-	-
Pb	2771	16971	4653	24395	7400
Li	-	578	-	578	-
Cr	147	-	470	617	-
Ca	2683	-	3735	6418	-
Ga	Not	Not	Not		18700
Ge	detected	detected	detected		300
	Not	Not	Not		
	detected	detected	detected		

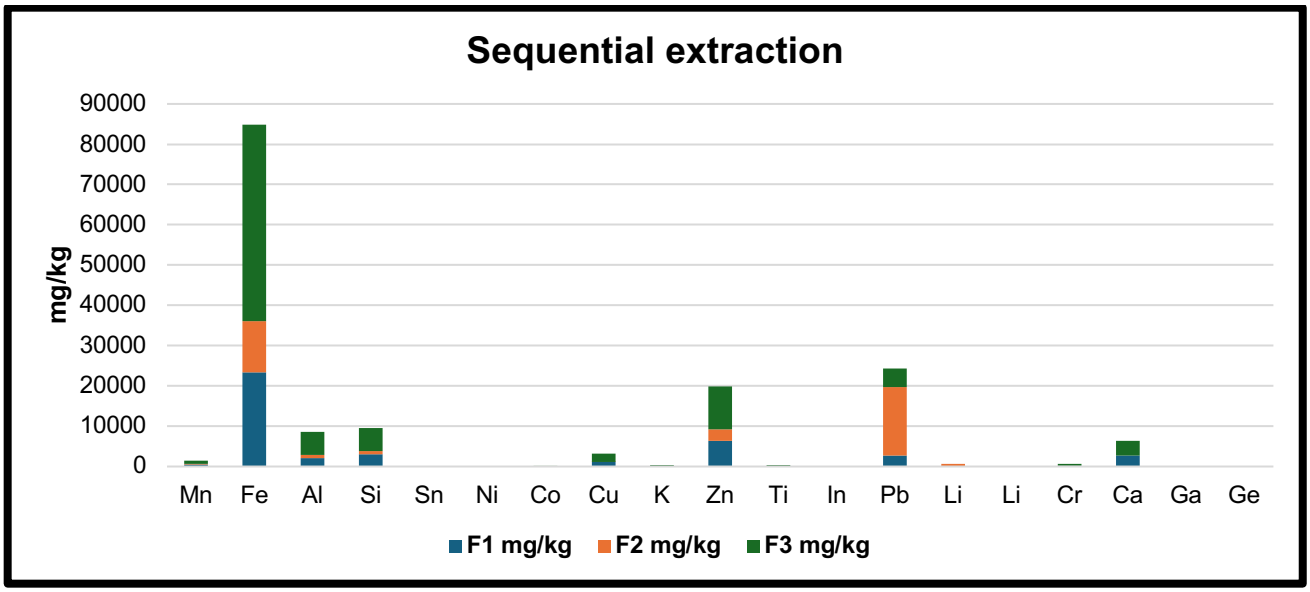

Figure 5.13: Sequential metal extraction of Tsumeb copper tailings.

5.3 Total Dissolution

Elemental characterization was performed by the total dissolution of the tailings sample, followed by analysis with an ICP-OES. An Anton Paar Ball Mill BM 500 (30 Hz, 5 min) was used to finely mill the tailings sample. Subsequently, 0.1 g (accurately weighed to 0.1 mg) of the finely milled tailings sample was digested with 1 g lithium metaborate in a muffle furnace for 3 hours. The resulting molten solution was cooled, and 4 ml of 65% HNO_3 was added. The percentage recoveries of the total dissolution were as follows: Ge (0.0300(2) %), Ga (1.870(5) %), Pb (0.740(5) %), Cu (9.01(12) %), Zn (23(2) %).

From the above results, it can be concluded that Ge is present in trace amounts (0.03 %) in the sample which can be regarded as substantial since Ge concentrations in the ore is about 0.0068 % (68 ppm). The 1.87 % Ga content is also regarded as substantial for a tailing sample, considering that the average reported Ga concentration in zinc sulfides is 0.0057 % (57 ppm) (Schulte and Foley, 2014; Lu *et al*., 2017). The three other dominant elements in the sample, namely Zn, Cu, and Pb, were unsurprisingly present at 23(2) %, 9.01(12) %, & 0.740(5) %, respectively.

Studies have been published on the elemental composition of metallurgical slags from the Tsumeb mine's that were subjected to different smelting technologies. Slags from the following processes were characterized: 1) carbonate processing in Cu-Pb smelter, 2) processing of sulfide ores in Cu and Pb smelting, and 3) granulated Cu smelting. The elemental characterization results were as follows: Zn (2.82-12.09 %), Cu (0.49-12.2 %), Pb (0.97-18.4 %), Ga (0.97 - 48 mg/kg) & Ge (2.4 -123 mg/kg) (Ettler *et al*., 2009). The total dissolution results are in range with published data on the composition of slags from the Tsumeb smelters. The study by Ettler *et al*. (2009) was to determine the speciation of pollutants and possible environmental effects, while the total dissolution done in this chapter serves as a base for developing a process to extract Ga and Ge from the Tsumeb mine tailings.

5.4 Conclusion

The aim of the sample characterization was to get different, but complementary information on the sample properties to ultimately get a cohesive "picture" of the composition of the Tsumeb tailing samples. The XRD results indicated the presence of quartz, magnetite, orthopyroxene, and olivine, the XRF results indicated the presence of quartz, magnetite, calcium oxide, magnesium oxide and aluminium oxide, while the EDS reported O 36.9(3) %, Fe 24.9(2) %, Si 16.2(1) %, Zn 3.6(2) %, Ca 3.1(0) %, Al 2.3 %, Mg 1.6%, Pb 1.5(1) % and Cu 1.2(2) %.

Sequential extraction and total dissolution indicated the presence of substantial amounts of Pb 0.740(5) %, Cu 9.01(12) %, Zn 23(2) % while economic value amounts of Ga 1.87 % and Ge 0.0300(2) % were observed. The combination of these results enabled the development of an effective extraction process for Ga and Ge from these tailings as discussed in **Chapter 6**.

Chapter 6 : Extraction and Isolation of Ga and Ge

6.1 Introduction

As stated in **Chapter 2,** this study aims to develop a hydrometallurgical process for the beneficiation of Ga and Ge from the Tsumeb tailings. The elemental composition and mineralogical phases have been established in **Chapter 5**. The key insights from **Chapter 5** are the trace but economically important amounts of Ga (1.87 %) and Ge (0.03 %) present, while it also contains 24 % quartz. The current price of gallium (11/11/2024) is $918/kg, up from $422/kg on 1/1/2021. In comparison, germanium currently trades at $4000/kg, up from $1984/kg for the same period. These price changes underline the market demand for the two elements with their monetary benefits, hence the importance of recovering the elements from the tailings (Strategic Metals Invest, 2024a, 2024b). It has already been established that low recoveries of Ga and Ge are possible in samples with significant amounts of quartz minerals. These possible low recoveries are due to the inert nature of quartz and the potential formation of SiO_2-GeO_2 and SiO_2-Ga complexes, which are complex to separate.

This chapter deals with two aspects of the beneficiation of Ga and Ge from the Tsumeb smelter tailings sample which contained 18 722 mg/kg/ 1.870(5) % Ga and 310 mg/kg/ 0.0300(2) % Ge (**Paragraph 5.3**). The first part of this chapter evaluates the extraction/leaching of Ga and Ge from the tailings sample, while the second part investigates the separation and isolation of Ga and Ge from these extraction solutions. Different mineral acids and a base were used to extract Ga and Ge from the tailings sample. Subsequently, the isolation of the elements was investigated with the aid of pH adjustment precipitation.

The leaching efficiencies of the different acids and bases were evaluated and compared, and the best candidates were selected for optimization. During the optimization steps, factors such as acid concentrations, stirring speed, sample mass, and leaching time were

varied to obtain the best conditions for chemical processing. Finally, solutions with higher Ga and Ge concentrations were obtained from the optimization step and subsequently used to isolate Ge and Ga from the leachate using pH adjustment precipitation.

6.2 Experimental Methods and Materials

6.2.1 General Experimental Procedures

The tailings sample was homogenized and finely milled (10 minutes at 30 Hertz) using an Anton Paar Ball Mill BM500 and passed through a sample splitter. The initial reactions were performed at 25 °C, while the post-optimization reactions were performed at 90 °C and their chemical analysis was performed in triplicates. All reactions preceding the optimization reactions were carried out on a 1 g tailing sample, leached for one hour at a stirring speed of 300 rpm.

6.2.2 Reagents

All chemicals and reagents used were of analytical grade (AR); the suppliers and purity of the reagents are provided in **Table 6.1.**

Table 6.1: Chemical reagents and suppliers used.

Reagent	Formula	Purity	Supplier
Nitric acid	HNO_3	65 %	Sigma-Aldrich
Sulfuric acid	H_2SO_4	98 %	Sigma-Aldrich
Phosphoric acid	H_3PO_4	85 %	Merck
Hydrochloric acid	HCl	32 %	Sigma-Aldrich
Sodium hydroxide	NaOH	AR	Sigma-Aldrich
Ga standard for ICP	Ga	-	Sigma-Aldrich
Ge standard for ICP	Ge	-	Sigma-Aldrich
ICP multi-element standard	-	-	Supelco
Germanium dioxide	GeO_2	99.99 %	Merck
Gallium chloride	$GaCl_3$	99.99 %	Merck

6.2.3 Equipment

- Anton Paar Ball Mill BM500
- Teledyne Leeman Prodigy 7 ICP-OES
- Eppendorf 5800R Centrifuge
- Sartorius CP64 analytical Balance
- Bruker Tensor 27 model FTIR

ICP-OES analysis calibration

Analytical standards were obtained from Sigma-Aldrich, South Africa, while ultra-pure water produced from a Hydro Health Reverse Osmosis Unit was used. Calibration standards for ICP analysis were prepared using 1005 mg/l ± 2mg/l Ge, 1000 mg/l ± 2 mg/l Ga and 100 mg/l multi-element standard (Sb, Al, As, Be, Cd, Ca, Cr, Co, Cu, Fe, Pb, Li, Mg, Mn, Mo, Ni, Se, Si, Sr, Tl, Ti, V, Zn). The calibration standards for Ga and Ge were prepared by quantitatively transferring 0.025, 0.05, 0.1, 0.15, 0.2, and 0.3 mL into 100.0 mL volumetric flasks and filled to the mark with 0.1 M HNO_3 solution. Similarly, the calibration curves for the other elements were prepared using the multi-element standard and quantitatively transferring 0.05, 0.1, 0.3, 0.5, 0.7, and 1.00 mL of the standard into

100.0 ml volumetric flasks and filling to the mark with 0.1 M HNO_3 solution. The selected wavelengths for ICP analysis are reported in **Table 6.2.**

Table 6.2: Selected wavelengths for ICP-OES analysis.

Element	Wavelength
Ga	287.424
Ge	219.871
Cu	327.396
Pb	280.200
Zn	202.548
Al	396.152
Fe	259.940
Mn	259.372
Si	288.158

6.3 Results and Discussion of Ga and Ge Leaching from Tailings

Initial Leaching Reactions

Four different mineral acids, namely nitric, sulfuric, phosphoric and hydrochloric acid, with concentrations of 1 M, were used to investigate the possible extraction/leaching of Ga and Ge, but also other important elements in the sample such as Cu, Pb, and Zn from the Tsumeb tailings. These preliminary/initial reactions were performed to determine a suitable reagent or a combination of reagents for extracting Ga and Ge from the tailings sample. The reactions were performed at room temperature on a 1 g (accurately weighed to 0.1 mg) sample. The reactions were performed at room temperature with a solid-to-liquid ratio of 1 g:10 mL. The reactions were stirred for one hour with a stirring speed of 300 rpm. The reaction mixture was filtered, and the filtrate was quantitatively transferred to a 100.0 mL volumetric flask and filled to the mark. The obtained leachates were analyzed using the ICP, and the results are reported in **Table 6.3.**

Table 6.3: Initial extraction (%) results using the various mineral acids.

Element	H_2SO_4	HCl	H_3PO_4	HNO_3
Cu	3.26	4.72	16.85	4.61
Zn	3.61	7.30	67.52	7.12
Pb	1.92	5.43	11.34	5.67
Ge	40.63	23.44	25.00	10.73
Ga	4.44	5.11	46.67	4.60

Promising results were obtained from these initial reactions. Phosphoric acid had the highest Ga extraction of 46.6(4) %, while simultaneously extracting 16.85(5) % Cu, 67.52(3) % Zn, and 11.3(5) % Pb while only extracting 25.0(6) % Ge. Meanwhile, sulfuric acid extracted 40,6(2) % Ge and only small quantities of the four other elements of interest, such as Ga (4.44(9) %), Cu (3.3(4) %), Zn (3.6(2) %), and Pb (1.9(2) %). These initial results were very promising and indicated a potential separation of Ga and Ge using these two acids. Hydrochloric acid demonstrated the second-best leaching efficiency for Ge at 23.4(4) %, as well as 5.11(7) % Ga, 4.7(2)

% Cu, 7.3(4) % Zn, and 5.4(4) % Pb. The extraction results for the five different elements using the varying four mineral acids are graphically displayed in **Figure 6.1.**

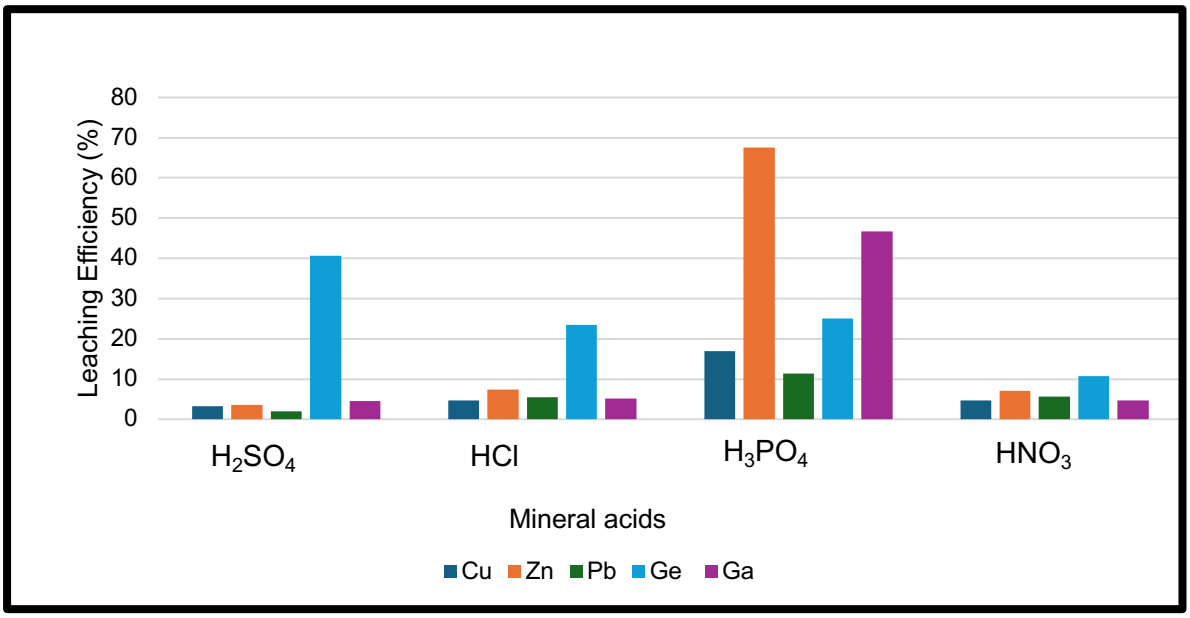

Figure 6.1: Extraction reactions comparing different mineral acids at 25 °C, a stirring speed of 300 rpm, and a mass-to-liquid ratio of 1 g:10 mL.

It was also decided to investigate the possible extraction of the main elements from the tailings using a base leachant, which was discussed in **Chapter 3,** as a method to circumvent silica gel formation (Rao *et al*., 2019). It was reported that Si and Ge exist in stable forms of $SiO_3(OH)^{3-}$ and $HGeO_3^-$ in solutions of pH higher than 12 and that the separation of the two complexes can be achieved by adjusting the solution pH. For this reason, alkaline leaching of the tailings sample using sodium hydroxide solutions of different concentrations was evaluated, and the results are reported in **Figure 6.2**. The reactions were performed at room temperature on a 1 g (accurately weighed to 0.1 mg) sample and quantitatively transferred to a 50 mL glass beaker. 10 mL of the different base concentrations were added to the solid samples and the mixtures was stirred on a hot plate for one hour with a speed of 300 rpm at 25 °C. The reaction mixture was filtered, and the filtrate was quantitatively transferred to a 100.0 mL volumetric flask and filled to the mark.

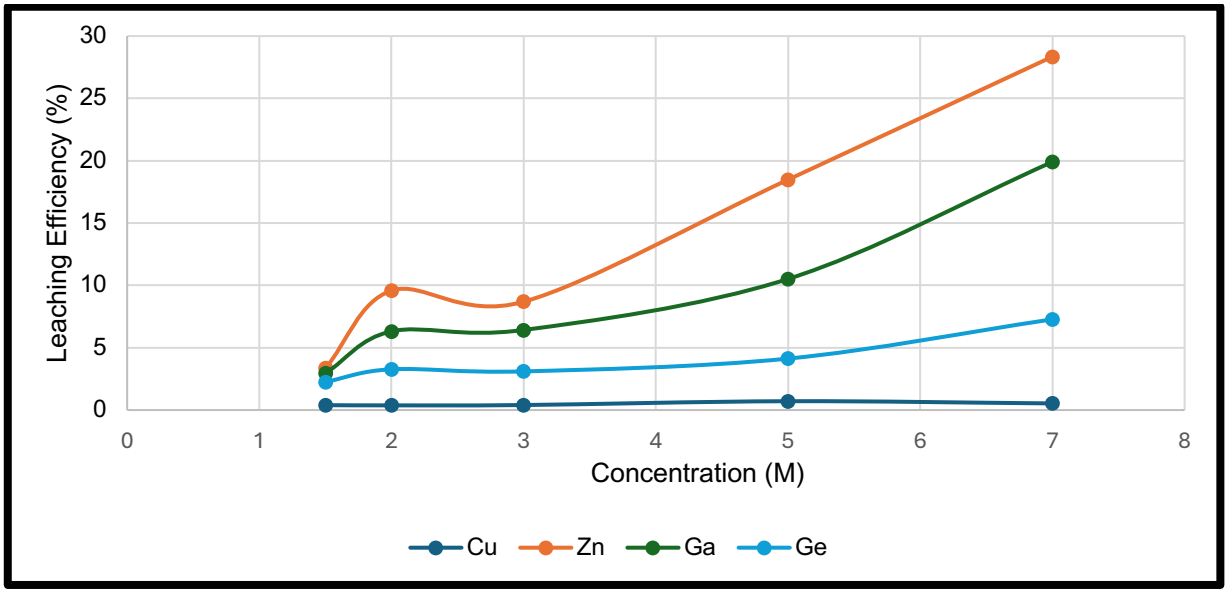

Figure 6.2: Elemental extractions using different sodium hydroxide concentration at 25 °C, a stirring speed of 300 rpm and mass to liquid ratio of 1 g:10 mL.

The initial elemental extraction at 1.5 M was very low, between 0.5 % and 4.5 % for the different elements, but increased steadily with an increase in alkali concentration. The leaching of Ga and Ge, in particular, increased substantially with Ga displaying a steep increase while Ge showed a more moderate increase. The leaching efficiencies at 1.5 M were 2.95 % Ga and 3.27 % Ge. The extraction of both target elements was highest at 7 M, the maximum concentration evaluated, with 19.91 % Ga and 7.27 % Ge. Even at high alkaline concentrations, the low extraction of Ga and Ge was deemed not economically feasible. Previous studies reported that alkaline extractants such as NaOH and CaO result in low extraction of Ga and Ge yields ranging from 9 to 51 %.

Nonetheless, a 70% Ga extraction yield was obtained from a different matrix (coal fly ash) sample after leaching for 24 hours performed by Arroyo *et al*. (2014). The publications in the current study showed that alkaline leaching is more likely to yield good recoveries of Ga than Ge (Xue *et al*., 2019). The same is true for this present study as observed at 7 M NaOH. The Ga was extracted more than double the quantity of Ge, with extractions of 19.9(4) % Ga at least double the 7.3(2) % achieved with Ge.

.

6.4 Extraction of Ga

Extraction of Ga with H_3PO_4

From the results reported in **Figure 6.1**, it is clear that phosphoric acid had the highest leaching efficiency for Ga and the second highest for Ge among the tested mineral acids. For this reason, phosphoric acid was chosen as the preferred leaching reagent that can successfully extract Ga from the Tsumeb tailings. Reactions with variation in phosphoric acid concentration were performed. The reactions were performed at room temperature on a 1 g (accurately weighed to 0.1 mg) sample and quantitively transferred to a 50 mL glass beaker. 10 mL of 1 M acids were added to the solid sample and the mixture was stirred on a hot plate for one hour with a speed of 300 rpm at 25 °C. The reaction mixture was filtered, and the filtrate was quantitatively transferred to a 100.0 mL volumetric flask and filled to the mark.

The results are graphically displayed in **Figure 6.3** and indicate the influence of different phosphoric acid concentrations on the Ga recovery. Furthermore, these results show that approximately 80 % of the Ga can be extracted with approximately 2 M H_3PO_4.

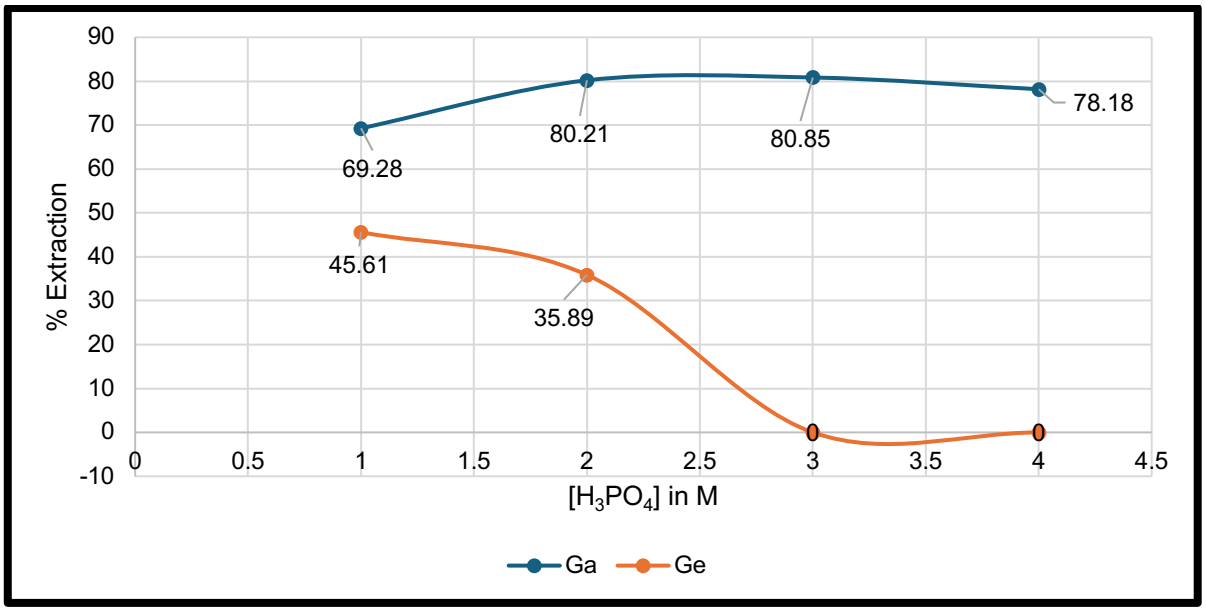

Figure 6.3: Ga and Ge extraction with varying phosphoric acid concentrations, 25 °C, a stirring speed of 300 rpm and mass to liquid ratio of 1 g:10 mL.

The optimum acid strength for extracting Ga and Ge from the tailings sample was investigated by varying the phosphoric acid concentration. In **Figure 6.3,** the highest extraction of Ga was obtained from leaching with 3 M H_3PO_4. However, the difference between the extraction of Ga with 3 M and 2 M acid is only 0.64 %. Therefore, the optimum H_3PO_4 concentration for Ga leaching was selected as 2 M since the 0.64 % increment from 2 M to 3 M was deemed negligible. The optimum H_3PO_4 concentration for the extraction of Ge was also found to be 2 M, as depicted in **Figure 6.3**.

At the same time, it is evident from **Figure 6.3** that very little Ge was extracted at 3 M H_3PO_4. At this concentration, a precipitate formation in the reaction vessel was observed. These results clearly indicated a possible way to separate Ga from Ge.

6.5 Extraction of Ge

In the previous subsection **(Paragraph 6.4.1)**, phosphoric acid clearly displayed good Ga extraction compared to Ge extraction. In this subsection, a suitable acid, including HNO_3 and H_2SO_4 and its corresponding optimum concentration for Ge extraction were investigated. Hydrochloric acid was excluded from the acid variation study due to its high acid consummation and low leaching efficiency for Ge (Patel & Karamalidis, 2021).

6.5.1 HNO_3 Leaching

From the initial reactions, nitric acid had overall low leaching efficiencies for all the elements; however, the leaching efficiencies for the different elements were of proximate similarities: 10.7(8) % Ge, 4.6(4) % Ga, 4.6(3) % Cu, 7.1(5) % Zn, and 5.7(6) % Pb. In order to verify the leaching efficiency of nitric acid for further inclusions or exclusion in this study, reactions with variation in nitric acid concentrations were performed in search of the optimum concentration that may possibly yield higher leaching efficiencies.

The reactions were performed at room temperature on a 1 g (accurately weighed to 0.1 mg) sample and quantitatively transferred to a 50 mL glass beaker. 10 mL of the different HNO_3 concentrations was added to the solid sample and the mixture was

stirred on a hot plate for one hour with a speed of 300 rpm at 25 °C. The reaction mixture was filtered, and the filtrate was quantitatively transferred to a 100.0 mL volumetric flask and filled to the mark. The results are graphically displayed in **Figure 6.4**

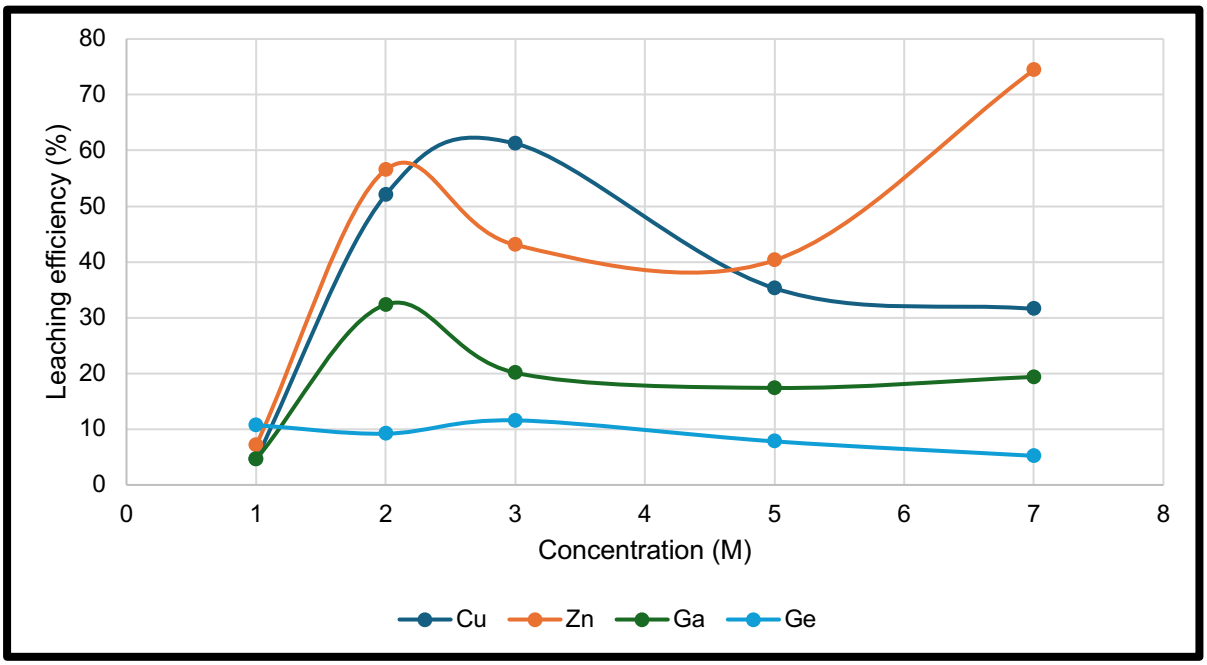

Figure 6.4: Variation of nitric acid concentration extractions at 25 °C, a stirring speed of 300 rpm and mass-to liquid-ratio of 1 g:10 mL.

With the variation of the nitric acid concentration presented in **Figure 6.4**, the extraction of Ga was the highest at 2 M concentration with 32 % Ga and 12 % Ge. The leaching efficiency of Ga increased from 1 M to 2 M, then decreased from 32 % to 20 % at 3 M and remained constant from 3 M concentration to 7 M HNO_3. The Ga extraction remained relatively stable between 19 and 20 %. A relatively small change in the Ge extraction was observed from 1 M to 3 M. At 1 M, Ge extraction is 10.73 %, whereas it is 9.19 % at 2 M, and 11.58 % at 3 M. From 3 M, a gradual decrease in Ge extraction is observed as the concentration is increased. From the nitric acid variation concentration reactions, it was decided that nitric acid was not a suitable leaching reagent due to its low extraction rates for the target elements while substantial amounts of Zn (56.53(5) %) and Cu (52.02(2) %) at 2 M HNO_3 were extracted.

6.5.2 H_2SO_4 Leaching

The final acid evaluated for its leaching capabilities was the sulfuric acid's influence. The reactions were performed at room temperature on a 1 g (accurately weighed to 0.1 mg) sample and quantitatively transferred to a 50 mL glass beaker. 10 mL of the different H_2SO_4 concentrations was added to the solid sample and the mixture was stirred on a hot plate for one hour with a speed of 300 rpm at 25 °C. The reaction mixture was filtered, and the filtrate was quantitatively transferred to a 100.0 mL volumetric flask and filled to the mark.

The effect of the different H_2SO_4 concentrations on the element leaching, as indicated in **Figure 6.1,** showed a pronounced influence on the leaching of Ge, while trace quantities of Ga and even less of Cu, Pb, and Zn were extracted. Subsequent reactions with varying sulfuric acid concentrations (1 M, 2 M, 3 M, and 4 M) were performed to try and find the optimum concentration that would yield the optimum Ge leaching and the results are displayed in **Figure 6.5**. The extraction of Ge increases with an increase in concentration until it reaches the highest extraction of 78 % at 3 M. After that, Ge extraction steadily decreases due to the possible formation of insoluble GeO_2.

The other elements of interest remained below 10 % as the sulfuric acid concentration increased. It was therefore decided that 3 M sulfuric acid would be the preferred acid concentration for Ge extraction. This result agrees well with those reported in the literature review chapter under **Paragraph 3.3 Leaching processes.** Although some of these studies reported high leaching efficiencies of Ga and Ge when using H_2SO_4, other studies reported low efficiencies due to the inability of H_2SO_4 to liberate Ga or Ge from the SiO_2 phase completely. XRD analysis results of the copper tailings sample used for this study revealed that 37 % comprises SiO_2 (reported in **4.3 Mineral Characterization)**.

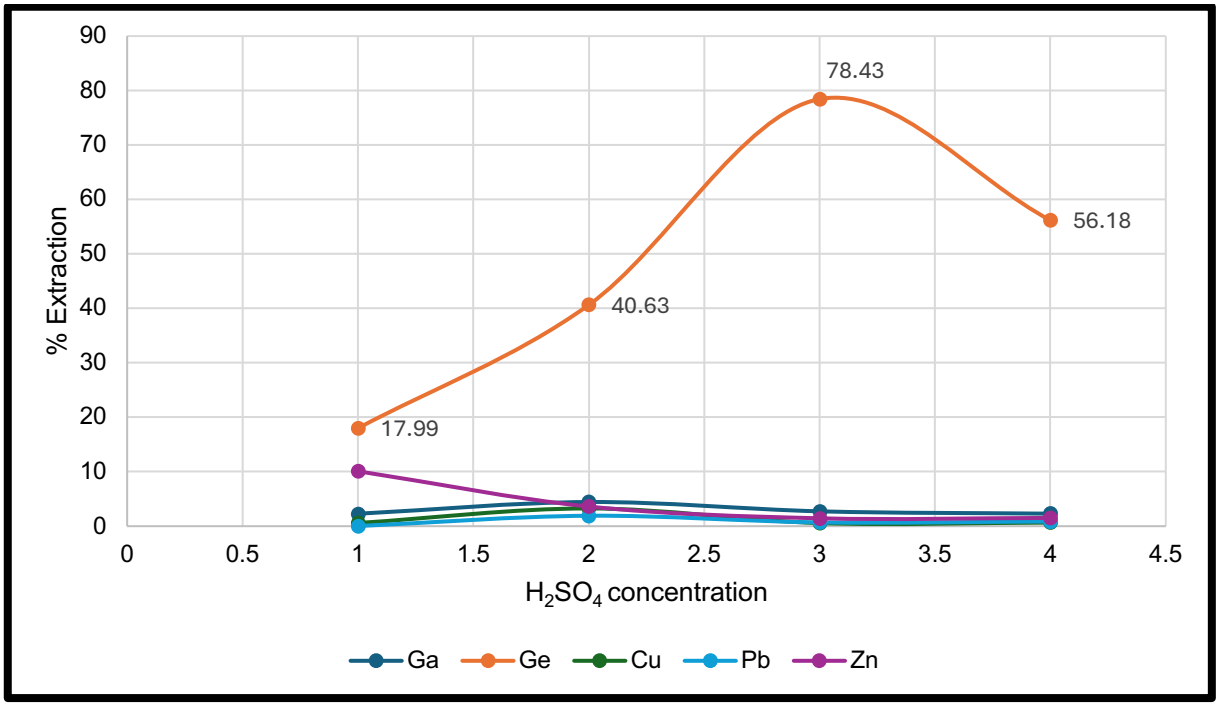

Figure 6.5: Extraction reaction results of sulfuric acid concentration variation. 25 °C, a stirring speed of 300 rpm and mass-to-liquid ratio of 1 g:10 mL.

6.6 Optimization of Ga Extraction using H_3PO_4

It is evident from **Figure 6.3** that H_3PO_4 is the preferred acid for Ga extraction at 2 M. Hence, it was decided to be used to optimize the rest of the experimental conditions for optimal Ga extraction. **Figures 6.6 – 6.9** depict optimization reactions wherein different experimental conditions (temperature, stirring speed, sample mass, and leaching time) were varied to identify the optimal conditions for extracting Ga. During these reactions, the behavior or extraction of Ge was also observed.

6.6.1 Temperature Variation

Leaching reactions of the Tsumeb tailings sample at various temperatures were performed in search of an optimal temperature for extracting Ga. The reactions were performed at different temperatures from 25 to 90 °C on a 1 g (accurately weighed to 0.1 mg) sample and quantitatively transferred to a 50 mL glass beaker. 10 mL of 2 M H_3PO_4 was added to the solid sample and the mixture was stirred on a hot plate for one hour with a speed of 300 rpm. The reaction mixture was filtered, and the filtrate was quantitatively transferred to a 100.0 mL volumetric flask and filled to the mark. From the temperature variation as indicated by the results displayed in **Figure 6.6**, the

highest extraction of 72 % Ga was observed at 90 °C. The Ge extraction also increased with an increase in temperature and reached a maximum of 46 % at the same temperature.

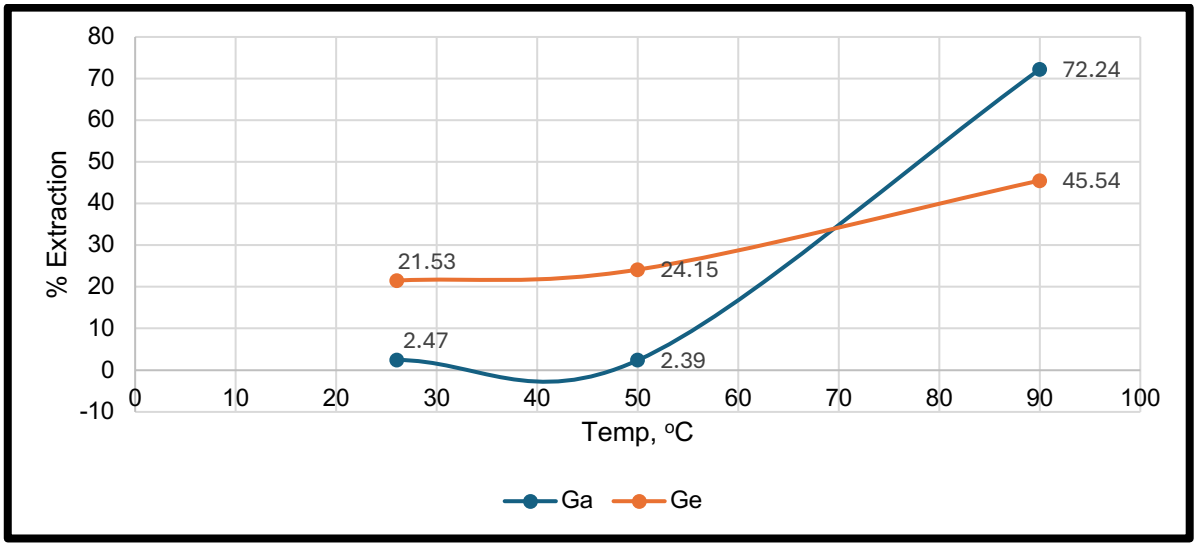

Figure 6.6: Effect of temperature variation on Ga and Ge extraction, temperature varied between 25 and 90 °C, 2 M H_3PO_4, a stirring speed of 300 rpm, and mass-to-liquid ratio of 1 g:10 mL.

6.6.2 Variation of Pulp Density

The effect of pulp density on the extraction of Ga is illustrated in **Figure 6.7.** Reactions using 2 M H_3PO_4 were conducted with sample mass varying from 0.1 g to 0.7 g per 10 mL volume of H_2SO_4. The reactions were performed at 90 °C, and the mixtures were stirred for one hour at 300 rpm. The reaction mixtures were filtered, and the filtrates were quantitatively transferred to 100.0 mL volumetric flasks and filled to the mark.

The leaching reaction that resulted in the highest extraction of Ga was 0.7 g in 10 ml acid at 90 °C. At 0.7 g, 82 % of Ga in the tailings sample is extracted compared to only 74 % extracted at 0.1 g. The extraction of Ga gradually increased with an increase in sample pulp density. Contrary to the observations made on the Ga extraction, Ge extraction gradually decreases as the pulp density increases. The highest Ge extraction of 54 % is obtained from the initial reaction with a pulp density of 0.1 g/10 mL.

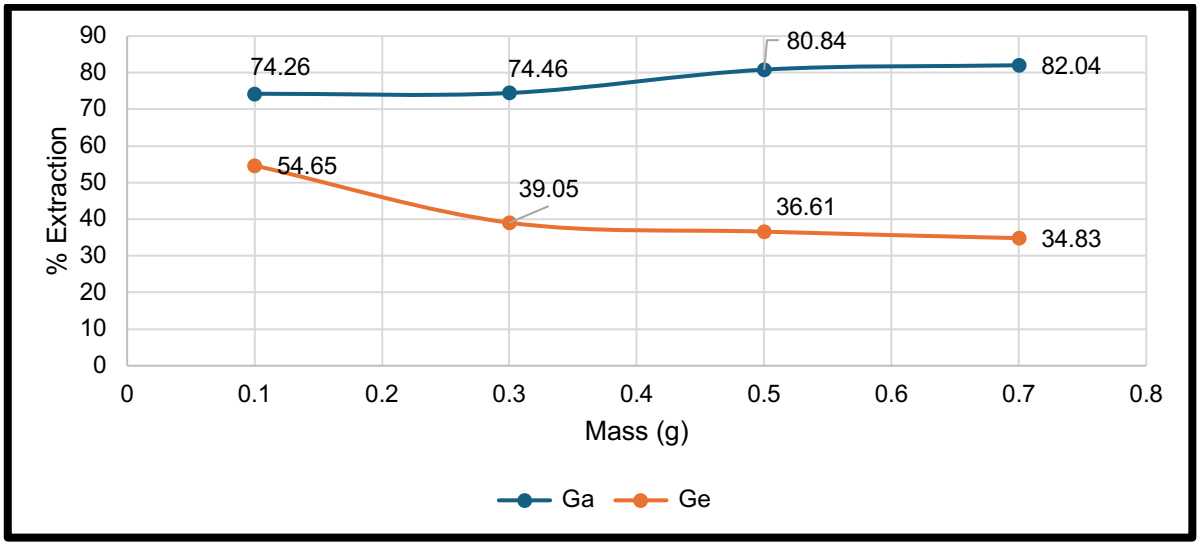

Figure 6.7: Effect of pulp density on Ga and Ge extraction, pulp density varied between 0.1 g/ 10 ml and 0.7 g/10 mL at various sample masses using 2 M H_3PO_4 at 90 °C, a stirring speed of 300 rpm.

6.6.3 Variation of Leaching Time

Reactions for extracting Ga from the Tsumeb tailings sample were performed at different leaching times to find the optimum leach time. The reactions were performed using 2 M H_3PO_4 at 90 °C, with a mass-to-liquid ratio of 1 g:10 mL. The various leaching times were between half an hour to five hours with a stirring speed of 300 rpm. The reaction mixtures were filtered, and the filtrates were quantitatively transferred to 100.0 mL volumetric flasks and filled to the mark.

The extraction behavior of Ge at these conditions is presented in **Figure 6.8** which illustrates the extraction of Ga at varying reaction times. The highest Ga extraction of just over 80 % was obtained after one hour of leaching. The Ga extraction sharply increases from half an hour to an hour and steadily decreases after one hour, reaching 73 % after five hours of leaching. The optimum leaching time for Ga from the Tsumeb tailings sample was decided to be one hour.

Similarly, the Ge extraction increased from half an hour to one hour, reaching a maximum of 45.61(11) %. The extraction remains roughly over 45 % after two hours of leaching and then steadily decreases, reaching 36 % after 5 hours. From these results it was decided that the optimum leaching time for Ge is one hour.

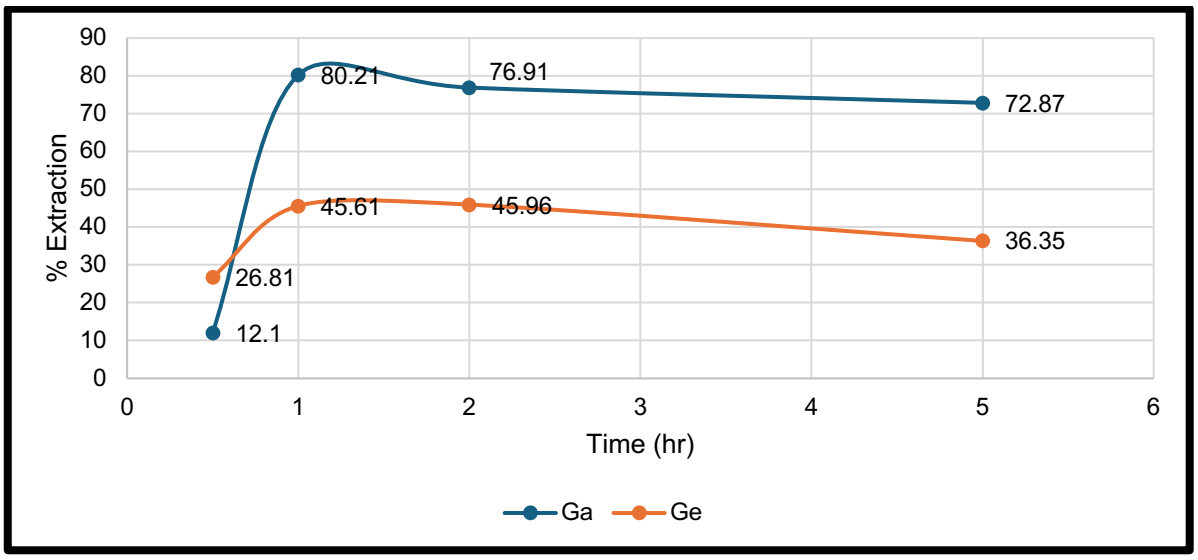

Figure 6.8: Effect of leaching time on Ga and Ge extraction, leaching time varied between 0.5 hour and 5 hours at 90 °C, 2 M H_3PO_4, mass to liquid ratio of 1 g:10 mL.

Possible reasons for the decrease in Ga and Ge extraction as the leaching time increases can be the precipitation of these elements and the formation of insoluble compounds from the reaction of Ga and Ge with the leaching reagent or components in solution. Furthermore, literature reports that the dissolved Ge hydrolyzes and polymerizes as the reaction time increases, which negatively affects the extraction of Ge (Geng *et al*., 2022). It is also deduced from the surveyed literature that the optimum leaching time will differ for the different matrices. For instance, one study reported a high extraction yield of 83% Ge after a 2-hour leaching time (Arroyo *et al*., 2014). Another study reported a recovery of 78% of Ge from a copper cake sample after a leaching time of 30 minutes (Kul & Topkaya, 2008).

6.6.4 Variation of Stirring Speed

In order to determine the possible influence of stirring speed on Ga extraction, the reactions were performed at 90° C on a 0.7 g (accurately weighed to 0.1 mg) samples and quantitively transferred to 50 mL glass beakers. 10 mL of 2 M H_3PO_4 was added to the solid samples and the mixtures were stirred on a hot plate for one hour with varied stirring speeds from 100 rpm to 500 rpm. The reaction mixtures were filtered, and the filtrates were quantitatively transferred to 100.0 mL volumetric flasks and filled to the mark. **Figure 6.9** compares the extraction of Ga at varying stirring speeds. The optimum leaching stirring speed for Ga was observed at 100 rpm. The Ga extraction

gradually decreased as the stirring speed increased. At a stirring speed of 500 rpm, the recovery of Ga dropped to 73 % from 82 % (100 rpm).

Similarly, the optimum stirring speed for Ge extraction was observed at 100 rpm. At 100 rpm, Ge was extracted with an efficiency of 60 %. Increasing the stirring speed also showed a gradual decrease in the Ge extraction. The extraction for Ge dropped to 36 % (500 rpm) from 60 % (100 rpm). A possible reason for the decrease in both Ga and Ge extraction, with a decrease in stirring speed, is the reduced contact time between particles and the leaching reagent, thus hindering effective extraction.

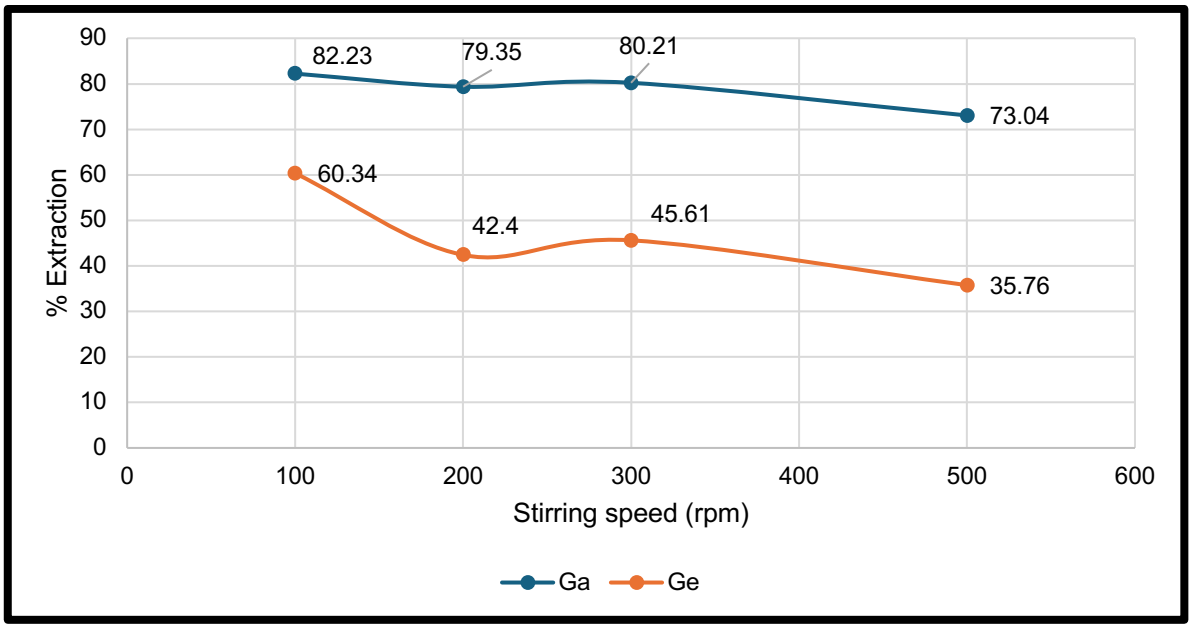

Figure 6.9: Effect of stirring speed on Ga and Ge extraction at various stirring speeds, stirring speed varied between 100 and 500 rpm, 90 °C, 2 M H_3PO_4 with mass to liquid ratio of 0.7 g:10 mL.

In order to simplify the separation process of Ga and Ge, to save both chemicals and reduce the waste, it was decided to use only the optimized conditions that were determined for the Ga/phosphoric leach process, to remove Ge with sulfuric acid. These reaction conditions were a stirring speed of 100 rpm, reaction temperature of 90 °C, pulp density of 0.7 g:10 mL. The only differences were the acid concentrations used during the separate process which were a [H_3PO_4] of 2 M for Ga and 3 M [H_2SO_4] for Ge (see **Paragraphs 6.8.1** and **6.8.2.**

6.7 Separation and Isolation of Ga and Ge in an artificial mixture

For the next part of this study, it was decided to investigate the possible separation and isolation of Ga and Ge from a synthetic mixture to observe and identify the reaction conditions of their separation/isolation prior to attempting it on the Tsumeb tailings with rather low Ga and Ge concentrations.

Based on the coordination chemistry of both Ga and Ge discussed in **Chapter 2**, it was established that the post-transitional element (Ga) and the metalloid (Ge) form complexes with hydroxides. As already established in literature, gallium precipitates as $Ga(OH)_3$ at a pH ranging between 9.4 and 9.7 (Lu *et al*., 2017). Germanium is precipitated mainly by the presence of H_2S and tannic acid. In this study, Ga and Ge were precipitated from phosphoric and sulfuric acid solutions by varying the pH with NaOH.

5 g (accurately weighed to 0.1 mg) samples of $GaCl_3$ and GeO_2 were separately dissolved in 150 mL of 2 M H_3PO_4 at 90 °C (**Table 6.3** indicated the substantial dissolution of both elements in phosphoric acid). The individual mixtures were stirred for one hour at 100 rpm stirring, and the pH of the solutions were incrementally changed by the dropwise addition 0.025 M NaOH. Aliquots of the two different mixtures were collected at various pH conditions as the pH was increased. The precipitates were collected, dried, weighed, redissolved in 2 M H_3PO_4, and analysed using ICP-OES.

The results indicating the Ga recovery with varying pH are reported in **Table 6.4,** while **Figure 6.10** graphically displays the Ga solubility at various pH conditions. The results indicate that at pH 1 all (100 %) of the Ga is dissolved in the acid. The increase in pH resulted in the accelerated precipitation of a Ga-OH product from a pH 1 to 2 (drop from 100 % to 10 %). The results indicate that at higher pH values (between pH 3 and 7), insignificant amounts of Ga remained in solution. Interestingly the results also indicate that the Ga-OH product starts to re-dissolves at pH of 7.

Table 6.4: Ga dissolution at various pH conditions.

pH	Ga in solution		Precipitated Ga	
	mg/kg	%	mg/kg	%
1	61871	100	0	0
2	6210	10	62	62
6	108	0	93.57	94
7	480	1	105.7	106
8	11003	18	51.52	52

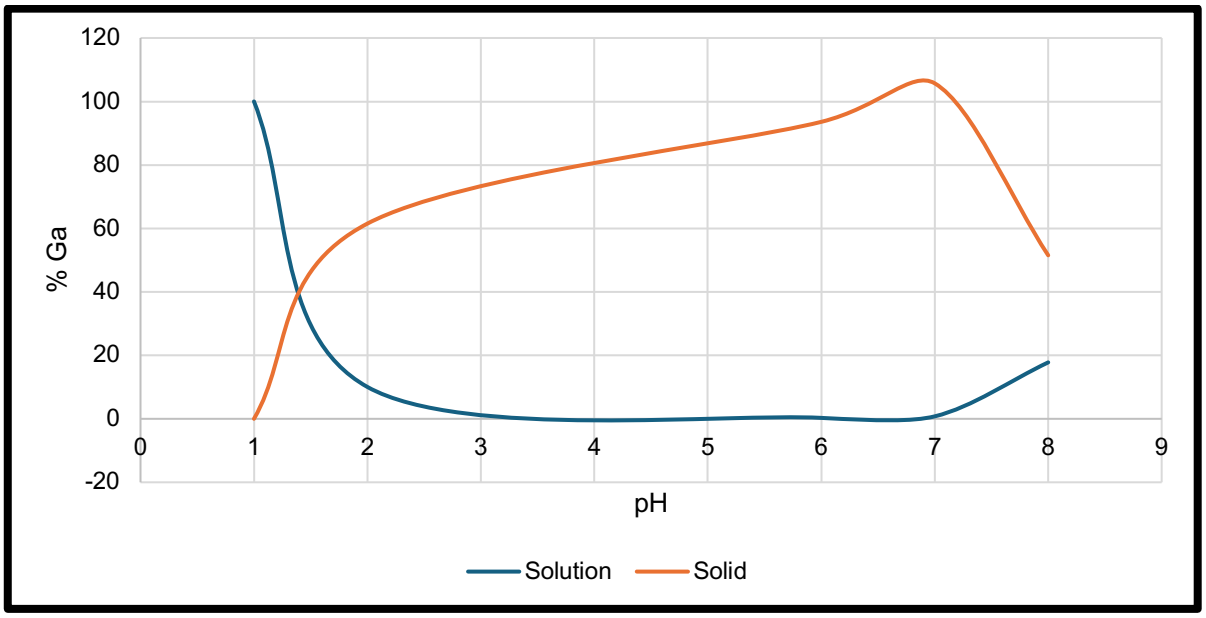

Figure 6.10: Behavior of Ga in solution at varying pH conditions, 2 M H_3PO_4 at 90 °C, with a mass-to-liquid ratio of 5 g:150 mL, stirring speed of 100 rpm.

The results for the Ge solubility at various pH conditions are reported in **Table 6.5** and the behavior of Ge in solution at the various pH conditions is graphically displayed in **Figure 6.11**. The results indicate that all the Ge was dissolved in the 2 M H_3PO_4 solution (pH =0). The results also show the gradual precipitation of the Ge-OH product with an increase in pH from pH 0 to 2 and then remains constant between pH 2 and 8. At pH 8, the Ge steadily starts to precipitate again.

These reactions clearly indicate that a solution with a pH of 3 may be very conducive for Ga and Ge separation or isolation from an aqueous solution. At a pH of 3 all the

Ga precipitated from the solution (**Figure 6.10**) while 78% of the Ge remained in solution (**Figure 6.11**).

Table 6.5: Ge solubilities at varying pH conditions.

pH	Ge in solution		Precipitated Ge	
	mg/kg	%	mg/kg	%
0	4878	100	0	0
2	3838.5	79	21	20
3	376.3	77	23	21
8	3833.5	79	21	20
11	2197.5	45	55	50

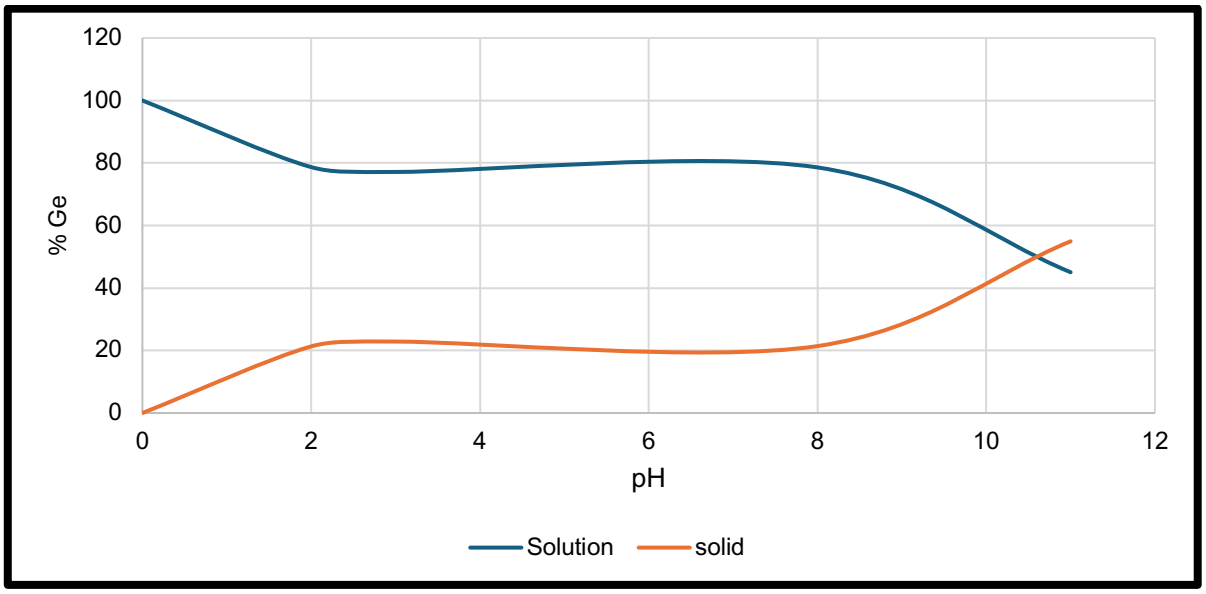

Figure 6.11: Behavior of Ge at various pH conditions using 2 M H_3PO_4 at 90 °C with mass to solid ratio of 5 g:150 mL, 100 rpm.

6.8 Separation of Ga and Ge in the Tsumeb tailings using Selective Acid leaching

It is clear from the results in **Table 6.3** that sequential use of H_2SO_4 and H_3PO_4 can have the potential to selectively separate the two target elements (two step process). The use of 3 M H_2SO_4 at optimal experimental conditions can selectively dissolve i) the Ge from the tailings, (which is also soluble in H_3PO_4) while ii) the subsequent reaction with H_3PO_4 will dissolve the remaining Ga and hence little Ga which is no longer present in the sample, (see **Reaction Scheme on Figure 6.12)**. Subsequent precipitation with NaOH at a pH of 3 (**Figures 6.13 and 14**) will precipitate the Ga in the H_3PO_4, while Ge in H_2SO_4 can be isolated at a pH higher than 12.

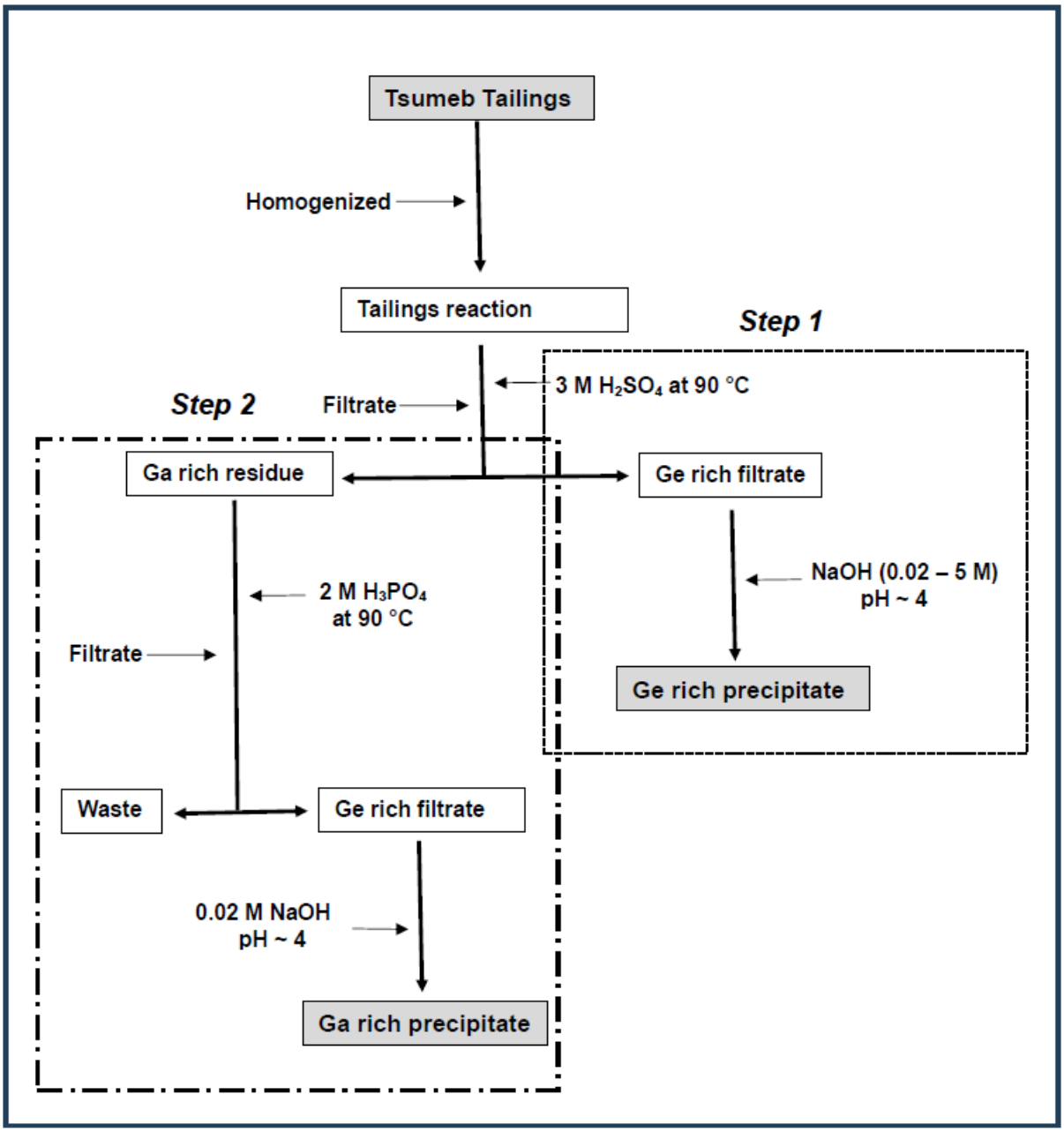

Figure 6.12: Flow diagram of proposed two step selective dissolution and extraction of Ga and Ge from Tsumeb Tailings.

6.8.1 Dissolution and Separation of Ge using H_2SO_4

This first step (**Step 1** in **Figure 6.12**) of the two-step extraction process evaluated the possible separation and isolation of Ge using sulfuric acid as leachant followed by its precipitation using NaOH. A larger scale reaction was chosen to increase the Ge amount for the isolation step.

Firstly, a 50 g (accurately weighed to 0.1 mg) tailings sample was leached with a 5 L of 3 M sulfuric acid solution. The solution was stirred for one hour at 100 rpm at 90 °C. The reaction mixture was filtered, and the filtrate was treated with NaOH (**Paragraph 6.8.3**). The remaining solid was used in the next step.

6.8.2 Dissolution and Separation of Ga using H_3PO_4

This step (**Step 2** in **Figure 6.12**), in the investigation involved the isolation of Ga with the phosphoric acid. The residue isolated after **Step 1** was washed with deionized water and dried. The residue was subsequently weighed, 6 g was obtained from the residue. From this residue 0.7 g (accurately weighed to 0.1 mg) was leached with 2 M H_3PO_4 at 90 °C. The mixture was stirred for one hour with a stirring speed of 100 rpm and finally filtered.

6.8.3 Isolation of Target Elements from Filtrates

In the final steps of this part of the study, the Ga and Ge were isolated from the two leachates by adjusting the pH of the solutions with 0.025 M NaOH.

H_2SO_4 Filtrate

Table 6.6 reports the result for the Ga and Ge content remaining in the solution after H_2SO_4 leaching and pH adjustment. The 100 % extraction at pH 1 refers to the amount that dissolved with H_2SO_4, approximately 4 % Ga (see **Table 6.3**). The pH of the aliquots of the filtrate obtained from the dissolution reactions performed as described in **Paragraph 6.8.1** were incrementally increased with 0.025 M NaOH. Samples of the different pH conditions were filtered and analysed using ICP-OES. The pH 4 solution in which good separation of Ga and Ge was observed, was further treated with NaOH to a pH of 8 to try and precipitate Ge. The precipitates were collected, dried, weighed,

redissolved in 2 M H_3PO_4, and analysed using ICP-OES and characterized by FTIR as detailed in **Paragraph 6.10.**

Table 6.6: Elemental extraction efficiencies using 3 M H_2SO_4 at varying pH.

pH	Ga (%)	Ge (%)
1	100	100
2	30.09	36.01
4	1.48	54.77
6	1.13	20.54
8	1.12	37.72

Figure 6.13 graphical displays the results reported in **Table 6.6.** These results show a sharp decrease in the Ga content in the sulfuric acid solution from the initial pH of 1 to pH 4, as well as a steady decrease in Ge content across the same pH values. A possible reason for the variable change in the Ge recovery is the precipitation of Ge in the form of GeO_2 and the formation of soluble germanate ions ($Ga(OH)_6^{2-}$). The results indicate good separation of Ga and Ge at pH 4. 54.77 % Ge remains in solution whereas only 1.48 % Ga is observed. From this pH, Ge should (according to previous results) precipitate with negligible amounts of Ga present.

Contrary to the expectations based on the results in **Table 6.3** and the subsequent results in **Paragraph 6.5.2** (**Figure 6.5**), the residue after the H_2SO_4 leaching still contained higher than expected Ge content, approximately 40 %. It was anticipated that the initial step H_2SO_4 leaching could remove the majority of Ge, leaving a residue predominantly composed of Ga which still contained some Ge. This higher-than-expected Ge percentage can also be attributed to a statistical or analytical error. The original Ge content in the tailings was only 0.03 % and any error on such as a small value will appear as abnormally high, and hence a false positive or large Ge concentration remaining in solution. Nonetheless, most of the Ga in **Step 2** was precipitated as the pH was adjusted from 1 to 2, from 100 % to 6 % as graphically depicted in **Figure 6.14**.

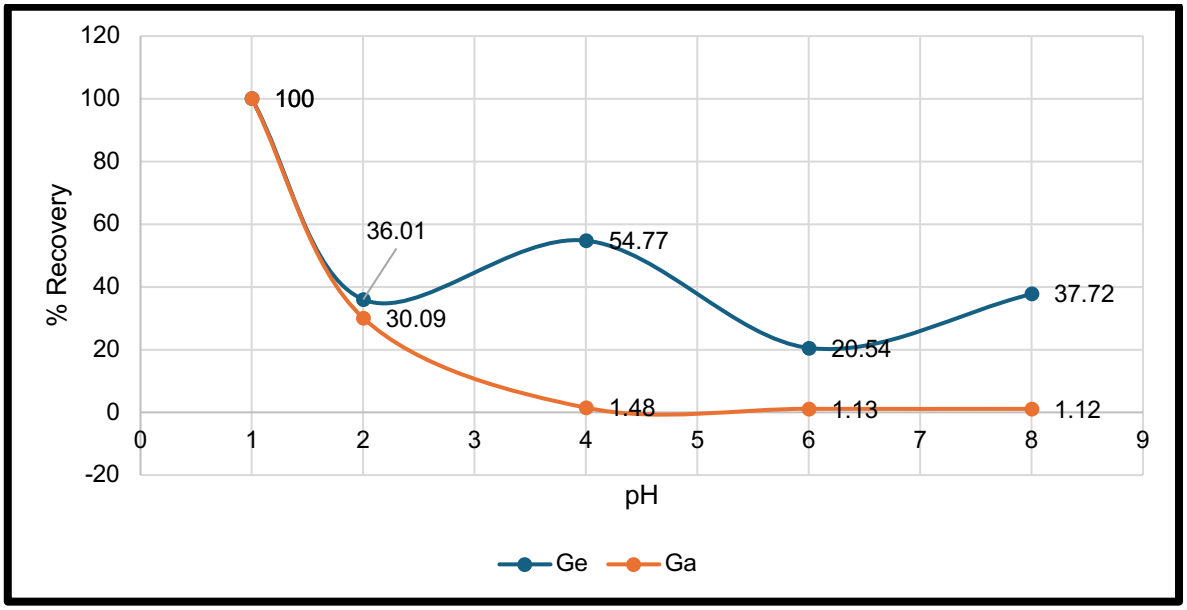

Figure 6.13: Elemental content in isolated product after **Step 1** of a two-step selective extraction process, 3 M H_2SO_4 at 90 °C, one hour leaching at 100 rpm.

H_3PO_4 Filtrate

The Ga and Ge content after H_3PO_4 leaching and isolated after pH adjustment are reported in **Table 6.7** and illustrated **in Figure 6.14.** The pH of aliquots of the filtrate obtained from the second step of the selective dissolution process, as described in **Paragraph 6.8.2** was incrementally changed by the dropwise addition 0.025 M NaOH. The solutions of the various pH conditions were filtered and analysed using ICP-OES. The precipitates were collected, dried, weighed, redissolved in 2 M H_3PO_4, and analysed using ICP-OES and characterized by FTIR as detailed in **Paragraph 6.10.**

Table 6.7: Elemental extraction efficiencies in 2 M H_3PO_4 at varying pH.

pH	Ga (%)	Ge (%)
1	100	100
2	6.66	60.70
4	4.79	70.37
6	6.73	86.31
8	4.08	72.51

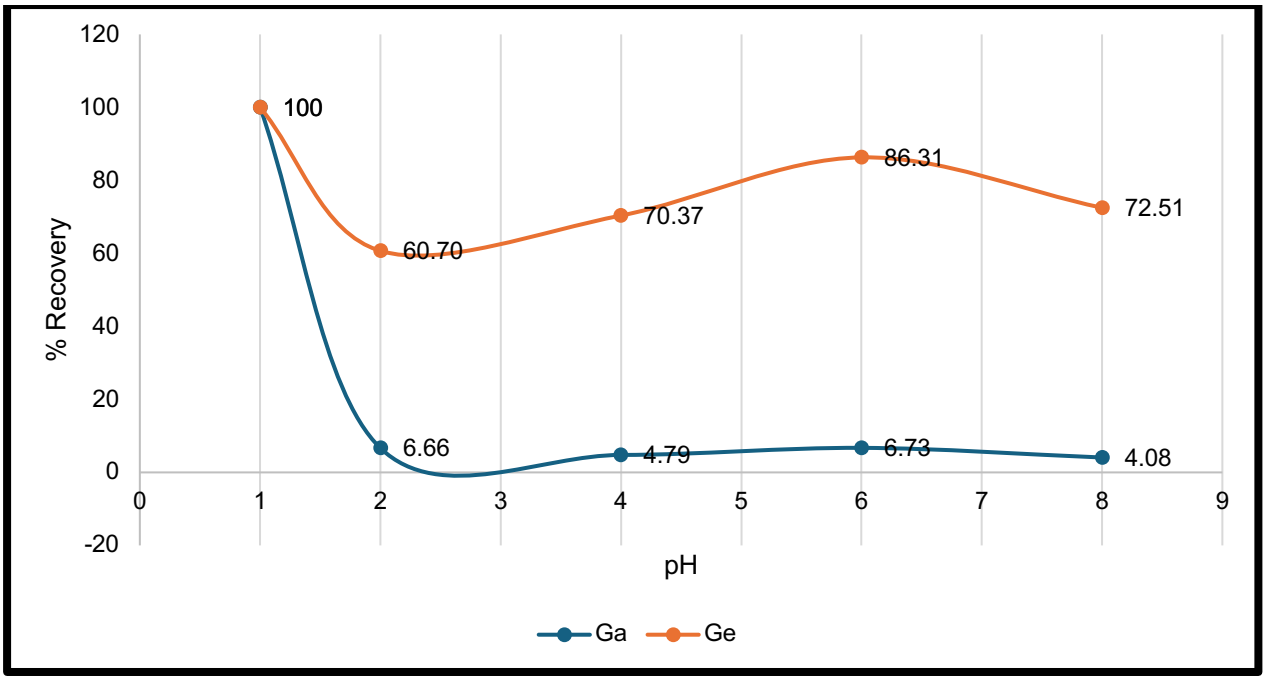

Figure 6.14: Step 2 of a two-step selective extraction process, using 2 M H_3PO_4 at 90 °C, one hour leaching at 100 rpm, mass-to-liquid of 0.7 g:10 mL.

The 100 % extraction at pH 1 refers to the amount that dissolved with H_2SO_4, approximately 25 % Ge (see **Table 6.3**). **Figure 6.14** illustrates the precipitation behavior of Ga in the phosphoric acid leachate as the pH is adjusted from 1 to 8. A significant portion of Ga, approximately 93 %, is precipitated as the pH is increased from an initial value of 1 to 2. Beyond this point, as the pH is further adjusted from 2 to 8, the Ga concentration in the solution stabilizes, remaining between 6 and 4 %. These results are similar to what is observed in the artificial mixture **(Figure 6.10)**, as the pH is adjusted from 1 to 2 more than 80 % Ga is precipitated.

In contrast, Ge predominantly remains in solution, about 30 %, across the pH range examined. A Ge-enriched solution is maintained between pH 2 and 8. It is important to note that for both the H_2SO_4 and H_3PO_4 leaching steps, about 30 - 40 % of the Ge remains in solution and does not precipitate with pH adjustment. However, a notable change in Ge concentration occurs when the pH is adjusted from 1 to 4, during which approximately 40 % Ge precipitates. In the artificial mixture, 40 % Ge only precipitated at pH 10 and higher.

6.9 pH Adjustment Precipitation from Phosphoric Acid Leachate (single step)

In the first leaching step of the two-step selective dissolution and separation process, the behaviour of Ge products differed from that observed in the synthetic mixture **(Figure 6.11)**. In the synthetic mixture, 80 % of Ge remained in solution across the pH range of 2 to 8, whereas 67 % of Ge was precipitated from the H_2SO_4 leachate when the pH was adjusted from 1 to 2. The fact is that Ge precipitation differed between the synthetic mixture and the Ge in tailings during pH adjustment. It begged the question whether the H_2SO_4 leaching reacted with the Ge species in the tailing sample (sulphate interactions) and hence influenced the precipitation behaviour or if different Ge species are present in the tailings, and thus the different behaviour.

Consequently, it was decided to explore Ge precipitation, only using H_3PO_4 (eliminate SO_4^{2-} from the reaction mixture) in an attempt to precipitate the majority of the Ge in the Tsumeb talings. The reactions were performed at 90 °C on 0.7 g (accurately weighed to 0.1 mg) samples and quantitatively transferred to 50 mL glass beakers. 10 mL of 2 M H_3PO_4 was added to the solid samples, and the mixtures were stirred on a hot plate for one hour at 100 rpm. The reaction mixtures were filtered, and the pH of the filtrates was adjusted dropwise with 0.025 M NaOH. The initial pH of the solutions was 1.25 and was subsequently adjusted to 2, 4, 6 and 8. The results are reported in **Table 6.8**. The 100 % refers to the elemental amount that was quantified in **Chapter 5 (Paragraph 5.3)** using ICP-OES.

Figure 6.15 displays the content of both Ga and Ge in solution at various pH conditions. The Ga and Ge content decreased when the pH was increased from its

initial 1.25 to pH 2. This happens as Ga and Ge complexes with hydroxide gradually precipitate from the solution. From the initial pH of 1.25 to pH 4, the amount of Ge in the solution steadily decreases from 100 % to 52 %, while the Ga content decreases from 100 % to 32.68(7) % from a pH of 1.24 to 2. About 67 % of Ga is precipitated at pH 2 compared to over 70 % of Ge remaining in solution. From pH 4 to pH 8, good separation of Ga and Ge is observed. At pH 6, 98 % of the initial Ga content that was initially in the solution was precipitated, leaving just 2 % Ga in the solution while 42 % Ge remained.

However, the outcome of the single step leaching process using H_3PO_4 was very similar to those obtained for the two-step process. In this one step process, approximately 40 % of the Ge did not precipitate with pH adjustment, compared to the 40 % in the H_2SO_4 leaching process ***(Step 1*** in **Figure 6.12)** and 30 % with the H_3PO_4 leaching step (***Step 2*** in **Figure 6.12**). These results strongly suggest that a fraction of Ge species in the Tsumeb tailing sample differ from those produced during the dissolution of GeO_2 in the synthetic mixture (**Paragraph 6.7**). Another explanation is that a portion of the Ge species in the Tsumeb taling sample reaction with both SO_4^{2-} and PO_4^{3-} in a very similar fashion, to produce Ge species that does not react with the added NaOH similar to the remaining 60 - 70 % of the Ge species present in the tailing sample.

It was decided to analyse and include (**Table 6.8)** some of the more important elements present in the Tsumeb tailings in order to identify and quantify the type of impurities that was isolated during the final steps of this investigation.

Table 6.8: Ga and Ge remaining in solution after precipitation with NaOH.

pH	Ga (%)	Ge (%)	Zn (%)	Cu (%)	Pb (%)
Initial	100	100	100	100	100
2	32.68	72.83	19.55	67.92	58.22
4	3.32	52.40	4.86	34.54	0
6	2.25	41.76	3.61	0	0
8	1.52	36.04	0	0	0

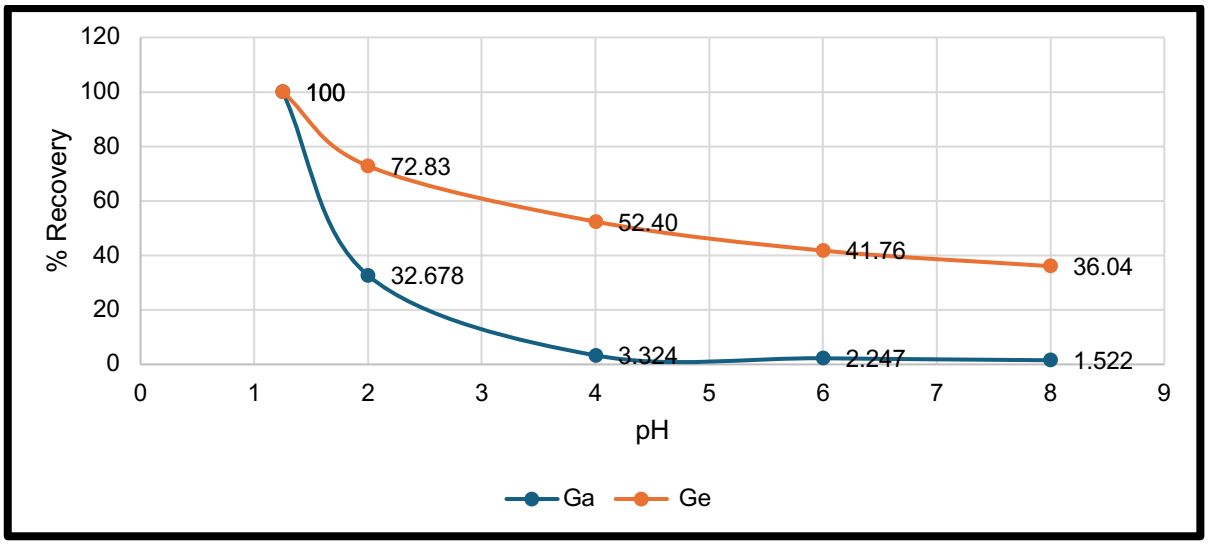

Figure 6.15: Ga and Ge content in solution at various pH conditions, 2 M H_3PO_4 at 90 °C, mass to liquid ratio of 0.7 g:10 mL, 100 rpm.

The results reported in **Table 6.8** clearly indicate that most of the elements (including Cu, Pb, and Ga) have precipitated at pH 6 and 8 in accordance to their normal pH behaviour.

6.10 Characterization of the products isolated at pH 4

The products that were isolated after the H_2SO_4 and H_3PO_4 leaching steps were characterized in order to verify the presence of the two target elements after the separation steps and their possible enrichment after the pH adjustment steps (**Paragraph 6.8.3**). The products were mainly characterized using Fourier transform Infrared Spectroscopy (FTIR) and while its purity was determined by the total dissolution of the samples using 2 M H_3PO_4 and elemental quantification done with ICP-OES.

Experimental conditions

The experimental conditions for the dissolution and separation of Ge are detailed in **Paragraph 6.8.1**, while those for Ga are described in **Paragraph 6.8.2**. The process for isolating both elements is outlined in **Paragraph 6.8.3.** The samples were analysed using a Bruker Tensor 27 model in the mid-IR region of 500 – 4000 cm^{-1} with 16 scan speed.

FTIR is a very useful method to analyze Ga-containing materials since gallium-containing compounds like gallium oxide, gallium nitride, and gallium arsenide have molecular vibrations exhibiting characteristic IR stretching frequencies between 950 and 1026 cm^{-1} which can be assigned to the Ga-OH vibrations while GaO stretching frequencies are present in the 620-725 cm^{-1} region (Yang *et al*., 2009).

Similarly, FTIR can also characterize Ge containing compounds that have Ge-O stretching frequencies between 400 – 900 cm^{-1} (Zhang *et al*., 2022).

The presence of large quantities of impurities can complicate the characterization of the target element species in the final product and caution should be taken not to put too much meaning on product characterization in the presence of other compounds.

Gallium Product Characterization

The spectrum obtained for the gallium precipitate **(Figure 6.16)** displays several peaks in the region between 519 and 1250 cm^{-1}. Some of these stretching may be assigned to Ga-OH peaks (between 965 and 1042 cm^{-1}), but the final product that was isolated was not pure (see the subsequent paragraph Product purity) which makes stretching frequency problematic. The IR spectrum for pure GaO_2 is presented in **Figure 6.17.** This product has fewer peaks compared to the isolated product, with one strong stretching frequency at 690 cm-1. Therefore, characterization of the product as a Ga product is dubious at its best. Further purification and its subsequent characterization as a pure Ga product are required to finally announce the isolation and purification of the Ga product.

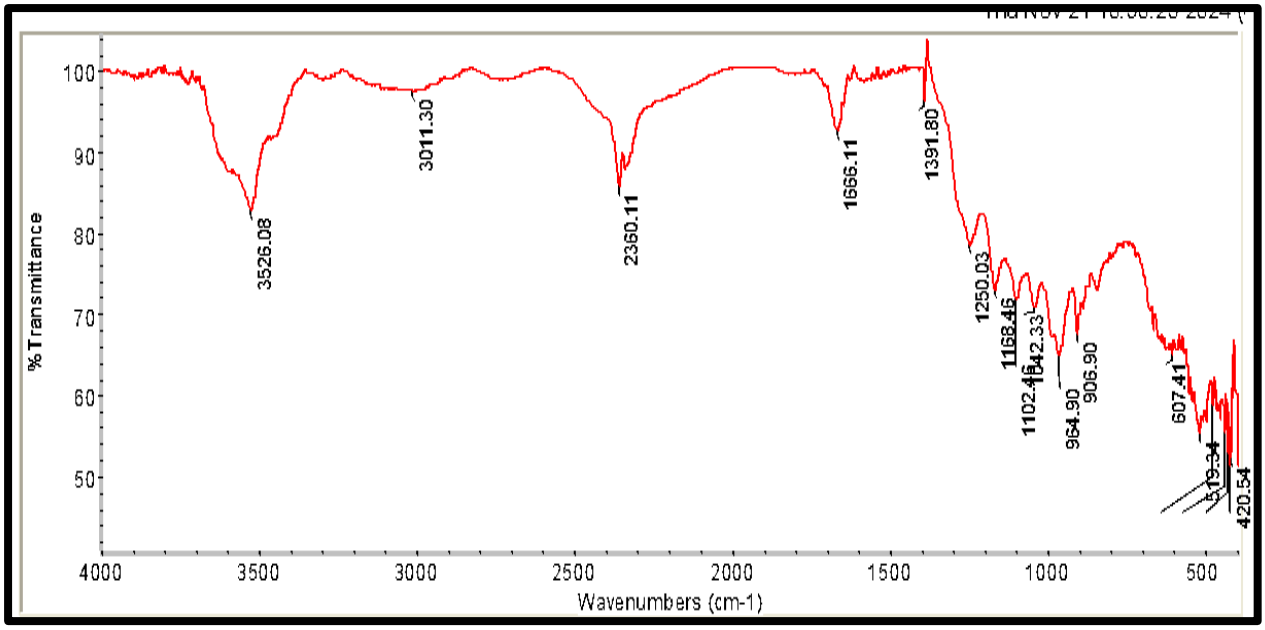

Figure 6.16: FTIR spectrum of Ga product precipitated at pH 4, extraction conditions: 2 M H_3PO_4 at 90 °C, one hour leaching at 100 rpm, mass-to-liquid of 0.7 g:10 mL.

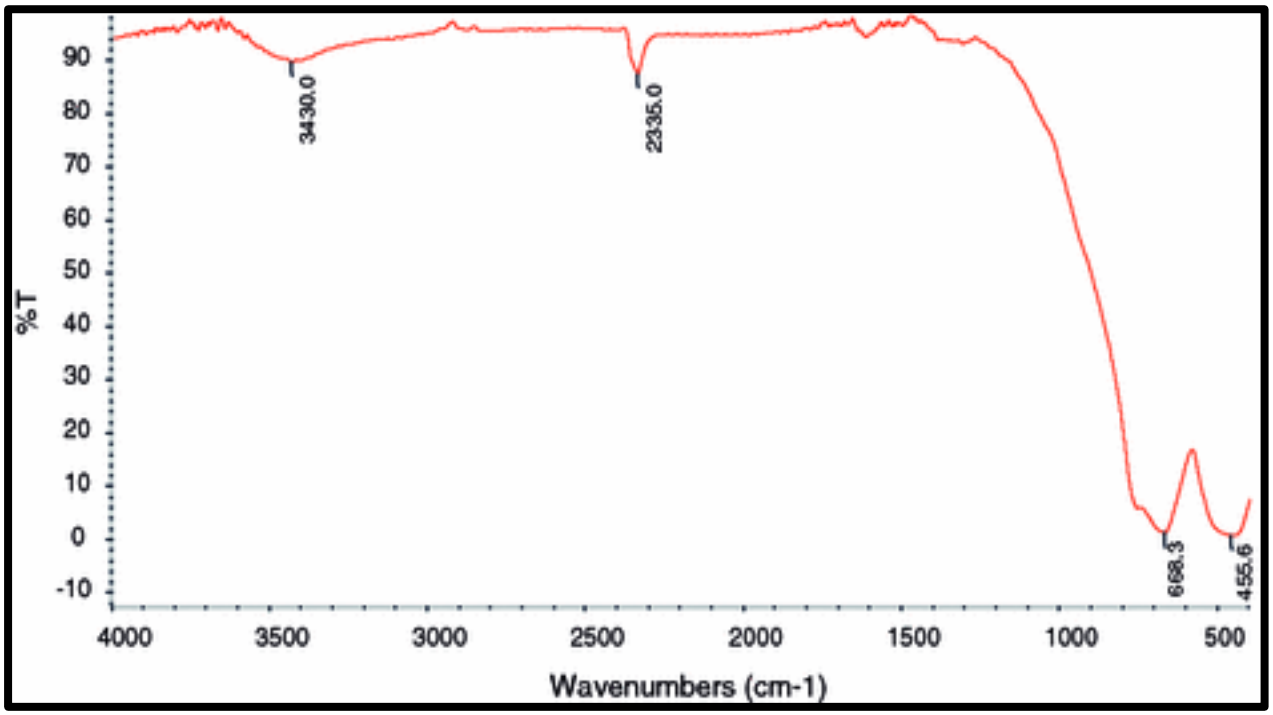

Figure 6.17: FTIR: Spectra of pure gallium oxide (Rambabu *et al*., 2007).

Germanium product Characterization

The solid isolated after the H_2SO_4 leaching (**Step 1**), hopefully containing Ge, was also analyzed using FTIR (**Figure 6.18)** and its spectrum was compared to that of GeO_2 (**Figure 6.19)**. According to literature germanium oxide exhibits stretching frequencies

between 400 and 900 cm^{-1}, and the spectrum of GeO_2 in this study displays a strong stretching frequency at 876 cm^{-1} which can be attributed to a Ge-O (double) bond. The isolated product had a strong stretching frequency at 1100 cm^{-1}, also pointing to a possible double Ga-oxygen bond, but the same argument holds as previously. The final product that was isolated was not pure (see the subsequent paragraph Product purity) which makes stretching frequency problematic.

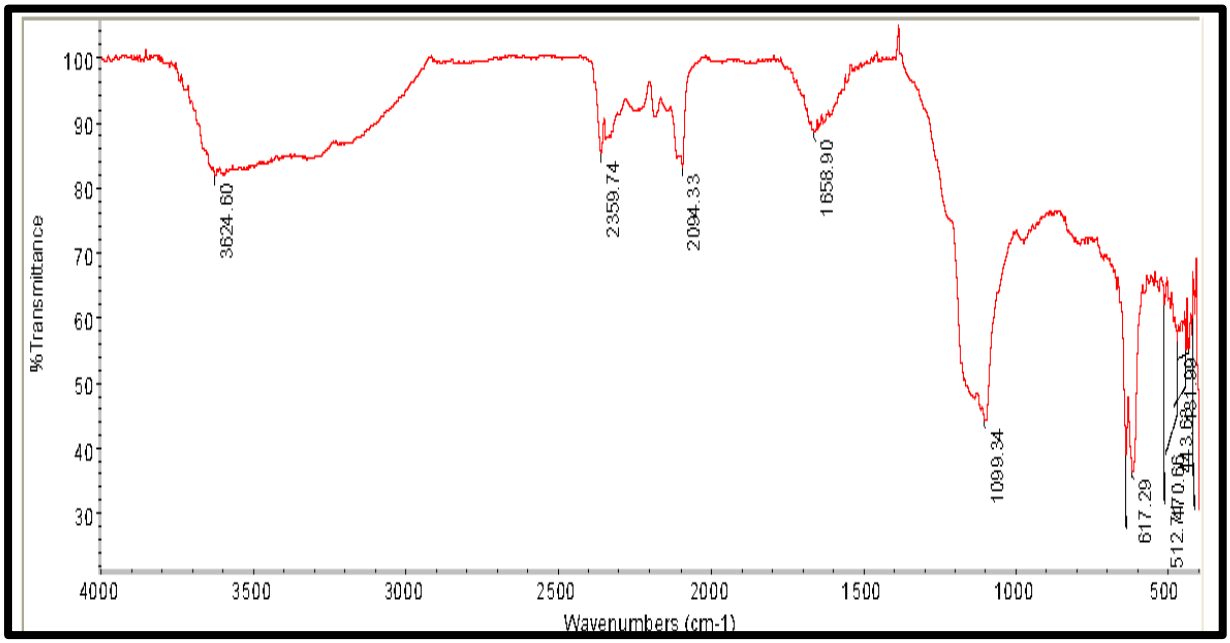

Figure 6.18: FTIR spectrum of Ge product precipitated at pH 8, extraction conditions 3 M H_2SO_4 90 °C, one hour leaching at 100 rpm.

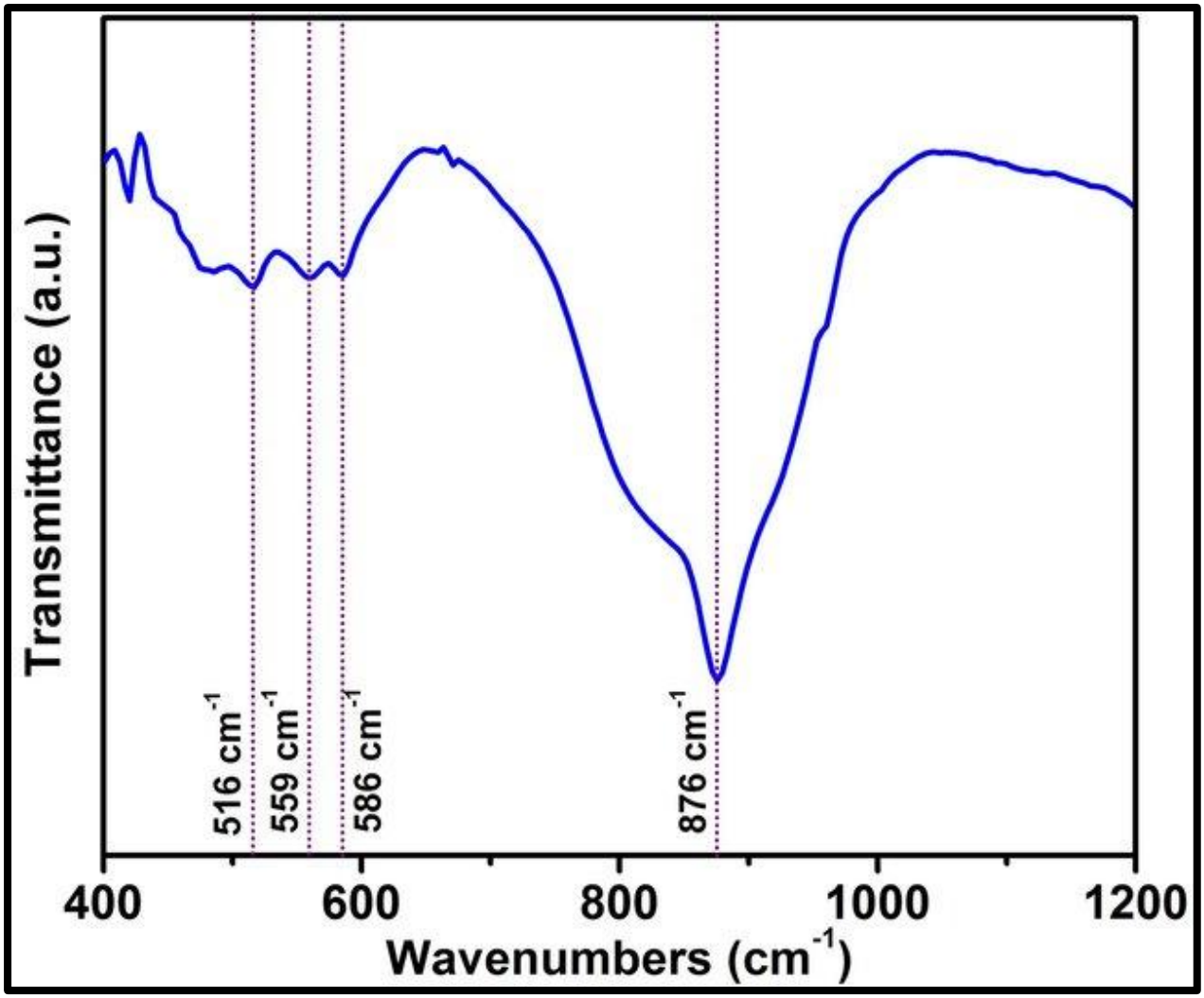

Figure 6.19: FTIR spectra of pure GeO2 (Ngo *et al*., 2015).

Product purity

The Ga and Ge products isolated as described in **Paragraph 6.8.3** were analysed for impurities using ICP-OES. Very promising results for the product isolated after Step 2 (**Figure 6.12**) were obtained. The product clearly shows the absence of Ge, while the Ga content increased from 1.9 % to approximately 24 %. It clearly validates the dissolution of the Ga and its separation from the Ge in the Tsumeb talings (**Step 2**), and hence the 'Two Step process' that were developed and applied in this study. The spectrum also indicated a substantial amount of Si and smaller amounts of Fe, Cu and Zn.

The product that was isolated after the H_2SO_4 leaching step (**Step 1**) indicated (**Figure 6.20)** the presence of 5 % Ge, up from 0.03 % in the original tailings, about 1 % Ga and a substantial amount of Fe and smaller amounts of Al, Zn, Mg and Cu. Again, these results validate the 'Two Step" separation process with the separation of the majority of the Ge from the Ga and increasing (100 fold) its concentration in the final product.

These results are extremely promising for the beneficiation (separation and isolation of Ge/Ga)) in the Tsumeb tailings and although the process were not completely selective, subsequent refining process steps (removing impurities prior to separation and isolation) and its experimental conditions (different experimental conditions for **Step 1**) may yield the target elements in high purity.

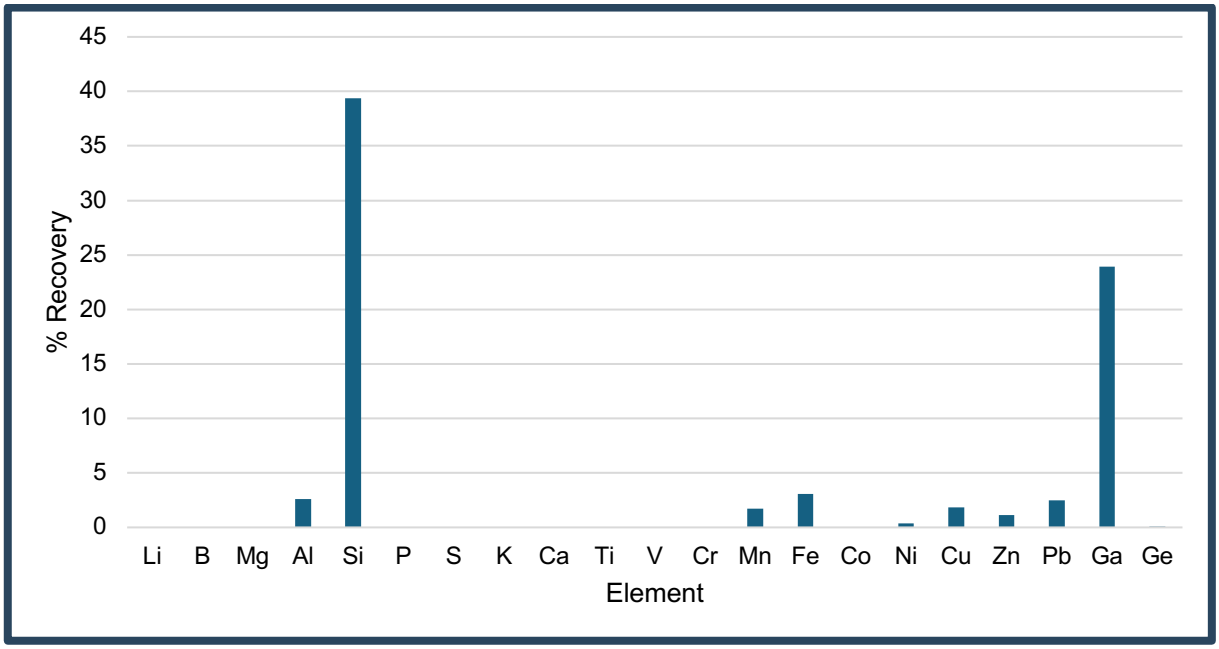

Figure 6.20: Impurities in the Ga product, extraction conditions: 2 M H_3PO_4 at 90 °C, one hour leaching at 100 rpm, mass-to-liquid of 0.7 g:10 mL, pH 4.

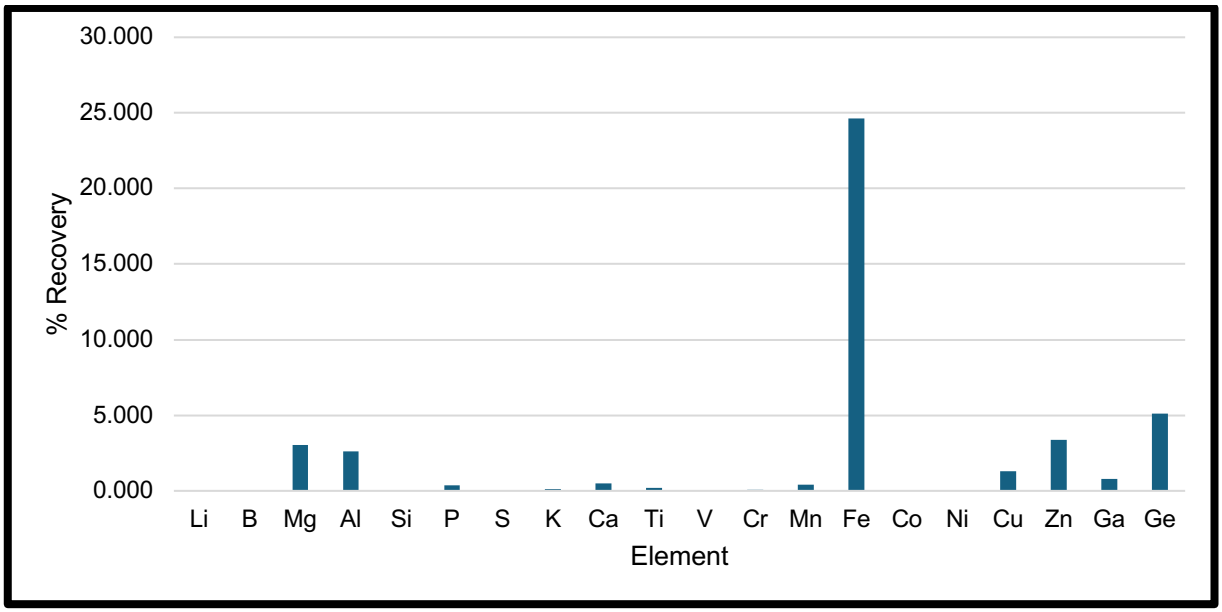

Figure 6.21: Impurities in the Ge product, extraction conditions 3 M H_2SO_4 90 °C, one hour leaching at 100 rpm, pH 8.

6.11 Conclusion

The results obtained for this study confirmed that the two target elements Ga and Ge can be separated using a 'Two Step' process which involves the dissolution of the Ge present in the Tsumeb using H_2SO_4 as leachant in the first step, followed by the dissolution of Ga in the second step using H_3PO_4 as leaching reagent. The results also indicated that approximately 40 % of the Ge is lost during this process and does not precipitate with the addition of NaOH. The loss of a large portion of the economically valuable Ge is not ideal and further studies may be needed to identify the Ge species in the tailings and its dissolution and finally its isolation to ensure optimum Ge recovery. It is also clear from the results that the final products contain a number of impurities, and some in large quantities, which may require additional beneficiation steps such as electro-winning, to remove them prior to Ga/Ge separation.

Previous studies conducted on Tsumeb mine waste only eluded to it as a potential source for the critical raw materials Ga and Ge (Ettler *et al*., 2009, 2021; Lohmeier *et al*., 2021). This study however not only confirmed its potential, but also its viability as Ga and Ge source using mild experimental conditions and unsophisticated chemicals.

Chapter 7 : Evaluation of the Study and Future Studies

7.1 Introduction

This study was motivated by the need to find alternative sources of the raw critical materials Ga and Ge. Considering that, Ga and Ge beneficiation from the Tsumeb tailings process was investigated. The history of the Tsumeb mine influenced the choice of sample for the study. The mine has produced tons of Cu, Pb, and Zn throughout the years. In addition to the mining of these metals, during a certain period of the mine, Ge was produced as a byproduct.

Previous studies concentrated on characterizing the metallurgical slags at the Tsumeb smelter and only alluded to its potential as a Ga and Ge source. No evidence was found in literature that involved both the characterization and the possible development of a process to extract Ga and Ge from the Tsumeb tailings. It was therefore decided to undertake a comprehensive study to characterize the Tsumeb tailings and to try and develop a hydrometallurgical process to separate and isolate Ga and Ge from these tailings.

This chapter critically evaluates the objectives set in the study and identifies possible future research projects emanating from the results obtained during the study.

7.2 Critical Evaluation of the Study

The overarching objective of this study was to develop a novel process to extract gallium and germanium from the Tsumeb copper mine tailings using inexpensive and readily available chemicals.

The objectives that were set in **Chapter 1**, **Paragraph 1.3** were as follows:

- In-depth literature study on Ga and Ge hydrometallurgy

- Chemical, geochemical, and mineralogical characterization of Ga and Ge bearing tailings
- Selective dissolution of Ga and Ge from the tailings
- Optimization of the reaction conditions
- Isolation of Ga and Ge from the digestion solution

The results and discussions made in the study will be evaluated according to the objectives cited above.

The in-depth literature study in **Chapter 3** provided valuable insights that guided this study. For instance, it was established that the selection of leaching reagents depended on the nature and source of the sample (whether the sample was tailings, ore, coal/fly ash, or industrial scrap). However, sulfuric acid was a common choice across samples from different sources, and high recoveries of Ga and Ge have been reported from extracting with this acid. Separation techniques such as solvent extraction, ion exchange, and precipitation were prevalent in the isolation of Ga and Ge. Solvent extraction is generally preferred among the three techniques due to its higher elemental recovery, selectivity, and efficiency. Nonetheless, precipitation by pH adjustment is also a suitable separation process due to its simplicity, cost-effectiveness, and minimal waste generation, hence its selection for the separation of Ga and Ge in this study.

The chemical, geochemical, and mineralogical characterization of the Tsumeb tailings are reported in **Chapter 5**. Non-destructive techniques such as XRF, XRD, and SEM-EDS were performed on the samples, while destructive techniques such as sequential extraction and lithium metaborate flux fusion were included to perform total elemental quantification of the sample. XRD analysis indicated the presence of quartz, orthopyroxene, olivine, and magnetite, while SEM/EDS and XRF indicated the presence of large amounts of Fe and Si and moderate amounts of Cu, Zn, and Pb. The total dissolution reactions indicated the presence of small quantities of Ga and Ge and confirmed the presence of moderate quantities of Cu, Zn, and Pb, as well as large amounts of Fe and Si in the Tsumeb tailings. The combination of these analytical techniques provided complementary information on the tailings.

Chapter 6 reports on the selective dissolution of Ga and Ge from the Tsumeb tailings using acid leaching. Different acids were evaluated, and H_2SO_4 proved to dissolve the majority of Ge in the sample and only small quantities of Ga, while H_3PO_4 proved selective towards Ga dissolution. Experimental conditions were optimized in terms of acid concentration, temperature, stirring speed, and pulp density.

Large portions of the tailing samples were subjected to a sequential two step leaching process involving its reaction with H_2SO_4 followed by a H_3PO_4 leaching step, applying the optimal conditions. Products were isolated from these reactions using NaOH as a precipitation reagent, characterized, and chemically quantified. Both the isolated products contained substantial amounts of impurities, but the H_2SO_4 leached product was enriched with Ge (from 0.03% to about 5 %) and 1 % Ga, while the H_3PO_4 product was enriched in Ga (from 1.8 to about 25 %) with no Ge present

From the above summary, it is clear that all the objectives set out in **Chapter 1** were successfully achieved. From the in-depth literature survey to the tailing characterization and finally, to the separation and isolation of enriched products, all the objectives were met.

I therefore regard the study as a success.

A number of questions and issues arose from this study, which may form the basis for future studies. From the loss of 30 - 40 % Ge during the NaOH precipitation to the presence of impurities in the final product are all important issues that can be addressed in future studies, which can only improve the process and may be the basis for possible industrial application.

7.3 Future Studies

Possible future studies emanating from this study include:

- The removal and recovery of the impurities such as Fe, Zn, Si, etc., prior to Ga and Ge separation and isolation
- Optimization of all reaction conditions for the different acids

- Investigate a more selective isolation process using bidentate ligands or other precipitants
- Optimization and purification of the Ga and Ge precipitation products
- Characterization of Ga and Ge precipitation products and
- Characterization of Ge products in tailing and its conversion to products suitable for pH precipitation
- Structural characterization using Raman Spectroscopy

Summary

The aim of this study was to develop a hydrometallurgical beneficiation process for extracting gallium (Ga) and germanium (Ge) from the Tsumeb mine tailings using readily available and cost-effective chemicals. Complete dissolution of the tailings was achieved using lithium metaborate, revealing the composition as 1.870(5) % Ga and 0.0300(2) % Ge. Other notable elements in the sample were 23(2) % Zn, 9.01(12) % Cu and 0.740(5) % Pb.

Geochemical and mineralogical characterizations were performed on the tailings. X-ray diffraction (XRD) analysis identified the sample composition as 24 % quartz, 19 % olivine, 24 % orthopyroxene and 33 % magnetite. Due to the high magnetite content, the feasibility of magnetite separation was investigated. However, the difference in Ga and Ge concentrations between the magnetic and the non-magnetic portions were insufficient to justify incorporating magnetic separation in the beneficiation process. The magnetic fraction contained 63 % Ga and 74 % Ge, while the non-magnetic fraction contained 53 % Ga and 91 % Ge.

The extraction of Ga and Ge using H_2SO_4, H_3PO_4, HCl and HNO_3 was evaluated. H_2SO_4 achieved the highest Ge extraction of 40.63 %, while H_3PO_4 was the most effective for Ga (46.67 %) and the second highest for Ge (25.00 %). These findings informed the development of a two-step selective dissolution and separation process. In the first step, H_2SO_4 was used to extract Ge, followed by Ga extraction from the residue using H_3PO_4. The reaction conditions were optimized. The optimal dissolution conditions for Ga were determined to be 2 M H_3PO_4, solid-to-liquid ratio of 0.7 g:10 mL, at 90 °C, for one hour leaching with stirring speed of 100 rpm. For Ge, the optimal conditions were 3 M H_2SO_4, solid-to-liquid ratio of 0.1 g:10 mL, at 90 °C, for one hour leaching with 100 rpm stirring.

Good separation of Ga and Ge was achieved at pH 4 in both steps of the process. Ge was isolated at pH 8 from the H_2SO_4 leachate, while Ga was isolated at pH 4 from the H_3PO_4 leachate. Products containing 5 % Ge and 25 % Ga were isolated.

Reference List

- Ahmed, I. M., El-Nadi, Y. A., & El-Hefny, N. E. (2013). Extraction of gallium(III) from hydrochloric acid by Cyanex 923 and Cyanex 925. *Hydrometallurgy*, *131–132*. https://doi.org/10.1016/j.hydromet.2012.09.010
- Ali, A., Chiang, Y. W., & Santos, R. M. (2022). X-Ray Diffraction Techniques for Mineral Characterization: A Review for Engineers of the Fundamentals, Applications, and Research Directions. *Minerals*, *12*(2). https://doi.org/10.3390/min12020205
- Ali, A., Zhang, N., & Santos, R. M. (2023). Mineral Characterization Using Scanning Electron Microscopy (SEM): A Review of the Fundamentals, Advancements, and Research Directions. In *Applied Sciences (Switzerland)* (Vol. 13, Issue 23). https://doi.org/10.3390/app132312600
- Araya, N., Kraslawski, A., & Cisternas, L. A. (2020). Towards mine tailings valorization: Recovery of critical materials from Chilean mine tailings. *Journal of Cleaner Production*, *263*. https://doi.org/10.1016/j.jclepro.2020.121555
- Arrambide Cruz, C., Marie, S., Arrachart, G., & Pellet-Rostaing, S. (2018). Selective extraction and separation of germanium by catechol-based resins. *Separation and Purification Technology*, *193*. https://doi.org/10.1016/j.seppur.2017.11.013
- Arroyo, F., Font, O., Chimenos, J. M., Fernández-Pereira, C., Querol, X., & Coca, P. (2014). IGCC fly ash valorisation. Optimisation of Ge and Ga recovery for an industrial application. *Fuel Processing Technology*, *124*, 222–227. https://doi.org/10.1016/j.fuproc.2014.03.004
- Arroyo, F., Font, O., Fernández-Pereira, C., Querol, X., Juan, R., Ruiz, C., & Coca, P. (2009). Germanium recovery from gasification fly ash: Evaluation of end-products obtained by precipitation methods. *Journal of Hazardous Materials*, *167*(1–3). https://doi.org/10.1016/j.jhazmat.2009.01.021
- Arroyo Torralvo, F., Fernández-Pereira, C., & Campanario, M. C. (2010). Recovery of germanium from aqueous solutions by ion-exchange

extraction of its catechol complex. *Industrial and Engineering Chemistry Research*, *49*(10). https://doi.org/10.1021/ie901020f

- Arroyo Torralvo, F., Fernández-Pereira, C., García Villard, E., Luna, Y., Leiva, C., Vilches, L., & Villegas, R. (2018). Low environmental impact process for germanium recovery from an industrial residue. *Minerals Engineering*, *128*. https://doi.org/10.1016/j.mineng.2018.07.022
- Bacon, J. R., & Davidson, C. M. (2008). Is there a future for sequential chemical extraction? In *Analyst* (Vol. 133, Issue 1). https://doi.org/10.1039/b711896a
- Balaram, V., & Subramanyam, K. S. V. (2022). Sample preparation for geochemical analysis: Strategies and significance. In *Advances in Sample Preparation* (Vol. 1). https://doi.org/10.1016/j.sampre.2022.100010
- Bautista, R. G. (2003). Processing to obtain high-purity gallium. *JOM*, *55*(3). https://doi.org/10.1007/s11837-003-0155-2
- Bayat, S., Aghazadeh, S., Noaparast, M., Gharabaghi, M., & Taheri, B. (2016). Germanium separation and purification by leaching and precipitation. *Journal of Central South University*, *23*(9). https://doi.org/10.1007/s11771-016-3279-6
- Bernstein, L. R. (n.d.). *Geology and Mineralogy of the Apex Germanium-Gallium Mine, Washington County, Utah*.
- Bernstein, L. R. (1985). Germanium geochemistry and mineralogy. *Geochimica et Cosmochimica Acta*, *49*(11). https://doi.org/10.1016/0016-7037(85)90241-8
- Bernstein, L. R., & Waychunas, G. A. (1987). Germanium crystal chemistry in hematite and goethite from the Apex Mine, Utah, and some new data on germanium in aqueous solution and in stottite. *Geochimica et Cosmochimica Acta*, *51*(3). https://doi.org/10.1016/0016-7037(87)90074-3
- Bock, R. (1979). *A Handbook of Decomposition Methods in Analytical Chemistry*.

- Bodénan, F., Guézennec, A.-G., Beaulieu, M., Bellenfant, G., Lemière, B., Lerouge, C., & Save, M. (2015). Re-processing of mine tailings: discussion on case studies. *13th SGA Biennial Meeting*, *July 2016*.
- Brennan, M. (2014). Gregarious gallium. In *Nature Chemistry* (Vol. 6, Issue 12). https://doi.org/10.1038/nchem.2116
- Brouwer, P. (2003). *Theory of XRF : getting acquainted with the principles*. PANalytical.
- Bruder-Hubscher, V., Lagarde, F., Leroy, M. J. F., Coughanowr, C., & Enguehard, F. (2002). Application of a sequential extraction procedure to study the release of elements from municipal solid waste incineration bottom ash. *Analytica Chimica Acta*, *451*(2). https://doi.org/10.1016/S0003-2670(01)01403-9
- Buchert, M., Schüler, D., & Bleher, D. (2009). Critical Metals for Future Sustainable Technologies and their Recycling Potential. *Unep*.
- Bunaciu, A. A., Udriştioiu, E. gabriela, & Aboul-Enein, H. Y. (2015). X-Ray Diffraction: Instrumentation and Applications. In *Critical Reviews in Analytical Chemistry* (Vol. 45, Issue 4). https://doi.org/10.1080/10408347.2014.949616
- Burdette, S., & Thornton, B. (2018). The germination of germanium. In *Nature Chemistry* (Vol. 10, Issue 2). https://doi.org/10.1038/nchem.2935
- Burton, J. D., Culkin, F., & Riley, J. P. (1959). The abundances of gallium and germanium in terrestrial materials. *Geochimica et Cosmochimica Acta*, *16*(1–3). https://doi.org/10.1016/0016-7037(59)90052-3
- Cairncross, B. (2017). The Where of Mineral Names: Tsumebite, Tsumeb Mine, Namibia. *Rocks and Minerals*, *92*(5). https://doi.org/10.1080/00357529.2017.1331402
- Cazaux, J. (2012). From the physics of secondary electron emission to image contrasts in scanning electron microscopy. In *Journal of Electron Microscopy* (Vol. 61, Issue 5). https://doi.org/10.1093/jmicro/dfs048
- Ceniceros-Gómez, A. E., Macías-Macías, K. Y., de la Cruz-Moreno, J. E., Gutiérrez-Ruiz, M. E., & Martínez-Jardines, L. G. (2018). Characterization of mining tailings in México for the possible recovery of strategic

elements. *Journal of South American Earth Sciences*, *88*. https://doi.org/10.1016/j.jsames.2018.08.013

- Charles, R. G., Douglas, P., Dowling, M., Liversage, G., & Davies, M. L. (2020). Towards Increased Recovery of Critical Raw Materials from WEEE– evaluation of CRMs at a component level and pre-processing methods for interface optimisation with recovery processes. *Resources, Conservation and Recycling*, *161*. https://doi.org/10.1016/j.resconrec.2020.104923
- Chen, L., Xu, J., & Chen, J. (2015). Applications of scanning electron microscopy in earth sciences. *Science China Earth Sciences*, *58*(10). https://doi.org/10.1007/s11430-015-5172-9
- Chen, W. S., Chang, B. C., & Chen, Y. J. (2018). Using Ion-Exchange to Recovery of Germanium from Waste Optical Fibers by Adding Citric Acid. *IOP Conference Series: Earth and Environmental Science*, *159*(1). https://doi.org/10.1088/1755-1315/159/1/012008
- Chen, W. S., Chang, B. C., & Chiu, K. L. (2017). Recovery of germanium from waste Optical Fibers by hydrometallurgical method. *Journal of Environmental Chemical Engineering*, *5*(5). https://doi.org/10.1016/j.jece.2017.09.048
- Chen, W. T., Chu, Y. C., Wei, J. M., Tsai, L. C., Tsai, F. C., Lin, C. P., & Shu, C. M. (2011). Gallium and arsenic recovery from waste gallium arsenide by wet refined methods. *Advanced Materials Research*, *194–196*. https://doi.org/10.4028/www.scientific.net/AMR.194-196.2115
- Cheng, T. H., Liu, C. J., Tsai, T. Y., & Shen, Y. H. (2019). A process for the recovery of gallium from gallium arsenide scrap. *Processes*, *7*(12). https://doi.org/10.3390/PR7120921
- Cieszynska, A., & Wiśniewski, M. (2012). Extractive recovery of palladium(II) from hydrochloric acid solutions with Cyphos®IL 104. *Hydrometallurgy*, *113–114*. https://doi.org/10.1016/j.hydromet.2011.12.006
- Coakley, G. J. (2002). *THE MINERAL INDUSTRY OF NAMIBIA-2001 THE MINERAL INDUSTRY OF NAMIBIA*. http://www.economist.com.na/2002/8feb/02-08-02.htm.

- Cook, N. J., Ciobanu, C. L., Pring, A., Skinner, W., Shimizu, M., Danyushevsky, L., Saini-Eidukat, B., & Melcher, F. (2009). Trace and minor elements in sphalerite: A LA-ICPMS study. *Geochimica et Cosmochimica Acta*, *73*(16). https://doi.org/10.1016/j.gca.2009.05.045
- Curtolo, D. C., Friedrich, S., & Friedrich, B. (2017). High Purity Germanium, a Review on Principle Theories and Technical Production Methodologies. *Journal of Crystallization Process and Technology*, *07*(04), 65–84. https://doi.org/10.4236/jcpt.2017.74005
- de Laeter, J. R., Böhlke, J. K., de Bièvre, P., Hidaka, H., Peiser, H. S., Rosman, K. J. R., & Taylor, P. D. P. (2003). Atomic weights of the elements: Review 2000 (IUPAC Technical Report). In *Pure and Applied Chemistry* (Vol. 75, Issue 6). https://doi.org/10.1351/pac200375060683
- de Oliveira, R. P., Benvenuti, J., & Espinosa, D. C. R. (2021). A review of the current progress in recycling technologies for gallium and rare earth elements from light-emitting diodes. In *Renewable and Sustainable Energy Reviews* (Vol. 145). https://doi.org/10.1016/j.rser.2021.111090
- Dennis L.M, & Hunter H.L. (1929). Germanium XXV11. *Journal of the American Chemical Society* , *51*(4), 1151–1154.
- Domaracka, L., Matuskova, S., Tausova, M., Senova, A., & Kowal, B. (2022). Efficient Use of Critical Raw Materials for Optimal Resource Management in EU Countries. *Sustainability (Switzerland)*, *14*(11). https://doi.org/10.3390/su14116554
- Douvris, C., Vaughan, T., Bussan, D., Bartzas, G., & Thomas, R. (2023). How ICP-OES changed the face of trace element analysis: Review of the global application landscape. In *Science of the Total Environment* (Vol. 905). https://doi.org/10.1016/j.scitotenv.2023.167242
- Drawell Analytical. (2023, October 23). *What is the Difference Between Powder Diffraction and Single Crystal Diffraction?* Drawell. https://www.drawellanalytical.com/what-is-the-difference-between-powder-diffraction-and-single-crystal-diffraction/
- Drzazga, M., Prajsnar, R., Chmielarz, A., Benke, G., Leszczyńska-Sejda, K., Ciszewski, M., Bilewska, K., & Krawiec, G. (2018). Germanium and indium recovery from zinc metallurgy by-products—Dross leaching in

sulphuric and oxalic acids. *Metals*, *8*(12). https://doi.org/10.3390/met8121041

- Du Laing, G. (2011). Redox Metal Processes and Controls in Estuaries. *Treatise on Estuarine and Coastal Science*, *4*, 115–141. https://doi.org/10.1016/B978-0-12-374711-2.00406-X
- Dumortier, R., Rodil, E., Weber, M. E., & Vera, J. H. (2004). Selective removal of gallium (III) from aqueous solutions containing zinc or aluminum using sodium di-(n-octyl) phosphinate. *Water Research*, *38*(7). https://doi.org/10.1016/j.watres.2004.01.004
- Dumortier, R., Weber, M. E., & Vera, J. H. (2005). Removal and recovery of gallium from aqueous solutions by complexation with sodium di-(n-octyl) phosphinate. *Hydrometallurgy*, *76*(3–4), 207–215. https://doi.org/10.1016/j.hydromet.2004.11.004
- Dutrizac, J. E., Jambor, J. L., & Chen, T. T. (1986). Host minerals for the gallium-germanium ores of the Apex mine, Utah. *Economic Geology*, *81*(4). https://doi.org/10.2113/gsecongeo.81.4.946
- Edraki, M., Baumgartl, T., Manlapig, E., Bradshaw, D., Franks, D. M., & Moran, C. J. (2014). Designing mine tailings for better environmental, social and economic outcomes: A review of alternative approaches. *Journal of Cleaner Production*, *84*(1). https://doi.org/10.1016/j.jclepro.2014.04.079
- Elshkaki, A., & Graedel, T. E. (2013). Dynamic analysis of the global metals flows and stocks in electricity generation technologies. *Journal of Cleaner Production*, *59*. https://doi.org/10.1016/j.jclepro.2013.07.003
- Epa, U., & Protection Division, R. (2004). *MARLAP Manual Volume II: Chapter 13, Sample Dissolution*.
- Ermrich, M., & Opper, D. (2013). XRD for the analyst: getting acquainted with the principles. In *PANalytical*.
- Esalah, J. O., Weber, M. E., & Vera, J. H. (1999). Removal of lead from aqueous solutions by precipitation with sodium di-(n-octyl) phosphinate. *Separation and Purification Technology*, *18*(1). https://doi.org/10.1016/S1383-5866(99)00046-5

- Esalah, J. O., Weber, M. E., & Vera, J. H. (2000). Removal of lead, cadmium and zinc from aqueous solutions by precipitation with sodium di-(n-octyl) phosphinate. *Canadian Journal of Chemical Engineering*, *78*(5). https://doi.org/10.1002/cjce.5450780512
- Etschmann, B., Liu, W., Li, K., Dai, S., Reith, F., Falconer, D., Kerr, G., Paterson, D., Howard, D., Kappen, P., Wykes, J., & Brugger, J. (2017). Enrichment of germanium and associated arsenic and tungsten in coal and roll-front uranium deposits. *Chemical Geology*, *463*, 29–49. https://doi.org/10.1016/j.chemgeo.2017.05.006
- Ettler, V., Johan, Z., Kříbek, B., Šebek, O., & Mihaljevič, M. (2009). Mineralogy and environmental stability of slags from the Tsumeb smelter, Namibia. *Applied Geochemistry*, *24*(1). https://doi.org/10.1016/j.apgeochem.2008.10.003
- Ettler, V., Mihaljevič, M., Strnad, L., Jedlicka, R., Kříbek, B., Bowell, R. J., Kamona, F., & Mapani, B. (2021). Mineralogy of Ga- and Ge-bearing metallurgical slags from Tsumeb, Namibia. *Mineralogical Magazine*, *85*(6). https://doi.org/10.1180/mgm.2021.83
- Ettler, V., Mihaljevič, M., Strnad, L., Kříbek, B., Hrstka, T., Kamona, F., & Mapani, B. (2022). Gallium and germanium extraction and potential recovery from metallurgical slags. *Journal of Cleaner Production*, *379*. https://doi.org/10.1016/j.jclepro.2022.134677
- European Commission. (2020). *Study on the EU's list of Critical Raw Materials-Final Report*. http://info.worldbank.org/governance/wgi/.
- European Commission. (2023). Study on the Critical Raw Materials for the EU 2023 Final Report. In *European Commission*. https://doi.org/10.2873/725585
- Eynard, U., Wittmer, D., Latunussa, C., & di Milano, P. (2020). *Study on the EU's list of Critical Raw Materials (2020) Non-Critical Raw Materials Factsheets BioSustain-Sustainable mobility: Perspectives for the future of biofuels production View project HARWIN-Harvesting solar energy with multifunctional glass-polymer windows (7FP) View project*. https://doi.org/10.2873/587825

- Falagán, C., Grail, B. M., & Johnson, D. B. (2017). New approaches for extracting and recovering metals from mine tailings. *Minerals Engineering*, *106*. https://doi.org/10.1016/j.mineng.2016.10.008
- Fang, Z., & Gesser, H. D. (1996). Recovery of gallium from coal fly ash. In *Hydrometallurgy* (Vol. 41).
- Feng, X., Zhang, H., & Yu, P. (2021). X-ray fluorescence application in food, feed, and agricultural science: a critical review. In *Critical Reviews in Food Science and Nutrition* (Vol. 61, Issue 14). https://doi.org/10.1080/10408398.2020.1776677
- Fink, D. A., & Culver-Hopper, J. (1991). *AD-A240 992 GERMANIUM REQUIREMENTS FOR NATIONAL DEFENSE Office of the Assistant Secretarv of Defense (Production and Logistics)*.
- Font, O., Querol, X., López-Soler, A., Chimenos, J. M., Fernández, A. I., Burgos, S., & García Peña, F. (2005). Ge extraction from gasification fly ash. *Fuel*, *84*(11). https://doi.org/10.1016/j.fuel.2004.06.041
- Foord, E. E., & Conklin, N. M. (1982). Stolzite from Tsumeb. *Mineralogical Record*, *13*(3).
- Fortier, S. M., Nassar, N. T., Graham, G. E., Hammarstrom, J. M., Day, W. C., Mauk, J. L., & Seal, R. R. (2022). USGS critical minerals review. In *Mining Engineering* (Vol. 74, Issue 5).
- Frentiu, T., Ponta, M., Levei, E., & Cordos, E. A. (2009). Study of partitioning and dynamics of metals in contaminated soil using modified four-step BCR sequential extraction procedure. *Chemical Papers*, *63*(2). https://doi.org/10.2478/s11696-008-0102-3
- Frenzel, M., Mikolajczak, C., Reuter, M. A., & Gutzmer, J. (2017). Quantifying the relative availability of high-tech by-product metals – The cases of gallium, germanium and indium. *Resources Policy*, *52*. https://doi.org/10.1016/j.resourpol.2017.04.008
- Fugleberg, S. (1999). *Finnish expert report on best available techniques in zinc production*.
- Funaiole, M. P., Hart, B., & Power-Riggs, A. (2023). *De-risking Gallium Supply Chains*.

- Geng, X., Liu, Y., Zhang, W., Wang, L., Wen, J., & Sun, J. (2022a). Recent advances in the recovery of germanium during the zinc refining process. In *Chemical Engineering Journal* (Vol. 446). Elsevier B.V. https://doi.org/10.1016/j.cej.2022.137445
- Geng, X., Liu, Y., Zhang, W., Wang, L., Wen, J., & Sun, J. (2022b). Recent advances in the recovery of germanium during the zinc refining process. In *Chemical Engineering Journal* (Vol. 446). Elsevier B.V. https://doi.org/10.1016/j.cej.2022.137445
- González, A., Font, O., Moreno, N., Querol, X., Arancibia, N., & Navia, R. (2017). Copper Flash Smelting Flue Dust as a Source of Germanium. *Waste and Biomass Valorization*, *8*(6). https://doi.org/10.1007/s12649-016-9725-8
- Gredilla, A., Fdez-Ortiz de Vallejuelo, S., Elejoste, N., de Diego, A., & Madariaga, J. M. (2016). Non-destructive Spectroscopy combined with chemometrics as a tool for Green Chemical Analysis of environmental samples: A review. In *TrAC - Trends in Analytical Chemistry* (Vol. 76). https://doi.org/10.1016/j.trac.2015.11.011
- Guevara-Riba, A., Sahuquillo, A., Rubio, R., & Rauret, G. (2004). Assessment of metal mobility in dredged harbour sediments from Barcelona, Spain. *Science of the Total Environment*, *321*(1–3). https://doi.org/10.1016/j.scitotenv.2003.08.021
- Gulley, A. L., McCullough, E. A., & Shedd, K. B. (2019). China's domestic and foreign influence in the global cobalt supply chain. *Resources Policy*, *62*. https://doi.org/10.1016/j.resourpol.2019.03.015
- Gunn, G. (2013). Critical Metals Handbook. In *Critical Metals Handbook*. https://doi.org/10.1002/9781118755341
- Gupta, M. K., & O'Sullivan, T. P. (2013). Recent applications of gallium and gallium halides as reagents in organic synthesis. In *RSC Advances* (Vol. 3, Issue 48, pp. 25498–25522). https://doi.org/10.1039/c3ra42316f
- Gutiérrez, B., Pazos, C., & Coca, J. (1997). Recovery of gallium from coal fly ash by a dual reactive extraction process. *Waste Management and Research*, *15*(4). https://doi.org/10.1006/wmre.1996.0093

- Guzik, K., Burkowicz, A., & Szlugaj, J. (2022). The EU's demand for selected critical raw materials used in the photovoltaic industry. *Gospodarka Surowcami Mineralnymi / Mineral Resources Management*, *38*(2). https://doi.org/10.24425/gsm.2022.141666
- Haque, A. K. F., Haque, M. M., Patoary, M. A. R., Uddin, M. A., Hossain, M. I., Mahbub, M. S., Basak, A. K., Maaza, M., & Saha, B. C. (2017). Electron impact secondary electron emissions from elemental and compound solids. *Vacuum*, *141*. https://doi.org/10.1016/j.vacuum.2017.04.004
- Harbuck, D. D. (1993). Increasing germanium extraction from hydrometallurgical zinc residues. *Mining, Metallurgy & Exploration*, *10*(1), 1–4.
- Harbuck, D. D., Judd, J. C., & Behunin, D. v. (1991). Germanium solvent extraction from sulfuric acid solutions (and co-extraction of germanium and gallium). *Solvent Extraction and Ion Exchange*, *9*(3). https://doi.org/10.1080/07366299108918060
- Harms, A. V. (2007). Complete dissolution of soil samples by fusion. In *Environmental Radiochemical Analysis II*. https://doi.org/10.1039/9781847550781-00167
- Hawthorne, F. C., Cooper, M. A., Abdu, Y. A., Ball, N. A., Back, M. E., & Tait, K. T. (2012). Davidlloydite, ideally Zn 3 (AsO 4) 2 (H 2 O) 4 , a new arsenate mineral from the Tsumeb mine, Otjikoto (Oshikoto) region, Namibia: description and crystal structure . *Mineralogical Magazine*, *76*(1). https://doi.org/10.1180/minmag.2012.076.1.45
- Hearth, S. (2021). The "world'S Greatest Mineral Locality": Haiom, Ndonga, Herero, and the Early Colonial Histories of Tsumeb, Namibia. In *Earth Sciences History* (Vol. 40, Issue 2). https://doi.org/10.17704/1944-6187-40.2.433
- Hirashita, T., Kawai, D., & Araki, S. (2007). GaCl3-catalyzed [4+2] annulations of allyltrimethylsilane and trimethyl(propargyl)silane with aldimines. *Tetrahedron Letters*, *48*(31). https://doi.org/10.1016/j.tetlet.2007.06.013

- Hoffmann, J. E. (1987). Extracting and Refining Germanium. *JOM*, *39*(6). https://doi.org/10.1007/BF03258062
- Höll, R., Kling, M., & Schroll, E. (2007). Metallogenesis of germanium-A review. In *Ore Geology Reviews* (Vol. 30, Issues 3–4, pp. 145–180). https://doi.org/10.1016/j.oregeorev.2005.07.034
- Hu, S. H., Xie, M. Y., Hsieh, Y. M., Liou, Y. S., & Chen, W. S. (2015). Resource recycling of gallium arsenide scrap using leaching-selective precipitation. *Environmental Progress and Sustainable Energy*, *34*(2). https://doi.org/10.1002/ep.12019
- Hughes, A. E., Haque, N., Northey, S. A., & Giddey, S. (2021). Platinum group metals: A review of resources, production and usage with a focus on catalysts. In *Resources* (Vol. 10, Issue 9). MDPI. https://doi.org/10.3390/resources10090093
- Jamieson, H. E., Walker, S. R., & Parsons, M. B. (2015). Mineralogical characterization of mine waste. In *Applied Geochemistry* (Vol. 57). https://doi.org/10.1016/j.apgeochem.2014.12.014
- Johnson, O. H. (1952). *GERMANIUM AND ITS INORGANIC COMPOUNDS*. https://pubs.acs.org/sharingguidelines
- Joy, D. C. (2019). Scanning Electron Microscopy: Theory, History and Development of the Field Emission Scanning Electron Microscope. In *Biological Field Emission Scanning Electron Microscopy: Volume I: Volume II* (Vols. 1–2). https://doi.org/10.1002/9781118663233.ch1
- Kamran Haghighi, H., & Irannajad, M. (2022). Roadmap for recycling of germanium from various resources: reviews on recent developments and feasibility views. In *Environmental Science and Pollution Research* (Vol. 29, Issue 32, pp. 48126–48151). Springer Science and Business Media Deutschland GmbH. https://doi.org/10.1007/s11356-022-20649-5
- KAWAKITA, H., MORISADA, S., & OHTO, K. (2014). Germanium Recovery Using Ion-Exchange Membrane and Solvent Extraction. *Journal of Ion Exchange*, *25*(4). https://doi.org/10.5182/jaie.25.88
- Khan, S. R., Sharma, B., Chawla, P. A., & Bhatia, R. (2022). Inductively Coupled Plasma Optical Emission Spectrometry (ICP-OES): a Powerful

Analytical Technique for Elemental Analysis. In *Food Analytical Methods* (Vol. 15, Issue 3). https://doi.org/10.1007/s12161-021-02148-4

- Kline, W. E., & Fogler, H. S. (1981). Dissolution of silicate minerals by hydrofluoric acid. *Industrial & Engineering Chemistry, Fundamentals*, *20*(2). https://doi.org/10.1021/i100002a008
- Kul, M., & Topkaya, Y. (2008). Recovery of germanium and other valuable metals from zinc plant residues. *Hydrometallurgy*, *92*(3–4). https://doi.org/10.1016/j.hydromet.2007.11.004
- Kuroiwa, K., Ohura, S. I., Morisada, S., Ohto, K., Kawakita, H., Matsuo, Y., & Fukuda, D. (2014). Recovery of germanium from waste solar panels using ion-exchange membrane and solvent extraction. *Minerals Engineering*, *55*. https://doi.org/10.1016/j.mineng.2013.10.002
- Levine, M. (2021, March 17). *ICP-OES – ICP Chemistry, ICP-OES Analysis, Strengths and Limitations*. Analysis & Separations. https://www.technologynetworks.com/analysis/articles/icp-oes-icp-chemistry-icp-oes-analysis-strengths-and-limitations-342265
- Li, F., Ge, L., Tang, Z., Chen, Y., & Wang, J. (2020). Recent developments on XRF spectra evaluation. In *Applied Spectroscopy Reviews* (Vol. 55, Issue 4). https://doi.org/10.1080/05704928.2019.1580715
- Li, X., Coles, B. J., Ramsey, M. H., & Thornton, I. (1995). Sequential extraction of soils for multielement analysis by ICP-AES. *Chemical Geology*, *124*(1–2). https://doi.org/10.1016/0009-2541(95)00029-L
- Li, X., Ma, B., Hu, D., Zhao, Q., Chen, Y., & Wang, C. (2022). Efficient separation and purification of indium and gallium in spent Copper indium gallium diselenide (CIGS). *Journal of Cleaner Production*, *339*. https://doi.org/10.1016/j.jclepro.2022.130658
- Li, X., & Thornton, I. (2001). Chemical partitioning of trace and major elements in soils contaminated by mining and smelting activities. *Applied Geochemistry*, *16*(15). https://doi.org/10.1016/S0883-2927(01)00065-8
- Liang, D., Wang, J., & Wang, Y. (2008). Germanium recovery by co-precipitation of germanium and iron in conventional zinc metallurgy.

Journal of the Southern African Institute of Mining and Metallurgy, *108*(11).

- Liang, D., Wang, J., Wang, Y., Wang, F., & Jiang, J. (2008). Behavior of tannins in germanium recovery by tannin process. *Hydrometallurgy*, *93*(3–4). https://doi.org/10.1016/j.hydromet.2008.03.006
- Licht, C., Peiró, L. T., & Villalba, G. (2015). Global substance flow analysis of gallium, germanium, and indium: Quantification of extraction, uses, and dissipative losses within their anthropogenic cycles. *Journal of Industrial Ecology*, *19*(5). https://doi.org/10.1111/jiec.12287
- Liu, F., Liu, Z., Li, Y., Liu, Z., Li, Q., & Zeng, L. (2016). Extraction of gallium and germanium from zinc refinery residues by pressure acid leaching. *Hydrometallurgy*, *164*. https://doi.org/10.1016/j.hydromet.2016.06.006
- Liu, F., Liu, Z., Li, Y., Wilson, B. P., Liu, Z., Zeng, L., & Lundström, M. (2017). Recovery and separation of gallium(III) and germanium(IV) from zinc refinery residues : Part II: Solvent extraction. *Hydrometallurgy*, *171*. https://doi.org/10.1016/j.hydromet.2017.05.009
- Liu, F., Liu, Z., Li, Y., Wilson, B. P., & Lundström, M. (2017a). Extraction of Ga and Ge from zinc refinery residues in $H_2C_2O_4$ solutions containing H_2O_2. *International Journal of Mineral Processing*, *163*. https://doi.org/10.1016/j.minpro.2017.04.005
- Liu, F., Liu, Z., Li, Y., Wilson, B. P., & Lundström, M. (2017b). Recovery and separation of gallium(III) and germanium(IV) from zinc refinery residues: Part I: Leaching and iron(III) removal. *Hydrometallurgy*, *169*. https://doi.org/10.1016/j.hydromet.2017.03.006
- Liu, Z., & Li, H. (2015). Metallurgical process for valuable elements recovery from red mud - A review. In *Hydrometallurgy* (Vol. 155). https://doi.org/10.1016/j.hydromet.2015.03.018
- Lohmeier, S., Lottermoser, B. G., Schirmer, T., & Gallhofer, D. (2021). Copper slag as a potential source of critical elements - A case study from Tsumeb, Namibia. *Journal of the Southern African Institute of Mining and Metallurgy*, *121*(3). https://doi.org/10.17159/2411-9717/1383/2021

- Lu, F., Xiao, T., Lin, J., Li, A., Long, Q., Huang, F., Xiao, L., Li, X., Wang, J., Xiao, Q., & Chen, H. (2018). Recovery of gallium from Bayer red mud through acidic-leaching-ion-exchange process under normal atmospheric pressure. *Hydrometallurgy*, *175*. https://doi.org/10.1016/j.hydromet.2017.10.032
- Lu, F., Xiao, T., Lin, J., Ning, Z., Long, Q., Xiao, L., Huang, F., Wang, W., Xiao, Q., Lan, X., & Chen, H. (2017). Resources and extraction of gallium: A review. *Hydrometallurgy*, *174*. https://doi.org/10.1016/j.hydromet.2017.10.010
- Lv, Y., Xing, P., Ma, B., Liu, B., Wang, C., Zhang, Y., & Zhang, W. (2019). Separation and Recovery of Valuable Elements from Spent CIGS Materials. *ACS Sustainable Chemistry and Engineering*, *7*(24). https://doi.org/10.1021/acssuschemeng.9b05121
- Ma, B., Li, X., Liu, B., Xing, P., Zhang, W., Wang, C., & Chen, Y. (2020). Effective Separation and Recovery of Valuable Components from CIGS Chamber Waste via Controlled Phase Transformation and Selective Leaching. *ACS Sustainable Chemistry and Engineering*, *8*(7). https://doi.org/10.1021/acssuschemeng.0c00138
- Ma, X. H., Qin, W. Q., & Wu, X. L. (2013). Extraction of germanium(IV) from acid leaching solution with mixtures of P204 and TBP. *Journal of Central South University*, *20*(7). https://doi.org/10.1007/s11771-013-1698-1
- Maarefvand, M., Sheibani, S., & Rashchi, F. (2020). Recovery of gallium from waste LEDs by oxidation and subsequent leaching. *Hydrometallurgy*, *191*. https://doi.org/10.1016/j.hydromet.2019.105230
- Macías-Macías, K. Y., Ceniceros-Gómez, A. E., Gutiérrez-Ruiz, M. E., González-Chávez, J. L., & Martínez-Jardines, L. G. (2019). Extraction and recovery of the strategic element gallium from an iron mine tailing. *Journal of Environmental Chemical Engineering*, *7*(2). https://doi.org/10.1016/j.jece.2019.102964
- Melcher, F. (2003). the Otavi Mountain Land in Nambia: Tsumeb, Germanium and Snowball Earth. *Mitteilungen der Österreichischen Mineralogischen Gesellschaft*, *148*.

- Melcher, F., & Buchhilz, P. (2012, April). Current and future germanium availability from primary sources. *Minor Metals Conference*.
- Melcher, F., Oberthür, T., & Rammlmair, D. (2006). Geochemical and mineralogical distribution of germanium in the Khusib Springs Cu-Zn-Pb-Ag sulfide deposit, Otavi Mountain Land, Namibia. *Ore Geology Reviews*, *28*(1). https://doi.org/10.1016/j.oregeorev.2005.04.006
- Meshram, P., & Abhilash. (2022). Strategies for Recycling of Primary and Secondary Resources for Germanium Extraction. In *Mining, Metallurgy and Exploration* (Vol. 39, Issue 2). https://doi.org/10.1007/s42461-022-00549-5
- Moskalyk, R. R. (2004). Review of germanium processing worldwide. In *Minerals Engineering* (Vol. 17, Issue 3, pp. 393–402). https://doi.org/10.1016/j.mineng.2003.11.014
- Muntau, H., Quevauviller, P., & Griepink, B. (1993). Speciation of heavy metals in soils and sediments an account of the improvement and harmonization of extraction techniques undertaken under the auspices of the bcr of the commission of the european communities. *International Journal of Environmental Analytical Chemistry*, *51*(1–4). https://doi.org/10.1080/03067319308027619
- Muratli, J. M., McManus, J., Mix, A., & Chase, Z. (2012). Dissolution of fluoride complexes following microwave-assisted hydrofluoric acid digestion of marine sediments. *Talanta*, *89*. https://doi.org/10.1016/j.talanta.2011.11.081
- Nadoll, P., Angerer, T., Mauk, J. L., French, D., & Walshe, J. (2014). The chemistry of hydrothermal magnetite: A review. In *Ore Geology Reviews* (Vol. 61). https://doi.org/10.1016/j.oregeorev.2013.12.013
- Nayak, S., & Devi, N. (2017). Separation and recovery of gallium(III) ions from aqueous phase by liquid–liquid extraction using a novel extractant, Cyphos IL 101. *Turkish Journal of Chemistry*, *41*(6). https://doi.org/10.3906/kim-1612-37
- Ngcephe, A. M., Sinha, M. K., & Purcell, W. (2020). Solvent extraction and separation of palladium from platinum group elements: Synthesis and characterization of 2-mercaptopyridine N-oxide-palladium (II)

complex. *Journal of Molecular Structure*, *1199*. https://doi.org/10.1016/j.molstruc.2019.127009

- Nguyen, T. H., & Lee, M. S. (2021). A Review on Germanium Resources and its Extraction by Hydrometallurgical Method. In *Mineral Processing and Extractive Metallurgy Review* (Vol. 42, Issue 6). https://doi.org/10.1080/08827508.2020.1756795
- Niu, P. P., Jiang, S. Y., & Muñoz, M. (2023). Two-stage enrichment of germanium in the giant Maoping MVT Pb-Zn deposit, southwestern China: Constraints from in situ analysis of multicolor sphalerites. *Ore Geology Reviews*, *157*. https://doi.org/10.1016/j.oregeorev.2023.105421
- Nora K. Foley, Brian W. Jaskula, Bryn E. Kimball, & Ruth F. Schulte. (2017). Gallium. In Klaus J. Schulz, Jr. , John H. DeYoung, & D. C. B. Robert R. Seal II (Eds.), *Critical mineral resources of the United States—Economic and environmental geology and prospects for future supply* (Vol. 1802, pp. H1–H35). U.S. Geological Survey. https://doi.org/10.3133/pp1802H
- Nozoe, A., Ohto, K., & Kawakita, H. (2012). Germanium Recovery using Catechol Complexation and Permeation through an Anion-Exchange Membrane. *Separation Science and Technology*, *47*(1). https://doi.org/10.1080/01496395.2011.613440
- Nyamangara, J. (1998). Use of sequential extraction to evaluate zinc and copper in a soil amended with sewage sludge and inorganic metal salts. *Agriculture, Ecosystems and Environment*, *69*(2). https://doi.org/10.1016/S0167-8809(98)00101-7
- Olivares, M., Tarriño, A., Murelaga, X., Baceta, J. I., Castro, K., & Etxebarria, N. (2009). Non-destructive spectrometry methods to study the distribution of archaeological and geological chert samples. *Spectrochimica Acta - Part A: Molecular and Biomolecular Spectroscopy*, *73*(3). https://doi.org/10.1016/j.saa.2008.12.036
- Oyedotun, T. D. T. (2018). X-ray fluorescence (XRF) in the investigation of the composition of earth materials: a review and an overview. *Geology, Ecology, and Landscapes*, *2*(2). https://doi.org/10.1080/24749508.2018.1452459

- Pan, X., Li, S., Li, Y., Guo, P., Zhao, X., & Cai, Y. (2022). Resource, characteristic, purification and application of quartz: a review. In *Minerals Engineering* (Vol. 183). https://doi.org/10.1016/j.mineng.2022.107600
- Papež, N., Dallaev, R., Ţălu, Ş., & Kaštyl, J. (2021). Overview of the current state of gallium arsenide-based solar cells. *Materials*, *14*(11). https://doi.org/10.3390/ma14113075
- Patel, M., & Karamalidis, A. K. (2021). Germanium: A review of its US demand, uses, resources, chemistry, and separation technologies. In *Separation and Purification Technology* (Vol. 275). Elsevier B.V. https://doi.org/10.1016/j.seppur.2021.118981
- Pesic, B., & Zhou, T. (1988). Recovering Gallium with Kelex 100. *JOM*, *40*(7). https://doi.org/10.1007/BF03258145
- Phatak, G. M., Gangadharan, K., & Rao, G. S. (1988). Electrochemical extraction of gallium from alkaline gallate solutions. *Transactions of the SAEST (Society for Advancement of Electrochemical Science and Technology)*, *23*(4).
- Pickering, W. F. (1986). Metal ion speciation — soils and sediments (a review). *Ore Geology Reviews*, *1*(1), 83–146.
- Pitiya, R. P., & Peter, L. J. (2021). A Review on the Deposit Geology and Mineralization Mechanism of Tsumeb Polymetallic Deposit, Namibia. *OALib*, *08*(11), 1–13. https://doi.org/10.4236/oalib.1108121
- Pourrahim, M., Rezai, B., & Gharabaghi, M. (2017). Comparison of Indium and Gallium Dissolution from Zinc Oxide Concentrate in Different Acidic Solutions. *Arabian Journal for Science and Engineering*, *42*(4). https://doi.org/10.1007/s13369-016-2407-9
- Qin, S., Sun, Y., Li, Y., Wang, J., Zhao, C., & Gao, K. (2015). Coal deposits as promising alternative sources for gallium. In *Earth-Science Reviews* (Vol. 150). https://doi.org/10.1016/j.earscirev.2015.07.010
- Rafiee, P., Ghassa, S., Moosakazemi, F., Khosravi, R., & Siavoshi, H. (2021). Recovery of a critical metal from electronic wastes: Germanium extraction with organic acid. *Journal of Cleaner Production*, *315*. https://doi.org/10.1016/j.jclepro.2021.128223

- Raiguel, S., Dehaen, W., & Binnemans, K. (2020). Extraction of gallium from simulated Bayer process liquor by Kelex 100 dissolved in ionic liquids. *Dalton Transactions*, *49*(11), 3532–3544. https://doi.org/10.1039/c9dt04623b
- Rao, S., Wang, D., Liu, Z., Zhang, K., Cao, H., & Tao, J. (2019). Selective extraction of zinc, gallium, and germanium from zinc refinery residue using two stage acid and alkaline leaching. *Hydrometallurgy*, *183*, 38–44. https://doi.org/10.1016/j.hydromet.2018.11.007
- Redlinger, M., Eggert, R., & Woodhouse, M. (2015). Evaluating the availability of gallium, indium, and tellurium from recycled photovoltaic modules. *Solar Energy Materials and Solar Cells*, *138*, 58–71. https://doi.org/10.1016/j.solmat.2015.02.027
- Rezaei, H., Ziaedin Shafaei, S., Abdollahi, H., Shahidi, A., & Ghassa, S. (2022). A sustainable method for germanium, vanadium and lithium extraction from coal fly ash: Sodium salts roasting and organic acids leaching. *Fuel*, *312*. https://doi.org/10.1016/j.fuel.2021.122844
- Robertz, B., Verhelle, J., & Schurmans, M. (2015). The Primary and Secondary Production of Germanium: A Life-Cycle Assessment of Different Process Alternatives. *JOM*, *67*(2), 412–424. https://doi.org/10.1007/s11837-014-1267-6
- Rochow, E. G., & Abel, E. W. (1997). Germanium, Tin and Lead. In *Chemistry of the Elements*. https://doi.org/10.1016/b978-0-7506-3365-9.50016-x
- Rodgers, K. J., Hursthouse, A., & Cuthbert, S. (2015). The potential of sequential extraction in the characterisation and management of wastes from steel processing: A prospective review. In *International Journal of Environmental Research and Public Health* (Vol. 12, Issue 9). https://doi.org/10.3390/ijerph120911724
- Rodil, E., Dumortier, R., & Vera, J. H. (2004). Removal of aluminum from aqueous solutions using sodium di-(n-octyl) phosphinate. *Chemical Engineering Journal*, *97*(2–3). https://doi.org/10.1016/S1385-8947(03)00213-4

- Ruiz, A. G., Sola, P. C., & Palmerola, N. M. (2018). Germanium: Current and Novel Recovery Processes. In *Advanced Material and Device Applications with Germanium*. InTech. https://doi.org/10.5772/intechopen.77997
- Schlüter, J., Malcherek, T., Mihailova, B., & Gebhard, G. (2013). The new mineral erikapohlite, Cu3(Zn,Cu,Mg)4Ca 2(AsO4)6 · 2H2O, the Ca-dominant analogue of keyite, from Tsumeb, Namibia. *Neues Jahrbuch Fur Mineralogie, Abhandlungen*, *190*(3). https://doi.org/10.1127/0077-7757/2013/0239
- Scholtz, J. J., Dijkkamp, D., & Schmitz, R. W. A. (1996). Secondary electron emission properties. *Philips Journal of Research*, *50*(3–4). https://doi.org/10.1016/S0165-5817(97)84681-5
- Schulte, R. F., & Foley, N. K. (2014). Compilation of gallium resource data for bauxite deposits. *United States Geological Survey*.
- Šebesta, M., Urík, M., Kolenčík, M., Bujdoš, M., & Matúš, P. (2020). Sequential extraction resulted in similar fractionation of ionic zn, nano- and microparticles of zno in acidic and alkaline soil. *Forests*, *11*(10). https://doi.org/10.3390/f11101077
- Shi, F., & Qiao, H. (2022). Preparations, properties and applications of gallium oxide nanomaterials – A review. *Nano Select*, *3*(2). https://doi.org/10.1002/nano.202100149
- Sill, C. W., & Sill, D. S. (1995). *FROM THE LAB Sample Dissolution* (Vol. 2).
- Song, H., Wang, C., Sen, B., & Liu, G. (2022). China Factor: Exploring the Byproduct and Host Metal Dynamics for Gallium-Aluminum in a Global Green Transition. *Environmental Science and Technology*, *56*(4). https://doi.org/10.1021/acs.est.1c04784
- Sook Lee, H., & Woo Nam, C. (1998). A study on the extraction of gallium from gallium arsenide scrap. In *Hydrometallurgy* (Vol. 49).
- Srinivasa Rao, K., Sarangi, D., Dash, P. K., & Chaudhury, G. R. (2003). Preferential extraction of gallium from Bayer liquor using ion exchange chelating resin containing hydroxamic acid functional group. *Journal of*

Chemical Technology and Biotechnology, *78*(5). https://doi.org/10.1002/jctb.819

- Sudarsan, V. (2017). Materials for Hostile Chemical Environments. *Materials Under Extreme Conditions: Recent Trends and Future Prospects*, 129–158. https://doi.org/10.1016/B978-0-12-801300-7.00004-8
- Surdu, V. A., & Győrgy, R. (2023). X-ray Diffraction Data Analysis by Machine Learning Methods—A Review. In *Applied Sciences (Switzerland)* (Vol. 13, Issue 17). https://doi.org/10.3390/app13179992
- Sutley, S., Gustkiewicz2, M.-S., Mayer, W., Leach, D., Sutley, S., Gustkiewicz, M.-S., Mayer, W., & Leach, D. (1999). *Mineralogy and chemistry of oxidized ores from the upper Silesia Mississippi valley-type zinc-lead deposits*.
- Swami, M., & Patel, K. (2021). Need of Gallium Recovery from Waste Samples: A Review. *Journal of Ravishankar University (PART-B)*, *34*(1). https://doi.org/10.52228/jrub.2021-34-1-2
- Takemura, H., Morisada, S., Ohto, K., Kawakita, H., Matsuo, Y., & Fukuda, D. (2013). Germanium recovery by catechol complexation and subsequent flow through membrane and bead-packed bed column. *Journal of Chemical Technology and Biotechnology*, *88*(8). https://doi.org/10.1002/jctb.3985
- Tan, Z., Jin, X., Zhen, Y., Wei, C., Li, X., Deng, Z., & Li, M. (2023). Recovery of indium and germanium from In-Ge residue leaching solution using solvent extraction and tannin precipitation. *Separation and Purification Technology*, *323*. https://doi.org/10.1016/j.seppur.2023.124416
- Tao, J., Tao, Z., & Zhihong, L. (2021). Review on resources and recycling of germanium, with special focus on characteristics, mechanism and challenges of solvent extraction. In *Journal of Cleaner Production* (Vol. 294). Elsevier Ltd. https://doi.org/10.1016/j.jclepro.2021.126217
- Tessier, A., Campbell, P. G. C., & Bisson, M. (1979). Downloaded via UNIV OF THE FREE STATE on August 18. In *ANALYTICAL CHEMISTRY* (Vol. 844, Issue 7). UTC. https://pubs.acs.org/sharingguidelines

- Thanh, L. H. V., & Liu, J. C. (2014). Flotation separation of soluble and colloidal indium from aqueous solution. *Industrial and Engineering Chemistry Research*, *53*(3). https://doi.org/10.1021/ie4032617
- The Editors of Encyclopaedia. (2024, June 3). *Electron configuration*. EncyclopediaBritannica. https://www.britannica.com/science/electronic-configuration
- Theodore Gray. (2007, August 11). *Gallium*. Photographic Periodic Table Poster.
- Torma, A. E., & Jiang, H. (1991). Extraction Processes for Gallium and Germanium. *Mineral Processing and Extractive Metallurgy Review*, *7*(3–4). https://doi.org/10.1080/08827509108952673
- Torralvo, F. A., & Fernández-Pereira, C. (2011). Recovery of germanium from real fly ash leachates by ion-exchange extraction. *Minerals Engineering*, *24*(1). https://doi.org/10.1016/j.mineng.2010.09.004
- *Tsumeb Specialty Smelter, Namibia*. (2024, February 1). Dundee Precious Metals Inc. https://dundeeprecious.com/assets/other/tsumeb-specialty-smelter/
- Vecchia, M. D., Ravyts, S., Broeck, G. van den, & Driesen, J. (2019). Gallium-nitride semiconductor technology and its practical design challenges in power electronics applications: An overview. In *Energies* (Vol. 12, Issue 14). https://doi.org/10.3390/en12142663
- Vernon-Parry, K. (2000). Scanning electron microscopy: an introduction. *III-Vs Review*, *13*(4), 40–44. https://doi.org/10.1016/S0961-1290(00)80006-X
- Wardell, M. P., & Davidson, C. F. (1987). Acid Leaching Extraction of Ga and Ge. *JOM*, *39*(6). https://doi.org/10.1007/BF03258061
    - W.C. Pat Shanks III, Bryn E. Kimball, Amy C. Tolcin, & David E. Guberman. (2017). Germanium and Indium. In Klaus J. Schulz, Jr. , John H. DeYoung, Robert R. Seal II, & Dwight C. Bradley (Eds.), *Critical Mineral Resources of the United States—Economic and Environmental Geology and Prospects for Future Supply* (Vol. 1802). U.S Geological Survey. https://doi.org/10.3133/pp1802I

- Webb, M. (2024, March 7). *Canadian miner Dundee Precious Metals (DPM) will sell its Tsumeb smelter, in Namibia, to Sinomine Resources for $49 million in cash.* Mining Weekly. https://www.miningweekly.com/article/dundee-sells-namibia-smelter-for-49m-2024-03-07
- Wegrzynek, D. (2004). *Commercial Applications of X-ray Spectrometric Techniques*.
- Wen, K., Jiang, F., Zhou, X. yang, & Sun, Z. ming. (2018). Leaching of gallium from corundum flue dust using mixed acid solution. *Transactions of Nonferrous Metals Society of China (English Edition)*, *28*(9). https://doi.org/10.1016/S1003-6326(18)64831-9
- Wenzel, W. W., Kirchbaumer, N., Prohaska, T., Stingeder, G., Lombi, E., & Adriano, D. C. (2001). Arsenic fractionation in soils using an improved sequential extraction procedure. *Analytica Chimica Acta*, *436*(2). https://doi.org/10.1016/S0003-2670(01)00924-2
- Xiaolong, Z., Shiyu, Z., Hui, L., & Yingliang, Z. (2021). Disposal of mine tailings via geopolymerization. In *Journal of Cleaner Production* (Vol. 284). https://doi.org/10.1016/j.jclepro.2020.124756
- Xu, Y., Xia, H., Zhang, Q., Jiang, G., Zhang, L., Xin, C., & Cai, W. (2023). Ultrasonic enhanced hydrazine sulfate acid leaching of low-grade germanium dust. *Applied Energy*, *332*. https://doi.org/10.1016/j.apenergy.2022.120485
- Žemberyová, M., Barteková, J., & Hagarová, I. (2006). The utilization of modified BCR three-step sequential extraction procedure for the fractionation of Cd, Cr, Cu, Ni, Pb and Zn in soil reference materials of different origins. *Talanta*, *70*(5), 973–978. https://doi.org/10.1016/J.TALANTA.2006.05.057
- Zhang, K., Liu, Z., Liu, Y., Cao, H., & Zhu, W. (2019). Recovery of gallium from strong acidic sulphate leach solutions of zinc refinery residues using a novel phosphate ester extractant. *Hydrometallurgy*, *185*. https://doi.org/10.1016/j.hydromet.2019.03.001

- Zhao, Z., Yang, Y., Xiao, Y., & Fan, Y. (2012). Recovery of gallium from Bayer liquor: A review. *Hydrometallurgy*, *125–126*. https://doi.org/10.1016/j.hydromet.2012.06.002
- Zhou, J., Zhu, N., Liu, H., Wu, P., Zhang, X., & Zhong, Z. (2019). Recovery of gallium from waste light emitting diodes by oxalic acidic leaching. *Resources, Conservation and Recycling*, *146*, 366–372. https://doi.org/10.1016/j.resconrec.2019.04.002
- Zhou, W., Apkarian, R., Wang, Z. L., & Joy, D. (2007). Fundamentals of scanning electron microscopy (SEM). In *Scanning Microscopy for Nanotechnology: Techniques and Applications*. https://doi.org/10.1007/978-0-387-39620-0_1
- Zimmerman, A. J., & Weindorf, D. C. (2010). Heavy Metal and Trace Metal Analysis in Soil by Sequential Extraction: A Review of Procedures. *International Journal of Analytical Chemistry*, *2010*. https://doi.org/10.1155/2010/387803